UNIVERSITÀ
DEGLI STUDI
DI PADOVA

Università degli Studi di Padova
Dipartimento di Ingegneria Civile, Edile ed Ambientale

Technische Universität Carolo-Wilhelmina zu Braunschweig
Fakultät Architektur, Bauingenieurwesen und Umweltwissenschaften

DOCTORAL SCHOOL IN
SCIENCE OF CIVIL AND ENVIROMENTAL ENGINEERING
XXXI CICLE

MODELING AND COMPUTATION OF CRACKING IN MULTIPHASE POROUS MEDIA WITH THE PHASE-FIELD APPROACH

Director of the School: Prof. Marco Marani
Supervisors: Prof. Lorenzo Sanavia
Prof. Laura De Lorenzis

PhD student: Claudio Gavagnin

Abstract

The development of mathematical and numerical models for the study of the problem of fracture in porous media is motivated by several real-world applications. In particular, the phase-field approach to fracture, based on the regularization of the variational formulation of the Griffith's theory, seems to be one of the most promising, due to its ability to model complicated fracture processes, such as nucleation and branching, and preserve the continuity of the displacement field. The majority of the phase-field models for fracture in porous media present in the literature are mainly oriented to the study the problem of fracture in saturated porous media. Anyway, certain phenomena, such as the cracking of clayey soils during a desiccation process, suggest the importance of the extension of these models to a partially saturated framework, in which also the flow of the gaseous phase can influence the mechanical behavior of the porous medium, and thus the process of formation and evolution of fractures.

The aim of this work is to develop a finite element model for the phase-field analysis of fracture in three-phase porous media, in which both the flux of the water and the flux of the dry air are taken into account. In the first part of the thesis particular attention is payed to the study of some numerical difficulties that such modeling implies, such as the errors in the evaluation of the mass conservation of the water and the occurrence of numerical locking when a volumetric-deviatoric energy split for the phase-field model is used. An original mass conservative formulation, which takes into account the deformability of the solid skeleton, and a new stabilized mixed finite element formulation for the phase-field model of fracture in saturated porous media have been proposed, and tested with different numerical applications. In the last part of the thesis the finite element discretization of the proposed three-phase model is derived and applied to the numerical simulation of two different desiccation problems, in order to to study the influence of the balance equation of the air in the development of fractures in the porous medium.

Sommario

Lo sviluppo di modelli matematici e numerici per lo studio della frattura nei mezzi porosi è motivato da numerose applicazioni nel mondo reale. In particolare, lo studio della frattura con la tecnica del phase-filed, basata sulla regolarizzazione della formulazione variazionale della teoria di Griffith, sembra essere una delle più promettenti, grazie alla sua abilità di modellare fenomeni complessi, come la formazione e la ramificazione di fratture, a preservare la continuità del campo di spostamenti. La maggior parte dei modelli phase-field presenti in letteratura sono principalmente orientati allo studio della frattura in mezzi porosi saturi. D'altro canto, alcuni fenomeni, come la formazione di fratture in argille durante un processo di essicazione, indicano l'importanza di estendere questi modelli in condizione di parziale saturazione, tenendo in considerazione la possibile influenza del flusso della fase gassosa sul comportamento meccanico dello scheletro solido e, di conseguenza, sul processo di formazione e evoluzione della frattura.

Lo scopo di questa tesi è la formulazione di un modello numerico agli elementi finiti per lo studio, con la tecnica del phase-field, della frattura in mezzi porosi trifase, in cui si considerino sia il flusso d'acqua che il flusso dell'aria all'interno del mezzo. Particolare attenzione è rivolta ad un approfondimento di alcune problematiche numeriche che tale modellazione comporta, come gli errori nella conservazione della massa della fase liquida e il locking numerico dovuto ad un eccesso di rigidezza volumetrica, quando lo split volumetrico-deviatorico dell'energia viene utilizzato nel modello phase-field. In particolare, vengono proposte e testate attraverso varie applicationi numeriche una nuova formulazione conservativa che tenga conto della deformabilità dello scheletro solido, e una nuova stabilizzazione per la formulazione mista del modello phase-field per la frattura in mezzi porosi saturi. Nell'ultima parte la discretizzazione agli elementi finiti del modello trifase proposto viene derivata, e applicata

alla simulazione numerica di due problemi di essicazione, con l'obiettivo di studiare l'influenza dell'equazione di bilancio dell'aria sullo sviluppo di fratture nel mezzo poroso.

Kurzfassung

Die Entwicklung von mathematischen und numerischen Modellen für die Untersuchung des Problems der Fraktur in porösen Medien wird durch mehrere reale Anwendungen motiviert. Insbesondere der Phasenfeldansatz für die Fraktur, der auf der Regularisierung der Variationsformulierung der Griffith'schen Theorie basiert, scheint einer der vielversprechendsten zu sein, da er in der Lage ist, komplizierte Frakturprozesse wie Keimbildung und Verzweigung zu modellieren und die Kontinuität des Verschiebungsfeldes zu erhalten. Die Mehrheit der in der Literatur vorhandenen Phasenfeldmodelle für den Bruch in porösen Medien ist hauptsächlich auf die Untersuchung des Problems des Bruchs in gesättigten porösen Medien ausgerichtet. Wie auch immer, bestimmte Phänomene, wie das Spalten von lehmigen Böden während eines Trocknungsprozesses, deuten darauf hin, wie wichtig die Erweiterung dieser Modelle zu einem teilweise gesättigten Gerüst ist, in dem auch der Fluss der Gasphase das mechanische Verhalten des porösen Mediums und damit den Prozess der Bildung und Entwicklung von Brüchen beeinflussen kann.

Ziel dieser Arbeit ist es, ein Finite-Elemente-Modell für die Phasenfeldanalyse von Brüchen in dreiphasigen porösen Medien zu entwickeln, bei dem sowohl der Fluss des Wassers als auch der Fluss der trockenen Luft berücksichtigt werden. Im ersten Teil der Arbeit wird besonderes Augenmerk auf die Untersuchung von einigen numerischen Schwierigkeiten, die eine solche Modellierung impliziert, wie z. B. die Fehler in der Bewertung der Massenkonservierung des Wassers und das Auftreten von numerischen Sperren, wenn eine volumetrisch-deviatorische Energie-Split für das Phasenfeld-Modell verwendet wird. Eine originale massenkonservative Formulierung, die die Verformbarkeit des festen Skeletts berücksichtigt, und eine neue stabilisierte gemischte Finite-Elemente-Formulierung für das Phasenfeldmodell der Fraktur in gesättigten porösen Medien wurden vorgeschlagen und mit verschiedenen numerischen Anwendungen getestet.

Im letzten Teil der Arbeit wird die Finite-Elemente-Diskretisierung des vorgeschlagenen Dreiphasenmodells abgeleitet und auf die numerische Simulation von zwei verschiedenen Trocknungsproblemen angewendet, um den Einfluss der Gleichgewichtsgleichung der Luft bei der Entwicklung von Frakturen im porösen Medium zu untersuchen.

Contents

Chapter 1

Introduction

1.1 Motivation and scope

The phenomenon of fracture in porous media characterizes a great variety of real world problems, both in the environmental [20, 49] and in the industrial fields. Particular attention has been devoted, in the last years, to the study of the problem of the hydraulic fracture [55, 56, 40], pushed by a growing demand for innovative, and sometimes controversial, methods of extraction of new oil resources. In this application, the fluid act as a fracture driving force, and the porous material is always considered saturated. On the other hand, especially looking at environmental problems, the development of cracks is strictly correlated to the process of desiccation. Therefore in this case the development of a model in which partially saturated conditions are considered becomes necessary. Some example of problems in which the fracture occurs in partially saturated materials are desiccation cracking in soils [49, 58], erosion of marsh borders in lagoons [20], or slope instability [52].

In general are defined as porous media all those materials with an heterogeneous internal structures characterized by the presence of a solid phase, which confers stiffness to the material, and some empty spaces, called pores, which may be filled by one or more fluids [37]. Due to this complicated internal microstructure, turns out to be more convenient to model the behavior of these material at the so-called macroscopic scale. Within this approach, the real structure of the material is substituted by ideally superimposed continua which occupies the entire domain at the same time [21], and the classical balance equation characteristic of the continuum mechanics can be applied without taking into account discontinuity at the interfaces between the real constituents. A comprehensive description of the balance equations that govern the mechanical behavior of the porous media can be found in [37]. What makes the porous media interesting, but at the same time complicated to be modeled, is the

coexistence and mutual influence of the mechanical deformation of the material and the flow of the fluids filling the pores of the material.

Concerning the modeling of fracture, a fundamental contribution to the study of the problem of evolution of preexisting cracks in elastic material is the energetic approach proposed by Griffith [29]. This approach is based on the definition of an energetic quantity related to the surfaces of the crack itself. A variational formulation of the Griffith's energetic criterion which allows the modeling of complex phenomena like fracture nucleation and branching was first proposed by Francfort and Marigo [25]. Anyway, this formulation requires to deal with the discontinuity of the displacement field in correspondence of the crack. The phase-field approach to fracture [12] is based on the regularization of this variational formulation, and solves the problem of the discontinuity of the displacement. Several models able to handle the crack discontinuity [43, 47, 35] have been proposed, but they are rely on an a priori definition of the crack propagation path, which is not the case of the phase-field approach. A review on several phase-field formulation present in the literature can be found in [1].

In order to couple the phase-field approach of fracture with the mechanical model for the porous media, several approaches can be followed. A variation formulation of the coupled problem, limited to the saturated case, has been proposed in [40]. Other possible strategies to realizes the coupling can be found in [41, 34, 11]. In this wok we follow the approach proposed in [17], where the coupling between the two problems is realized including a dependency on the phase-field parameter into the constitutive law for the effective stress $\boldsymbol{\sigma}'$, which is the portion of the stress directly correlated with the elastic deformations of the solid matrix of the porous medium.

Due to the continuity of that displacement field that the phase-field approach imply, the numerical formulation of the problem can be derived using a standard finite element approach [46].

The aim of this work is to develop a model able to capture the process of crack formation in partially saturated porous media, with particular attention on the role played by the air flow in the porous medium. In order to apply this model to the simulation of complex real-world problems, a robust numerical implementation, derived taking into account several numerical issues that this modeling implies, is needed.

1.2 Outline of the thesis

This thesis is organized as follows. In Chapter 2 the governing equations of the model are presented. In the first part the balance equations characterizing the problem of

water and air flow in deforming porous media are derived, while the second part deals with the variational phase-field formulation of fracture in elastic material. Finally the two problem are coupled, using the concept of effective stress.

Chapter 3 deals with the problem of the derivation of a mass conservative scheme for the numerical solution of water flow in a partially saturated porous medium. The first part is a review of the problem, limited to the numerical solution of the Richards equation. In the second part the problem is extended, considering also the influence of the deformation of the solid matrix. Four different solution schemes are presented, and tested in a numerical application.

In Chapter 4 the problem of the numerical locking due to the excess of volumetric stiffness is treated. In the first part we review the results presented in literature, limited to the case of saturated elastic porous media with low permeability. The second part deals with the stability of phase-field model with a volumetric-deviatoric energy split. It is shown how the numerical instabilities occurring in this two distinct problems share the same nature, and can be solved using a stable mixed finite element formulation. A new stabilized mixed formulation of the problem of fracture in dry and saturated porous media is derived, applying a polynomial pressure-projection technique. Several numerical examples are included, in order to show the occurrence of the numerical locking, and the efficiency of the stabilization proposed.

Finally, Chapter 5 deals with the application of the general model derived in Chapter 2. In the first part the Finite Element Method is applied, in order to derive the numerical formulation of the governing equations. Then the numerical simulation of two different problems of desiccation of initially saturated soil is presented, focusing on the influence of the flow of the air phase in the development of fractures.

Chapter 2

Governing equations

2.1 Introduction

The aim of this chapter is to introduce the equations governing the fracture propagation in partially saturated deforming porous media. In Section 2.2 the equilibrium equations and the mass balance equations for the constituents (solid, water and air) and for the whole multiphase material are introduced within the framework of the theory of mixtures [63, 61, 62] restricted by the volume fraction concept [14, 21]. The closure of the problem is obtained adding some necessary constitutive relations for the solid and the fluid phases, and the key concept of effective stress [59, 28, 10]. This results into a system of three differential equations, which can be solved with respect to the displacement $\boldsymbol{u}$, the water pressure p^w and the air pressure p^a. This system of equations form the so-called $\boldsymbol{u} - p^w - p^a$ formulation of the problem of air and water flow in a deforming porous medium [37].

In Section 2.3 the phase-field approach to brittle fracture is reviewed. This approach is based on the regularization [12] of the variational formulation of the Griffith's theory of brittle fracture [25], and the differential equations governing the problems of equilibrium and evolution of the phase-field variable d are derived as Euler's equations of a constrained energy minimization problem. Different formulations for the elastic and the fracture components of the total energy, as well as different techniques for the enforcing of the irreversibility constraint on the phase-field parameter d, are taken into account.

Finally, in Section 2.4, the equations governing the phase-field model of fracture in partially saturated porous media proposed in this thesis are presented. The model is obtained coupling the evolution equation for the phase-field parameter d, presented in Section 2.3, with the $\boldsymbol{u}-p^w-p^a$ formulation presented in Section 2.2. The coupling is obtained assuming a dependency on the phase-field parameter in the constitutive

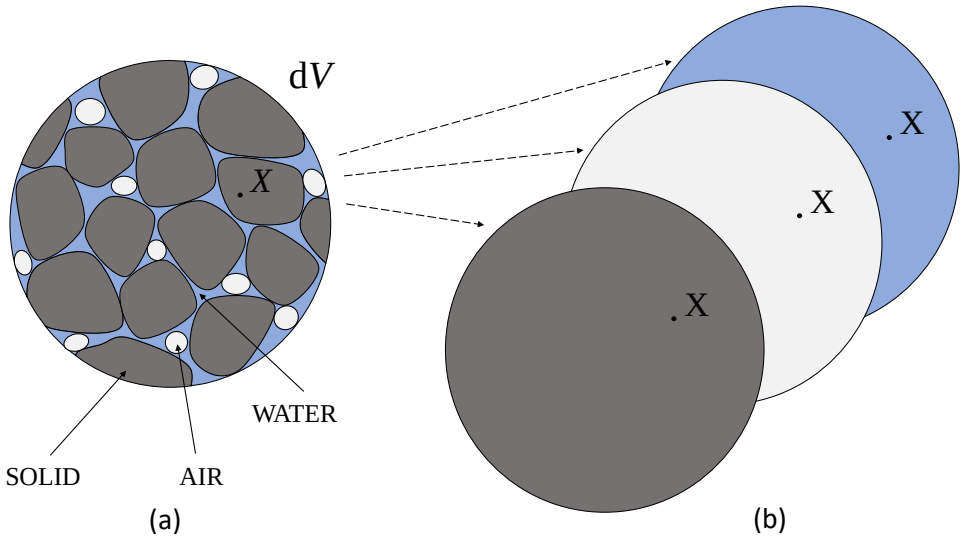

Figure 2.1: Schematic representation of the real internal structure of an infinitesimal potion dV of a partially saturated porous medium (a), and its corresponding representation as a mixture consisting of smeared overlapping continuous phases (b).

equation for the effective stress [17], i.e. the portion of the stress which is responsible of the deformation of the solid skeleton of the material. We call the resulting system of equation the $\boldsymbol{u} - p^w - p^a - d$ formulation of the problem.

2.2 Two-phase flow in deforming porous media

2.2.1 The volume fraction concept

A porous medium is a material which consists in a solid matrix, with close and open pores inside. When the open pores are filled by one ore more fluid phases the material is called multiphase porous medium. In the case of partially saturated geomaterials, which are the object of this thesis, two fluid phases filling the pore space are taken into account: one liquid phase, consisting of water, and one gas phase, consisting of dry air (i.e. in absence of the vapor species, and the consequent mass exchange between vapor and water). Furthermore, the three phases are considered immiscible, and without mutual exchange of mass. A representation of this structure can be seen in Figure 2.1.a.

Due to the complicated pore structure which characterizes geomaterials, such as soils, rocks or concrete, and to the presence of interaction forces at the interfaces of the constituents, the development of a mechanical model at the microscopic level,

i.e. the level of investigation in which the real non-homogeneous structure of the material is considered, becomes rather complicated, as well as unnecessary for practical applications. From an engineering point of view, it is instead more interesting the development of a model at a less detailed scale, in order to provide an average description of the mechanical behavior of the porous medium, but still keeping track of the nature and the mechanical properties of the constituents. This scale of investigation is called macroscopic scale, and at this level the real multiphase system is substituted by a model in which every constituent is assumed to occupy the entire domain, as represented in Figure 2.1.b. Therefore, at each point $\boldsymbol{X} \in \Omega$, with Ω being the domain of the multiphase material, all the phase are assumed to by simultaneously present (overlapping continua), and the characteristic balance equations (mass, momentum, energy) of the continuum mechanics can be used, for each phase, on the entire domain Ω.

In order to derive the macroscopic equations describing the behavior of these substitute continua, several theories have been developed in the field of mechanics of porous media. These theories can be classified into two main approaches [37]. One approach start from the mechanical description of the behavior of the real constituents at the microscopic scale, with the derivation of balance equations in which interaction forces and discontinuities at the interfaces between the constituents are taken into account. The macroscopic equations are then derived using an averaging process based on the integration of the microscopic quantities over a control volume, called representative element volume (REV). These averaging theories, based on the upscaling of microscopic quantities, are known as hybrid mixture theories [30, 31, 32, 65].

A second possible approach is to start the derivation of the balance equations for the single phases directly at the macroscopic level, and is based on the fundamental concept of volume fraction, defined as the ratio of the volume of the constituents to the volume of the control space [37]. The volume fraction allows the smearing operation of the intrinsic mechanical properties of the single phases over the entire domain Ω. Phenomenological approaches, such as the Biot's theory [4, 5], and mixture theories [63, 61, 62] restricted by the volume fraction concept belong to this approach [44, 27, 51, 14]. The latter, in particular will be adopted in this thesis, to the derive the macroscopic mass balance and equilibrium equations governing the mechanical behavior of the multiphase material.

Let us define the volume fraction ϕ^α relative to the phase α as

$$\phi^\alpha = \frac{dV^\alpha}{dV} \tag{2.1}$$

where $\alpha = s$, w, a (solid,water,air) and dV^α is the volume occupied by the phase α within a certain control volume dV, assumed to be tied to the solid matrix. The volume fractions of the single phases are subjected to the closure condition

$$\sum_{n_{phases}} \phi^\alpha = 1 \tag{2.2}$$

For applications of the mixture theory to the modeling of partially saturated porous media, is also useful to introduce two additional volumetric quantities, commonly use in the field of geomechanics: the porosity n, defined as

$$n = 1 - \phi^s \tag{2.3}$$

and the water saturation S^w, defined as

$$S^w = \frac{\phi^w}{\phi^a + \phi^w} \tag{2.4}$$

Based on the closure condition (2.2), and on the definition (2.3) and (2.4), the volume fractions ϕ^s, ϕ^w and ϕ^a can be expressed as function of n and S^w, obtaining

$$\phi^s = 1 - n \tag{2.5}$$

$$\phi^w = nS^w \tag{2.6}$$

$$\phi^a = n\left(1 - S^w\right) \tag{2.7}$$

We define as "intrinsic" a quantity ε^α defined with respect to the phase volume dV^α. Its corresponding quantity ε_α, defined with respect to the control volume dV , is then called "partial", and is related to the intrinsic one by the relation

$$\varepsilon_\alpha = \phi^\alpha \varepsilon^\alpha \tag{2.8}$$

The volume fraction ϕ^α can be seen as a link between some averaged properties of the real constituents, and the corresponding distributed properties which characterizes the substitute continua. The partial quantities ε_α are fundamental for the development of the balance equations at a macroscopic level. In particular we define the partial density ρ_α of the phase α as

$$\rho_\alpha = \phi^\alpha \rho^\alpha \tag{2.9}$$

where ρ^α is the intrinsic density of the constituent, and the partial Cauchy stress tensor of the phase α as

$$\boldsymbol{\sigma}_\alpha = \phi^\alpha \boldsymbol{\sigma}^\alpha \tag{2.10}$$

where $\boldsymbol{\sigma}^\alpha$ is the intrinsic stress of the constituent.

A other important fundamental assumption for the kinematic description of the mixture is that an independent state of motion is assigned to each constituent [22]. This means that the individual constituents follows different motions and, therefore, the time evolution of a certain material point of a phase α, described by a mathematical operator called material time derivative, has to be described with respect to the intrinsic velocity $\boldsymbol{v}^\alpha$ of that particular phase. The material time derivative, with respect to the motion of the phase α, of a certain differentiable function $f(\boldsymbol{x}, t)$ is defined as

$$\frac{\mathrm{d}^\alpha f}{\mathrm{d}t} = \frac{\partial f}{\partial t} + \boldsymbol{v}^\alpha \cdot \nabla f \tag{2.11}$$

When studying the fluid flow in deforming porous media, anyway, it is more useful to focus on the relative motion of the fluids with respect to the solid matrix, rather then on their absolute motion. We define then the relative velocity of the fluid phase α with respect of solid phase as

$$\tilde{\boldsymbol{v}}^\alpha = \boldsymbol{v}^\alpha - \boldsymbol{v} \tag{2.12}$$

where $\boldsymbol{v} = \boldsymbol{v}^s$ is the intrinsic velocity of the solid phase. It is then possible to express the material time derivative with respect to a fluid phase α as a function of the material time derivative with respect to the solid, using the expression

$$\frac{\mathrm{d}^\alpha f}{\mathrm{d}t} = \dot{f} + \tilde{\boldsymbol{v}}^\alpha \cdot \nabla f \tag{2.13}$$

obtained inserting (2.12) in (2.11), and where the symbol

$$\dot{(\,)} = \frac{\mathrm{d}^s (\,)}{\mathrm{d}t} \tag{2.14}$$

indicates the material time derivative with respect to the solid phase.

In the next sections we introduce the macroscopic balance equations that govern the problem, starting from the integral form of balance equation of the single phase formulated at the macroscopic scale, and under the assumption of small strains.

2.2.2 Mass balance equation

Let's consider an arbitrary volume $V \in \Omega$, where $\Omega \in \mathbb{R}^d$ is a domain representing a d-dimensional three-phase porous medium ($d = 2$ in 2D, $d = 3$ in 3D). The total mass of the phase α in V is defined as

$$M_\alpha = \int_V \rho_\alpha \mathrm{d}V \tag{2.15}$$

The law of conservation of mass states that the total mass of each phase must preserve over time, that is

$$\frac{\mathrm{d}^\alpha M_\alpha}{\mathrm{d}t} = \int_V \left(\frac{\mathrm{d}^\alpha \rho_\alpha}{\mathrm{d}t} + \rho_\alpha \nabla \cdot \boldsymbol{v}^\alpha \right) \mathrm{d}V = 0 \tag{2.16}$$

where the Reynolds transport theorem has been applied, in order to move the time derivative into the integral. This conservation law must hold for every arbitrary volume V, so we can derive the following localized form of the mass conservation law for the phase α:

$$\frac{\mathrm{d}^\alpha \rho_\alpha}{\mathrm{d}t} + \rho_\alpha \nabla \cdot \boldsymbol{v}^\alpha = 0 \tag{2.17}$$

Applying the definition of relative velocity (2.12) and the relation for the material time derivative (2.13), we obtain for each phase

$$\dot{\rho}_s + \rho_s \nabla \cdot \boldsymbol{v} = 0 \tag{2.18}$$

$$\dot{\rho}_w + \rho_w \nabla \cdot \boldsymbol{v} + \nabla \cdot (\phi^w \tilde{\boldsymbol{v}}^w) = 0 \tag{2.19}$$

$$\dot{\rho}_a + \rho_a \nabla \cdot \boldsymbol{v} + \nabla \cdot (\phi^a \tilde{\boldsymbol{v}}^a) = 0 \tag{2.20}$$

Now we want to transform the partial densities into intrinsic densities, which have a more clear physical meaning. On order to do that, we apply the relation (2.9), specified for each phase α, obtaining, from equations (2.18), (2.19) and (2.20):

$$\dot{(\phi^s \rho^s)} + \phi^s \rho^s \nabla \cdot \boldsymbol{v} = 0 \tag{2.21}$$

$$\dot{(\phi^w \rho^w)} + \phi^w \rho^w \nabla \cdot \boldsymbol{v} + \nabla \cdot (\phi^w \tilde{\boldsymbol{v}}^w) = 0 \tag{2.22}$$

$$\dot{(\phi^a \rho^a)} + \phi^a \rho^a \nabla \cdot \boldsymbol{v} + \nabla \cdot (\phi^a \tilde{\boldsymbol{v}}^a) = 0 \tag{2.23}$$

If we assume the hypothesis of incompressible solid grains ($\dot{\rho^s} = 0$), and we express the volume fractions as function of the porosity n and the water saturation S^w throw equations (2.5), (2.6) and (2.7), we can rewrite equations (2.21), (2.22) and (2.23) as

$$-\rho^s \dot{n} + \rho^s (1-n) \nabla \cdot \boldsymbol{v} = 0 \tag{2.24}$$

$$S^w \rho^w \dot{n} + n \rho^w \dot{S^w} + S^w n \dot{\rho^w} + S^w \rho^w n \nabla \cdot \boldsymbol{v} + \nabla \cdot \bar{\boldsymbol{v}}^w = 0 \tag{2.25}$$

$$(1-S^w)\rho^a \dot{n} - n\rho^a \dot{S^w} + (1-S^w) n \dot{\rho^a} + (1-S^w)\rho^a n \nabla \cdot \boldsymbol{v} + \nabla \cdot \bar{\boldsymbol{v}}^a = 0 \tag{2.26}$$

where $\bar{\boldsymbol{v}}^w$ and $\bar{\boldsymbol{v}}^a$ are the so-called Darcy velocities of water and air, defined as

$$\bar{\boldsymbol{v}}^w = n S^w \tilde{\boldsymbol{v}}^w \tag{2.27}$$

$$\bar{\boldsymbol{v}}^a = n(1 - S^w)\tilde{\boldsymbol{v}}^a \tag{2.28}$$

Due to the constraint (2.2), only $n_{phase} - 1$ equation are necessary to ensure the conservation of mass. If we sum up the equations (2.24) and (2.25), we obtain the mass conservation equation of solid and water:

$$n\rho^w \dot{S^w} + S^w n\dot{\rho^w} + S^w \rho^w \nabla \cdot \boldsymbol{v} + \nabla \cdot \bar{\boldsymbol{v}}^w = 0 \tag{2.29}$$

With a similar procedure, if we sum up the equations (2.24) and (2.26), we obtain the mass conservation equation of solid and air:

$$-n\rho^a \dot{S^w} + (1 - S^w)n\dot{\rho^a} + (1 - S^w)\rho^a \nabla \cdot \boldsymbol{v} + \nabla \cdot \bar{\boldsymbol{v}}^a = 0 \tag{2.30}$$

In order to be able to express equation (2.29) and equation (2.30) as function of the only variables $\boldsymbol{u}$, p^w and p^a, we need to define a set of constitutive repations for the variable ρ^w, ρ^a, S^w, $\bar{\boldsymbol{v}}^w$ and $\bar{\boldsymbol{v}}^a$. Under the hypotesis of small deformations, the porosity n is normally assumed constant, and con be considered as a material parameter.

2.2.3 Equilibrium equation and effective stress

Let's consider again an arbitrary volume V of our domain. The balance of the internal and external forces applied to the phase α in V is defined as

$$\int_V \rho_\alpha \boldsymbol{g} \mathrm{d}V + \int_V \boldsymbol{h}_\alpha \mathrm{d}V + \int_{\partial V} \boldsymbol{t}_\alpha \mathrm{d}A = \boldsymbol{0} \tag{2.31}$$

where $\boldsymbol{g}$ is the gravity acceleration vector, $\boldsymbol{t}_\alpha$ is the partial traction vector, defined as

$$\boldsymbol{t}_\alpha = \phi^\alpha \boldsymbol{t}^\alpha \tag{2.32}$$

and $\boldsymbol{h}_\alpha$ is the force, per unit of total volume, exerted by the other phases on the phase α, and subjected to the constraint

$$\sum_{n_{phase}} \boldsymbol{h}^\alpha = \boldsymbol{0} \tag{2.33}$$

Now, applying the Cauchy theorem

$$\boldsymbol{t}_\alpha = \boldsymbol{\sigma}_\alpha \cdot \boldsymbol{n} \tag{2.34}$$

we introduce the Cauchy partial stress tensor $\boldsymbol{\sigma}_\alpha$. Using the divergence theorem, it is than possible to rewrite (2.31) as

$$\int_V (\nabla \cdot \boldsymbol{\sigma}_\alpha + \rho_\alpha \boldsymbol{g} + \boldsymbol{h}_\alpha) \mathrm{d}V = \mathbf{0} \tag{2.35}$$

This equation must hold for every arbitrary volume V, so we can derive, for each phase, the following localized forms of the equilibrium law:

$$\nabla \cdot \boldsymbol{\sigma}_s + \rho_s \boldsymbol{g} + \boldsymbol{h}_s = \mathbf{0} \tag{2.36}$$

$$\nabla \cdot \boldsymbol{\sigma}_w + \rho_w \boldsymbol{g} + \boldsymbol{h}_w = \mathbf{0} \tag{2.37}$$

$$\nabla \cdot \boldsymbol{\sigma}_a + \rho_a \boldsymbol{g} + \boldsymbol{h}_a = \mathbf{0} \tag{2.38}$$

Due to the low velocities of the fluids in the pores, the viscous dissipating component of the stress tensor for the fluids is assumed negligible [37]. As consequence of this assumption, the partial stress tensors $\boldsymbol{\sigma}_w$ and $\boldsymbol{\sigma}_a$ have the following isotropic forms

$$\boldsymbol{\sigma}_w = -\phi^w p^w \mathbf{I} = -n S^w p^w \mathbf{I} \tag{2.39}$$

$$\boldsymbol{\sigma}_a = -\phi^a p^a \mathbf{I} = -n \left(1 - S^w\right) p^a \mathbf{I} \tag{2.40}$$

where $\mathbf{I}$ is the identity tensor, and p^w and p^a are the intrinsic relative pressure of water and air respectively. The relative pressure of a fluid is a measure of the difference between the absolute pressure of the fluid itself and the atmospheric air pressure p_0^a, which leads to the following definition for p^w and p^a:

$$p^w = p_{abs}^w - p_0^a \tag{2.41}$$

$$p^a = p_{abs}^a - p_0^a \tag{2.42}$$

where p_{abs}^w and p_{abs}^a are the absolute values of the pore pressure of water and air respectively.

We define now the total Cauchy stress tensor of the mixture as the sum of the partial stress tensor of the components, namely [37]

$$\boldsymbol{\sigma} = \boldsymbol{\sigma}_s + \boldsymbol{\sigma}_w + \boldsymbol{\sigma}_a \tag{2.43}$$

Taking into account the isotropic forms (2.39) and (2.40) of the partial stress tensors$\boldsymbol{\sigma}_w$ and $\boldsymbol{\sigma}_a$, the definition of the total stress (2.43) can be rewritten as

$$\boldsymbol{\sigma} = \boldsymbol{\sigma}_s - n \left[S^w p^w + \left(1 - S^w\right) p^a\right] \mathbf{I} \tag{2.44}$$

Summing up equations (2.36), (2.37) and (2.38), and taking into account the definitions (2.43) and (2.46), we obtain the following equilibrium equation of the whole mixture:

$$\nabla \cdot \boldsymbol{\sigma} + \bar{\rho}\boldsymbol{g} = \mathbf{0} \tag{2.45}$$

where $\bar{\rho}$ is the averaged density of the whole mixture, defined as

$$\bar{\rho} = \rho_s + \rho_w + \rho_a = (1-n)\rho^s + nS^w\rho^w + n(1-S^w)\rho^a \tag{2.46}$$

In order to be able to express the equation (2.45) as a function of the only variables $\boldsymbol{u}$, p^w and p^a, the subdivision (2.44) of the total stress unto the sum of the partial stresses of the single components is not the most appropriate. The partial stress tensor $\boldsymbol{\sigma}_s$ relative to the solid phase, in fact, takes into account not only the contact forces between the grains, which are responsible of the deformation of the solid matrix, but also the pressure exerted on the grains by the fluids filling the pores, which does not imply a deformation of the solid matrix. Therefore $\boldsymbol{\sigma}_s$ is not as suitable variable for the definition of a stress-deformation constitutive law. It is therefore useful to introduce the concept of effective stress $\boldsymbol{\sigma}'$, which is defined as the portion of the total stress $\boldsymbol{\sigma}$ directly responsible of the deformation of the solid matrix (not to be confused with the solid grains, which are assumed incompressible). The concept of effective stress was first introduced by Terzaghi [59], who, in the case of saturated porous media, proposed the expression

$$\boldsymbol{\sigma}' = \boldsymbol{\sigma} + p^w\mathbf{I} \tag{2.47}$$

The extension of the concept of effective stress to partially saturated porous media is not straightforward, and several definition are present in literature. A very well know definition of the effective stress for partially saturated porous media is the one proposed by Bishop [6], and experimentally validated by Skempton [57]. In Bishop's formulation, the effective stress $\boldsymbol{\sigma}'$ is defined as

$$\boldsymbol{\sigma}' = \boldsymbol{\sigma} + [\chi p^w + (1-\chi)p^a]\,\mathbf{I} \tag{2.48}$$

where χ is a coefficient related to the area of contact between the water and the solid, and must be determined experimentally, based on the type of problem into analysis. In this work we adopt an alternative expression, derived by Schrefler *et al.* [53] by using volume averaging, in which the effective stress $\boldsymbol{\sigma}'$ is defined as

$$\boldsymbol{\sigma}' = \boldsymbol{\sigma} + [S^w p^w + (1-S^w)p^a]\,\mathbf{I} \tag{2.49}$$

The expression (2.49) can be seen as a particular case of (2.48), in which the coefficient χ is defined as

$$\chi = S^w \tag{2.50}$$

and does not need any experimental characterization. The quantity

$$p^p = S^w p^w + (1 - S^w) p^a \tag{2.51}$$

is called intrinsic mean pore pressure, and represent the intrinsic averaged value of the pressure exerted on the grains by the fluids filling the pores. If we define the partial mean pore pressure as

$$p_p = (1 - n)\, p^p \tag{2.52}$$

and we insert the definition of the effective stress (2.49) into equation (2.44), we obtain the following relation between the partial stress tensor $\boldsymbol{\sigma}_s$ and the effective stress $\boldsymbol{\sigma}'$:

$$\boldsymbol{\sigma}_s = \boldsymbol{\sigma}' + p_p \mathbf{I} \tag{2.53}$$

It can be seen how the effective stress $\boldsymbol{\sigma}'$ can be obtained subtracting from the partial stress $\boldsymbol{\sigma}_s$ the partial mean pore pressure p_p, i.e. the portion of $\boldsymbol{\sigma}_s$ which does not imply a deformation of the solid matrix. Furthermore, as a difference between two partial quantity, $\boldsymbol{\sigma}'$ is also a partial quantity, resulting to be a good candidate for the definition of a constitutive relation with the deformation of the solid matrix, which, in turn, is a quantity defined with respect of the whole mixture, and not an intrinsic characteristic of the solid phase.

Introducing (2.49) in (2.45), we obtain the following form of the equilibrium equation of the whole mixture

$$\nabla \cdot \left[\boldsymbol{\sigma}' - (S^w p^w + (1 - S^w) p^a)\, \mathbf{I}\right] + \bar{\rho} \boldsymbol{g} = \mathbf{0} \tag{2.54}$$

2.2.4 Constitutive equations

To solve the system of equations (2.29), (2.30) and (2.54) using, as main variables, the displacement of the solid matrix $\boldsymbol{u}$, the water pressure p^w, and the air pressure p^a, we need a set of constitutive equations for the variables S^w, ρ^w, ρ^a, $\bar{\boldsymbol{v}}^w$, $\bar{\boldsymbol{v}}^a$ and $\boldsymbol{\sigma}'$. We underline at this point the important role payed by the choice of the effective stress $\boldsymbol{\sigma}'$. Even if, looking at the balance equations of the mixture, several alternative choices of the effective stress seems to be possible, only a correct derivation of $\boldsymbol{\sigma}'$ from the entropy inequality ensure the thermodynamic consistency of the constitutive equations introduced in this section (see [10]).

Constitutive law for the effective stress

It is well know in the field of geomechanics that soils are material that develops irreversible deformations, well described within the framework of the theory of plasticity. Anyway, the scope of this thesis is the development of a model for brittle fracture in partially saturated porous media, and therefore we need to define a constitutive low for the effective stress $\boldsymbol{\sigma'}$ only inside the elastic domain. We assume, in particular, a linear elastic constitutive equation for the effective stress $\boldsymbol{\sigma'}$, defined as

$$\boldsymbol{\sigma'} = \frac{\partial \Psi_0(\boldsymbol{\varepsilon}(\boldsymbol{u}))}{\partial \boldsymbol{\varepsilon}} = \mathbb{C} : \boldsymbol{\varepsilon} \tag{2.55}$$

where

$$\varepsilon = \nabla^s \boldsymbol{u} \tag{2.56}$$

is the infinitesimal stress tensor, and

$$\Psi_0(\boldsymbol{\varepsilon}(\boldsymbol{u})) = \frac{1}{2}\lambda \mathrm{tr}^2(\boldsymbol{\varepsilon}) + \mu \mathrm{tr}(\boldsymbol{\varepsilon}^2) \tag{2.57}$$

is the density of elastic energy. Finally

$$\mathbb{C} = \frac{\partial^2 \Psi_0}{\partial \boldsymbol{\varepsilon}^2} \tag{2.58}$$

is the forth order elasticity tensor, depending on the Lamè constants λ and μ.

Constitutive laws for the density of the fluids

Concerning the density of the fluids, we assume that, at constant temperature, both water and air behaves as barotropic fluids. That means that exist a function $f(\rho^\alpha, p^\alpha)$ such that

$$f(\rho^\alpha, p^\alpha) = 0 \tag{2.59}$$

For the water we assume the relation [37]

$$p^w = K^w \ln(\rho^{\mathrm{w}} - \rho_0^{\mathrm{w}}) \tag{2.60}$$

where K^w is a material constant called bulk modulus of the water, and is an intrinsic property of the fluid, ρ_0^w is the density of water at the atmospheric pressure, and p^w the water pressure. We can then derive the equations

$$\rho^w = \rho_0^{\mathrm{w}} \exp\left(\frac{p^w}{K^w}\right) \tag{2.61}$$

$$\dot{\rho^w} = \frac{\dot{p^w}}{K^w}\rho^w \tag{2.62}$$

We assume the water intrinsic density as constant ($\rho^w = \rho_0^w$), maintaining the validity of the rate equation (2.62).

For the air we assume the equation of state of ideal gas [37], namely

$$p^a + p_0^a = RT\rho^a \tag{2.63}$$

where R is the specific gas constant of air, T is the absolute temperature, p_0^a is the air atmospheric pressure and p^a the relative pressure. Knowing the air density ρ_0^a at the atmospheric pressure, we obtain

$$\rho^a = \frac{p^a + p_0^a}{K^a} \tag{2.64}$$

$$\dot{\rho}^a = \frac{\dot{p}^a}{K^a} \tag{2.65}$$

where $K^a = \frac{p_0^a}{\rho_0^a}$.

Constitutive law for the saturation

Let us introduce a new variable, called capillary pressure p^c, defined, at equilibrium, as

$$p^c = p^a - p^w \tag{2.66}$$

It is now possible to formulate for water saturation a constitutive relation of the kind $S^w = S^w(p^c)$. In soil mechanics, this constitutive model is called Soil-Water Characteristics Curve (SWCC). The SWCC used in this work is the well-established empirical model proposed by Van Genuchten [64]. In this model the water saturation is defined as

$$\begin{cases} S^w = 1 & \text{for } p^c \leq 0 \\ S^w = (1 - S_r^w)\left[1 + \left(\frac{\alpha_{vg} p^c}{\rho^w g}\right)^{n_{vg}}\right]^{-m_{vg}} + S_r^w & \text{for } p^c > 0 \end{cases} \tag{2.67}$$

where α_{vg} and n_{vg} are parameters of the model depending on the nature of the soil, $m_{vg} = 1 - \frac{1}{n_{vg}}$ and S_r^w is the residual water saturation, which is a lower bound for the water saturation S^w.

Constitutive laws for fluid relative velocities

Based on thermodynamic studies on the dissipative nature of the interaction forces $\boldsymbol{h}^w$ and $\boldsymbol{h}^a$ between the the fluids and the solid phase [33, 32, 54], starting from the

equilibrium equations of the fluid phases (2.37) and (2.38), the Darcy's law for water and air phase can be derived, obtaining respectively

$$\bar{\boldsymbol{v}}^w = nS^w\tilde{\boldsymbol{v}}^w = \frac{k^{rw}k^s\boldsymbol{I}}{\mu^w}(-\nabla p^w + \rho^w\boldsymbol{g}) \tag{2.68}$$

$$\bar{\boldsymbol{v}}^a = n(1-S^w)\tilde{\boldsymbol{v}}^a = \frac{k^{ra}k^s\boldsymbol{I}}{\mu^a}(-\nabla p^w + \rho^w\boldsymbol{g}) \tag{2.69}$$

where $\bar{\boldsymbol{v}}^w$ and $\bar{\boldsymbol{v}}^a$ are called Darcy velocities of water and air,k^s is the intrinsic permeability, $\boldsymbol{I}$ is the identity matrix, k^s is the intrinsic permeability of the solid matrix, μ^w and μ^a are the dynamic viscosity of water and air respectively. Finally the two coefficient k^{rw} and k^{ra} are called relative permeability of water and air respectively, and they take into account how the saturated Darcy velocity of a fluid phase is reduced by the presence of the other fluids. Therefore the relative permeability can be determined as functions of the water saturation. For the Van Genuchten model, the following expressions have been derived [45]

$$k^{rw} = \sqrt{S_e^w}\left\{1 - \left[1 - (S_e^w)^{\frac{1}{m_{vg}}}\right]^{m_{vg}}\right\}^2 \tag{2.70}$$

$$k^{ra} = \left\{(1-S_e^w)\left[1 - (S_e^w)^{\frac{1}{m_{vg}}}\right]^{m_{vg}}\right\}^2 + k^{ra}_{RES} \tag{2.71}$$

where $S_e^w = (S^w - S_r^w)/(1-S_r^w)$ is called effective saturation, m_{vg} is the same parameter used in the Van Genuchten model, and $k^{ra}_{RES} \ll 1$ is an artificial residual air relative permeability, fundamental in the numerical application because it allows to maintain the mass balance equation of solid and air (2.30) always "active", also when $S^w = 1$.

2.2.5 Governing equations

Applying the previous set of constitutive equations to the systems of equations (2.29), 2.30 and 2.45, we obtain the following form of the differential equations governing the problem of water and air flow in a deforming linear elastic porous material:

$$\nabla\cdot(\mathbb{C}:\boldsymbol{\varepsilon}) - \nabla\left[S^w p^w + (1-S^w)p^a\right] + \rho\boldsymbol{g} = \boldsymbol{0} \tag{2.72}$$

$$n\rho^w\dot{S^w} + S^w n\rho^w\frac{\dot{p^w}}{K^w} + S^w\rho^w\nabla\cdot\boldsymbol{v} + \nabla\cdot\left[\rho^w\frac{k^{rw}k^s\boldsymbol{I}}{\mu^w}(-\nabla p^w + \rho^w\boldsymbol{g})\right] = 0 \tag{2.73}$$

$$-n\rho^a\dot{S^w} + (1-S^w)n\frac{\dot{p^a}}{K^a} + (1-S^w)\rho^a\nabla\cdot\boldsymbol{v} + \nabla\cdot\left[\rho^a\frac{k^{ra}k^s\boldsymbol{I}}{\mu^a}(-\nabla p^a + \rho^a\boldsymbol{g})\right] = 0 \tag{2.74}$$

that can now be solved with respect of the displacement $\boldsymbol{u}$, the water pressure p^w, and the air pressure p^a.

Finally, the following initial conditions (ICs) boundary conditions (BCs) have to be specified on the boundary Γ of the domain Ω of the problem:

$$\begin{array}{ll}
\boldsymbol{u}(\boldsymbol{x},t)) = \boldsymbol{u}(\boldsymbol{x},0)) & \text{at } t=0 \\
p^w(\boldsymbol{x},t)) = p^w(\boldsymbol{x},0)) & \text{at } t=0 \\
p^a(\boldsymbol{x},t)) = p^a(\boldsymbol{x},0) & \text{at } t=0 \\
\boldsymbol{u} = \overline{\boldsymbol{u}} & \text{on } \Gamma_{\boldsymbol{u}}^D \\
p^w = \bar{p}^w & \text{on } \Gamma_{p^w}^D \\
p^a = \bar{p}^a & \text{on } \Gamma_{a}^D \\
\boldsymbol{\sigma}\cdot\boldsymbol{n} = \bar{\boldsymbol{t}} & \text{on } \Gamma_{\boldsymbol{u}}^N \\
\tilde{\boldsymbol{v}}^w\cdot\boldsymbol{n} = \bar{q}^w & \text{on } \Gamma_{p^w}^N \\
\tilde{\boldsymbol{v}}^w\cdot\boldsymbol{n} = \bar{q}^a & \text{on } \Gamma_{p^a}^N
\end{array} \tag{2.75}$$

where Γ^D and Γ^N are the Dirichlet and the Neumann boundary respectively.

2.3 Phase-field model of brittle fracture

2.3.1 Griffith's theory of brittle fracture

The first energetic approach of classical fracture mechanics was proposed in 1921 by Griffith [29], who introduced the following criterion of propagation of preexisting fractures:

$$\frac{\mathrm{d}W^{ext}}{\mathrm{d}A} - \frac{\mathrm{d}E^{el}}{\mathrm{d}A} = \frac{\mathrm{d}E^{s}}{\mathrm{d}A} \tag{2.76}$$

where W^{ext} is the work of the external loads, E^{el} is the elastic energy, E^s is the energy associated to the surface A of the growing crack $\Gamma_c(A)$. The evolution of the problem is considered quasi-static, so the kinetic energy is not taken into account in the equation (2.76). If we consider a pure elastic body and conservative external forces, we can define the total potential energy P as

$$P = E^{el} - W^{ext} \tag{2.77}$$

and identify the left-hand side of equation (2.76) as the the release of the potential energy upon an infinitesimal increment of the fracture surface dA, defined as

$$G = -\frac{\mathrm{d}P}{\mathrm{d}A} \tag{2.78}$$

The condition (2.76) can be therefore rewritten as

$$G = G_c \tag{2.79}$$

where the quantity

$$G_c = \frac{\mathrm{d}E^s}{\mathrm{d}A} \tag{2.80}$$

is postulated to be a material property, called fracture toughness, and is a fundamental energetic quantity in fracture mechanics. The Griffith's criterion states that a preexisting fracture in an elastic body can propagate only if the condition (2.79) is fulfilled, that is only if the release of the potential energy upon an infinitesimal increment of the fracture surface dA equals the surface energy related to the increment dA itself. Additionally, the fracture toughness G_c is postulated to be also an upper bound for the release rate G, namely

$$G \leq G_c \tag{2.81}$$

A fundamental characteristic of the Griffith's theory is that the crack path $\hat{\Gamma}_c$is assumed to be known *a priori* [13], which means that the growing crack $\Gamma_c(A)$ has to be considered as a subset of the prescribed crack path $\hat{\Gamma}_c$, namely

$$\Gamma_c(A) \subseteq \hat{\Gamma}_c \tag{2.82}$$

The crack growth along the path $\hat{\Gamma}_c$ has to be considered an irreversible process, so the time evolution of the crack surface A must fulfill the irreversibility condition

$$\dot{A} \geq 0 \tag{2.83}$$

where the time t has to be considered as a pseudo-time parameter governing the loading history of the quasi-static problem. If we subdivide the entire loading process into a finite sequence of time steps $(t_n)_{n=1,N}$, the condition (2.83) can be rewritten as

$$A_{n+1} \geq A_n \tag{2.84}$$

where $n+1$ is the current time step, and n is the previous time step. We can finally summarize the Griffith's theory into the following three conditions [19]

$$A_{n+1} \geq A_n \tag{2.85}$$

$$G \leq G_c \tag{2.86}$$

$$(G - G_c)(A_{n+1} - A_n) = 0 \tag{2.87}$$

where (2.85) is the irreversibility condition, (2.86) is the upper bound on the release rate of the potential energy, and (2.87) is the Griffith's criterion written in the form of complementary condition.

2.3.2 Variational approach to fracture mechanics

A variational formulation of the problem of brittle fracture based on Griffith's theory has been first proposed in 1998 by Francfort and Marigo [25]. The problem of equilibrium and quasi-static evolution of the crack is governed by the minimization of the functional

$$E(\boldsymbol{u},\Gamma_c) = \underbrace{\int\limits_{\Omega/\Gamma_c} \Psi_0(\boldsymbol{\varepsilon}(\boldsymbol{u}))\mathrm{d}V}_{E^{el}(\boldsymbol{u},\Gamma_c)} + \underbrace{G_c\mathscr{H}^{n-1}(\Gamma_c)}_{E^s(\Gamma_c)} - \underbrace{\int\limits_{\Omega/\Gamma_c} \boldsymbol{b}\cdot\boldsymbol{u}\mathrm{d}V - \int\limits_{\Gamma_{\boldsymbol{u}}^N} \bar{\boldsymbol{t}}_{n+1}\cdot\boldsymbol{u}\mathrm{d}S}_{W^{ext}(\boldsymbol{u},\Gamma_c)} \quad (2.88)$$

where

$$\Psi_0(\boldsymbol{\varepsilon}(\boldsymbol{u})) = \frac{1}{2}\lambda \mathrm{tr}^2(\boldsymbol{\varepsilon}) + \mu \mathrm{tr}(\boldsymbol{\varepsilon}^2) \quad (2.89)$$

is the elastic energy density, $\Omega \in \mathbb{R}^d$ is a domain representing an elastic d-dimensional body ($d = 2$ in 2D, $d = 3$ in 3D), $\boldsymbol{b}$ is the body force defined on the domain Ω and $\bar{\boldsymbol{t}}_n$ is the prescribed surface traction acting, at the current time t_{n+1}, on the portion of the boundary with Neumann conditions on the displacement field $\Gamma_{\boldsymbol{u}}^N$. Finally $\mathscr{H}^{n-1}(\Gamma_c)$ is the Hausdorff measure of the crack Γ_c of dimension $d-1$ which, for $d = 3$, corresponds to the area A of the growing crack Γ_c. The functional (2.88) depends on the the displacement $\boldsymbol{u}$ and on the crack itself Γ_c, and the discrete irreveresibility condition (2.84) becomes

$$\Gamma_{c,n+1} \supseteq \Gamma_{c,n} \quad (2.90)$$

The main advantage of the formulation based on the minimization of (2.88), compared to the Griffith's theory, is that the crack Γ_c itself is now a variable of the problem, so it is not constrained to follow a prescribed crack path $\hat{\Gamma}_c$ anymore. Therefore, the minimization of (2.88) allows to model not only the evolution of preexisting cracks on prescribed path, but also crack initiation and branching. However, in order to obtain a numerical solution of the problem based on the minimization of (2.88), a computational model able to perform the numerical tracking of the evolving discontinuity boundary Γ_c is needed. This tacking operation, anyway, requires complex and costly computations, especially when complicated phenomena like interaction between multiple cracks, or branching, need to be modeled [9].

In order to enable an efficient numerical treatment of the variational problem based on (2.88), the following regularized version of the functional $E(\boldsymbol{u},\Gamma)$ has been proposed by Bourdin *et al.* [12]:

$$E_l(\boldsymbol{u},d) = \underbrace{\int_\Omega \Psi(\boldsymbol{\varepsilon}(\boldsymbol{u}),d)\mathrm{d}V}_{E^{el}(\boldsymbol{u},d)} + \underbrace{\frac{G_c}{4C_v}\int_\Omega \left(\frac{w(d)}{l} + l\left|\nabla d\right|^2\right)\mathrm{d}V}_{E^s(d)} - \underbrace{\int_\Omega \boldsymbol{b}\cdot\boldsymbol{u}\mathrm{d}V - \int_{\Gamma_{\boldsymbol{u}}^N} \bar{\boldsymbol{t}}_n\cdot\boldsymbol{u}\mathrm{d}S}_{W^{ext}(\boldsymbol{u})} \tag{2.91}$$

where d is the phase-field parameter, which varies from $d=0$ (undamaged material) to $d=1$ (damaged material), $w(d)$ is the local part of the so-called dissipated energy density function, whose definition depends on the chosen phase-field model, l the so-called characteristic length, and C_v a normalization constant, which ensures the consistency with (2.88). The elastic energy density, now depending also from the phase-field parameter, is defined as

$$\Psi(\boldsymbol{\varepsilon}(\boldsymbol{u}),d) = \left[(1-d^2)+\eta\right]\ \Psi_0(\boldsymbol{\varepsilon}(\boldsymbol{u})) \tag{2.92}$$

where Ψ_0 is the undamaged elastic energy density defined in (2.89), and η is an artificial residual stiffness introduced for numerical stability purposes. The discrete irreversibility condition (2.90) needs now to be formulated as function of the phase-field variable d, and becomes

$$d \geq d_n \tag{2.93}$$

where d and d_{n-1} are the values of the phase-field at the current and at the previous time step respectively [26] (the subscript $n+1$ has been omitted).

The advantage of the regularized formulation based on the minimization of (2.91), when compared to the free-discontinuity formulation based on (2.88), is that in the former no integrals over the discontinuity surfaces are present. The discontinuity surface is, in fact, transformed into a volume in which a regular transition between the undamaged and the broken state of the material is modeled. The width of this transition zone is controlled by the parameter l, and it is mathematically proved that, for $l \to 0$, the solution of the regularized formulation, based on the minimization of the functional (2.91), converges, in the sense of Γ-convergence, to the solution based on the minimization of (2.88).

The solution of the problem of equilibrium and quasi-static evolution of the phase-field variable d consists in finding a couple $(\boldsymbol{u},d)$ that minimizes the functional (2.91), namely

$$\arg\min\left\{E_l(\boldsymbol{u},d):\ \boldsymbol{u}\in T_u,\ d\in T_d\right\} \tag{2.94}$$

where T_u and T_d are the admissible displacement space and the admissible phase-field space, respectively, and are defined as

$$\begin{aligned} T_u &= \left\{ \boldsymbol{u} : \Omega \to \mathbb{R}^2 \mid \boldsymbol{u} \in \boldsymbol{H}^1, \boldsymbol{u} = \overline{\boldsymbol{u}} \text{ on } \Gamma_{\boldsymbol{u}}^D \right\} \\ T_d &= \left\{ d : \Omega \to \mathbb{R} \mid d \in H^1, d \geq d_n \text{ in } \Omega \right\} \end{aligned} \tag{2.95}$$

The minimization of the functional (2.91) is a constrained minimization problem, where the discrete irreversibility condition (2.93) is acting as unilateral constrain. In order to derive the weak form of the constrained minimization problem, we start defining the Lagrangian functional

$$L_l(\boldsymbol{u}, d, \lambda) = E_l(\boldsymbol{u}, d) + \int_\Omega \lambda c\left(d\right) \mathrm{d}V \tag{2.96}$$

where $\lambda = \lambda\left(\boldsymbol{x}\right)$ is a function called Karush-Kuhn-Tucker (KKT) multiplier, enforcing on the domain Ω and on the portion of the boundary with Neumann BCs on the phase-field Γ_d^N the unilateral constrain

$$c\left(d\right) = d_n - d \leq 0 \tag{2.97}$$

which, in turn, coincides with the discrete irreversibility condition (2.93).

Now, the necessary conditions for a pair $(\boldsymbol{u}, d)$ to be a minimum of the constrained minimization problem, known as Karush-Kuhn-Tucker (KKT) conditions, are

$$L_l'(\boldsymbol{u}, d, \lambda)\left(\boldsymbol{v}\right) = \int_\Omega \frac{\partial \Psi(\boldsymbol{\varepsilon}(\boldsymbol{u}), d)}{\partial \boldsymbol{\varepsilon}(\boldsymbol{u})} : \boldsymbol{\varepsilon}(\boldsymbol{v}) \mathrm{d}V = 0 \; \forall \boldsymbol{v} \in T_u \tag{2.98}$$

$$\begin{aligned} L_l'(\boldsymbol{u}, d, \lambda)\left(\alpha\right) = &\int_\Omega \frac{\partial \Psi(\boldsymbol{\varepsilon}(\boldsymbol{u}), d)}{\partial d}\left(\alpha - d\right) \mathrm{d}V + \frac{G_c}{4C_v} \int_\Omega \frac{\left(\alpha - d\right)}{l} \mathrm{d}V \\ &+ \frac{G_c}{4C_v} \int_\Omega 2l \nabla d \cdot \nabla\left(\alpha - d\right) \mathrm{d}V - \int_\Omega \lambda\left(\alpha - d\right) = 0 \; \forall \alpha \in T_d \end{aligned} \tag{2.99}$$

$$\lambda\left(\boldsymbol{x}\right) \geq 0 \tag{2.100}$$

$$\int_\Omega \lambda\left(d_n - d\right) \mathrm{d}V = 0 \tag{2.101}$$

where $L_l'(\boldsymbol{u}, d, \lambda)\left(\boldsymbol{v}\right)$ and $L_l'(\boldsymbol{u}, d, \lambda)\left(\alpha\right)$ are the directional derivatives of the functional $E_l(\boldsymbol{u}, d)$. Equations (2.98) and (2.99) are the stationarity condition of the Lagrangian, with respect of $\boldsymbol{u}$ and d. The inequality (2.100), called dual feasibility

condition, ensure the KKT multiplier to be positive. Finally equation (2.101) is called complementary conditions, and ensure the KKT multipliers to be non-zero only if the constraint (2.97) is active, i.e. if the inequality becomes an equality.

Considering the condition

$$\alpha - d \geq d_n - d$$

which derives directly form the definition of the phase-field admissible space T_d, equations (2.98), (2.99), (2.100) and (2.101) can be condensed into the three equaitons

$$\int_{\Omega} \frac{\partial \Psi(\boldsymbol{\varepsilon}(\boldsymbol{u}), d)}{\partial \boldsymbol{\varepsilon}(\boldsymbol{u})} : \boldsymbol{\varepsilon}(\boldsymbol{v}) \mathrm{d}V = 0 \; \forall \boldsymbol{v} \in T_u \tag{2.102}$$

$$\int_{\Omega} \frac{\partial \Psi(\boldsymbol{\varepsilon}(\boldsymbol{u}), d)}{\partial d} (\alpha - d) \, \mathrm{d}V + \frac{G_c}{4C_v} \int_{\Omega} \frac{w'(d)}{l} (\alpha - d) \, \mathrm{d}V + \frac{G_c}{4C_v} \int_{\Omega} 2l \nabla d \cdot \nabla (\alpha - d) \, \mathrm{d}V \geq 0 \; \forall \alpha \in T_d \tag{2.103}$$

$$\int_{\Omega} \frac{\partial \Psi(\boldsymbol{\varepsilon}(\boldsymbol{u}), d)}{\partial d} (d_n - d) \, \mathrm{d}V + \frac{G_c}{4C_v} \int_{\Omega} \frac{w'(d)}{l} (d_n - d) \, \mathrm{d}V + \frac{G_c}{4C_v} \int_{\Omega} 2l \nabla d \cdot \nabla (d_n - d) \, \mathrm{d}V = 0 \tag{2.104}$$

which represent the weak form of the problem (2.94), and are non longer dependent on the KKT multiplier λ. If we define the stress tensor $\boldsymbol{\sigma}$ as

$$\boldsymbol{\sigma} = \frac{\partial \Psi(\boldsymbol{\varepsilon}(\boldsymbol{u}), d)}{\partial \boldsymbol{\varepsilon}} = \left[(1 - d^2) + \eta \right] \frac{\partial \Psi_0(\boldsymbol{\varepsilon}(\boldsymbol{u}))}{\partial \boldsymbol{\varepsilon}} \tag{2.105}$$

and we apply the Green's Lemma to the equations (2.102), (2.103) and (2.104), it is possible to derive the strong form of the variational problem, which consists of the following Euler's equation, defined on the domain Ω

$$- \nabla \cdot \boldsymbol{\sigma} = \boldsymbol{b} \tag{2.106}$$

$$- 2(1 - d) \Psi_0 + \frac{G_c}{4C_v} (\frac{w'(d)}{l} - 2l\Delta d) \geqslant 0 \tag{2.107}$$

$$\left[-2(1 - d) \Psi_0 + \frac{G_c}{4C_v} (\frac{w'(d)}{l} - 2l\Delta d) \right] (d - d_n) = 0 \tag{2.108}$$

together with the BCs

$$\boldsymbol{\sigma} \cdot \boldsymbol{n} = \bar{\boldsymbol{t}}_n \quad \text{on } \Gamma_{\boldsymbol{u}}^N \tag{2.109}$$

$$\nabla d \cdot \boldsymbol{n} \geqslant 0 \quad \text{on } \Gamma_d^N \tag{2.110}$$

$$(\nabla d \cdot \boldsymbol{n})\,(d - d_n) \quad \text{on } \Gamma_d^N \tag{2.111}$$

where equation (2.106) is the equilibrium equation, equation (2.107) is the evolution equation of the phase-field variable d and equation (2.108) is the complementary condition,

2.3.3 Particularization of the model

The energy split

The phase-field model presented, with the energy $\Psi(\boldsymbol{\varepsilon}(\boldsymbol{u}), d)$ defined as (2.92), is called *isotropic*, because the total undamaged energy $\Psi_0(\boldsymbol{\varepsilon}(\boldsymbol{u}))$ is degraded by the phase-field variable d. This is the simplest constitutive assumption for the energy, but allows the development of fractures also in compression, leading to possible unrealistic interpenetration of the material. Therefore several energy splits have been proposed in the literature [3, 36, 39] in order to maintain undamaged a certain portion of the elastic energy related to the compressive behavior of the material. These models are called *anisotropic*, and are all based on the general energy split definition

$$\Psi(\boldsymbol{\varepsilon}(\boldsymbol{u}), d) = \left[(1 - d^2) + \eta\right] \Psi_0^+(\boldsymbol{\varepsilon}(\boldsymbol{u})) + \Psi_0^-(\boldsymbol{\varepsilon}(\boldsymbol{u})), \quad \Psi_0 = \Psi_0^+ + \Psi_0^- \tag{2.112}$$

The isotropic model can be seen as a particular anisotropic model in which $\Psi_0^- = 0$. Therefore, from now on in this work, the strain energy $\Psi(\boldsymbol{\varepsilon}(\boldsymbol{u}), d)$ is always intended to be defined as in (2.112). Starting from the general definition of the anisotropic split of the elastic energy density (2.112), it is possible to derive from $\Psi(\boldsymbol{\varepsilon}(\boldsymbol{u}), d)$ the expression for the stress tensor $\boldsymbol{\sigma}$ in the anisotropic case, namely

$$\boldsymbol{\sigma} = \frac{\partial \Psi(\boldsymbol{\varepsilon}(\boldsymbol{u}), d)}{\partial \boldsymbol{\varepsilon}} = \left[(1 - d^2) + \eta\right] \frac{\partial \Psi_0^+(\boldsymbol{\varepsilon}(\boldsymbol{u}))}{\partial \boldsymbol{\varepsilon}} + \frac{\partial \Psi_0^-(\boldsymbol{\varepsilon}(\boldsymbol{u}))}{\partial \boldsymbol{\varepsilon}} \tag{2.113}$$

As for the energy split (2.112), it can be notice that the expression (2.105) for the stress tensor $\boldsymbol{\sigma}$ in the isotropic model can be seen as a particular case of the more general definition (2.113). Therefore, from now on in this work, the stress tensor $\boldsymbol{\sigma}$ is always intended to be defined as in (2.113).

As follows we present two models, both based on the definition of volumetric-deviatoric decomposition of the energy. The first one is the model proposed by Lancioni and Royer-Carfagni [36], in which the positive and negative components of the energy $\Psi_0(\boldsymbol{\varepsilon}(\boldsymbol{u}))$ are defined as

$$\begin{cases} \Psi_0^+ = \mu(\boldsymbol{\varepsilon}^{\text{dev}} : \boldsymbol{\varepsilon}^{\text{dev}}) \\ \Psi_0^- = K_n \text{tr}^2(\boldsymbol{\varepsilon}) \end{cases} \tag{2.114}$$

where $K_n = \lambda + \frac{\mu}{n}$ is the bulk modulus, $\boldsymbol{\varepsilon}^{\text{dev}} = \boldsymbol{\varepsilon} - \frac{\text{tr}(\boldsymbol{\varepsilon})}{n}\boldsymbol{I}$ is the deviatoric part of the strain tensor and n is the dimension of the problem. In this split only the deviatoric component of the elastic energy is considered as driving force for the fracture, and the elastic constitutive equation (2.113) remains linear.

The second model that we consider is the one proposed by Amor *et al.* [3], in which the positive and negative components of the energy $\Psi_0(\boldsymbol{\varepsilon}(\boldsymbol{u}))$ are defined as

$$\begin{cases} \Psi_0^+ = K_n \langle \text{tr}(\boldsymbol{\varepsilon}) \rangle_+^2 + \mu(\boldsymbol{\varepsilon}^{\text{dev}} : \boldsymbol{\varepsilon}^{\text{dev}}) \\ \Psi_0^- = K_n \langle \text{tr}(\boldsymbol{\varepsilon}) \rangle_-^2 \end{cases} \tag{2.115}$$

where $\langle \text{tr}(\boldsymbol{\varepsilon}) \rangle_\pm = \frac{1}{2}(\text{tr}(\boldsymbol{\varepsilon}) \pm |\text{tr}(\boldsymbol{\varepsilon})|)$. In addition to the deviatoric part, this model considers as a fracture driving force also the volumetric part of the elastic energy, if its sign is positive (that is, if the hydrostatic component of the stress tensor is positive). Because of the presence of the Macaulay brackets in (2.115), the elastic constitutive equation (2.113) is no longer linear.

Based on (2.112) and (2.113), the strong form of the problem of constrained minimization of the functional (2.91), becomes, for the anisotropic case:

$$-\nabla \cdot \boldsymbol{\sigma} = \boldsymbol{b} \tag{2.116}$$

$$-2(1-d)\,\Psi_0^+ + \frac{G_c}{4C_v}\left(\frac{w'(d)}{l} - 2l\Delta d\right) \geqslant 0 \tag{2.117}$$

$$\left[-2(1-d)\,\Psi_0^+ + \frac{G_c}{4C_v}\left(\frac{w'(d)}{l} - 2l\Delta d\right)\right](d - d_n) = 0 \tag{2.118}$$

together with the BCs (2.109), (2.110) and (2.111).

Choice of the function $w\,(d)$

Now, in order to be able to solve the phase-field evolution equation (2.117), we still need to choose a expression for the local part of the dissipated fracture energy density

function $w(d)$, and define the corresponding normalization coefficient [50]

$$C_v = \int_0^1 \sqrt{w(s)} ds \tag{2.119}$$

Two models are taken into account in this work, both commonly use in the phase-field community. The first one, called AT1 (AT stands for Ambrosio-Tortorelli, see [2]) assumes a linear expression for the local part of the dissipated fracture energy density function $w(d)$, namely

$$w(d) = d \tag{2.120}$$

The corresponding normalization coefficient C_v, derived inserting (2.120) into (2.119), is

$$C_v = \frac{2}{3} \tag{2.121}$$

The advantage of this model is that there is an undamaged elastic phase at the beginning of the loading history (see Figure 2.2.a). But this good property of the model has a cost: during the elastic phase the phase-field equation (2.117) would lead to negative values of d, so the the additional positiveness condition

$$d \geq 0 \tag{2.122}$$

needs to be explicitly formulated.

The system of differential equations (2.116), (2.117) and (2.118) becomes, for the AT1 model

$$-\nabla \cdot \boldsymbol{\sigma} = \boldsymbol{b} \tag{2.123}$$

$$-2(1-d)\,\Psi_0^+ + \frac{3G_c}{8}\left(\frac{1}{l} - 2l\Delta d\right) \geqslant 0 \tag{2.124}$$

$$\left[-2(1-d)\,\Psi_0^+ + \frac{3G_c}{8}\left(\frac{1}{l} - 2l\Delta d\right)\right](d - d_n) = 0 \tag{2.125}$$

together with the irreversibility condition (2.93), the positiveness condition (2.122) and the BCs (2.109), (2.110) and (2.111).

The second model taken into account in this thesis is the so-called AT2 model, in which a quadratic expression for the local part of the dissipated fracture energy density function $w(d)$ is considered, namely

$$w(d) = d^2 \tag{2.126}$$

The corresponding normalization coefficient C_v is

$$C_v = \frac{1}{2} \tag{2.127}$$

Due to the choice of a quadratic expression for $w(d)$, in this case the constraint $0 \leq d \leq 1$ is implicitly satisfied by the model. On the other hand, the evolution of the phase-field parameter stars directly at the beginning of the loading history, so, unlike the AT1 model, for the AT2 model there is no undamaged elastic region (see Figure 2.2.b).

The system of differential equations (2.116), (2.117) and (2.118) becomes, for the AT2 model

$$-\nabla \cdot \boldsymbol{\sigma} = \boldsymbol{b} \tag{2.128}$$

$$-2(1-d)\,\Psi_0^+ + G_c(\frac{d}{l} - l\Delta d) \geqslant 0 \tag{2.129}$$

$$\left[-2(1-d)\,\Psi_0^+ + G_c(\frac{d}{l} - l\Delta d)\right](d - d_n) = 0 \tag{2.130}$$

together with the irreversibility condition (2.93) and the BCs (2.109), (2.110) and (2.111).

Figure 2.2 shows the homogeneous (that is, without considering the gradient term in the phase-field equation) and the localized stress-strain curves for the one-dimensional problem of tension of an elastic bar. We can notice that the solution bifurcates (localization of the fracture) in correspondence of the maximum value of the stress. This value is called critical stress σ_c and, for the one dimensional tension problem, its value can be derived analytically. In particular, for the AT1 model

$$\sigma_c^{AT1} = \sqrt{\frac{3G_cE}{8l}} \tag{2.131}$$

while for the AT2 model

$$\sigma_c^{AT2} = \frac{9}{16}\sqrt{\frac{G_cE}{3l}} \tag{2.132}$$

These two expressions define a relation between the variables G_c, E, l and σ_c that allows, knowing three parameters, to determine the value of the fourth.

It is possible, at this point, to recognize how the internal length l plays a dual role in the phase-field model. If we consider the functional (2.91) just as a variational regularization of Griffith's theory, the internal length is only a regularization parameter, which has to be chosen as small as possible, in order to ensure that the solution tends to the one of the Griffith's theory. The latter, in fact, can be applied only to

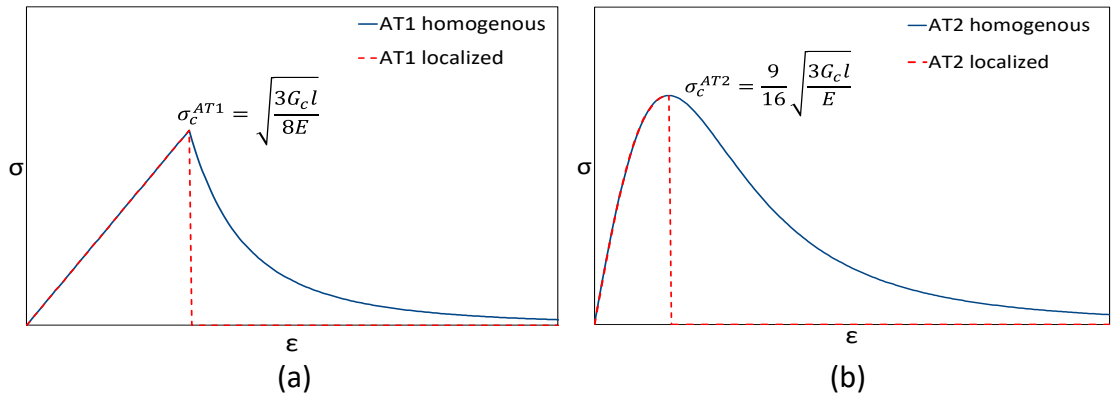

Figure 2.2: Homogeneous and localized stress-strain curves for the 1-D traction problem of an elastic bar: (a) AT1 model, (b) AT2 model.

already existing cracks, requiring no other parameters in addition to G_c and E. If we focus instead on the capability of a phase-field model to estimate the nucleation of new cracks in a initially undamaged material, the internal length l assume a precise physical meaning, allowing, throw equation (2.131) or (2.132), to indirectly insert into the model the tensile strength of the material.

Irreversibility and positiveness conditions

In order to find the pair $(\boldsymbol{u}, d)$, solution of the system of differential equations (2.116), (2.117) and (2.118) constrained by the irreversibility condition (2.93), it is necessary to deal with the inequalities (2.117) and (2.93). We present in this section two possible techniques which allow to transform the evolution equation of the phase-field variable d into an equality, in which the satisfaction of the irreversibility condition is implicitly ensure.

The first technique is the penalty method. This method consists into adding to the functional $E_l(\boldsymbol{u}, d)$ a penalty term $P_\gamma(d)$, defined as [26]

$$P_\gamma(d) = \frac{\gamma}{2} \int_\Omega \langle d - d_n \rangle_-^2 \, \mathrm{d}V \tag{2.133}$$

where γ is the so-called penalty parameter, and the term

$$\langle d - d_{n-1} \rangle_- = \frac{(d - d_{n-1} - |d - d_n|)}{2} \tag{2.134}$$

ensure that the penalty term $P_\gamma(d)$ is active only when the irreversibility condition (2.93) is violated. The penalty parameter γ has to be large enough (ideally $\gamma \to \infty$) to ensure an accurate enforcement of the irreversibility condition (2.93), but not so

large to result into ill-conditioning of the numerical solution [26]. With the addition of the penalty term $P_\gamma(d)$ the functional $E_l(\boldsymbol{u}, d)$ becomes:

$$E_{l,\gamma}(\boldsymbol{u}, d) = \underbrace{\int_\Omega \Psi(\boldsymbol{\varepsilon}(\boldsymbol{u}), d)\mathrm{d}V}_{E^{el}(\boldsymbol{u},d)} + \underbrace{\frac{G_c}{4C_v}\int_\Omega \left(\frac{w(d)}{l} + l\,|\nabla d|^2\right)\mathrm{d}V}_{E^s(d)}$$
$$\underbrace{- \int_\Omega \boldsymbol{b}\cdot\boldsymbol{u}\mathrm{d}V - \int_{\Gamma_{\boldsymbol{u}}^N} \bar{\boldsymbol{t}}_n\cdot\boldsymbol{u}\mathrm{d}S}_{W^{ext}(\boldsymbol{u})} + \underbrace{\frac{\gamma}{2}\int_\Omega \langle d - d_n\rangle_-^2\,\mathrm{d}V}_{P_\gamma(d)} \quad (2.135)$$

The advantage of the penalty method, is that the variational framework is preserved, and the problem of constrained minimization of the functional $E_l(\boldsymbol{u}, d)$, defined in (2.91), has been transformed into a unconstrained minimization problem, based on the functional $E_{l,\gamma}(\boldsymbol{u}, d)$, defined in (2.135). The solution of the problem of equilibrium and quasi-static evolution of the phase-field variable d consists in finding a couple $(\boldsymbol{u}, d)$ that minimizes the functional (2.91), namely

$$\arg\min\left\{E_{l,\gamma}(\boldsymbol{u}, d) :\ \boldsymbol{u}\in T_u,\ d\in T_d\right\} \quad (2.136)$$

where T_u and T_d are the admissible displacement space and the admissible phase-field space, respectively, and are defined as

$$\begin{aligned} T_u &= \left\{\boldsymbol{u} : \Omega\to\mathbb{R}^2 \mid \boldsymbol{u}\in\boldsymbol{H}^1, \boldsymbol{u} = \overline{\boldsymbol{u}} \text{ on } \Gamma_{\boldsymbol{u}}^D\right\} \\ T_d &= \left\{d : \Omega\to\mathbb{R} \mid d\in H^1\right\} \end{aligned} \quad (2.137)$$

We notice that the irreversibility constraint is no longer present in the definition of the admissible phase-field space T_d. A necessary condition for $(\boldsymbol{u}, d)$ to be a minimum of $E_{l,\gamma}(\boldsymbol{u}, d)$, is that $E_{l,\gamma}(\boldsymbol{u}, d)$ has to be stationary in $(\boldsymbol{u}, d)$. We obtain the following weak form of the minimization problem

$$\int_\Omega \frac{\partial\Psi(\boldsymbol{\varepsilon}(\boldsymbol{u}), d)}{\partial\boldsymbol{\varepsilon}(\boldsymbol{u})} : \boldsymbol{\varepsilon}(\boldsymbol{v})\mathrm{d}V = 0\ \forall\boldsymbol{v}\in T_u \quad (2.138)$$

$$\int_\Omega \frac{\partial\Psi(\boldsymbol{\varepsilon}(\boldsymbol{u}), d)}{\partial d}\alpha\mathrm{d}V + \frac{G_c}{4C_v}\int_\Omega \frac{w'(d)}{l}\alpha\mathrm{d}V + \frac{G_c}{4C_v}\int_\Omega 2l\nabla d\cdot\nabla\alpha\mathrm{d}V$$
$$+\gamma\int_\Omega \langle d - d_n\rangle_-\,\alpha\mathrm{d}V = 0\ \forall\alpha\in T_d \quad (2.139)$$

After the application of the Green's Lemma, it is possible to derive from equations (2.138) and (2.139) the strong form of the problem (2.136), which consists in the Euler's equaitions

$$-\nabla \cdot \boldsymbol{\sigma} = \boldsymbol{b} \tag{2.140}$$

$$-2(1-d)\,\Psi_0^+ + \frac{G_c}{4C_v}\left(\frac{w'(d)}{l} - 2l\Delta d\right) + \gamma\,\langle d - d_n\rangle_- = 0 \tag{2.141}$$

together with the BCs

$$\boldsymbol{\sigma}\cdot\boldsymbol{n} = \bar{\boldsymbol{t}}_n \quad \text{on } \Gamma_{\boldsymbol{u}}^N \tag{2.142}$$

$$\nabla d \cdot \boldsymbol{n} = 0 \quad \text{on } \Gamma_d^N \tag{2.143}$$

Equation (2.140) is the equilibrium equation, and equation (2.141) is the evolution equation of the phase-field variable d, which has now become an equality.

The mathematical derivation of a lower bound for γ has been provide in [26], where the following expression of γ, for the AT1 and AT2 model respectively, are proposed:

$$\gamma = \begin{cases} \frac{G_c}{l}\frac{27}{64\mathtt{TOL}_{\mathtt{ir}}^2}, & \text{when } w(d) = d \\ \frac{G_c}{l}\left(\frac{1}{\mathtt{TOL}_{\mathtt{ir}}^2} - 1\right), & \text{when } w(d) = d^2 \end{cases} \tag{2.144}$$

The parameter $0 < TOL_{ir} \ll 1$ indicates the error in the approximation of the Γ-convergence of the fracture energy $E^s(d)$ committed using the phase-field profile obtained by the solution of equation (2.141), instead of the optimal phase-field profile, obtain by the solution of the system of equations (2.117), (2.118) and (2.93). In addition, in [26] the value

$$\mathtt{TOL}_{\mathtt{ir}} = 0.01 \tag{2.145}$$

has been suggested as a practical irreversibility threshold for both the AT1 and the AT2 models.

The second technique consists in the use of the notion of history field, and was proposed in [39]. This technique is based on the idea that the undamaged portion of the energy $\Psi_0^+(\boldsymbol{\varepsilon}(\boldsymbol{u}))$ can be seen as the *driving force* of the the evolution of the phase-field variable d. Therefore, once defined the energy history variable $\mathcal{H}^+$ as

$$\mathcal{H}^+ = \max_{\tau\in[0,t]} \Psi_0^+(\boldsymbol{\varepsilon},\tau) \tag{2.146}$$

the following evolution equation for the phase-field d is proposed in [39]:

$$-2(1-d)\mathcal{H}^+ + \frac{G_c}{4C_v}\left(\frac{w'(d)}{l} - 2l\Delta d\right) = 0 \tag{2.147}$$

where the phase-field d is expected to be always and increasing function, driven by the energy history variable $\mathcal{H}^+$, which, in turn, is an increasing function by definition. This irreversibility technique has two main drawbacks: the first is that, due to the introduction of the history variable in the phase-field equation, the variational framework of the formulation is lost. The second is that the role of the variable $\Psi_0^+(\boldsymbol{\varepsilon}(\boldsymbol{u}))$ as driving force for the evolution of d, and the consequent connection with its irreversibility, are not clearly demonstrated [26]. On the other hand, this method results to be very easy to implement, and, after the numerical discretization, the phase-field equation (2.147) results to be linear with respect to d, which turns to be a computational advantage if a staggered solution approach is used.

Finally, if the AT1 model is used, the additional positiveness condition

$$d \geq 0 \tag{2.148}$$

has to be taken into account. If the penalty method is used to enforce the irrevesibility, the positiveness condition (2.148) can be simply incorporated into the discrete irreversibility condition (2.93) by setting the following initial condition on the phase-field d

$$d\left(x, t=0\right) = d_0\left(x\right) = 0, \quad \forall x \in \Omega \cup \Gamma_d^N \tag{2.149}$$

On the other hand, if the method of the energy history variable is used, the positiveness condition (2.148) has to be explicitly treated using, for example, a penalty method very similar to the one exposed for the irreversibility condition [26].

2.4 Phase-field model of fracture in three-fase porous media

The framework for the modeling of partially saturated porous media, presented in Section 2.2, and the one for the phase-field modeling of brittle fracture, presented in Section 2.3, are now unified. In this coupling process, several approaches can be followed. A variation formulation of the coupled problem, limited to the saturated case, has been proposed [40]. Anyway, due to the non-linearity that the partially saturated model implies, to develop an extension of this variational formulation is a hard task. Other possible strategies to realizes the coupling can be found in [41, 34, 11], where different phase-field formulations for the modeling of hydraulic fracture in saturated porous media are proposed.

In this wok we follow the approach proposed in [17], where the coupling between the two problem is realized including a dependency on the phase-field d into the constitutive law for the effective stress $\boldsymbol{\sigma}'$, which is the portion of the stress directly correlated with the elastic deformations of the solid matrix of the porous medium, and therefore considered as the most natural responsible of the accumulation of the elastic energy necessary for the development of fractures. In particular, the coupling between the two problem is obtained defining the following constitutive law for the effective stress:

$$\boldsymbol{\sigma}'(\boldsymbol{\varepsilon}, d) = \frac{\partial \Psi(\boldsymbol{\varepsilon}(\boldsymbol{u}), d)}{\partial \boldsymbol{\varepsilon}} \tag{2.150}$$

where the elastic energy density $\Psi(\boldsymbol{\varepsilon}(\boldsymbol{u}), d)$ is the one defined into equation (2.112), namely

$$\Psi(\boldsymbol{\varepsilon}, d) = \left[(1-d^2) + \eta\right] \Psi_0^+(\boldsymbol{\varepsilon}(\boldsymbol{u})) + \Psi_0^-(\boldsymbol{\varepsilon}(\boldsymbol{u})) \tag{2.151}$$

We can now derive the differential equations governing the phase-field model of fracture in partially saturated porous media proposed in this work. In particular, the model is based on the equilibrium equation

$$\nabla \cdot \boldsymbol{\sigma}'(\boldsymbol{\varepsilon}, d) - \nabla \left[S^w p^w + (1 - S^w) p^a\right] + \rho \boldsymbol{g} = \boldsymbol{0} \tag{2.152}$$

the mass balance equation for solid and water phases

$$n\rho^w \dot{S^w} + S^w n \rho^w \frac{\dot{p^w}}{K^w} + S^w \rho^w \nabla \cdot \boldsymbol{v} + \nabla \cdot \left[\rho^w \frac{k^{rw} k^s \boldsymbol{I}}{\mu^w} (-\nabla p^w + \rho^w \boldsymbol{g})\right] = 0 \tag{2.153}$$

the mass balance equation for solid and air phases

$$--n\rho^a \dot{S^w} + (1-S^w) n \frac{\dot{p^a}}{K^a} + (1-S^w)\rho^a \nabla \cdot \boldsymbol{v} + \nabla \cdot \left[\rho^a \frac{k^{ra} k^s \boldsymbol{I}}{\mu^a} (-\nabla p^a + \rho^a \boldsymbol{g})\right] = 0 \tag{2.154}$$

and the evolution equation for the phase-field variable d, which takes the form

$$-2(1-d)\,\Psi_0^+ + \frac{G_c}{4C_v}\left(\frac{w'(d)}{l} - 2l\Delta d\right) + \gamma \left\langle d - d_n \right\rangle_- = 0 \tag{2.155}$$

if the irreversibility condition (2.93) is enforced with the penalty method, or the alternative form

$$-2(1-d)\mathcal{H}^+ + \frac{G_c}{4C_v}\left(\frac{w'(d)}{l} - 2l\Delta d\right) = 0 \tag{2.156}$$

if the irreversibility condition (2.93) is enforced using the energy history variable $\mathcal{H}^+$. The ICs and the BCs of the problem are the following:

$$\begin{array}{ll}
\boldsymbol{u}\left(\boldsymbol{x},t\right)) = \boldsymbol{u}\left(\boldsymbol{x},0\right)) & \text{at } t=0 \\
p^w\left(\boldsymbol{x},t\right)) = p^w\left(\boldsymbol{x},0\right)) & \text{at } t=0 \\
p^a\left(\boldsymbol{x},t\right)) = p^a\left(\boldsymbol{x},0\right) & \text{at } t=0 \\
\boldsymbol{u} = \overline{\boldsymbol{u}} & \text{on } \Gamma_{\boldsymbol{u}}^D \\
p^w = \bar{p}^w & \text{on } \Gamma_{p^w}^D \\
p^a = \bar{p}^a & \text{on } \Gamma_{a}^D \\
\boldsymbol{\sigma}\cdot\boldsymbol{n} = \bar{\boldsymbol{t}} & \text{on } \Gamma_{\boldsymbol{u}}^N \\
\tilde{\boldsymbol{v}}^w\cdot\boldsymbol{n} = \bar{q}^w & \text{on } \Gamma_{p^w}^N \\
\tilde{\boldsymbol{v}}^w\cdot\boldsymbol{n} = \bar{q}^a & \text{on } \Gamma_{p^a}^N \\
\nabla d\cdot\boldsymbol{n} = 0 & \text{on } \Gamma_{d}^N
\end{array} \tag{2.157}$$

The system of equations (2.152), (2.153), (2.154) and (2.155) (or alternatively (2.156)), together with the ICs and BCs (2.157), can be solved with respect of the displacement $\boldsymbol{u}$, the water pressure p^w, and the air pressure p^a, and the phase field variable d.

Chapter 3

Mass conservative numerical schemes for FEM analysis of deforming variably saturated porous media

3.1 Introduction

The mass balance equation, whose general strong form is given by equation (2.17), is a parabolic equation, which needs therefore to be integrated in time. In particular, several discretization schemes are avaiable in literature, and it has been found in [18, 24] that the way in which the time discretization scheme is applied plays a fundamental role, leading to a conservative or a non-conservative numerical scheme. This problem is well known in hydrology, where the flow of one or more fluids is usually studied assuming a rigid porous skeleton. Less attention on this problem has been paid in the field of geomechanics, where the flow of the fluids is coupled with the deformation of the solid matrix.

The first part of this chapter reviews this topic, including the derivation of a mass-conservative scheme for the solution of the Richards equation, and the numerical study of an infiltration problem [67]. Then, in the second part of this chapter we study the mass conservation problem taking into account the deformability of the solid skeleton. Several numerical discretization schemes are compared, and we propose an original alternative solution scheme, which is shown to be conservative in a numerical application.

3.2 Conservative scheme for the Richards equation

3.2.1 Governing equation and numerical discretization

The aim of this section is the derivation of a conservative numerical scheme for the resolution of the Richards equation, based on [18, 24].

The Richards equation can be obtained, starting from the general form of the mass balance of water (2.19). If the solid matrix is assumed to be rigid, which means that $\nabla \cdot \boldsymbol{v} = 0$ and $n = n_0$, and the density of the liquid water ρ^w is assumed constant, which implies that $\dot{\rho^w} = 0$, the equation (2.19) can be written as

$$n_0 \rho^w \frac{\partial S^w}{\partial t} + \rho^w \nabla \cdot [\bar{\boldsymbol{v}}^w] = 0 \tag{3.1}$$

where $\bar{\boldsymbol{v}}^w$ is the so-called Darcy's water velocity, defined as

$$\bar{\boldsymbol{v}}^w = n S^w \tilde{\boldsymbol{v}}^w \tag{3.2}$$

where $\tilde{\boldsymbol{v}}^w$ is the relative water velocity, with respect to the solid matrix. Equation (3.1) has to hold for each point of the domain Ω. We introduce now, as constitutive law for the water, the Darcy's Law (2.68), which allows to calculate the Darcy's velocity $\bar{\boldsymbol{v}}^w$ as

$$\bar{\boldsymbol{v}}^w = \frac{k^{rw} k^s \boldsymbol{I}}{\mu^w} (-\nabla p^w + \rho^w \boldsymbol{g}) \tag{3.3}$$

Introducing (3.3) in (3.1) we obtain

$$n_0 \rho^w \frac{\partial S^w}{\partial t} + \rho^w \nabla \cdot \left[\frac{k^{rw} k^s \boldsymbol{I}}{\mu^w} (-\nabla p^w + \rho^w \boldsymbol{g}) \right] = 0 \tag{3.4}$$

This equation depends, not only on the water pressure p^w, but also on the air pressure p^a, throw the Soil Water Characteristic Curve (SWCC), a constitutive equation that defines the water saturation S^w as a function of the type

$$S^w = S^w(p^w, p^a) \tag{3.5}$$

It would be therefore necessary to solve also the balance equation for the air mass, in order to obtain the air pressure p^a. Anyway, assuming a constant relative air pressure $p^a = 0$, the SWCC takes the form

$$S^w = S^w\left(p^w\right) \tag{3.6}$$

and the equation (3.4) can be solved with respect of the only variable p^w.

In order to be (3.4) a well-posed problem, we need to specify some boundary conditions (BCs) on the boundary $\Gamma = \partial\Omega$ of the domain Ω, together with some initial conditions (ICs) at the time $t = 0$. First of all, we have to define on the boundary Γ the portionΓ_p^D, where the BCs are applied on the water pressure (Dirichlet BCs), and the portion Γ_p^N, where BCs are applied on the water flux (Neumann BCs). This decomposition must fulfill the relations:

$$\Gamma = \Gamma_p^D \cup \Gamma_p^N \tag{3.7}$$

$$\Gamma_p^D \cap \Gamma_p^N = \oslash \tag{3.8}$$

The ICs and the BCs are then expressed as

$$\begin{array}{ll} p^w = p_0^w & \text{at } t = 0 \\ p^w = \bar{p}^w & \text{on } \Gamma_p^D \\ \rho^w \bar{\boldsymbol{v}}^w \cdot \boldsymbol{n}_q = \bar{q} & \text{on } \Gamma_p^N \end{array} \tag{3.9}$$

where p_0^w is the initial water pressure, $\bar{p}^w$ is the imposed water pressure on the portion of the boundary Γ_p^N, $\bar{q}$ is the imposed flux on the portion of the boundary Γ_p^N, and $\boldsymbol{n}_q$ is the unit vector perpendicular to the portion of the boundary Γ_p^N.

Now, in order to move, before the discretization, all the derivatives with respect to time and space on the main variable p^w, it is possible to apply the chain rule to the time derivative of the water saturation, namely

$$\frac{\partial S^w}{\partial t} = \frac{\partial S^w}{\partial p^w}\frac{\partial p^w}{\partial t} \tag{3.10}$$

and recast the equation (3.4) in the alternative formulation

$$n_0 \rho^w \frac{\partial S^w}{\partial p^w}\frac{\partial p^w}{\partial t} + \nabla \cdot \left[\rho^w \frac{k^{rw} k^s \boldsymbol{I}}{\mu^w}(-\nabla p^w + \rho^w \boldsymbol{g})\right] = 0 \tag{3.11}$$

We apply now the Backward Euler scheme for the discretization in time. First of all, we define as $n+1$ and n the current and the previous time steps respectively, and we call Δt the dimension of the current time step. In the Backward Euler scheme (known also as Implicit Euler scheme) a certain differential equation is solved at the current time step $n + 1$, replacing the derivatives with respect of time with their discrete counterpart, namely

$$\dot{()} = \frac{()_{\,n+1} - ()_{\,n}}{\Delta t} \tag{3.12}$$

We obtain for equation (3.4)

$$n_0 \rho^w \frac{S_{n+1}^w - S_n^w}{\Delta t} + \nabla \cdot \left[\rho^w \frac{k_{n+1}^{rw} k^s \boldsymbol{I}}{\mu^w}(-\nabla p_{n+1}^w + \rho^w \boldsymbol{g})\right] = 0 \tag{3.13}$$

and for equation (3.11)

$$n\rho^w \left.\frac{\partial S^w}{\partial p^w}\right|_{n+1} \frac{p^w_{n+1} - p^w_n}{\Delta t} + \nabla \cdot \left[\rho^w \frac{k^{rw}_{n+1} k^s \boldsymbol{I}}{\mu^w}(-\nabla p^w_{n+1} + \rho^w \boldsymbol{g})\right] = 0 \tag{3.14}$$

Now, while the two analytical equations (3.4) and (3.11) are two equivalent formulations of the problem, this is not true anymore for the time-discrete equations (3.13) and (3.14). The key point of this loss of equivalence after the time discretization is the application of the chain rule (3.10) to transform (3.4) into (3.11) . The chain rule is, in fact, mathematically correct only when we consider infinitesimal differentials, that means infinitesimal variation of the quantities. In the time discrete equations these variations are not infinitesimal anymore, leading to a loss of the validity of the chain rule, namely

$$\frac{\Delta S^w_{n+1}}{\Delta t} \neq \left.\frac{\partial S^w}{\partial p^w}\right|_{n+1} \frac{\Delta p^w_{n+1}}{\Delta t} \tag{3.15}$$

where

$$\Delta S^w_{n+1} = S^w_{n+1} - S^w_n \tag{3.16}$$

$$\Delta p^w_{n+1} = p^w_{n+1} - p^w_n \tag{3.17}$$

In particular, the bigger is the variation of the derivative $\frac{\partial S^w}{\partial p^w}$ in the interval Δt, the bigger become the error in the evaluation of the discrete quantity $\frac{\Delta S^w}{\Delta t}$. That is exactly the case of the SWCC curves $S^w = S^w(p^w)$, which shows a highly nonlinear behavior. A consequence of (3.15) is that the total water mass in the mixture, which depends on the saturation S^w, is not conserved anymore, when the scheme (3.14) is used.

For the dicretization in space the finite element method (FEM) is used, starting from the weak form of the problem. Defined the following spaces for the test function p^w and for the weighting function w_p

$$\begin{aligned} T_p &= \left\{p^w : \Omega \to \mathbb{R} \mid p^w \in H^1, p^w = \bar{p}^w \text{ on } \Gamma_p^D\right\} \\ W_p &= \left\{w_p : \Omega \to \mathbb{R} \mid w_p \in H^1, w_p = 0 \text{ on } \Gamma_p^D\right\} \end{aligned} \tag{3.18}$$

the solution of the problem (3.13), together with the BCs (3.9), is the function p^w

that solves, for any admissible test function w_p, the following weak formulation

$$W^c_{n+1} = \int_\Omega w_p n_0 \rho^w \left(S^w_{n+1} - S^w_n\right) \mathrm{dV} + \Delta t \int_\Omega \nabla w_p \cdot \left[\frac{k^{rw}_{n+1} k^s \boldsymbol{I}}{\mu^w}(\nabla p^w_{n+1} - \rho^w \boldsymbol{g})\right] \mathrm{dV} + \Delta t \int_{\Gamma^N_p} w_p \bar{q}^w_{n+1} \mathrm{d}\Gamma = 0 \quad (3.19)$$

Similarly, the solution of the problem (3.14), together with the BCS (3.9), is the function p^w that solves, for any admissible test function w_p, the weak formulation

$$W^{nc}_{n+1} = \int_\Omega w_p n_0 \rho^w \left.\frac{\partial S^w}{\partial p^w}\right|_{n+1} \left(p^w_{n+1} - p^w_n\right) \mathrm{dV} + \Delta t \int_\Omega \nabla w_p \cdot \left[\rho^w \frac{k^{rw}_{n+1} k^s \boldsymbol{I}}{\mu^w}(\nabla p^w_{n+1} - \rho^w \boldsymbol{g})\right] \mathrm{dV} + \Delta t \int_{\Gamma^N_p} w_p \bar{q}^w_{n+1} \mathrm{d}\Gamma = 0 \quad (3.20)$$

In the weak formulations (3.19) and (3.20), the apex c stands for conservative, while the apex nc stands for non-conservative.

The corresponding discrete system of equations is obtained applying the Bubnov-Galerkin approach. We subdivide our domain in a mesh of finite elements, and we consider an approximation of the spaces T_p and W_p, based on polynomial shape functions with local support, namely

$$\begin{aligned} \tilde{p}^w &= \boldsymbol{N}_p \hat{\boldsymbol{p}}^w \\ \tilde{w}_p &= \boldsymbol{N}_p \hat{\boldsymbol{w}}_p \end{aligned} \quad (3.21)$$

where $\tilde{()}$ are the approximated trials and weighting functions, $\hat{()}$ are the vectors containing the values of those functions on the mesh nodes, and $\boldsymbol{N}_p$ is the vector of dimension $1 \times nn$ containing the shape function for the water pressure N^i_p, relative to an arbitrary node i of the nn nodes defined on the domain Ω by the finite element mesh. What characterizes the the Bubnov-Galerkin approach is that the same shape functions are used for the trial and the weighting functions.

We can now obtain the discrete counterpart of the weak form (3.19), namely

$$\boldsymbol{R}^c_{n+1} = \boldsymbol{ds}_{n+1} + \boldsymbol{H}_{n+1} \hat{\boldsymbol{p}}^w_{n+1} + \boldsymbol{f}_{p,n+1} = \boldsymbol{0} \quad (3.22)$$

where $\boldsymbol{R}^c_{n+1}$ is the so-called residual for the conservative scheme, at the current time step $n+1$. The matrix $\boldsymbol{H}_{n+1}$ and the vectors $\boldsymbol{s}_{n+1}$ and $\boldsymbol{f}_{p,n+1}$ are defined as

$$\boldsymbol{H}_{n+1} = \Delta t \int_{\Omega} (\nabla \boldsymbol{N}_p)^T \rho^w \frac{k^{rw}_{n+1} k^s \boldsymbol{I}}{\mu^w} \nabla \boldsymbol{N}_p \mathrm{dV} \tag{3.23}$$

$$\boldsymbol{ds}_{n+1} = \int_{\Omega} \boldsymbol{N}_p^T n_0 \rho^w \left(S^w_{n+1} - S^w_n \right) \mathrm{dV} \tag{3.24}$$

$$\boldsymbol{f}_{p,n+1} = -\Delta t \int_{\Omega} (\nabla \boldsymbol{N}_p)^T (\rho^w)^2 \frac{k^{rw}_{n+1} k^s \boldsymbol{I}}{\mu^w} \boldsymbol{g} d\Omega + \Delta t \int_{\Gamma^N_p} \boldsymbol{N}_p^T \bar{q} \mathrm{d}\Gamma \tag{3.25}$$

Similarly, we can write the discrete counterpart of the weak form (3.20) as

$$\boldsymbol{R}^{nc}_{n+1} = \boldsymbol{S}_{n+1} \left(\hat{\boldsymbol{p}}^w_{n+1} - \hat{\boldsymbol{p}}^w_n \right) + \boldsymbol{H}_{n+1} \hat{\boldsymbol{p}}^w_{n+1} + \boldsymbol{f}_{p,n+1} = \boldsymbol{0} \tag{3.26}$$

where $\boldsymbol{R}^{nc}_{n+1}$ is the residual for the non-conservative scheme, at the current time step $n+1$, and the matrix $\boldsymbol{S}_{n+1}$ is define as

$$\boldsymbol{S}_{n+1} = \int_{\Omega} \boldsymbol{N}_p^T n_0 \rho^w \left. \frac{\partial S^w}{\partial p^w} \right|_{n+1} \boldsymbol{N}_p \mathrm{dV} \tag{3.27}$$

Due to the nonlinearity, with respect of p^w, of some integrals in the equations (3.19) and (3.20), the system of equations has to be linearized and solved using an iterative scheme. A general iterative procedure is based on the solution of the system

$$\boldsymbol{T}^k_{n+1} \Delta \hat{\boldsymbol{p}}^{w,k+1}_{n+1} = -\boldsymbol{R}^k_{n+1} \tag{3.28}$$

where $k+1$ and k are the current and the previous iterations whithin the time step $n+1$, and $\boldsymbol{T}^k_{n+1}$ is a "tangent-like" matrix, whose exact definition depens on the chosen iterative scheme. During the computation of each time step, the solution $\hat{\boldsymbol{p}}^{w,k+1}_{n+1}$ is updated after each nonlinear iteration, i.e.

$$\hat{\boldsymbol{p}}^{w,k+1}_{n+1} = \hat{\boldsymbol{p}}^{w,k}_{n+1} + \Delta \hat{\boldsymbol{p}}^{w,k+1}_{n+1} \tag{3.29}$$

The iteration loop is repeated until the residual $\boldsymbol{R}^k_{n+1}$ becomes smaller than a certain tolerance, which means that the equilibrium has been reached.

A well know iterative scheme, characterized by a quadratic rate of convergence in the neighborhood of the solution, is the Newton-Raphson method, in which the matrix $\boldsymbol{T}_{n+1}$ is the Jacobian matrix $\boldsymbol{J}_{n+1}$ of the residual $\boldsymbol{R}$ in $\hat{\boldsymbol{p}}^{w,k}_{n+1}$. Therefore, from the residual vectors $\boldsymbol{R}^c_{n+1}$ and $\boldsymbol{R}^{nc}_{n+1}$, we obtain

$$\boldsymbol{J}^{c,k}_{n+1} = \left. \frac{\partial \boldsymbol{R}^c_{n+1}}{\partial \hat{\boldsymbol{p}}^w_{n+1}} \right|_k = \left. \frac{\partial \boldsymbol{ds}_{n+1}}{\partial \hat{\boldsymbol{p}}^w_{n+1}} \right|_k + \left. \frac{\partial \left(\boldsymbol{H}_{n+1} \hat{\boldsymbol{p}}^w_{n+1} \right)}{\partial \hat{\boldsymbol{p}}^w_{n+1}} \right|_k + \left. \frac{\partial \boldsymbol{f}_{p,n+1}}{\partial \hat{\boldsymbol{p}}^w_{n+1}} \right|_k \tag{3.30}$$

$$\boldsymbol{J}_{n+1}^{nc,k} = \left.\frac{\partial \boldsymbol{R}_{n+1}^{nc}}{\partial \hat{\boldsymbol{p}}^{w}}\right|_{k} = \left.\frac{\partial \left[\boldsymbol{S}_{n+1}\left(\hat{\boldsymbol{p}}_{n+1}^{w} - \hat{\boldsymbol{p}}_{n}^{w}\right)\right]}{\partial \hat{\boldsymbol{p}}_{n+1}^{w}}\right|_{k} + \left.\frac{\partial \left(\boldsymbol{H}_{n+1}\hat{\boldsymbol{p}}_{n+1}^{w}\right)}{\partial \hat{\boldsymbol{p}}_{n+1}^{w}}\right|_{k} + \left.\frac{\partial \boldsymbol{f}_{p,n+1}}{\partial \hat{\boldsymbol{p}}_{n+1}^{w}}\right|_{k} \tag{3.31}$$

Anyway, due to the fact that the quadratic convergence is only local, the convergence rate of the Newton-Raphson method can be significantly worse than quadratic in the first iterations. In addition to that, the matrix $\boldsymbol{J}_{n+1}$ results to be nonsymmetric. For these reasons, together with the elevated cost of the computation of the Jacobian matrix $\boldsymbol{J}_{n+1}$, several author used the Picard's method, in order to linearize the non conservative residual $\boldsymbol{R}_{n+1}^{nc}$ [48], and a modify version of it, in order to linearize the non conservative residual $\boldsymbol{R}_{n+1}^{c}$ [18].

The Picard's method, known also as fixed-point iteration, is a simplified version of the Newton-Raphson method, in which, in the derivation of $\boldsymbol{R}_{n+1}^{c}$ and $\boldsymbol{R}_{n+1}^{nc}$ with respect to $\hat{\boldsymbol{p}}_{n+1}^{w}$, the dependency of $\boldsymbol{S}_{n+1}$, $\boldsymbol{H}_{n+1}$ and $\boldsymbol{f}_{p,n+1}$ on the vector $\hat{\boldsymbol{p}}_{n+1}^{w}$ is not take into account. Therefore, for both the residual vectors $\boldsymbol{R}_{n+1}^{c}$ and $\boldsymbol{R}_{n+1}^{nc}$, the matrix $\boldsymbol{T}_{n+1}$ is defined as

$$\boldsymbol{T}_{n+1}^{PC,k} = \boldsymbol{S}_{n+1}^{k} + \boldsymbol{H}_{n+1}^{k} \tag{3.32}$$

Finally we notice that, when the linearization with respect to $p^{w}$is performed, the term $\frac{\partial S^{w}}{\partial p^{w}}$ appears in the conservative scheme too. But in this case it is present only in the tangent matrix, which is updated every iteration, without affecting the computation of the residual.

3.2.2 Verification of the mass balance

The aim of this chapter is a numerical comparison of several discretization scheme, in order to evaluate their efficiency in terms of mass conservation. It is therefore necessary to find a suitable definition of the error obtained with each numerical scheme in the evolution of the time-discrete Water Mass Balance statement:

$$\Delta M_{stor}^{n+1} + \bar{M}_{in/out}^{n+1} = 0 \tag{3.33}$$

where:

- $\Delta M_{stor}^{n+1} = M_{stor}^{n+1} - M_{stor}^{n}$ is the variation of the mass of water stored in the domain during the time step $n+1$.
- $\bar{M}_{in/out}^{n+1}$ is the average mass of water entering/exiting the domain during the time interval $[t_n, t_{n+1}]$.

The mass of the water stored in the domain M_{stor} is defined as

$$M_{stor} = \sum_{el=1}^{ne} \int_{\Omega_e} n_0 S^w \mathrm{dV} \tag{3.34}$$

where Ω_e is the volume of a finite element, and ne is the number of elements in which the total domain Ω is subdivided. The quantity ΔM_{stor}^{n+1} can be therefore calculated as

$$\Delta M_{stor}^{n+1} = \sum_{el=1}^{ne} \int_{\Omega_e} n_0 (S_{n+1}^w - S_n^w) \mathrm{dV} \tag{3.35}$$

In order to compute the average mass of water entering or exiting the domain during the time step $n+1$, we need to compute the flux of water throw the Dirichlet and the Neumann boundaries. The mass of water $M_{in/out}^{D,n+1}$ passing throw the Dirichlet boundary at the time $n+1$ is defined as

$$M_{in/out}^{D,n+1} = \sum_{el=1}^{neD} \int_{\Gamma_p^N} \rho^w \bar{\boldsymbol{v}}^w \cdot \boldsymbol{n}_p \mathrm{d}\Gamma \tag{3.36}$$

where neD is the number of finite elements having a portion of their boundary belonging to the Dirichlet boundary Γ_p^D, and $\boldsymbol{n}_p$ is the unit vector perpendicular to Γ_p^D. Anyway, it can be shown that, ones the convergence of the time step is reached, the residual vector $\boldsymbol{R}_{n+1}$, as it is defined, has null components on every node, except for the nodes on the Dirichlet boundary Γ_p^D, where its value correspond to the value of the flux on the area of influence of a particular node. Therefore flux of water throw the Dirichlet boundary can be calculated as

$$M_{in/out}^{D,n+1} = \sum_{i=1}^{nn} R_{n+1}^i \tag{3.37}$$

where nn is the total number of nodes in the domain.

Regarding the Neumann boundary conditions, we simply obtain from the flux $\bar{q}$ applied onΓ_q, the expression

$$M_{in/out}^{N,n+1} = \Delta t \int_{\Gamma_p^N} \boldsymbol{N}_p^T \bar{q} \mathrm{d}\Gamma \tag{3.38}$$

Now, we can calculate the average mass of water $\bar{M}_{in/out}^{n+1}$ entering/exiting the domain during the time interval $[t_n, t_{n+1}]$, simply taking the average of the value at the extremes of the interval, obtaining

$$\bar{M}_{in/out}^{n+1} = \frac{\left(M_{in/out}^{D,n} + M_{in/out}^{N,n}\right) + \left(M_{in/out}^{D,n+1} + M_{in/out}^{N,n+1}\right)}{2} \tag{3.39}$$

Finally we define the relative mass error (expressed in percentage %) as

$$e_{rel,mass} = 100 \frac{\Delta M_{stor}^{n+1} - \bar{M}_{in/out}^{n+1}}{\bar{M}_{in/out}^{n+1}} \tag{3.40}$$

In the example a numerical scheme will be consider conservative, if it leads always to relative mass errors

$$e_{rel,mass} \leq 5\% \tag{3.41}$$

3.2.3 Numerical simulation of water infiltration in a dry sandbox

In this section we propose a numerical analysis of the problem of infiltration in a sandbox initially dry. The example is proposed in [67], as re-adaption of an example originally presented in [42], and solved using a conservative numerical formulation for the mass balance equation, which takes into account the flux of the water and the air phases. Anyway, the results obtained in [67] show that the presence of an active air phase does not influence significantly the results. Therefore, this example is used for a double scope: test whether the Richards equation, where passive air pressure is assumed, leads to similar results to the one shown in [67], and also to show the difference between the solutions obtained with the conservative and the non-conservative formulations.

The domain of the problem consists in a square sandbox , with a length of the side $L = 3\,m$, initially dry, subject to an infiltration process driven by a pond of water, $h_p = 0.1\,m$ high and $l_p = 1\,m$ wide, located over the central section of the dry upper boundary. As ICs of the problem, we assume hydrostatic relative water pressure distribution, with with relative water pressure $p^w = 0$ at the depth $z = 3\,m$, namely

$$p^w = (z-3)\rho^w g \quad \text{at } t = 0 \tag{3.42}$$

The same hydrostatic pressure distribution is imposed as Dirichlet boundary condition on the entire boundary, except for the portion of the boundary in contact with the water pond, where a positive water pressure, corresponding to the height of the pond, is applied. We can resume the Dirichlet boundary conditions as

$$\begin{cases} p^w = 0 & \text{at } z = 3,\ x \in [0,3] \\ p^w = (z-3)\rho^w g & \text{at } x = 0,\ z \in [0,3] \\ p^w = (z-3)\rho^w g & \text{at } x = 3,\ z \in [0,3] \\ p^w = -3\rho^w g & \text{at } z = 0,\ x \in [0,1) \cup (2,3] \\ p^w = h_p \rho^w g & \text{at } z = 0,\ x \in [2,3] \end{cases} \tag{3.43}$$

Regarding the SSWC, the Van Genuchten model [64] is used. In this empirical model the function $S^w = S^w(p^w)$ consists in the expression

$$S^w(p^w) = (1 - S^{wr}) \left[1 + \left(\alpha_{vg} \frac{-p^w}{\rho^w g}\right)^{n_{vg}}\right]^{-m_{vg}} + S^{wr} \tag{3.44}$$

where, $m_{vg} = 1 - 1/n_{vg}$, S^{wr} is the residual water saturation, and α_{vg} and n_{vg} are parameters of the model. For the Van Genuchten model, an expression for the relative water permeability function $k^{rw} = k^{rw}(S^w)$ has been proposed by Mualem [45], that is

$$k^{rw}(S^w) = \sqrt{S_e} \left[1 - \left(1 - S_e^{\frac{1}{m_{vg}}}\right)^{m_{vg}}\right]^2 \tag{3.45}$$

where S_e is the effective water saturation, defined as

$$S_e = \frac{S^w - S^{wr}}{1 - S^{wr}} \tag{3.46}$$

The material parameters of the problem are resumed in table 3.1, while figure 3.1 shows the plot of the functions $S^w = S^w(p^w)$ and $k^{rw} = k^{rw}(S^w)$.

$n_0\,[-]$	$k^s\,[m^2]$	$\mu^w\,[Pa \cdot s]$	$\rho^w\,[Kg/m^3]$	$\alpha_{vg}\,[m^{-1}]$	$n_{vg}\,[-]$	$S^{wr}\,[-]$
$0,301$	$5,83\,e^{-12}$	$0,001$	1000	5.47	4.264	0.309

Table 3.1: Material parameters

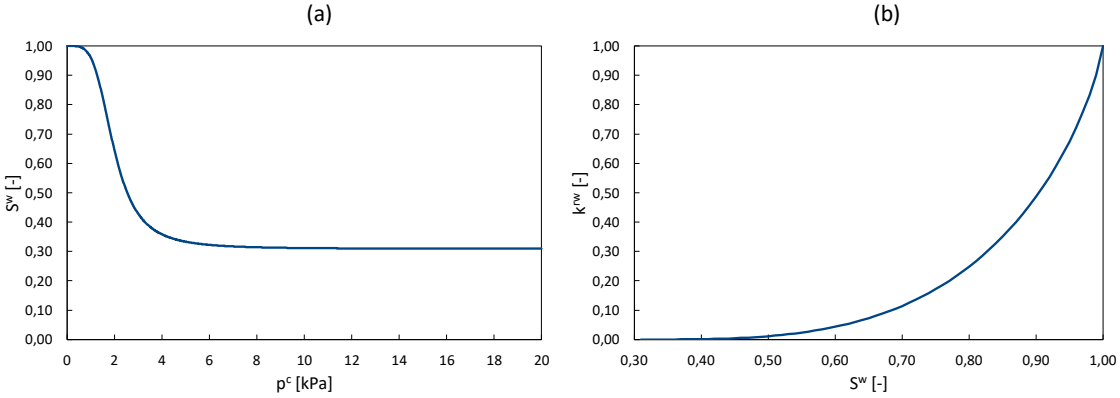

Figure 3.1: (a) Soil Water Characteristic Curve $S^w = S^w(p^w)$. (b) Water relative permeability function $k^{rw} = k^{rw}(S^w)$.

For the discretization in time, an increasing dimension of the time step is used, as in [67], following the relation

$$\Delta t_{n+1} = 1.05 \Delta t_n$$

The dimension of the first time step is $\Delta t_1 = 10^{-7}\, s$, and the total number of time steps is $N_{ts} = 451$. Every time step is solved iteratively, using the Picard's method, with a tolerance $toll = 10^{-3}$ on the relative residual used as exiting criterion. A maximum number of iterations $iter_{max} = 50$ is set, in case the tollerance is not reached.

Regarding the discretization in space, the domain has been divided in a mesh of triangular linear elements, with regular horizontal discretization ($\Delta x = 0,1\, m$) and variable vertical discretization ($\Delta y_{bottom} = 0,1\, m$,$\Delta y_{top} = 0.0125\, m$). The scheme of the problem, and the finite element mesh used for the numerical solution are represented in Figure 3.2, while in Figure 3.3 the initial conditions for the water pressure p^w and the water saturation $S^w$are shown.

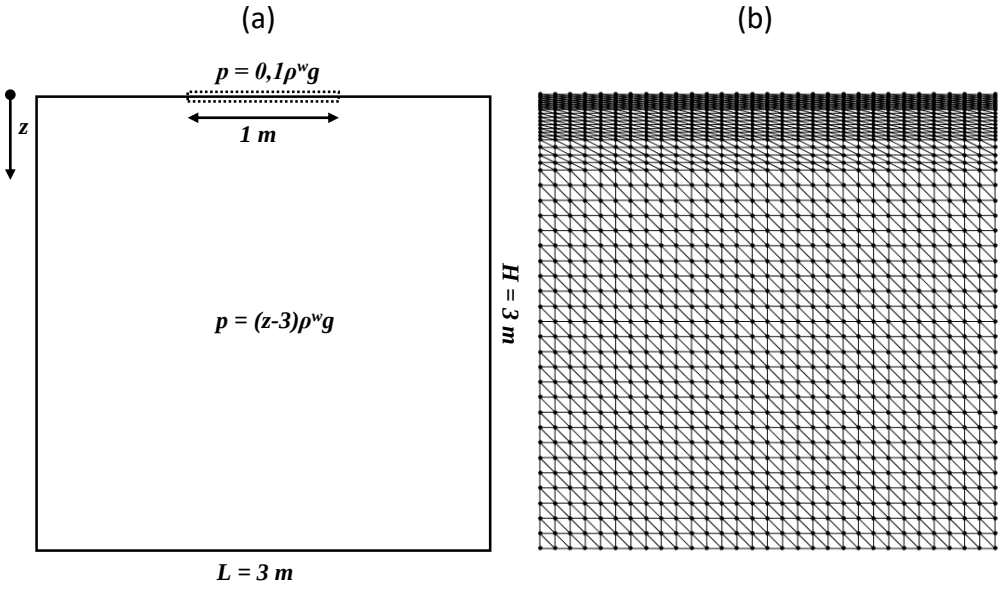

Figure 3.2: (a) Scheme of the problem. (b) Finite element mesh.

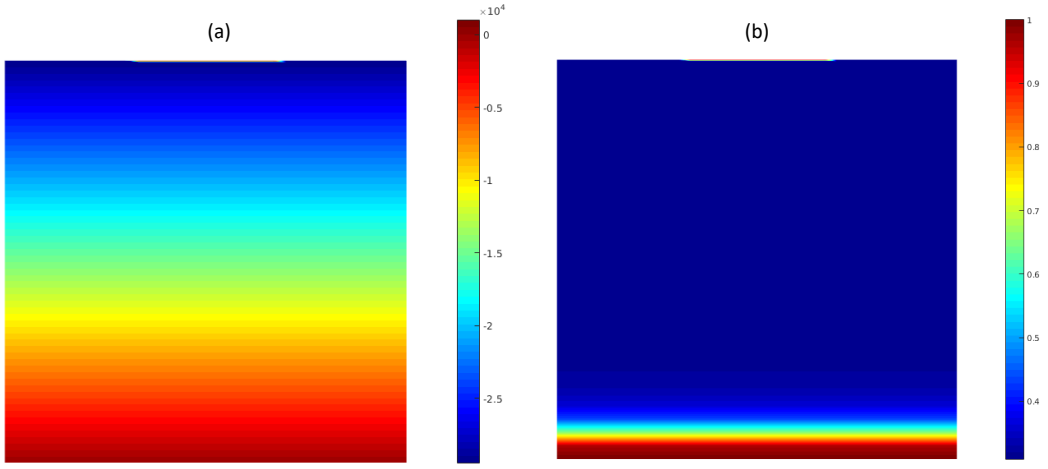

Figure 3.3: Initial conditions for (a) the water pressure $p^w$and (b) the water saturation S^w.

At the end of the simulation, the model based on the conservative formulation reaches the convergence in every time step, while the model based on the non-conservative formulation stops to converge at $T_{step} = 387$. In figure 3.4 the contour of the water saturation for the both model at this time step is shown, and an a small difference in the dimension of the front of infiltrating water can be already noticed.

In order to have a better qualitative evidence of the phenomenon of water loss in the numerical model, the simulation has been carried on till the last time step also for the non-conservative scheme, even if, in the last time steps, the convergence was not reached. In Figure 3.5 the contour of the water saturation for the both model, at the last time step $T_{step} = 451$, is shown, and it can be noticed how the mass of infiltrated water obtained with the non-conservative model is clearly smaller than the one obtained with the conservative model.

Finally, in Figure 3.6, the relative errors in the mass balance at every time step, for the two model, are shown. It can be noticed that, for the conservative model, the error is always less than 5%, while with the non-conservative scheme, pick values greater then 10% are reached already before the loss of convergence of the model.

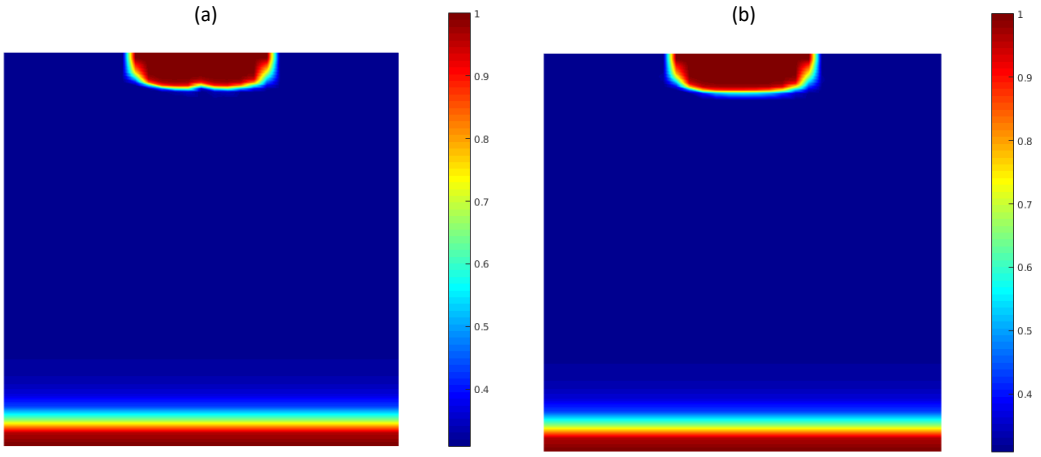

Figure 3.4: Contours of the water saturation S^w at $T_{step} = 387$ (last converged step of the non-conservative scheme): (a) non-conservative scheme, (b) conservative scheme.

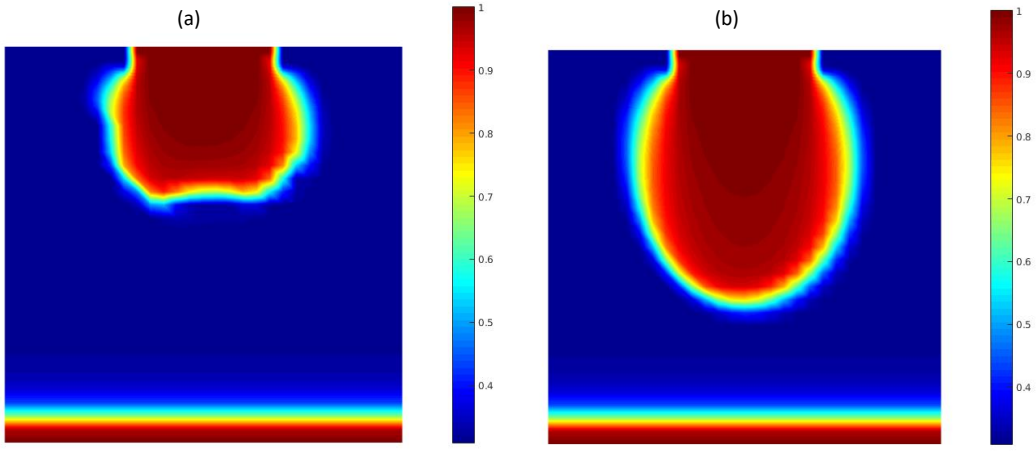

Figure 3.5: Contours of the water saturation S^w at $T_{step} = 451$ (last step of the simulation): (a) non-conservative scheme, (b) conservative scheme.

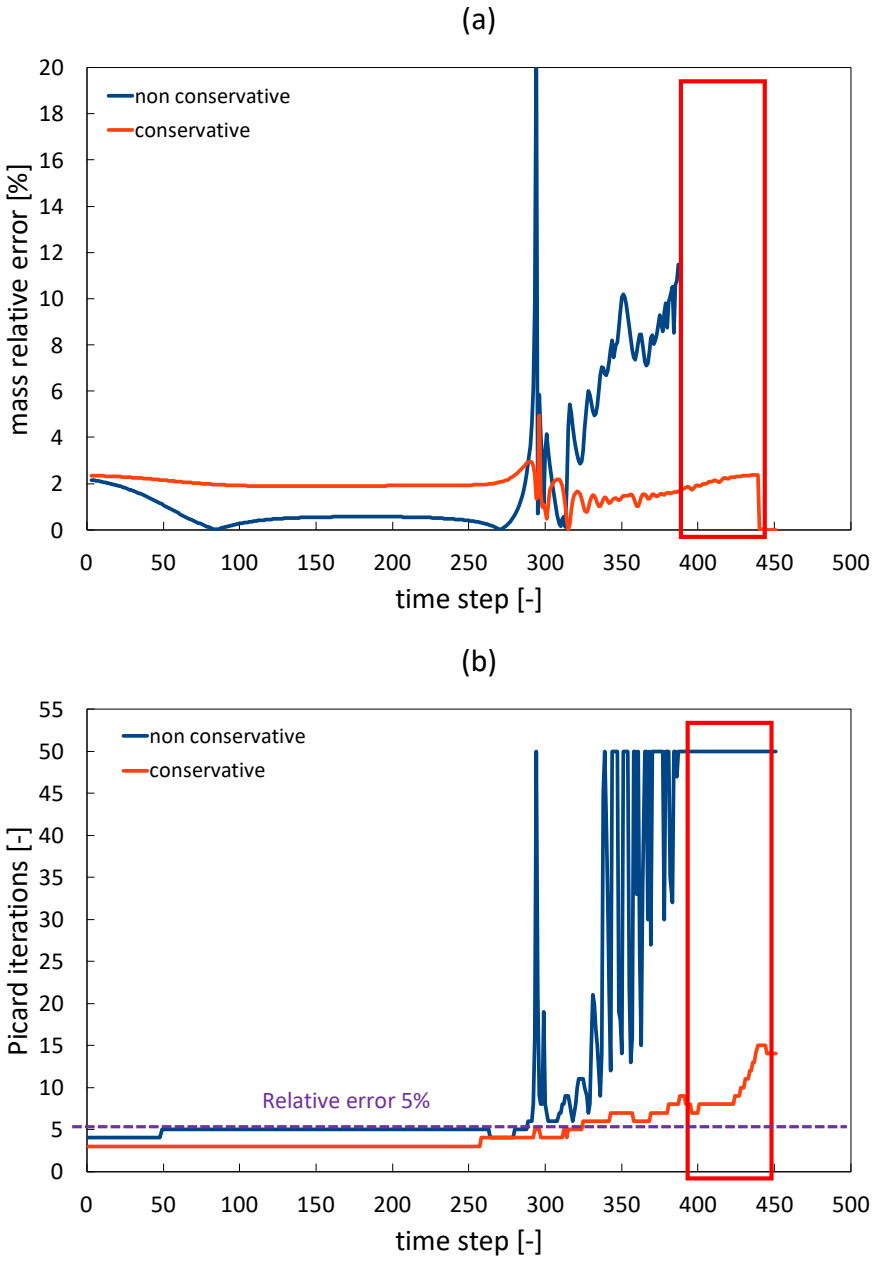

Figure 3.6: (a) relative mass errors and (b) number of nonlinear iterations at each time steps, for the two schemes. The time steps in wich the non-conservative scheme did not reached the convergence are marked in red.

3.3 Extension including the deformability of the solid matrix

3.3.1 Governing equations and numerical discretization

We extend now the model considered in the previous section, including the deformability of the solid matrix. The model is now characterized by two equations, the equilibrium equation (2.72) and the mass conservation equation (2.73), derived in Section 2.2, and simplified by assuming the passive air condition $p^a = 0$, a constant liquid water density ρ^w and a constant porosity $n = n_0$. Due to the fact that the relative (to the atmospheric pressure $p^{atm} = 101325\,Pa$) air pressure p^a is assumed constant, the mass balance equation of solid and air (2.30) is not needed. The equilibrium equation of the mixture (2.72) becomes

$$\nabla \cdot \boldsymbol{\sigma}' - \nabla \left(S^w p^w\right) + \rho \boldsymbol{g} = \mathbf{0} \tag{3.47}$$

where $\boldsymbol{\sigma}'$ is the effective stress tensor, $\rho = (1 - n_0)\rho^s + n_0 S^w \rho^w$ is the density of the mixture, $\boldsymbol{g}$ is the vector of gravity acceleration. We suppose a linear elastic behavior of the solid matrix, expressed by the constitutive equation

$$\boldsymbol{\sigma}' = \mathbb{C} : \boldsymbol{\varepsilon} \tag{3.48}$$

where $\boldsymbol{\varepsilon} = \nabla^s \boldsymbol{u}$ is the strain tensor, defined as the symmetric part of the displacement gradient, and $\mathbb{C}$ is the fourth order elasticity tensor. Equation (3.47) can be rewritten as

$$\nabla \cdot (\mathbb{C} : \boldsymbol{\varepsilon}) - \nabla \left(S^w p^w\right) + \rho \boldsymbol{g} = \mathbf{0} \tag{3.49}$$

The equilibrium equation (3.49) is accompanied by a set of BCs on the boundary Γ of the domain Ω. First of all, we define on the boundary Γ the portion$\Gamma_{\boldsymbol{u}}^D$, where Dirichlet BCs are applied, and the portion $\Gamma_{\boldsymbol{u}}^N$, where Neumann BCs are. This decomposition must fulfill the relation:

$$\Gamma = \Gamma_{\boldsymbol{u}}^D \cup \Gamma_{\boldsymbol{u}}^N \tag{3.50}$$

$$\Gamma_{\boldsymbol{u}}^D \cap \Gamma_{\boldsymbol{u}}^N = \oslash \tag{3.51}$$

The BCs associated to the equilibrium equation (3.49) are

$$\begin{aligned} \boldsymbol{u} &= \bar{\boldsymbol{u}} \quad && \text{on } \Gamma_{\boldsymbol{u}}^D \\ \boldsymbol{\sigma} \cdot \boldsymbol{n}_t &= \bar{\boldsymbol{t}} && \text{on } \Gamma_{\boldsymbol{u}}^N \end{aligned} \tag{3.52}$$

where $\bar{\boldsymbol{u}}$ is the prescribed displacement on the portion of the boundary $\Gamma_{\boldsymbol{u}}^D$, $\bar{\boldsymbol{t}}$ is the prescribed traction on the portion of the boundary $\Gamma_{\boldsymbol{u}}^N$, and $\boldsymbol{n}_t$ is the unit vector perpendicular to the portion of the boundary $\Gamma_{\boldsymbol{u}}^N$.

The mass balance equation of the solid and the liquid water (2.73), together with the assumption of the passive air condition $p^a = 0$ and a constant liquid water density ρ^w, becomes

$$n_0 \rho^w \dot{S^w} + S^w \rho^w \nabla \cdot \boldsymbol{v} + \nabla \cdot \left[\rho^w \frac{k^{rw} k^s \boldsymbol{I}}{\mu^w} (-\nabla p^w + \rho^w \boldsymbol{g}) \right] = 0 \tag{3.53}$$

The mass balance equation (3.53) is accompanied by the ICs and BCs (3.9), introduced in the previous section, with the addition of the initial condition on the displacements

$$\boldsymbol{u} = \boldsymbol{u}_0 \quad \text{at } t = 0 \tag{3.54}$$

From a closer look at the mass balance equation (3.53), it can be easily seen that, when $\nabla \cdot \boldsymbol{v} \to 0$, the conservative form of the Richards equations (3.4) is resumed. In the majority of the applications in geomechanics, anyway, equation (3.53) is rewritten in the form

$$n_0 \rho^w \frac{\partial S^w}{\partial p^w} \dot{p^w} + S^w \rho^w \nabla \cdot \boldsymbol{v} + \nabla \cdot \left[\rho^w \frac{k^{rw} k^s \boldsymbol{I}}{\mu^w} (-\nabla p^w + \rho^w \boldsymbol{g}) \right] = 0 \tag{3.55}$$

before the numerical discretization. Also in this case, it can be easily seen that, when $\nabla \cdot \boldsymbol{v} \to 0$, the non-conservative form of the Richards equation (3.11) is resumed. It is already clear that, also when the solid matrix is not rigid, the formulation (3.53) is preferable.

Looking at the definition of water mass in the mixture

$$M_w = \int_V n S^w \rho^w \mathrm{d}V, \tag{3.56}$$

we notice that, also the variation of the porosity n influences the evaluation of the water mass, and hence can influence the mass conservative properties of the discretized mass balence equation. The porosity n is, in fact, directly related to the volumetric deformation of the solid matrix by the expression

$$n = \frac{n_0 - 1}{1 + \boldsymbol{\varepsilon}_v} + 1, \tag{3.57}$$

where $\boldsymbol{\varepsilon}_v = \nabla \cdot \boldsymbol{u}$ is the volumetric strain, and we would expect that taking into account this dependency into equation (3.53) could imply a better performance in

terms of mass conservation. In this case equation (3.53) becomes

$$n\rho^w \dot{S^w} + S^w \rho^w \nabla \cdot \boldsymbol{v} + \nabla \cdot \left[\rho^w \frac{k^{rw} k^s \boldsymbol{I}}{\mu^w} (-\nabla p^w + \rho^w \boldsymbol{g}) \right] = 0 \tag{3.58}$$

A numerical scheme for the equations (3.53), (3.55) or (3.58) can be derived, following a procedure similar to the one developed in Section 3.2, obtaining a system of equations coupled with the discrete counterpart of the equilibrium equation (3.47).

First of all we apply the Backward Euler scheme for the discretization in time of the different versions of the mass balance equation, obtaining for equation (3.55)

$$n_0 \rho^w \left. \frac{\partial S^w}{\partial p^w} \right|_{n+1} \frac{p^w_{n+1} - p^w_n}{\Delta t} + S^w_{n+1} \rho^w \nabla \cdot \frac{\boldsymbol{u}_{n+1} - \boldsymbol{u}_n}{\Delta t} + \nabla \cdot \left[\rho^w \frac{k^{rw}_{n+1} k^s \boldsymbol{I}}{\mu^w} (-\nabla p^w_{n+1} + \rho^w \boldsymbol{g}) \right] = 0 \tag{3.59}$$

for equation (3.53)

$$n_0 \rho^w \frac{S^w_{n+1} - S^w_n}{\Delta t} + S^w_{n+1} \rho^w \nabla \cdot \frac{\boldsymbol{u}_{n+1} - \boldsymbol{u}_n}{\Delta t} + \nabla \cdot \left[\rho^w \frac{k^{rw}_{n+1} k^s \boldsymbol{I}}{\mu^w} (-\nabla p^w_{n+1} + \rho^w \boldsymbol{g}) \right] = 0 \tag{3.60}$$

and for equation (3.58)

$$n_{n+1} \rho^w \frac{S^w_{n+1} - S^w_n}{\Delta t} + S^w_{n+1} \rho^w \nabla \cdot \frac{\boldsymbol{u}_{n+1} - \boldsymbol{u}_n}{\Delta t} + \nabla \cdot \left[\rho^w \frac{k^{rw}_{n+1} k^s \boldsymbol{I}}{\mu^w} (-\nabla p^w_{n+1} + \rho^w \boldsymbol{g}) \right] = 0 \tag{3.61}$$

For the discretization in space the finite element method (FEM) is used, starting from the weak formulation of the problem. First, we define the following spaces for the test functions $\boldsymbol{u}$ and p^w and of the weighting functions $\boldsymbol{w}_u$ and w_p

$$\begin{aligned} T_u &= \left\{ \boldsymbol{u} : \Omega \to \mathbb{R}^3 \mid \boldsymbol{u} \in H^1, \boldsymbol{u} = \bar{\boldsymbol{u}} \text{ on } \Gamma^D_{\boldsymbol{u}} \right\} \\ T_p &= \left\{ p^w : \Omega \to \mathbb{R} \mid p^w \in H^1, p^w = \bar{p}^w \text{ on } \Gamma^D_p \right\} \\ W_u &= \left\{ \boldsymbol{w}_u : \Omega \to \mathbb{R}^3 \mid \boldsymbol{w}_u \in H^1, \boldsymbol{w}_u = \boldsymbol{0} \text{ on } \Gamma^D_{\boldsymbol{u}} \right\} \\ W_p &= \left\{ w_p : \Omega \to \mathbb{R} \mid w_p \in H^1, w_p = 0 \text{ on } \Gamma^D_p \right\} \end{aligned} \tag{3.62}$$

The weak formulation of the equilibrium equation (3.53), together with the BCs (3.52), results to be

$$W^u_{n+1} = \int_\Omega (\nabla^s \boldsymbol{w}_u : \mathbb{C} : \boldsymbol{\varepsilon}_{n+1} - \nabla \cdot \boldsymbol{w}_u S^w p^w_{n+1} - \boldsymbol{w}_u \cdot \rho_{n+1} \boldsymbol{g}) \mathrm{dV} - \int_{\Gamma^N_{\boldsymbol{u}}} \boldsymbol{w}_u \cdot \bar{\boldsymbol{t}} \mathrm{d}\Gamma = 0 \tag{3.63}$$

while, the weak formulation of the mass conservation equation (3.59), together with the BCs (3.9), results to be

$$W^{p1}_{n+1} = \int_\Omega w_p n_0 \rho^w \left.\frac{\partial S^w}{\partial p^w}\right|_{n+1} \left(p^w_{n+1} - p^w_n\right) \mathrm{dV} + \int_\Omega w_p S^w_{n+1} \rho^w \nabla \cdot (\boldsymbol{u}_{n+1} - \boldsymbol{u}_n)\, \mathrm{dV}$$
$$+ \Delta t \int_\Omega \nabla w_p \cdot \left[\rho^w \frac{k^{rw}_{n+1} k^s \boldsymbol{I}}{\mu^w} (\nabla p^w_{n+1} - \rho^w \boldsymbol{g})\right] \mathrm{dV} + \Delta t \int_{\Gamma^N_p} w_p \bar{q}^w \mathrm{d}\Gamma = 0 \quad (3.64)$$

Similarly, the solution of the problem (3.60), together with the BCs (3.9), results to be

$$W^{p2}_{n+1} = \int_\Omega w_p n_0 \rho^w \left(S^w_{n+1} - S^w_n\right) \mathrm{dV} + \int_\Omega w_p S^w_{n+1} \rho^w \nabla \cdot (\boldsymbol{u}_{n+1} - \boldsymbol{u}_n)\, \mathrm{dV}$$
$$+ \Delta t \int_\Omega \nabla w_p \cdot \left[\rho^w \frac{k^{rw}_{n+1} k^s \boldsymbol{I}}{\mu^w} (\nabla p^w_{n+1} - \rho^w \boldsymbol{g})\right] \mathrm{dV} + \Delta t \int_{\Gamma^N_p} w_p \bar{q}^w \mathrm{d}\Gamma = 0 \quad (3.65)$$

and the solution of the problem (3.61), together with the BCs (3.9), results to be

$$W^{p3}_{n+1} = \int_\Omega w_p n_{n+1} \rho^w \left(S^w_{n+1} - S^w_n\right) \mathrm{dV} + \int_\Omega w_p S^w_{n+1} \rho^w \nabla \cdot (\boldsymbol{u}_{n+1} - \boldsymbol{u}_n)\, \mathrm{dV}$$
$$+ \Delta t \int_\Omega \nabla w_p \cdot \left[\rho^w \frac{k^{rw}_{n+1} k^s \boldsymbol{I}}{\mu^w} (\nabla p^w_{n+1} - \rho^w \boldsymbol{g})\right] \mathrm{dV} + \Delta t \int_{\Gamma^N_p} w_p \bar{q}^w \mathrm{d}\Gamma = 0 \quad (3.66)$$

Again, we apply now the Bobnov-Galerkin method, in order to obtain the discrete counterpart of the previous weak formulations. An approximation of the trial functions T_u, T_p and of the weighting functions W_u, W_p is defined, based on polynomial shape functions with local support, obtaining

$$\begin{aligned} \tilde{\boldsymbol{u}} &= \boldsymbol{N}_u \hat{\boldsymbol{u}} \\ \tilde{p}^w &= \boldsymbol{N}_p \hat{\boldsymbol{p}}^w \\ \tilde{\boldsymbol{w}}_u &= \boldsymbol{N}_u \hat{\boldsymbol{w}}_u \\ \tilde{w}_p &= \boldsymbol{N}_p \hat{\boldsymbol{w}}_p \end{aligned} \quad (3.67)$$

where $\tilde{()}$ are the approximated trials and weighting functions, $\hat{()}$ are the vectors containing the values of those functions on the mesh nodes. In particular, due to the vectorial nature of the displacement field, $\hat{\boldsymbol{u}}$, $\hat{\boldsymbol{w}}_u$ and $\boldsymbol{N}_u$ are defined as

$$\begin{aligned} \hat{\boldsymbol{u}} &= \{\boldsymbol{u}^1, \boldsymbol{u}^2, ..., \boldsymbol{u}^{nn}\}^T \\ \hat{\boldsymbol{w}}_u &= \{\boldsymbol{w}_u^1, \boldsymbol{w}_u^2, ..., \boldsymbol{w}_u^{nn}\}^T \\ \boldsymbol{N}_u &= \{\boldsymbol{N}_u^1, \boldsymbol{N}_u^2, ..., \boldsymbol{N}_u^{nn}\}^T \end{aligned} \tag{3.68}$$

where, for a problem in two dimensions,

$$\begin{aligned} \boldsymbol{u}^i &= \left\{u_x^i, u_y^i\right\} \\ \boldsymbol{w}_u^i &= \left\{w_{u,x}, w_{u,y}^i\right\} \\ \boldsymbol{N}_u^i &= I_2 N_u^i \end{aligned} \tag{3.69}$$

where I_2 is the identity matrix of dimension two, and N_u^i is the shape function for the displacement, relative to an arbitrary node i of the nn nodes defined on the domain. In addition, it is useful to represent the elastic constitutive law (3.48) using the Voigt notation, namely

$$[\![\boldsymbol{\sigma}']\!] = \boldsymbol{D}\,[\![\boldsymbol{\varepsilon}]\!] \tag{3.70}$$

where $[\![\boldsymbol{\sigma}']\!]$ and $[\![\boldsymbol{\varepsilon}]\!]$ are the vectorial forms of the effective stress tensor $\boldsymbol{\sigma}'$ and the strain tensor $\boldsymbol{\varepsilon} = \nabla^s \tilde{\boldsymbol{u}}$ respectively, defined as

$$[\![\boldsymbol{\sigma}']\!] = \left\{\sigma'_{xx}, \sigma'_{yx}, \sigma'_{xy}\right\}^{\mathrm{T}} \tag{3.71}$$

$$[\![\boldsymbol{\varepsilon}]\!] = \left\{\varepsilon_{xx}, \varepsilon_{yy}, 2\varepsilon_{xy}\right\}^{\mathrm{T}} \tag{3.72}$$

and $\boldsymbol{D}$ is the so-called elasticity matrix, which, for a plain strain problem, is defined as

$$\boldsymbol{D} = \begin{bmatrix} \lambda + 2\mu & \lambda & 0 \\ \lambda & \lambda + 2\mu & 0 \\ 0 & 0 & \mu \end{bmatrix} \tag{3.73}$$

where λ and μ are the Lamè coefficients.

We can now obtain the discrete counterpart of the weak form of the equilibrium equation (3.63), namely

$$\boldsymbol{R}_{n+1}^u = \boldsymbol{K}_e \hat{\boldsymbol{u}}_{n+1} - \boldsymbol{Q}_{n+1} \hat{\boldsymbol{p}}_{n+1}^w + \boldsymbol{f}_{u,n+1} = \boldsymbol{0} \tag{3.74}$$

where the matrices and vectors $\boldsymbol{K}_e$, $\boldsymbol{Q}_{n+1}$ and $\boldsymbol{f}_{u,n+1}$ are defined as

$$\boldsymbol{K}_e = \int_{\Omega} (\boldsymbol{B}^T \boldsymbol{D} \boldsymbol{B} \mathrm{dV} \tag{3.75}$$

$$\boldsymbol{Q}_{n+1} = \int_{\Omega} (\boldsymbol{b}^T S^w \boldsymbol{N}_p \mathrm{dV} \tag{3.76}$$

$$\boldsymbol{f}_{u,n+1} = -\int_{\Omega} \boldsymbol{N}_u^T \rho \boldsymbol{g} d\Omega - \int_{\Gamma_{\boldsymbol{u}}^N} \boldsymbol{N}_u^T \bar{\boldsymbol{t}} \mathrm{d}\Gamma \tag{3.77}$$

with the matrices $\boldsymbol{B}$ and $\boldsymbol{b}$ defined such that $\boldsymbol{B}\hat{\boldsymbol{u}} = \{\boldsymbol{\varepsilon}\}$ and $\boldsymbol{b}\hat{\boldsymbol{u}} = \nabla \cdot \tilde{\boldsymbol{u}}$.

Regarding the discrete counterpart of the weak form of the mass balance equation, we obtain three discrete algebraic systems of equations, one for each formulation that has been introduced. Applying again the Bobnov-Galerkin method, from the weak form (3.64) we obtain

$$\boldsymbol{R}_{n+1}^{p1} = \boldsymbol{S}_{n+1}\left(\hat{\boldsymbol{p}}_{n+1}^w - \hat{\boldsymbol{p}}_n^w\right) + \boldsymbol{Q}_{n+1}^T\left(\hat{\boldsymbol{u}}_{n+1} - \hat{\boldsymbol{u}}_n\right) + \boldsymbol{H}_{n+1}\hat{\boldsymbol{p}}_{n+1}^w + \boldsymbol{f}_{p,n+1} = \boldsymbol{0} \tag{3.78}$$

from the weak form (3.65) we obtain

$$\boldsymbol{R}_{n+1}^{p2} = \boldsymbol{ds}_{n+1} + \boldsymbol{Q}_{n+1}^T\left(\hat{\boldsymbol{u}}_{n+1} - \hat{\boldsymbol{u}}_n\right) + \boldsymbol{H}_{n+1}\hat{\boldsymbol{p}}_{n+1}^w + \boldsymbol{f}_{p,n+1} = \boldsymbol{0} \tag{3.79}$$

and from the weak form (3.66) we obtain ,

$$\boldsymbol{R}_{n+1}^{p3} = \boldsymbol{ds}_{n+1}^* + \boldsymbol{Q}_{n+1}^T\left(\hat{\boldsymbol{u}}_{n+1} - \hat{\boldsymbol{u}}_n\right) + \boldsymbol{H}_{n+1}\hat{\boldsymbol{p}}_{n+1}^w + \boldsymbol{f}_{p,n+1} = \boldsymbol{0} \tag{3.80}$$

where the matrices and the vectors $\boldsymbol{S}_{n+1}$, $\boldsymbol{H}_{n+1}$, $\boldsymbol{ds}_{n+1}$and $\boldsymbol{f}_{p,n+1}$ are the same derived in Section 3.2.1; the vector $\boldsymbol{ds}_{n+1}^*$ is a modification of $\boldsymbol{ds}_{n+1}$, in which the variation of n with the volumetric deformation is taken into account, obtaining

$$\boldsymbol{ds}_{n+1}^* = \int_{\Omega} \boldsymbol{N}_p^T n \rho^w \left(S_{n+1}^w - S_n^w\right) \mathrm{dV} \tag{3.81}$$

If we define now the generalized solution vector $\hat{\boldsymbol{U}}_{n+1}$ and the generalized residual vector $\boldsymbol{R}_{n+1}$ as

$$\hat{\boldsymbol{U}}_{n+1} = \left\{ \begin{array}{c} \hat{\boldsymbol{u}}_{n+1} \\ \hat{\boldsymbol{p}}_{n+1}^w \end{array} \right\} \tag{3.82}$$

$$\boldsymbol{R}_{n+1} = \left\{ \begin{array}{c} \boldsymbol{R}_{n+1}^u \\ \boldsymbol{R}_{n+1}^{p1/2/3} \end{array} \right\} \tag{3.83}$$

the FEM formulation of the coupled flow-deformation problem can be written in the compact form

$$\boldsymbol{R}_{n+1} = \boldsymbol{R}_{n+1}\left(\hat{\boldsymbol{U}}_{n+1}\right) = \boldsymbol{0} \tag{3.84}$$

Due to the presence of nonlinear expressions for the variables S^w, k^{rw} and n, the system of equations (3.84) results to be a nonlinear function in $\hat{\boldsymbol{U}}_{n+1}$, and so has to be linearized and solved using an iterative scheme. In this section we apply the Newton-Raphson method, in which the solution of the current time step $n+1$ is searched

iteratively, approximating the function $\boldsymbol{R}_{n+1}$ with its tangent. The approximation solution $\hat{\boldsymbol{U}}_{n+1}^{k+1}$, where $k+1$ indicates the current Newton-Raphson iteration $k+1$, , is obtained solving the linear system of equations

$$\boldsymbol{J}_{n+1}^{k} \Delta \hat{\boldsymbol{U}}_{n+1}^{k+1} = -\boldsymbol{R}_{n+1}^{k} \tag{3.85}$$

and then computing

$$\hat{\boldsymbol{U}}_{n+1}^{k+1} = \hat{\boldsymbol{U}}_{n+1}^{k} + \Delta \hat{\boldsymbol{U}}_{n+1}^{k+1} \tag{3.86}$$

The matrix $\boldsymbol{J}_{n+1}^{k}$, known as Jacobian matrix of $\boldsymbol{R}_{n+1}^{k}$, is defined as

$$\boldsymbol{J}_{n+1}^{k} = \frac{\partial \boldsymbol{R}_{n+1}^{k}}{\partial \hat{\boldsymbol{U}}_{n+1}^{k}} \tag{3.87}$$

From now on, due to the fact that, in the expression for the residual $\boldsymbol{R}_{n+1}^{k}$ and the Jacobian $\boldsymbol{J}_{n+1}^{k}$, all the values relative to the current time step $n+1$ are intended to be the one computed during the previous nonlinear iteration k, we omit the iteration index k. Due to the presence of two subsystems of equations, one for the field variable $\boldsymbol{u}$, and one for the field variable p^w, the matrix $\boldsymbol{J}_{n+1}$ can be subdivided in blocks, namely

$$\boldsymbol{J}_{n+1} = \begin{bmatrix} \boldsymbol{J}_{n+1}^{uu} & \boldsymbol{J}_{n+1}^{up} \\ \boldsymbol{J}_{n+1}^{pu1/2/3} & \boldsymbol{J}_{n+1}^{pp1/2/3} \end{bmatrix} \tag{3.88}$$

where the blocks are defined as

$$\boldsymbol{J}_{n+1}^{uu} = \frac{\partial \boldsymbol{R}_{n+1}^{u}}{\partial \hat{\boldsymbol{u}}_{n+1}}, \quad \boldsymbol{J}_{n+1}^{up} = \frac{\partial \boldsymbol{R}_{n+1}^{u}}{\partial \hat{\boldsymbol{p}}_{n+1}^{w}}, \quad \boldsymbol{J}_{n+1}^{pu1/2/3} = \frac{\partial \boldsymbol{R}_{n+1}^{p}}{\partial \hat{\boldsymbol{u}}_{n+1}}, \quad \boldsymbol{J}_{n+1}^{pp1/2/3} = \frac{\partial \boldsymbol{R}_{n+1}^{p}}{\partial \hat{\boldsymbol{p}}_{n+1}^{w}} \tag{3.89}$$

In particular, the non-zero blocks $\boldsymbol{J}_{n+1}^{up}$ and $\boldsymbol{J}_{n+1}^{pu}$ represents the coupling between the two fields.

The blocks $\boldsymbol{J}_{n+1}^{uu}$ and $\boldsymbol{J}_{n+1}^{up}$, are derived from the residual $\boldsymbol{R}_{n+1}^{u}$, relative to the equilibrium equation, obtaining

$$\boldsymbol{J}_{n+1}^{uu} = \frac{\partial \boldsymbol{R}_{n+1}^{u}}{\partial \hat{\boldsymbol{u}}_{n+1}} = \boldsymbol{K}_{e} \tag{3.90}$$

$$\boldsymbol{J}_{n+1}^{up} = \frac{\partial \boldsymbol{R}_{n+1}^{u}}{\partial \hat{\boldsymbol{p}}_{n+1}^{w}} = \boldsymbol{Q}_{n+1} + \boldsymbol{dF}_{u,n+1} \tag{3.91}$$

where the matrices $\boldsymbol{K}_{e}$ and $\boldsymbol{Q}_{n+1}$ are the same derived in the calculation of $\boldsymbol{R}_{n+1}^{u}$, and $\boldsymbol{dF}_{u,n+1}$ is defined as

$$\boldsymbol{dF}_{u,n+1} = \int_{\Omega} \left(\boldsymbol{N}_{u}^{T} n_0 \rho^w \boldsymbol{g} \right) \left. \frac{\partial S^w}{\partial p^w} \right|_{n+1} \boldsymbol{N}_{p} \mathrm{dV} \tag{3.92}$$

Regarding the residual $\boldsymbol{R}^{p}_{n+1}$, we have three different expressions, one for each derived formulation of the mass balance equation. From the first formulation of the residual $\boldsymbol{R}^{p1}_{n+1}$, defined in (3.78), we derive

$$\boldsymbol{J}^{pu1}_{n+1} = \frac{\partial \boldsymbol{R}^{p1}_{n+1}}{\partial \hat{\boldsymbol{u}}_{n+1}} = \boldsymbol{Q}^{T}_{n+1} \tag{3.93}$$

$$\boldsymbol{J}^{pp1}_{n+1} = \frac{\partial \boldsymbol{R}^{p1}_{n+1}}{\partial \hat{\boldsymbol{p}}^{w}_{n+1}} = \boldsymbol{S}_{n+1} + \boldsymbol{C}_{n+1} + \boldsymbol{G}_{n+1} + \boldsymbol{H}_{n+1} + \boldsymbol{P}_{n+1} + \boldsymbol{dF}_{p,n+1} \tag{3.94}$$

from the second formulation of the residual $\boldsymbol{R}^{p2}_{n+1}$, defined in (3.79), we derive

$$\boldsymbol{J}^{pu2}_{n+1} = \frac{\partial \boldsymbol{R}^{p2}_{n+1}}{\partial \hat{\boldsymbol{u}}_{n+1}} = \boldsymbol{Q}^{T}_{n+1} \tag{3.95}$$

$$\boldsymbol{J}^{pp2}_{n+1} = \frac{\partial \boldsymbol{R}^{p2}_{n+1}}{\partial \hat{\boldsymbol{p}}^{w}_{n+1}} = \boldsymbol{S}_{n+1} + \boldsymbol{H}_{n+1} + \boldsymbol{P}_{n+1} + \boldsymbol{dF}_{p,n+1} \tag{3.96}$$

and from the third formulation of the residual $\boldsymbol{R}^{p3}_{n+1}$, defined in (3.80), we derive

$$\boldsymbol{J}^{pu3}_{n+1} = \frac{\partial \boldsymbol{R}^{p3}_{n+1}}{\partial \hat{\boldsymbol{u}}_{n+1}} = \boldsymbol{Q}^{T}_{n+1} + \boldsymbol{N}_{n+1} \tag{3.97}$$

$$\boldsymbol{J}^{pp3}_{n+1} = \frac{\partial \boldsymbol{R}^{p3}_{n+1}}{\partial \hat{\boldsymbol{p}}^{w}_{n+1}} = \boldsymbol{S}^{*}_{n+1} + \boldsymbol{C}_{n+1} + \boldsymbol{H}_{n+1} + \boldsymbol{P}_{n+1} + \boldsymbol{dF}_{p,n+1} \tag{3.98}$$

The matrices $\boldsymbol{S}_{n+1}$ and $\boldsymbol{H}_{n+1}$ are the same derived in Section 3.2.1, while the matrices $\boldsymbol{C}_{n+1}$, $\boldsymbol{G}_{n+1}$, $\boldsymbol{P}_{n+1}$, $\boldsymbol{dF}_{p,n+1}$, $\boldsymbol{N}_{n+1}$ and $\boldsymbol{S}^{*}_{n+1}$ are defined as

$$\boldsymbol{C}_{n+1} = \int_{\Omega} \boldsymbol{N}_{p}^{T} n_{0} \rho^{w} \left.\frac{\partial^{2} S^{w}}{\partial p^{w2}}\right|_{n+1} \boldsymbol{N}_{p} \mathrm{dV} \tag{3.99}$$

$$\boldsymbol{G}_{n+1} = \int_{\Omega}\int_{\Omega} \left[\boldsymbol{N}_{p}^{T} \boldsymbol{b} \left(\hat{\boldsymbol{u}}_{n+1} - \hat{\boldsymbol{u}}_{n}\right)\right] \left.\frac{\partial S^{w}}{\partial p^{w}}\right|_{n+1} \boldsymbol{N}_{p} \mathrm{dV} \tag{3.100}$$

$$\boldsymbol{P}_{n+1} = \Delta t \int_{\Omega} \left[(\nabla \boldsymbol{N}_{p})^{T} \rho^{w} \frac{k^{s} \boldsymbol{I}}{\mu^{w}} \nabla \boldsymbol{N}_{p} \hat{\boldsymbol{p}}^{w}_{n+1}\right] \left.\frac{\partial k^{rw}_{n+1}}{\partial S^{w}}\right|_{n+1} \left.\frac{\partial S^{w}}{\partial p^{w}}\right|_{n+1} \boldsymbol{N}_{p} \mathrm{dV} \tag{3.101}$$

$$\boldsymbol{dF}_{p,n+1} = -\Delta t \int_{\Omega} \left[(\nabla \boldsymbol{N}_{p})^{T} \left(\rho^{w}\right)^{2} \frac{k^{s} \boldsymbol{I}}{\mu^{w}} \boldsymbol{g}\right] \left.\frac{\partial k^{rw}_{n+1}}{\partial S^{w}}\right|_{n+1} \left.\frac{\partial S^{w}}{\partial p^{w}}\right|_{n+1} \boldsymbol{N}_{p} \mathrm{dV} \tag{3.102}$$

$$\boldsymbol{N}_{n+1} = \int_{\Omega} \boldsymbol{N}_{p}^{T} \rho \left(S^{w}_{n+1} - S^{w}_{n}\right) \left.\frac{\partial n}{\partial \boldsymbol{\varepsilon}_{v}}\right|_{n+1} \boldsymbol{b} \mathrm{dV} \tag{3.103}$$

$$\boldsymbol{S}^{*}_{n+1} = \int_{\Omega} \boldsymbol{N}_{p}^{T} n \rho^{w} \left.\frac{\partial S^{w}}{\partial p^{w}}\right|_{n+1} \boldsymbol{N}_{p} \mathrm{dV} \tag{3.104}$$

3.3.2 An alternative mass conservative formulation

If we retrace the procedure, followed in Section 2.2.2, to obtain the mass balance equation of water (2.73), we notice that the product rule of derivation has be applied to the rate term $\dot{\rho}_w = (n\dot{S^w}\rho^w)$, in order to be able to sum up the mass balance equation of the solid with the one of the fluid, eliminating the material derivative of the porosity $\dot{n}$. When the numerical discretization in time is applied, the product rule is subjected to the same restrictions exposed in Section 3.2 for the chain rule. From that point of view, also the formulation of the mass balance (3.53) is already expected to be not conservative. We propose in this section a formulation of the mass balance of solid and water, obtained without applying this two rules of derivation.

The mass balance equation for a specie α can be expressed in two alternative forms, called *Lagrangian form* and *Eulerian form*. In the Lagrangian form the conservation of ρ_α is stated relatively to an infinitesimal control volume moving together with a physical particle of the body, and the conservation of mass for α takes the form

$$\frac{\mathrm{d}^\alpha \rho_\alpha}{\mathrm{d}t} + \rho_\alpha \nabla \cdot \boldsymbol{v}^\alpha = 0 \tag{3.105}$$

where

$$\frac{\mathrm{d}^\alpha \rho_\alpha}{\mathrm{d}t} = \dot{\rho}_\alpha = \frac{\partial \rho_\alpha}{\partial t} + \nabla \rho_\alpha \cdot \boldsymbol{v}^\alpha$$

is the material derivative of the density ρ_α, already introduce in the previous chapter.

On the other hand, in the Eulerian form the conservation of ρ_α is stated relatively to an infinitesimal control volume fixed in the space, and the conservation of mass for α takes the form

$$\frac{\partial \rho_\alpha}{\partial t} + \nabla \cdot (\rho_\alpha \boldsymbol{v}^\alpha) = 0 \tag{3.106}$$

The Eulerian form is known also as *conservation form* of the equation, in the sense that leads to conservative numerical schemes, due to the fact the the time integration is done on the time partial derivative, and not on the material derivative.

In our case we have two mass conservation equations, one for the solid and one for the liquid phase. Our objective is, therefore, to derive a mass conservation equation for the both species together, staring from the Eulerian form of the conservation equations of the single phases, and avoiding the use of the chain rule or the product rule of the derivation.

Based on the Lagrangian form of the mass balance of the solid and of the water, derived in Section 2.2.2, we can write the corresponding equations in the Eulerian

form, obtaining

$$-\rho^s \frac{\partial n}{\partial t} + \rho^s \nabla \cdot (1-n)\,\boldsymbol{v} = 0 \tag{3.107}$$

$$\rho^w \frac{\partial (S^w n)}{\partial t} + \rho^w \nabla \cdot [n S^w (\boldsymbol{v} + \tilde{\boldsymbol{v}}^w)] = 0 \tag{3.108}$$

Summing up these two equations we obtain

$$\rho^w \frac{\partial [-n(1-S^w)]}{\partial t} + \rho^w \nabla \cdot [1 - n(1-S^w)\,\boldsymbol{v}] + \rho^w \nabla \cdot (n S^w \tilde{\boldsymbol{v}}^w) = 0 \tag{3.109}$$

If we notice now that the term

$$\phi^a = n(1-S^w) \tag{3.110}$$

is the volume fraction of air ϕ^a, and we apply the Darcy's law (2.68), then equation (3.109) can be rewritten as

$$-\rho^w \frac{\partial \phi^a}{\partial t} + \rho^w \nabla \cdot [(1-\phi^a)\,\boldsymbol{v}] + \rho^w \nabla \cdot \left[\frac{k^{rw} k^s \boldsymbol{I}}{\mu^w}(-\nabla p^w + \rho^w \boldsymbol{g})\right] = 0 \tag{3.111}$$

After the application of the discretization in time (Backward Euler) we obtain

$$-\frac{\rho^w \phi^a_{n+1} - \phi^a_n}{\Delta t} + \rho^w \nabla \cdot \left[\left(1-\phi^a_{n+1}\right)\frac{\boldsymbol{u}_{n+1} - \boldsymbol{u}_n}{\Delta t}\right] + \rho^w \nabla \cdot \left[\frac{k^{rw}_{n+1} k^s \boldsymbol{I}}{\mu^w}(-\nabla p^w_{n+1} + \rho^w \boldsymbol{g})\right] = 0 \tag{3.112}$$

We apply now the Weighted Residual method, obtaining the following time-discrete weak formulation

$$W^{p4}_{n+1} = -\int_\Omega w_p \rho^w \left(\phi^a_{n+1} - \phi^a_n\right) \mathrm{dV} + \int_\Omega w_p \rho^w \nabla \cdot \left[\left(1-\phi^a_{n+1}\right)(\boldsymbol{u}_{n+1} - \boldsymbol{u}_n)\right] \mathrm{dV} + \Delta t \int_\Omega \nabla w_p \cdot \left[\rho^w \frac{k^{rw}_{n+1} k^s \boldsymbol{I}}{\mu^w}(\nabla p^w_{n+1} - \rho^w \boldsymbol{g})\right] \mathrm{dV} + \Delta t \int_{\Gamma^N_p} w_p \bar{q}^w_{n+1} \mathrm{dV} = 0 \tag{3.113}$$

In order tho simplify the numerical treatment of the second term on the left hand

side of equation (3.113), we apply the Green's Lemma, deriving the equivalent form

$$W_{n+1}^{p4} = -\int_{\Omega} w_p \rho^w \left(\phi_{n+1}^a - \phi_n^a\right) \mathrm{dV} - \int_{\Omega} \nabla w_p \cdot \rho^w \left[\left(1-\phi_{n+1}^a\right)\left(\boldsymbol{u}_{n+1}-\boldsymbol{u}_n\right)\right] \mathrm{dV}$$

$$+\int_{\partial\Omega} w_p \rho^w \left(1-\phi_{n+1}^a\right)\left(\boldsymbol{u}_{n+1}-\boldsymbol{u}_n\right)\cdot\boldsymbol{n}_\Gamma \mathrm{d}\Gamma + \Delta t \int_{\Omega} \nabla w_p \cdot \left[\rho^w \frac{k_{n+1}^{rw}\boldsymbol{K}}{\mu^w}\left(\nabla p_{n+1}^w - \rho^w \boldsymbol{g}\right)\right] \mathrm{dV}$$

$$+ \Delta t \int_{\Gamma_p^N} w_p \bar{q}_{n+1}^w \mathrm{dV} = 0 \quad (3.114)$$

The corresponding discrete system of equations is obtained applying the Bubnov-Galerkin approach, following the same procedure used in the previous section. We obtain the following expression for the residual

$$\boldsymbol{R}_{n+1}^{p4} = \boldsymbol{d\phi}_{n+1} + \boldsymbol{dv}_{n+1} + \boldsymbol{da}_{n+1} + \boldsymbol{H}_{n+1}\hat{\boldsymbol{p}}_{n+1}^w + \boldsymbol{f}_{p,n+1} = \boldsymbol{0} \quad (3.115)$$

where the vectors $\boldsymbol{d\phi}_{n+1}$, $\boldsymbol{dv}_{n+1}$ and $\boldsymbol{da}_{n+1}$ are

$$\boldsymbol{d\phi}_{n+1} = -\int_{\Omega} \boldsymbol{N}_p^T \rho^w \left(\phi_{n+1}^a - \phi_n^a\right) \mathrm{dV} \quad (3.116)$$

$$\boldsymbol{dv}_{n+1} = -\int_{\Omega} (\nabla \boldsymbol{N}_p)^T \rho^w \left[\left(1-\phi_{n+1}^a\right)\left(\boldsymbol{u}_{n+1}-\boldsymbol{u}_n\right)\right] \mathrm{dV} \quad (3.117)$$

$$\boldsymbol{da}_{n+1} = \int_{\partial\Omega} \boldsymbol{N}_p^T \rho^w \left(1-\phi_{n+1}^a\right)\left[\boldsymbol{n}_\Gamma^T\left(\boldsymbol{u}_{n+1}-\boldsymbol{u}_n\right)\right] \mathrm{d}\Gamma \quad (3.118)$$

Equation (3.115) is coupled with the discrete form of the equilibrium equation (3.74), obtaining again the nonlinear system of equations

$$\boldsymbol{R}_{n+1} = \left\{ \begin{array}{c} \boldsymbol{R}_{n+1}^u \\ \boldsymbol{R}_{n+1}^{p4} \end{array} \right\} = \boldsymbol{0} \quad (3.119)$$

which has to be linearized and solved using an iterative scheme. As in the previous section, the Newton-Raphson method is used, leading to linear system of equations

$$\boldsymbol{J}_{n+1}^k \Delta\hat{\boldsymbol{U}}_{n+1}^{k+1} = -\boldsymbol{R}_{n+1}^k \quad (3.120)$$

where $\Delta\hat{\boldsymbol{U}}_{n+1}^{k+1}$ is defined in (3.86). The Jacobian matrix $\boldsymbol{J}_{n+1}$ results to be

$$\boldsymbol{J}_{n+1} = \left[\begin{array}{cc} \boldsymbol{J}_{n+1}^{uu} & \boldsymbol{J}_{n+1}^{up} \\ \boldsymbol{J}_{n+1}^{pu4} & \boldsymbol{J}_{n+1}^{pp4} \end{array} \right] \quad (3.121)$$

where $\boldsymbol{J}^{uu}_{n+1}$ and $\boldsymbol{J}^{up}_{n+1}$ are defined in (3.90) and (3.91) respectively, and $\boldsymbol{J}^{pu4}_{n+1}$ and $\boldsymbol{J}^{pp4}_{n+1}$ must be derived from the residual $\boldsymbol{R}^{p4}_{n+1}$. In particular, for the block matrix $\boldsymbol{J}^{pu4}_{n+1}$ we obtain the expression

$$\boldsymbol{J}^{pu4}_{n+1} = \frac{\partial \boldsymbol{R}^{p4}_{n+1}}{\partial \hat{\boldsymbol{u}}_{n+1}} = \boldsymbol{\Theta}^{u}_{n+1} + \boldsymbol{V}^{u1}_{n+1} + \boldsymbol{V}^{u2}_{n+1} + \boldsymbol{A}^{u1}_{n+1} + \boldsymbol{A}^{u2}_{n+1} \tag{3.122}$$

where

$$\boldsymbol{\Theta}^{u}_{n+1} = -\int_{\Omega} \boldsymbol{N}_p^T \rho^w \left(1 - S^w\right) \left.\frac{\partial n}{\partial \boldsymbol{\varepsilon}_v}\right|_{n+1} \boldsymbol{b}\mathrm{dV} \tag{3.123}$$

$$\boldsymbol{V}^{u1}_{n+1} = -\int_{\Omega} (\nabla \boldsymbol{N}_p)^T \rho^w \left(1 - \phi^a_{n+1}\right) \boldsymbol{N}_u \mathrm{dV} \tag{3.124}$$

$$\boldsymbol{V}^{u2}_{n+1} = -\int_{\Omega} \left[(\nabla \boldsymbol{N}_p)^T \rho^w \left(\boldsymbol{u}_{n+1} - \boldsymbol{u}_n\right)\right] \left(1 - S^w\right) \left.\frac{\partial n}{\partial \boldsymbol{\varepsilon}_v}\right|_{n+1} \boldsymbol{b}\mathrm{dV} \tag{3.125}$$

$$\boldsymbol{A}^{u1}_{n+1} = \int_{\Gamma^N_p} \boldsymbol{N}_p^T \rho^w \left(1 - \phi^a_{n+1}\right) \left(\boldsymbol{n}_\Gamma^T \boldsymbol{N}_u\right) \mathrm{d}\Gamma \tag{3.126}$$

$$\boldsymbol{A}^{u2}_{n+1} = \int_{\Gamma^N_p} \left\{\boldsymbol{N}_p^T \rho^w \left[\boldsymbol{n}_\Gamma^T \left(\boldsymbol{u}_{n+1} - \boldsymbol{u}_n\right)\right]\right\} \left(1 - S^w\right) \left.\frac{\partial n}{\partial \boldsymbol{\varepsilon}_v}\right|_{n+1} \boldsymbol{b}\mathrm{d}\Gamma \tag{3.127}$$

Finally, for the block matrix $\boldsymbol{J}^{pu4}_{n+1}$ we obtain the expression

$$\boldsymbol{J}^{pp4}_{n+1} = \frac{\partial \boldsymbol{R}^{p4}_{n+1}}{\partial \hat{\boldsymbol{p}}^{w}_{n+1}} = \boldsymbol{\Theta}^{p}_{n+1} + \boldsymbol{V}^{p}_{n+1} + \boldsymbol{A}^{p}_{n+1} + \boldsymbol{H}_{n+1} + \boldsymbol{P}_{n+1} + \boldsymbol{dF}_{p,n+1} \tag{3.128}$$

where $\boldsymbol{H}_{n+1}$, $\boldsymbol{P}_{n+1}$ and $\boldsymbol{dF}_{p,n+1}$ are the same defined in the previous sections, and the remaining matrices are defined as

$$\boldsymbol{\Theta}^{p}_{n+1} = \int_{\Omega} \boldsymbol{N}_p^T \rho^w n \left.\frac{\partial S^w}{\partial p^w}\right|_{n+1} \boldsymbol{N}_p \mathrm{dV} \tag{3.129}$$

$$\boldsymbol{V}^{p}_{n+1} = \int_{\Omega} \left[(\nabla \boldsymbol{N}_p)^T \rho^w \left(\boldsymbol{u}_{n+1} - \boldsymbol{u}_n\right)\right] n \left.\frac{\partial S^w}{\partial p^w}\right|_{n+1} \boldsymbol{N}_p \mathrm{dV} \tag{3.130}$$

$$\boldsymbol{A}^{p}_{n+1} = -\int_{\Gamma^N_p} \left\{\boldsymbol{N}_p^T \rho^w \left[\boldsymbol{n}_\Gamma^T \left(\boldsymbol{u}_{n+1} - \boldsymbol{u}_n\right)\right]\right\} n \left.\frac{\partial S^w}{\partial p^w}\right|_{n+1} \boldsymbol{N}_p \mathrm{d}\Gamma \tag{3.131}$$

3.3.3 Verification of the mass balance

In order to verify the conservation of mass for the four proposed formulations in this section, it is again necessary to evaluate the time-discrete water mass balance statement

$$\Delta M_{stor}^{n+1} + \bar{M}_{in/out}^{n+1} = 0 \tag{3.132}$$

which, this time, needs to take also the deformability of the solid skeleton into account.

If we consider negligible the variation of length of the boundary with the deformation, the average mass of water entering/exiting the domain $\bar{M}_{in/out}^{n+1}$ can be evaluated, as in the previous section, throw equation (3.39), together with equations (3.37) and (3.38).

Regarding the evaluation of the storaged water mass M_{stor}, it becomes necessary to take into account the variation of the porosity n and of the volume of integration with the deformation, obtaining the following the definition of storage mass

$$M_{stor} = \sum_{el=1}^{ne} \int_{\bar{\Omega}_e} n S^w \mathrm{dv} \tag{3.133}$$

where n is the current value of the porosity, dv is and infinitesimal volume of the deformed body and $\bar{\Omega}_{e,def}$ the deformed volume of a finite element.

Starting from the definition of volumetric strain $\boldsymbol{\varepsilon}_v$, in the framework of the infinitesimal theory of deformation, is it possible to obtain the following relationship between the infinitesimal deformed volume dv and the infinitesimal undeformed volume dV:

$$\mathrm{dv} = (1 + \boldsymbol{\varepsilon}_v)\, \mathrm{dV} \tag{3.134}$$

Inserting (3.134) into (3.133), together with equation (3.57) for the porosity n, we obtain

$$M_{stor} = \sum_{el=1}^{ne} \int_{\Omega_e} (n_0 + \boldsymbol{\varepsilon}_v)\, S^w \mathrm{dV} \tag{3.135}$$

which can be now integrated on the undeformed volume of the finite elements. The variation of storaged mass during the current time step $n+1$ is therefore defined as

$$\Delta M_{stor}^{n+1} = \sum_{el=1}^{ne} \int_{\Omega_e} (n_0 + \boldsymbol{\varepsilon}_{v,n+1})\, S_{n+1}^w \mathrm{dV} - \sum_{el=1}^{ne} \int_{\Omega_e} (n_0 + \boldsymbol{\varepsilon}_{v,n})\, S_n^w \mathrm{dV} \tag{3.136}$$

3.3.4 Numerical simulation of the Liakopoulos experiment

In this example we show the results of the numerical simulation of the Liakopouls experiment [38]. This test consists in the study of the drainage of an initially saturated soil column of Del Monte sand due to gravitational effects. The initial and the boundary conditions, together with the dimensions of the domain are shown in Figure 3.7. The initial conditions in the experiment have been set regulating the water flux on the top of the column, in order to obtain the condition $p^w = 0$ in all the domain. Once this condition has been reached, the water supply on the top has been removed, starting the desaturation process. The parameter of the model are listed in Table 3.2.

$n_0\,[-]$	$k^s\,[m^2]$	$\mu^w\,[Pa \cdot s]$	$\rho^w\,[Kg/m^3]$	$\rho^s\,[Kg/m^3]$	$E\,[MPa]$	$\nu\,[-]$
0.2975	$4.5\,e^{-13}$	0.001	1000	2000	1.3	0.4

Table 3.2: Material parameters

The SWCC curve and the relative permeability-saturation curve used by Liakopoulos are

$$S^w = 1 - 1,9722e^{-11}\,(p^c)^{2,4279} \tag{3.137}$$

$$k^{rw} = 1 - 2,207\,(1 - S^w)^{0.9529} \tag{3.138}$$

The mesh is discretized with 40 elements in the vertical direction, and the time step $\Delta t = 1\,s$ is used. Finally the tolerance of the non-linear solver is set to $toll = 10^{-7}$.

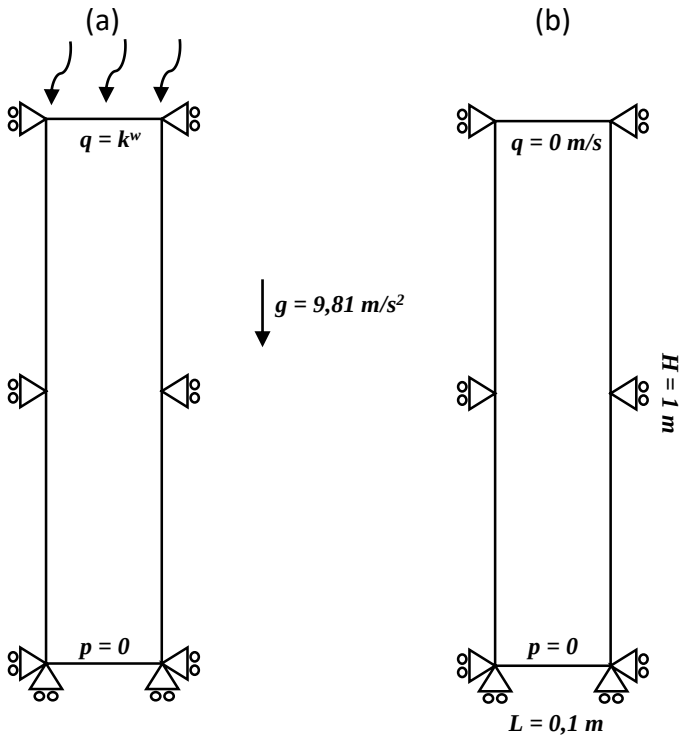

Figure 3.7: Scheme of the Liakopoulos experiment: in (a) the initial conditions at $t = 0$ s, in (b) the boundary conditions for the desaturation process.

Four different numerical schemes are considered, analyzing their mass conservation property:

- *Scheme* 1: it is obtained from the formulation (3.55) of the mass conservation equation, with the chain rule applied to the rate of water saturation.
- *Scheme* 2: it is obtained from the formulation (3.53) of the mass conservation equation. This scheme is mass conservative at the rigid skeleton limit.
- *Scheme* 3: it is obtained from the formulation (3.58) of the mass conservation equation, considering the porosity n dependent on the deformation (equation (3.57))
- *Scheme* 4: it is the new conservative scheme (3.114), derived from the strong form (3.111), obtained without applying neither the chain rule nor the product rule to the time derivatives.

In a first analysis the elastic properties of the reference test case ($E = 1.3\,MPa$, $\nu = 0.4$) are used, and the numerical results from *Scheme* 2 for the capillary pressure are compared with the experimental ones (Figure 3.8); moreover, a comparison

with an analytical solution for the initial conditions (constant flux and $p^w = 0$ everywhere) and the steady state drained limit for the displacement is also provided (Figure 3.9), showing a good agreement between the numerical/experimental and numerical/analytical results. Finally the evolution in time of the saturation S^w is shown in Figure 3.10.

In a second analysis we compare the results obtain with the *Schemes* $1-4$, for three different values of the Young modulus E. The first value is the one of the reference test case ($E = 1,3\,MPa$, $\nu = 0,4$), the second one is a very high value of the Young modulus, and the third one correspond to a less rigid material ($E = 0,13\,MPa$, $\nu = 0,4$).

Figure 3.11.a shows the results obtained assuming a rigid solid skeleton (very big value of E). It can be clearly seen how the *Scheme* 1 leads to considerable errors in the first part of the desiccation analysis, while the solutions of the other three schemes coincide, and are characterized by a relative mass error always lower then 5%, considered as limit of acceptability. In this case only the saturation S^w influences the mass conservation. Figure 3.11.b shows the results relative to the Young modulus of the material used in the experiment. It can be seen how the relative mass error obtained with the *Scheme* 1 remains bigger then 5%, while the other schemes perform well. In particular the last two schemes, capable to capture the variation of the porosity with the deformation, lead to slightly better results at the end of the desiccation process. In this case both S^w and n influences the mass conservation. In the last example, shown in Figure 3.11.c, a Young modulus $E = 0,13\,MPa$ is considered. It can be seen that the both first two schemes leads to bigger error in the final part of the desiccation process, while the last two performs again well. In particular the error obtained with the *Scheme* 1 are slightly lower then the one obtained with the *Scheme* 3. In this case n influences the mass conservation the most.

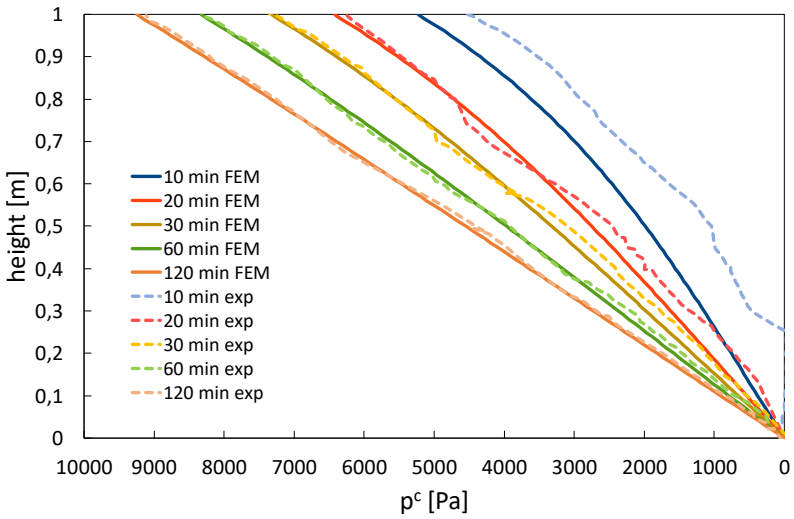

Figure 3.8: Comparison between the numerical results (*Scheme* 2) and the experimental evolution in time of the capillary pressure p^c.

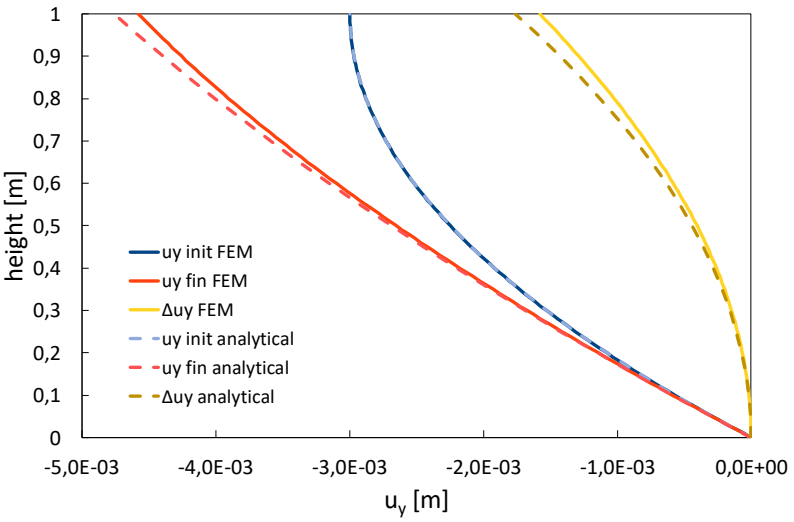

Figure 3.9: Comparison between the numerical and the analytical steady state solution for the vertical displacement.

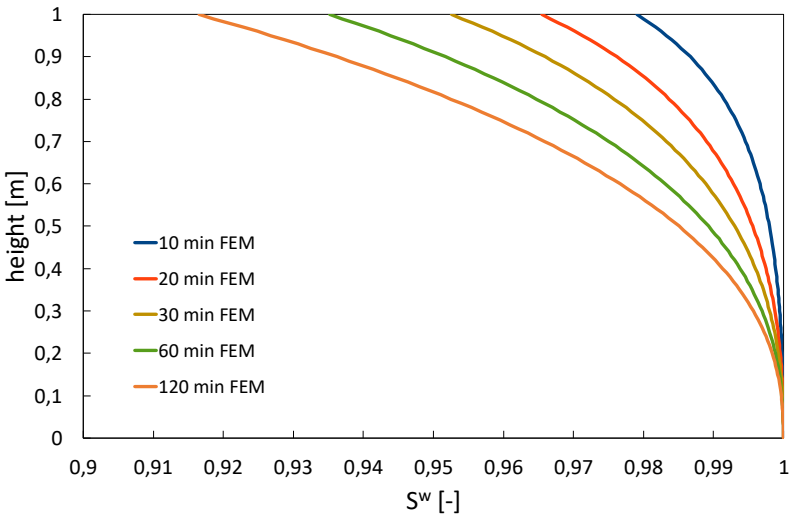

Figure 3.10: Evolution in time of the water saturation S^w obtained with the numerical model (*Scheme* 2) and the elastic parameters of the reference test.

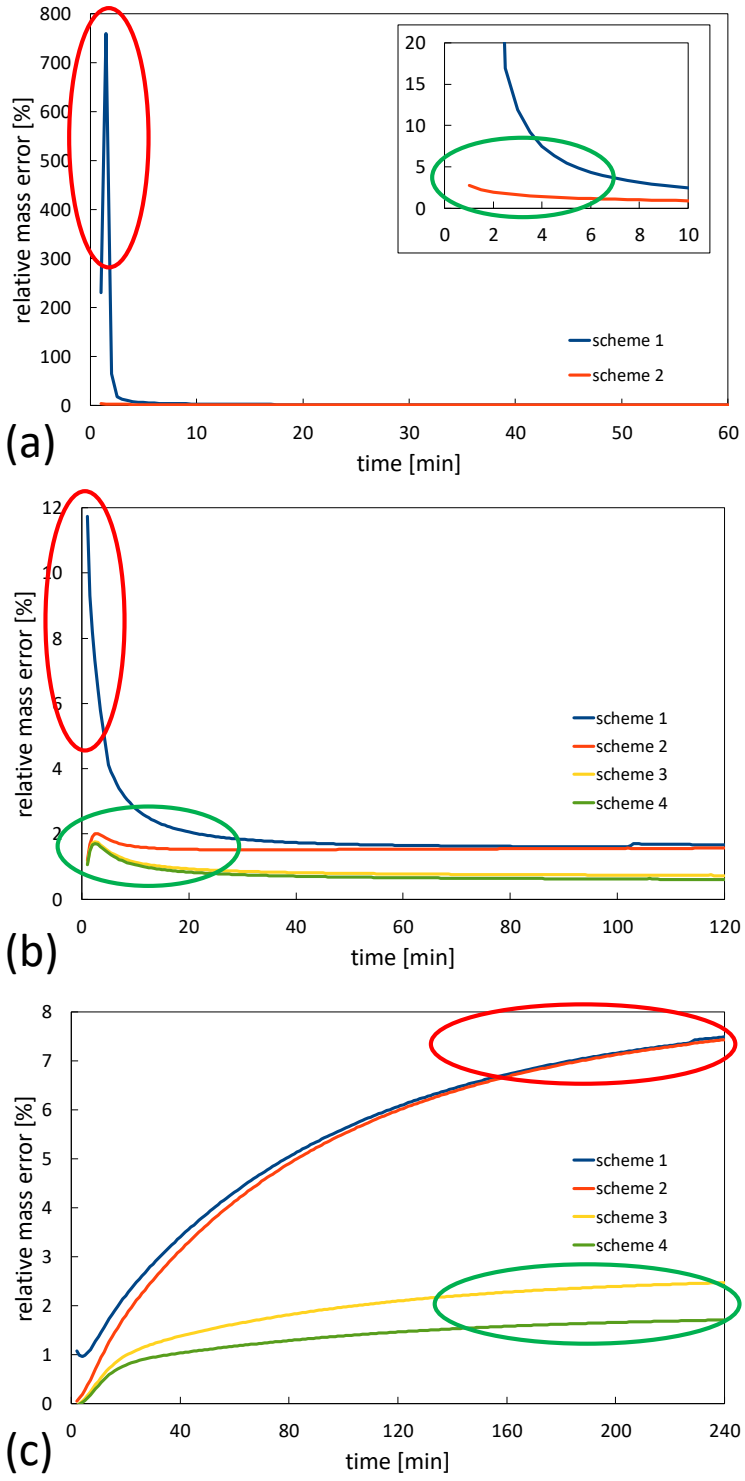

Figure 3.11: Relative mass errors for the *Scheme* $1-4$: in (a) $E \to \infty$, in (b) $E = 1,3\,MPa$, in (c) $E = 0,13\,MPa$. The solutions showing a maximum relative error greater than 5% are highlighted with a red circle, while the ones showing a maximum relative error smaller than 5% are highlighted with a green circle.

3.4 Conclusions

In this chapter the attention has been posed on the development of conservative numerical schemes for the discretization of the mass conservation equation in partially saturated porous media. In the first part of the chapter we focused on the numerical modeling of porous media with rigid solid skeleton, for which the mass balance equation of water becomes the so-called Richards equation. The problem of the conservation of mass after the numerical discretization has been introduced, and the main conservative and non-conservative formulations present in the literature have been reviewed. The two formulations have been used in the numerical simulation of an infiltration problem, showing that the non-conservative formulation, not only leads to significant errors in the mass conservation, but also shows some convergence issues, not observed using a conservative scheme.

The problem has been after extended, taking into account the deformability of the solid skeleton, consider as a linear elastic material. Four different formulations of the mass balance equation of water and solid have been discussed, including an original formulation obtained starting from the eulerian form of the mass balance of the single species, and without the use of neither the chain rule nor the product rule of derivation in the treatment of the equations before the numerical discretization.

Finally, the four different numerical schemes, obtained after the discretization in time and space, have been used in the simulation of a benchmark desiccation experiment [38]. The problem has been solved using three different values of the Young modulus, and, compared to the other schemes adopted, the new scheme proposed leads to the lowest values of relative mass error in all the three cases analyzed. Anyway, the implementation of this scheme is more complicated and the resolution is the most computational expensive. For a normal engineering application, probably the best compromise between accuracy and numerical efficiency is the so-called *Scheme* 2, that can be modified into the *Scheme* 3 when the deformability of the material becomes bigger.

Chapter 4

Stabilized mixed formulation for phase-field modeling of deviatoric fractures in saturated porous media

4.1 Introduction

In the numerical approximation of a phase-field model of fracture in porous media with the Finite Element Method (FEM), the problem of the numerical locking due to high volumetric stiffness of the medium can occur. The causes of this state of incompressibility can be traced both to the hydraulic and the mechanical properties of the material. Regarding the hydraulic properties, it is well known in the literature [68, 37, 10] that, in the early stage of the consolidation process of porous media with low permeability, oscillating solutions for the pore pressure can be found when using finite elements that violate the so-called Ladyzenskaja-Babuska-Brezzi (LBB) condition [15]. Regarding the mechanical properties, has been shown in [60] that, when using a deviatoric-volumetric energy split in the phase-field simulation of brittle fractures subjected to compressive loading, the phase-field solution may feature a much larger thickness of the localization band than expected based on the chosen characteristic length, or the simulation may even not converge at all. To the knowledge of the author, the combination of these two phenomena has not been studied yet.

The objective of this chapter is, therefore, to study the occurrence of these instabilities, generally defined as locking phenomena, in the phase-field modeling of brittle fracture in saturated porous media, and to introduce a new stabilized mixed formulation for low-order finite elements, based on the polynomial-pressure-projection technique, first proposed in [7, 23, 8] in the field of fluid dynamics, and successively applied in [66] to the field of saturated porous media. The chapter is subdivided as

follows: Section 4.2 focuses on the introduction of the stabilization technique and on a review of its application to the modeling of saturated porous media; in Section 4.3 the same stabilization technique to phase-field modeling of fracture in elastic solids and, in Section 4.4, the two problems are combined. Here three alternative formulations of the poroelastic-fracture problem and their relative stabilization are studied.

4.2 Water flow in a linear elastic saturated porous medium

4.2.1 Mathematical formulation

The balance equations for the coupled problem of saturated water flow in a deforming porous medium briefly introduced. The following assumptions are made: isothermal fully saturated condition ($\boldsymbol{u} - p^w$ formulation), incompressibility of both solid and liquid phase, and geometric linearity. With these assumptions, we can rewrite the strong form of the equilibrium (2.72) equation as

$$\nabla \cdot \boldsymbol{\sigma}^t + \rho \boldsymbol{g} = \boldsymbol{0} \tag{4.1}$$

and the strong form of the mass balance equation of solid and water mass (2.73) as

$$\nabla \cdot \dot{\boldsymbol{u}} + \nabla \cdot \boldsymbol{v}^{ws} = 0 \tag{4.2}$$

where $\boldsymbol{\sigma}^t$ is the Cauchy total stress tensor, $\boldsymbol{g}$ is the vector of gravity acceleration, $\boldsymbol{u}$ the solid matrix displacement, and $\boldsymbol{v}^{ws}$ the relative water velocity with respect to the solid matrix, and

$$\rho = (1 - n)\rho^s + n\rho^w \tag{4.3}$$

is the density of the mixture, with ρ^s and ρ^w indicating the intrinsic density of the solid and of the water phase respectively, and n indicating the porosity of the material. Equations (4.1) and (4.2) are defined on the domain Ω of the body.

Based on the Terzaghi's effective stress principle (2.47), the Cauchy total stress tensor$\boldsymbol{\sigma}^t$ can be decomposed as

$$\boldsymbol{\sigma}^t = \boldsymbol{\sigma}^e - \boldsymbol{I}p^w \tag{4.4}$$

where p^w is the water pore pressure, and $\boldsymbol{\sigma}^e$ is the so-called effective stress, namely the portion of the total stress directly related to the deformation of the solid matrix.

In order to be able to solve the system of differential equations (4.1) and (4.2) we need to add some constitutive laws. Concerning the mechanical behavior of the solid

matrix, we assume a linear elastic constitutive relation between the effective stress tensor $\boldsymbol{\sigma}^e$ and the infinitesimal strain tensor $\boldsymbol{\varepsilon}$, namely

$$\boldsymbol{\sigma}^e = \mathbb{C} : \boldsymbol{\varepsilon} \tag{4.5}$$

where $\mathbb{C}$ is the fourth-order elastic tensor depending on the two Lamè constants λ and μ. Note that $\boldsymbol{\varepsilon} = \nabla^s \boldsymbol{u}$, where ∇^s is the symmetric part of the gradient operator.

For the fluid phase we introduce, as a constitutive equation, the Darcy's law (2.68), which for a saturated porous medium takes the form

$$\boldsymbol{v}^{ws} = -\frac{k^w}{\rho^w g}\boldsymbol{I}(\nabla p^w - \rho^w \boldsymbol{g}) \tag{4.6}$$

where $k^w$is the hydraulic conductivity (expressed in m/s).

Introducing (4.5), (4.6) and (4.4) into (4.1) and (4.2) we obtain the system of equations

$$\nabla \cdot (\mathbb{C} : \nabla^s \boldsymbol{u} - \boldsymbol{I} p^w) + \rho \boldsymbol{g} = \boldsymbol{0} \tag{4.7}$$

$$\nabla \cdot \dot{\boldsymbol{u}} - \nabla \cdot \left[\frac{k^w}{\rho^w g}\boldsymbol{I} \cdot (\nabla p^w - \rho^w \boldsymbol{g})\right] = 0 \tag{4.8}$$

that now can be solved for $\boldsymbol{u}$ and p^w.

In order for the system of equations (4.7) and (4.8) to be a well-posed problem, we need to specify some boundary conditions on the boundary $\Gamma = \partial\Omega$ of the domain Ω, together with some initial condition at the time $t = 0$. First of all, we have to define on the boundary Γ the portions $\Gamma_{\boldsymbol{u}}^D$ and Γ_p^D , where boundary conditions are applied on displacements and water pressure respectively (Dirichlet BCs), and the portions $\Gamma_{\boldsymbol{u}}^N$ and Γ_q^N, where boundary conditions are applied on traction and water flux respectively (Neumann BCs). This decomposition must fulfill the relationships:

$$\Gamma = \Gamma_{\boldsymbol{u}}^D \cup \Gamma_{\boldsymbol{u}}^N = \Gamma_p^D \cup \Gamma_p^N \tag{4.9}$$

$$\Gamma_{\boldsymbol{u}}^D \cap \Gamma_{\boldsymbol{u}}^N = \Gamma_p^D \cap \Gamma_p^N = \oslash \tag{4.10}$$

The initial and boundary conditions are then expressed as

$$\begin{array}{ll} \boldsymbol{u} = \boldsymbol{u}_0 & \text{at } t = 0 \\ p^w = p_0^w & \text{at } t = 0 \\ \boldsymbol{u} = \overline{\boldsymbol{u}} & \text{on } \Gamma_{\boldsymbol{u}}^D \\ p^w = \bar{p}^w & \text{on } \Gamma_p^D \\ \boldsymbol{\sigma} \cdot \boldsymbol{n} = \bar{\boldsymbol{t}} & \text{on } \Gamma_{\boldsymbol{u}}^N \\ \boldsymbol{v}^{ws} \cdot \boldsymbol{n} = \bar{q} & \text{on } \Gamma_q^N \end{array} \tag{4.11}$$

where $\boldsymbol{u}_0$ arep_0^w the initial values of the displacement and water pressure, $\overline{\boldsymbol{u}}$ and $\bar{p}^w$ are the imposed values of the displacement and water pressure on the portion of Γ with Dirichlet BCs, $\bar{\boldsymbol{t}}$ and $\bar{q}$ are the imposed values of the traction and the water flux on the portion of Γ with Neumann BCs, and $\boldsymbol{n}$ is the unit vector perpendicular to the boundary Γ.

4.2.2 Finite element discretization

We apply now the Weighted Residual Method to derive a weak formulation of the boundary value problem represented by the differential equations (4.1) and (4.2), together with the BCs (4.11), and starting point for the application of the Finite Element Method. Defining the following spaces for the trial functions $\boldsymbol{u}$ and p^w and of the test (or weighting) functions $\boldsymbol{w}_u$ and w_p

$$\begin{aligned} T_u &= \left\{\boldsymbol{u} : \Omega \to \mathbb{R}^2 \mid \boldsymbol{u} \in \boldsymbol{H}^1, \boldsymbol{u} = \overline{\boldsymbol{u}} \text{ on } \Gamma_{\boldsymbol{u}}^D\right\} \\ T_p &= \left\{p^w : \Omega \to \mathbb{R} \mid p^w \in H^1, p^w = \bar{p}^w \text{ on } \Gamma_p^D\right\} \\ W_u &= \left\{\boldsymbol{w}_u : \Omega \to \mathbb{R}^2 \mid \boldsymbol{w}_u \in \boldsymbol{H}^1, \boldsymbol{w}_u = \boldsymbol{0} \text{ on } \Gamma_{\boldsymbol{u}}^D\right\} \\ W_p &= \left\{w_p : \Omega \to \mathbb{R} \mid w_p \in H^1, w_p = 0 \text{ on } \Gamma_p^D\right\} \end{aligned} \tag{4.12}$$

the solution of the problem (4.1), (4.2) and (4.11) is the pair $\{\boldsymbol{u}, p^w\}$ that solves, for any admissible pair $\{\boldsymbol{w}_u, w_p\}$, the following weak formulation

$$\begin{aligned} &\int_\Omega (\nabla^s \boldsymbol{w}_u : \boldsymbol{D} : \nabla^s \boldsymbol{u} - p^w \nabla \cdot \boldsymbol{w}_u - \boldsymbol{w}_u \cdot \rho \boldsymbol{g}) \mathrm{d}V - \int_{\Gamma_{\boldsymbol{u}}^N} \boldsymbol{w}_u \cdot \bar{\boldsymbol{t}} \mathrm{d}\Gamma = 0 \\ &\int_\Omega \left\{ w_p \nabla \cdot \dot{\boldsymbol{u}} + \nabla w_p \cdot \left[\tfrac{k^w}{\rho^w g} \boldsymbol{I} \cdot (\nabla p^w - \rho^w \boldsymbol{g})\right] \right\} \mathrm{d}V + \int_{\Gamma_p^N} w_d \bar{q} \mathrm{d}\Gamma = 0 \end{aligned} \tag{4.13}$$

Starting from this weak form, it is now possible to discretize the problem in space and in time. Concerning the discretization in space, we subdivide our domain in a mesh of quadrilateral elements, and we consider an approximation of the spaces T_u, T_p, W_u, W_p based on polynomial shape functions with local support, namely

$$\begin{aligned} \tilde{\boldsymbol{u}} &= \boldsymbol{N}_u \hat{\boldsymbol{u}} \\ \tilde{p}^w &= \boldsymbol{N}_p \hat{\boldsymbol{p}}^w \\ \tilde{\boldsymbol{w}}_u &= \boldsymbol{N}_u \hat{\boldsymbol{w}}_u \\ \tilde{w}_p &= \boldsymbol{N}_p \hat{\boldsymbol{w}}_p \end{aligned} \tag{4.14}$$

where $\tilde{()}$ are the approximated trials and weighting functions, $\hat{()}$ are the vectors containing the values of these functions on the mesh nodes, $\boldsymbol{N}_p$ is the vector of dimension $1 \times nn$ containing the shape function for the water pressure N_p^i, relative to an arbitrary node i of the nn nodes defined on the domain Ω by the finite element mesh, and $\boldsymbol{N}_u$ is a matrix defined as defined as

$$\boldsymbol{N}_u = \{\boldsymbol{N}_u^1, \boldsymbol{N}_u^2, ..., \boldsymbol{N}_u^{nn}\}^T \tag{4.15}$$

where, for a problem in two dimensions,

$$\boldsymbol{N}_u^i = I_2 N_u^i \tag{4.16}$$

where I_2 is the identity matrix of dimension two, and N_u^i is the shape function for the displacement, relative to an arbitrary node i of the nn nodes defined on the domain. The same shape functions are used for the corresponding trial and weighting functions, so the Bobnov-Galerkin Method is recovered.

Concerning the discretization in time, we apply the Backward Euler scheme. First of all, we define as $n+1$ and n the current and the previous time steps respectively, and we call Δt the dimension of the current time step. In the Backward Euler scheme (known also as Implicit Euler scheme) a certain differential equation is solved at the current time step $n+1$, replacing the derivatives with respect of time with their discrete counterpart, namely

$$\dot{(\,)} = \frac{(\,)_{\,n+1} - (\,)_{\,n}}{\Delta t} \tag{4.17}$$

We can therefore write the discrete version of the weak form (4.13) as

$$\begin{aligned} \boldsymbol{R}_{u,n+1} &= \boldsymbol{K}_{n+1}\hat{\boldsymbol{u}}_{n+1} - \boldsymbol{Q}_{n+1}\hat{\boldsymbol{p}}^w_{n+1} - \boldsymbol{f}_{u,n+1} = \boldsymbol{0} \\ \boldsymbol{R}_{p,n+1} &= \boldsymbol{Q}^T_{n+1}(\hat{\boldsymbol{u}}_{n+1} - \hat{\boldsymbol{u}}_n)/\Delta t + \boldsymbol{H}_{n+1}\hat{\boldsymbol{p}}^w_{n+1} - \boldsymbol{f}_{p,n+1} = \boldsymbol{0} \end{aligned} \tag{4.18}$$

with

$$\boldsymbol{K} = \int_{\Omega} \boldsymbol{B}^T \boldsymbol{D} \boldsymbol{B} \mathrm{d}V \tag{4.19}$$

$$\boldsymbol{Q} = \int_{\Omega} \boldsymbol{b}^T \boldsymbol{N}_p \mathrm{d}V \tag{4.20}$$

$$\boldsymbol{H} = \int_{\Omega} (\nabla \boldsymbol{N}_p)^T \frac{k^w \mathbf{I}}{\rho^w g} \nabla \boldsymbol{N}_p \mathrm{d}V \tag{4.21}$$

$$\boldsymbol{f}_u = \int_{\Omega} \boldsymbol{N}_u^T \rho \boldsymbol{g} d\Omega + \int_{\Gamma} \boldsymbol{N}_u^T \bar{\boldsymbol{t}} \mathrm{d}\Gamma \tag{4.22}$$

$$\boldsymbol{f}_p = \int_{\Omega} (\nabla \boldsymbol{N}_p)^T \frac{k^w}{g} \boldsymbol{g} d\Omega - \int_{\Gamma} \boldsymbol{N}_p^T \bar{q} \mathrm{d}\Gamma \tag{4.23}$$

where the matrices $\boldsymbol{B}$ and $\boldsymbol{b}$ are defined such that $\boldsymbol{B}\hat{\boldsymbol{u}} = [\![\boldsymbol{\varepsilon}]\!]$ and $\boldsymbol{b}\hat{\boldsymbol{u}} = \nabla \cdot \tilde{\boldsymbol{u}}$, with $[\![\boldsymbol{\varepsilon}]\!]$ being the infinitesimal strain tensor $\boldsymbol{\varepsilon}$ represented in Voigt notation. The matrix

$\boldsymbol{D}$ is the elasticity matrix , which for a plain strain problem (assumption made for all the applications in this chapter) is defined as

$$\boldsymbol{D} = \begin{bmatrix} \lambda + 2\mu & \lambda & 0 \\ \lambda & \lambda + 2\mu & 0 \\ 0 & 0 & \mu \end{bmatrix} \tag{4.24}$$

where λ and μ are the Lamè coefficients.

We can now notice that the expressions (4.19) - (4.23) do not depend on the solution at the current time step, so the problem is linear and the solution can be directly calculated solving the system

$$\begin{bmatrix} \boldsymbol{K} & -\boldsymbol{Q} \\ \boldsymbol{Q}^T & \Delta t \boldsymbol{H} \end{bmatrix} \begin{Bmatrix} \hat{\boldsymbol{u}} \\ \hat{\boldsymbol{p}}^w \end{Bmatrix}_{n+1} = \begin{bmatrix} \boldsymbol{0} & \boldsymbol{0} \\ \boldsymbol{Q}^T & \boldsymbol{0} \end{bmatrix} \begin{Bmatrix} \hat{\boldsymbol{u}} \\ \hat{\boldsymbol{p}}^w \end{Bmatrix}_{n} + \begin{Bmatrix} \boldsymbol{f}_u \\ \Delta t \boldsymbol{f}_p \end{Bmatrix}_{n+1} \tag{4.25}$$

Now the next step is the choice of the functions $\boldsymbol{N}_u$ and $\boldsymbol{N}_p$: it is well known in the literature that, for a coupled solid deformation-fluid flow problem, this choice is subjected to some restrictions, as the pair ($\boldsymbol{N}_u$, $\boldsymbol{N}_p$) has to fulfill the so called LBB condition in order to ensure the stability of the solution in the locally undrained limit. The study of the stability of the formulation is the goal of this chapter, and will be treated in the next section.

4.2.3 Stable, unstable and stabilized formulations

We consider know the algebraic structure of the problem in the local undrained limit, i.e. when the product $\Delta t k^w \to 0$ [66]. The differential equations (4.7) and (4.8) become

$$\begin{gathered} \nabla \cdot (\boldsymbol{D} : \nabla^s \boldsymbol{u} - \boldsymbol{I} p^w) + \rho \boldsymbol{g} = \boldsymbol{0} \\ \nabla \cdot \dot{\boldsymbol{u}} = 0 \end{gathered} \tag{4.26}$$

and the discrete counterpart (4.25) becomes

$$\begin{bmatrix} \boldsymbol{K} & -\boldsymbol{Q} \\ -\boldsymbol{Q}^T & \boldsymbol{0} \end{bmatrix} \begin{Bmatrix} \hat{\boldsymbol{u}} \\ \hat{\boldsymbol{p}}^w \end{Bmatrix} = \begin{Bmatrix} \boldsymbol{f}_u \\ \boldsymbol{0} \end{Bmatrix} \tag{4.27}$$

We can notice that the lower diagonal block in the system (4.27) is now zero, and the matrix assumes the typical structure of the problems in mechanics where incompressibility acts as a constraint. From a physical point of view, this is exactly what is happening: if we consider a arbitrary portion of our domain, in the undrained limit the water can not move in our out of that volume, because of the condition $\nabla \cdot \dot{\boldsymbol{u}} = 0$, and, due to its incompressibility, constrains the solid matrix to develop pure deviatoric deformations. In order to obtain a stable solution, the choice of the spaces

W_u and W_p has to satisfy the LBB conditions. The combination of quadratic displacements and linear pressure interpolations (Q9P4 for quadrilateral finite elements) satisfies this condition, while the combination of linear displacements and linear pressure interpolations (Q4P4 for quadrilateral finite elements) does not. In spite of its stability, the Q9P4 quadrilateral element, with its 22 degrees of freedom (DOFs), is computationally more expensive than the Q4P4 quadrilateral element, which has only 12 DOFs. The computational advantage of the linear-displacements/linear-pressure interpolation becomes even more evident in three-dimensional problems, where every hexagonal element has 32 degrees of freedom (DOF), while using a quadratic-displacements/linear-pressure interpolation the number of DOFs per hexagonal element rises to 89.

A smart approach to stabilize the linear-displacements/linear-pressure interpolation has been introduced by Bochev and Dohrmann in [23, 7, 8], in the context of fluid mechanics, and successively applied by White and Borja in [66], in the field of porous mechanics. We briefly resume the stabilization technique proposed in [23] for the Stokes equations. The strong form of the equations is

$$\begin{aligned} -\nu\Delta\boldsymbol{u} + \nabla p &= \boldsymbol{f} \\ \nabla\cdot\boldsymbol{u} &= 0 \end{aligned} \tag{4.28}$$

where $\boldsymbol{u}$ is the water velocity, p the water pressure and ν the water viscosity, along with the homogeneous boundary condition

$$\boldsymbol{u} = 0 \text{ on } \Gamma \tag{4.29}$$

The algebraic system obtained after the finite element discretization of the weak form of the problem is

$$\begin{bmatrix} \boldsymbol{A} & -\boldsymbol{B} \\ -\boldsymbol{B}^T & \boldsymbol{0} \end{bmatrix} \begin{Bmatrix} \hat{\boldsymbol{u}} \\ \hat{\boldsymbol{p}} \end{Bmatrix} = \begin{Bmatrix} \boldsymbol{f}_u \\ \boldsymbol{0} \end{Bmatrix} \tag{4.30}$$

where

$$\boldsymbol{A} = \int_\Omega \nu(\nabla\boldsymbol{N}_u)^T\nabla\boldsymbol{N}_u \mathrm{d}V, \quad \boldsymbol{B} = \int_\Omega \nu(\nabla\cdot\boldsymbol{N}_u)^T\boldsymbol{N}_p \mathrm{d}V, \quad \boldsymbol{f}_u = \int_\Omega \boldsymbol{N}_u^T\boldsymbol{f}\mathrm{d}V \tag{4.31}$$

Due to the zero low diagonal block in the stiffness matrix in (4.30), it is well known in the literature that finite elements with the same order of interpolation for the velocity $\boldsymbol{u}$ and the pressure p do not fulfill the LBB condition, and therefore can lead to an oscillating solution for the pressure. In this unstable category falls the linear-velocity/linear-pressure interpolation. The idea proposed in [23] is to add a stabilization term in the weak formulation of the problem, resulting in a non-zero low

diagonal block in the corresponding discrete equation. Let us first define an element piecewise constant projector operator for the pressure as

$$\Pi p|_{\Omega_e} = \frac{1}{V_e} \int_{\Omega} p d\Omega \tag{4.32}$$

where Π is the projection operator and V_e is the volume of the element domain Ω_e. This is nothing but the definition of the average element pressure. Having this definition in mind, the discrete version of the new stabilized problem becomes

$$\begin{bmatrix} \boldsymbol{A} & -\boldsymbol{B} \\ -\boldsymbol{B}^T & -\boldsymbol{C} \end{bmatrix} \begin{Bmatrix} \hat{\boldsymbol{u}} \\ \hat{\boldsymbol{p}} \end{Bmatrix} = \begin{Bmatrix} \boldsymbol{f}_u \\ \boldsymbol{0} \end{Bmatrix} \tag{4.33}$$

where the new low diagonal block $\boldsymbol{C}$ is introduced. This is defined as

$$\boldsymbol{C} = \int_{\Omega} \frac{1}{\nu} (\boldsymbol{N}_p - \Pi \boldsymbol{N}_p)^T (\boldsymbol{N}_p - \Pi \boldsymbol{N}_p) \mathrm{d}V \tag{4.34}$$

The idea behind this stabilization is substantially to 'penalize' the oscillations of the pressure around their element average value. This is actually more than a simple penalization: Bochev and Dohrmann demonstrated that the additional terms proposed quantify, and therefore correct, the deficiency of the linear-velocity/linear-pressure interpolation with respect to the LBB condition [66]. There are two main advantages in the use of this stabilization:

- The stabilization term is a local additional term: it requires only the computation of average value of the element shape functions, so no additional information need to be sent to the subroutine calculating the element stiffness matrix and residual. Therefore the stabilization can be easily implemented without changing the overall structure of the finite element code, and requiring furthermore a minimum additional computational cost (specially when compared with the saving in therms of DOF due to the use of linear interpolation for the velocity instead of the quadratic one necessary to satisfy the LBB condition)

- No additional stabilization coefficients are required: the penalization factor is the inverse of a physical parameter characterizing the problem, the water viscosity ν, and the risk of an insufficient or excessive stabilization due to an arbitrary coefficient set by the user is avoided.

Starting from this idea, and noticing the clear similarity between the equations (4.27) and (4.30), White and Borja introduced a similar stabilization term in order to be

able to use the Q4P4s element in the consolidation analysis of saturated porous media with low permeability. In [66] they propose the following modified version the discrete residual (4.18):

$$\begin{aligned} \boldsymbol{R}_{u,n+1} &= \boldsymbol{K}_{n+1}\hat{\boldsymbol{u}}_{n+1} - \boldsymbol{Q}_{n+1}\hat{\boldsymbol{p}}^w_{n+1} - \boldsymbol{f}_{u,n+1} = \boldsymbol{0} \\ \boldsymbol{R}_{p,n+1} &= \boldsymbol{Q}^T_{n+1}(\hat{\boldsymbol{u}}_{n+1} - \hat{\boldsymbol{u}}_n)/\Delta t + \boldsymbol{H}_{n+1}\hat{\boldsymbol{p}}^w_{n+1} - \boldsymbol{f}_{p,n+1} + \boldsymbol{R}^{stab}_{n+1} = \boldsymbol{0} \end{aligned} \tag{4.35}$$

where the stabilization vector $\boldsymbol{R}^{stab}_{n+1}$ has been included in the definition of the residual $\boldsymbol{R}_{p,n+1}$. The vector $\boldsymbol{R}^{stab}_{n+1}$ is defined in [66] as

$$\boldsymbol{R}^{stab}_{n+1} = \mathbf{S}^{WB}(\hat{\boldsymbol{p}}^w_{n+1} - \hat{\boldsymbol{p}}^w_n)/\Delta t \tag{4.36}$$

where

$$\boldsymbol{S}^{WB} = \int_\Omega \frac{\tau}{2\mu}(\boldsymbol{N}_p - \mathit{\Pi}\boldsymbol{N}_p)^T(\boldsymbol{N}_p - \mathit{\Pi}\boldsymbol{N}_p)\mathrm{d}V \tag{4.37}$$

Here μ is the shear modulus of the solid matrix, and τ an additional coefficient introduced mainly to compensate a possible excess of stabilization ($\tau = 0.04$ has been used in [66] for a two-dimensional numerical application). Being the permeability $k^w > 0$ (even if very small), the problem is always characterized by a transient evolution (even if very slow) and, therefore, the stabilized quantity is the time derivative of the water pressure. Now it is interesting to notice that, in analogy with what has been done for the Stokes equations, also in this case the stabilization term is penalized by a physical parameter of the problem, namely 2μ. However, while in the current case of the Stokes equations the parameter multiplying the velocity was a scalar value and so the choice of the penalization was unique (the inverse of that value), in the case in analysis the strain tensor $\boldsymbol{\varepsilon}$ is multiplied by the fourth order elasticity tensor $\mathbb{C}$, depending itself from the two Lamè constants λ and μ. Thus a criterion for the choice of a scalar value representative of the tensor $\mathbb{C}$ is needed. We suggest, as a general criterion, to use as a stabilization coefficient

$$c^{stab} = (\mathrm{tr}(\mathbb{C})/n)^{-1} = \frac{1}{\lambda + 2\mu} \tag{4.38}$$

where n is the dimension of the problem. Following this criterion a modified definition of the stabilization (4.37) arises, namely

$$\boldsymbol{S}^{mod} = \int_\Omega \frac{1}{\lambda + 2\mu}(\boldsymbol{N}_p - \mathit{\Pi}\boldsymbol{N}_p)^T(\boldsymbol{N}_p - \mathit{\Pi}\boldsymbol{N}_p)\mathrm{d}V \tag{4.39}$$

We notice that, in this case, the stabilization coefficient is always greater or equal to (4.37), proposed in [66], leading to a weaker stabilization effect. With the introduction

of the stabilization matrix $\boldsymbol{S}$ ($\boldsymbol{S}^{WB}$ or $\boldsymbol{S}^{mod}$), the stabilized counterpart of the (4.25) can be derived, namely

$$\begin{bmatrix} \boldsymbol{K} & -\boldsymbol{Q} \\ \boldsymbol{Q}^T & \Delta t\boldsymbol{H}+\boldsymbol{S} \end{bmatrix} \begin{Bmatrix} \hat{\boldsymbol{u}} \\ \hat{\boldsymbol{p}}^w \end{Bmatrix}_{n+1} = \begin{bmatrix} \boldsymbol{0} & \boldsymbol{0} \\ \boldsymbol{Q}^T & \boldsymbol{S} \end{bmatrix} \begin{Bmatrix} \hat{\boldsymbol{u}} \\ \hat{\boldsymbol{p}}^w \end{Bmatrix}_{n} + \begin{Bmatrix} \boldsymbol{f}_u \\ \Delta t\boldsymbol{f}_p \end{Bmatrix}_{n+1} \tag{4.40}$$

4.2.4 Numerical example

In this example we show the numerical solution of a classical problem of geomechanics, Terzaghi's problem, whose analytical solution is well known. The domain of the problem is a layer of poroelastic material of height H and infinite extension, subjected to a constant load w applied at the top and vertically constrained at the bottom (see Figure 4.1). The water flux is free at the top, but constrained at the bottom. On the lateral boundaries zero horizontal displacement and water flux are imposed. The problem is a plane state of deformation and the mesh used for the discretization of the domain consists into a column of 20 quadrilateral elements. Although the analytical solution for displacement and water pressure is known for the entire consolidation process, our goal is to compare the numerical solutions of the pressure obtained using different stable and unstable finite elements at the early stage of the consolidation. The problem is solved using the classical finite elements Q9P4, Q4P4, and the stabilized bilinear elements Q4P4s-WB (the original proposed by White and Borja with the stabilization (4.37)) and Q4P4s (with the modified stabilization term (4.39) proposed in this thesis).The parameters of the models are: $E = 1\,kPa$, $k^w = 10^{-5}\,m/s$, $\rho^s = 0$, $\rho^w = 1000\,kg/m^3$, $\Delta t = 1\,s$; two different Poisson ratios are considered, $\nu = 0$ and $\nu = 0.4$ (very high value for soils, but chosen order to accentuate the differences between the two stabilizations analyzed).

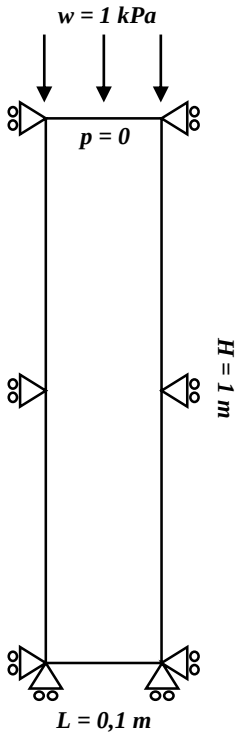

Figure 4.1: Scheme of the Terzaghi's problem [66].

In order to study the stability of the different finite elements, we focus our attention on the initial stage of the consolidation process: it is immediately after the application of the load that, for a factor $k^w \Delta t$ small enough, the porous medium is subjected to undrained conditions, behaving as a incompressible material. Under this condition unstable finite elements are expected to show oscillations for the pressure solution. If we look at Figure 4.2.a, we can notice that the solution obtained for the pressure with the element Q4P4 shows large oscillations that propagate also far away from the boundary where the load is applied (pressure jump). The solution obtained with the stable Taylor-Hood element Q9P4 shows a small initial oscillation, that disappears at a small distance from the boundary where the load is applied. Both stabilized elements Q4P4s-WB and Q4P4s work perfectly, in the sense that they reproduce perfectly the solution of the stable element Q9P4. The two solutions coincides because, for $\nu = 0$, the two stabilization terms (4.37) and (4.39) coincide.

In Figure 4.2.b the results obtained using a Poisson modulus $\nu = 0.4$ are shown. For the element Q4P4 the results show again large oscillations along the entire domain, although slightly smaller than in the previous case. Again the Taylor-Hood element, as expected, leads to a stable pressure distribution. In this case, however, the difference in the choice of the 'penalty' coefficient in the stabilization term becomes

evident. While the proposed stabilized element Q4P4s delivers again exactly the same solution obtained with the stable Q9P4, the Q4P4s-WB shows a total absence of oscillation. This result, which seems to indicate and advantage of Q4P4s-WB, because it is the closest to the analytical solution (constant pressure equal to the applied load along the column, and sharp jump in the solution at the top, where Dirichlet boundary conditions are applied), is instead an indicator of an excess of stabilization. In fact, we consider as and indicator of the correctness of the stabilization coefficient the agreement with the numerical solution obtained with a stable formulation, more than the agreement with the analytical solution itself. This excess of stabilization for the element Q4P4s-WB was noticed by the authors themselves, and is possibly the reason why they introduce in the stabilization (4.37) an additional coefficient τ , set smaller than 1, in other to reduce the excess of diffusion that they noticed in some simulations [66]. Except for the choice of the penalty coefficient, the stabilization technique proposed in [66] results very effective and, at the same time, easy to implement.

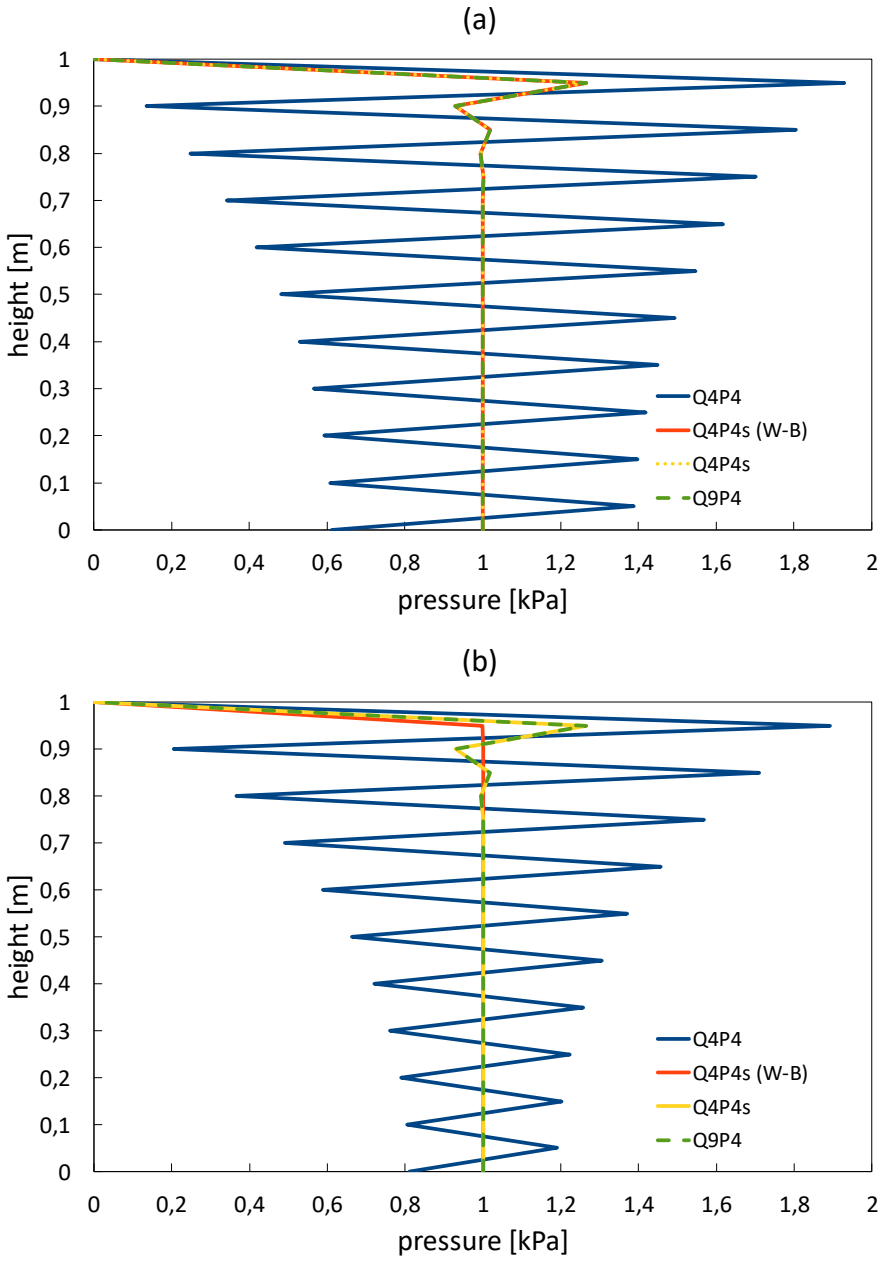

Figure 4.2: Pressure distribution along the column at the first time step for different finite elements. In (a) $\nu = 0$, in (b) $\nu = 0.4$.

4.3 Phase-field modeling of deviatoric fractures in elastic materials

4.3.1 Mathematical formulation

In Section 2.3 the regularized functional (2.135) for the phase-field modeling of brittle fracture ha been introduced. This functional reads

$$E_l(\boldsymbol{u},d) = \underbrace{\int_\Omega \Psi(\boldsymbol{\varepsilon}(\boldsymbol{u}),d)\mathrm{d}V}_{E^{el}(\boldsymbol{u},d)} + \underbrace{\frac{G_c}{4C_v}\int_\Omega \left(\frac{w(d)}{l} + l\,|\nabla d|^2\right)\mathrm{d}V}_{E_l^s(d)} + \underbrace{\frac{\gamma}{2}\int_\Omega \langle d-d_n\rangle_-^2\,\mathrm{d}V}_{P_\gamma(d)} \tag{4.41}$$

where $\boldsymbol{u}$ is the displacement vector, $\boldsymbol{\varepsilon}(\boldsymbol{u})$ is the infinitesimal strain tensor, d is the phase-field variable, G_c is the fracture toughness, l the so-called characteristic length, C_v a normalization constant, depending on the model used for the local part of the dissipation function $w(d)$, $\Psi(\boldsymbol{\varepsilon}(\boldsymbol{u}),d)$ is the elastic energy density, $P_\gamma(d)$ is a penalty term, introduce to enforce the irreversibility of the phase-field variable d, and the subscript n indicated the previous step the loading process, which is divided into a finite sequence of pseudo-time steps $(t_n)_{n=1,N}$. The functional (4.41) is a general expression, which need to be particularized by choosing and specific model for the functions $w(d)$ and $\Psi(\boldsymbol{\varepsilon}(\boldsymbol{u}),d)$. Concerning the the local part of the dissipation function, we choose the AT1 model (see Section 2.3.3), characterized by the following expression for $w(d)$ and C_v:

$$w(d) = d, \quad C_v = \tfrac{2}{3} \tag{4.42}$$

For the energy density function $\Psi(\boldsymbol{\varepsilon}(\boldsymbol{u}),d)$, we use and expression base on volumetric-deviatoric energy split proposed by Lancioni and Royer-Carfagni [36], namely

$$\Psi(\boldsymbol{\varepsilon}(\boldsymbol{u}),d) = [(1-d^2)+\eta]\;\Psi_0^{\mathrm{dev}}(\boldsymbol{\varepsilon}(\boldsymbol{u})) + \Psi_0^{\mathrm{vol}}(\boldsymbol{\varepsilon}(\boldsymbol{u})) \tag{4.43}$$

where η is the residual stiffness, and $\Psi_0^{\mathrm{vol}}(\boldsymbol{\varepsilon}(\boldsymbol{u}))$ and $\Psi_0^{\mathrm{dev}}(\boldsymbol{\varepsilon}(\boldsymbol{u}))$ are the volumetric and the deviatoric component of the undamaged elastic energy $\Psi_0(\boldsymbol{\varepsilon}(\boldsymbol{u}))$, such that

$$\Psi_0(\boldsymbol{\varepsilon}(\boldsymbol{u})) = \Psi_0^{\mathrm{dev}}(\boldsymbol{\varepsilon}(\boldsymbol{u})) + \Psi_0^{\mathrm{vol}}(\boldsymbol{\varepsilon}(\boldsymbol{u}))$$

In particular, if a linear elastic model is assumed for the undamaged material, $\Psi_0(\boldsymbol{\varepsilon}(\boldsymbol{u}))$, $\Psi_0^{\mathrm{dev}}(\boldsymbol{\varepsilon}(\boldsymbol{u}))$ and $\Psi_0^{\mathrm{vol}}(\boldsymbol{\varepsilon}(\boldsymbol{u}))$ are defined as

$$\Psi_0(\boldsymbol{\varepsilon}(\boldsymbol{u})) = \tfrac{1}{2}\lambda \mathrm{tr}^2(\boldsymbol{\varepsilon}(\boldsymbol{u})) + \mu \mathrm{tr}(\boldsymbol{\varepsilon}^2) = \tfrac{1}{2}\boldsymbol{\varepsilon} : \mathbb{C} : \boldsymbol{\varepsilon}$$
$$\Psi_0^{\mathrm{dev}}(\boldsymbol{\varepsilon}(\boldsymbol{u})) = \mu \boldsymbol{\varepsilon}^{\mathrm{dev}}(\boldsymbol{u}) : \boldsymbol{\varepsilon}^{\mathrm{dev}}(\boldsymbol{u})$$
$$\Psi_0^{\mathrm{vol}}(\boldsymbol{\varepsilon}(\boldsymbol{u})) = \tfrac{1}{2} K \mathrm{tr}^2(\boldsymbol{\varepsilon}(\boldsymbol{u})) \tag{4.44}$$

where $\boldsymbol{\varepsilon}^{\mathrm{dev}} = \boldsymbol{\varepsilon} - \frac{1}{3}\mathrm{tr}(\boldsymbol{\varepsilon})\boldsymbol{I}$ is the deviatoric component of the strain tensor $\boldsymbol{\varepsilon}$, $K = \lambda + \frac{2}{3}\mu$ is the material bulk modulus and $\mathbb{C}$ is the fourth-order elastic tensor depending on the two Lamè constants λ and μ. Inserting (4.42) and (4.43) in (4.41), we obtain

$$E_l(\boldsymbol{u}, d) = \int_\Omega [(1-d)^2 + \eta] \underbrace{\mu \boldsymbol{\varepsilon}^{\mathrm{dev}}(\boldsymbol{u}) : \boldsymbol{\varepsilon}^{\mathrm{dev}}(\boldsymbol{u})}_{\Psi_0^{\mathrm{dev}}} \mathrm{d}V + \int_\Omega \underbrace{\frac{1}{2} K \mathrm{tr}^2(\boldsymbol{\varepsilon}(\boldsymbol{u}))}_{\Psi_0^{\mathrm{vol}}} \mathrm{d}V$$
$$+ \frac{3}{8} G_c \int_\Omega \left(\frac{d}{l} + l \left| \nabla d \right|^2 \right) \mathrm{d}V + \frac{\gamma}{2} \int_\Omega \langle d - d_n \rangle_-^2 \, \mathrm{d}V \tag{4.45}$$

It is now useful, for the following the developments, to express $E_l(\boldsymbol{u}, d)$ as a function of the total strain $\boldsymbol{\varepsilon}$, and not of its components $\boldsymbol{\varepsilon}^{\mathrm{dev}}$ and $\mathrm{tr}(\boldsymbol{\varepsilon})$. We introduce, therefore, the following split of the elasticity tensor

$$\mathbb{C} = \mathbb{C}^{\mathrm{vol}} + \mathbb{C}^{\mathrm{dev}} \tag{4.46}$$

where the volumetric tensor $\mathbb{C}^{\mathrm{vol}}$ and the deviatoric tensor $\mathbb{C}^{\mathrm{dev}}$ are defined by the equivalences

$$\Psi_0^{\mathrm{vol}} = \frac{1}{2} \boldsymbol{\varepsilon} : \mathbb{C}^{\mathrm{vol}} : \boldsymbol{\varepsilon} = \frac{1}{2} K \mathrm{tr}^2(\boldsymbol{\varepsilon}(\boldsymbol{u})) \tag{4.47}$$

$$\Psi_0^{\mathrm{dev}} = \frac{1}{2} \boldsymbol{\varepsilon} : cc = \mu \boldsymbol{\varepsilon}^{\mathrm{dev}}(\boldsymbol{u}) : \boldsymbol{\varepsilon}^{\mathrm{dev}}(\boldsymbol{u}) \tag{4.48}$$

The functional (4.45) can be rewritten as

$$E_l(\boldsymbol{u}, d) = \int_\Omega \frac{1}{2} \boldsymbol{\varepsilon}(\boldsymbol{u}) : \left\{ [(1-d)^2 + \eta] \mathbb{C}^{\mathrm{dev}} + \mathbb{C}^{\mathrm{vol}} \right\} : \boldsymbol{\varepsilon}(\boldsymbol{u}) \mathrm{d}V$$
$$+ \frac{3}{8} G_c \int_\Omega \left(\frac{d}{l} + l \left| \nabla d \right|^2 \right) \mathrm{d}V + \frac{\gamma}{2} \int_\Omega \langle d - d_n \rangle_-^2 \, \mathrm{d}V \tag{4.49}$$

The phase-field formulation of brittle fracture is based on the minimization of the functional (4.49). More precisely. the solution of the problem of equilibrium and

evolution of the phase-field variable d consists in finding a couple $(\boldsymbol{u}, d)$ that minimizes the functional (4.45), namely

$$\arg\min \{E_l(\boldsymbol{u}, d) : \ \boldsymbol{u} \in T_u, \ d \in T_d\} \tag{4.50}$$

where T_u and T_d are the admissible displacement space and the admissible phase-field space, defined as

$$\begin{aligned} T_u &= \left\{\boldsymbol{u} : \Omega \to \mathbb{R}^2 \mid \boldsymbol{u} \in \boldsymbol{H}^1, \boldsymbol{u} = \overline{\boldsymbol{u}} \text{ on } \Gamma_{\boldsymbol{u}}^D\right\} \\ T_d &= \{d : \Omega \to \mathbb{R} \mid d \in H^1\} \end{aligned} \tag{4.51}$$

A necessary optimality condition for $(\boldsymbol{u}, d)$ ti be a minimum of $E_l(\boldsymbol{u}, d)$ is that

$$E_l'(\boldsymbol{u}, d)\,(\boldsymbol{v}) = \int_\Omega \boldsymbol{\varepsilon}(\boldsymbol{u}) : \left\{[(1-d)^2 + \eta]\mathbb{C}^{\text{dev}} + \mathbb{C}^{\text{hyd}}\right\} : \boldsymbol{\varepsilon}(\boldsymbol{v})\mathrm{d}V = 0 \tag{4.52}$$

$$\begin{aligned} E_l'(\boldsymbol{u}, d)\,(\alpha) = \int_\Omega \left[-2(1-d)\,\Psi_0^{\text{dev}}\left(\boldsymbol{\varepsilon}(\boldsymbol{u})\right)\right]\alpha \mathrm{d}V + \frac{3}{8}G_c \int_\Omega \frac{\alpha}{l}\mathrm{d}V \\ + \frac{3}{4}G_c l \int_\Omega \nabla d \cdot \nabla \alpha \mathrm{d}V + \gamma \int_\Omega \langle d - d_n\rangle_- \,\alpha \mathrm{d}V = 0 \end{aligned} \tag{4.53}$$

for every $(\boldsymbol{v}, \alpha) \in W_v \times W_d$, where $E_l'(\boldsymbol{u}, d)\,(\boldsymbol{v})$ and $E_l'(\boldsymbol{u}, d)\,(\alpha)$ are the directional derivatives of the functional $E_l(\boldsymbol{u}, d)$, and W_v and W_α are the displacement and the phase-field test space, defined as

$$\begin{aligned} W_v &= \left\{\boldsymbol{v} : \Omega \to \mathbb{R}^2 \mid \boldsymbol{v} \in \boldsymbol{H}^1, \boldsymbol{v} = \boldsymbol{0} \text{ on } \Gamma_{\boldsymbol{u}}^D\right\} \\ W_\alpha &= \{\alpha : \Omega \to \mathbb{R} \mid \alpha \in H^1\} \end{aligned} \tag{4.54}$$

Equations (4.52) and (4.53) represent the weak for of the variational problem(4.50). Applying the Green's Lemma to the equations (4.52), it is possible to derive the following Euler's equations of the variational formulation

$$-\nabla \cdot \boldsymbol{\sigma}(\boldsymbol{\varepsilon}, d) = \boldsymbol{0} \tag{4.55}$$

$$-2(1-d)\,\Psi_0^{\text{dev}} + \frac{G_c}{4C_v}\left(\frac{w'(d)}{l} - 2l\Delta d\right) + \gamma\,\langle d - d_{n-1}\rangle_- = 0 \tag{4.56}$$

where equation (4.55) is the equilibrium equation, equation (4.56) the phase-field evolution equation, and $\boldsymbol{\sigma}(\boldsymbol{\varepsilon}, d)$ is the stress tensor, defined as

$$\begin{aligned} \boldsymbol{\sigma}(\boldsymbol{\varepsilon}, d) = \frac{\partial \Psi(\boldsymbol{\varepsilon}(\boldsymbol{u}), d)}{\partial \boldsymbol{\varepsilon}} = \left\{[(1-d)^2 + \eta]\mathbb{C}^{\text{dev}} + \mathbb{C}^{\text{hyd}}\right\} : \boldsymbol{\varepsilon} \\ = [(1-d)^2 + \eta]2\mu\boldsymbol{\varepsilon}^{\text{dev}} + K\text{tr}(\boldsymbol{\varepsilon})\boldsymbol{I} \end{aligned} \tag{4.57}$$

Together with the BCs

$$\boldsymbol{\sigma} \cdot \boldsymbol{n} = \mathbf{0} \quad \text{on } \Gamma_{\boldsymbol{u}}^{N} \tag{4.58}$$

$$\nabla d \cdot \boldsymbol{n} = 0 \quad \text{on } \Gamma_{d}^{N} \tag{4.59}$$

the equations (4.55) and (4.56) form the strong form of the variational problem.

We introduce now an approximation of the spaces T_u, T_p, W_u, W_p based on polynomial shape functions with local support, namely

$$\begin{aligned} \tilde{\boldsymbol{u}} &= \boldsymbol{N}_u \hat{\boldsymbol{u}} \\ \tilde{d} &= \boldsymbol{N}_d \hat{\boldsymbol{d}} \\ \tilde{\boldsymbol{v}} &= \boldsymbol{N}_u \hat{\boldsymbol{v}} \\ \tilde{\alpha} &= \boldsymbol{N}_d \hat{\boldsymbol{\alpha}} \end{aligned} \tag{4.60}$$

where $\tilde{()}$ are the approximated trials and weighting functions, $\hat{()}$ are the vectors containing the values of these functions on the mesh nodes, $\boldsymbol{N}_d$ is the vector of dimension $1 \times nn$ containing the shape function for the water pressure N_d^i, relative to an arbitrary node i of the nn nodes defined on the domain Ω by the finite element mesh, and $\boldsymbol{N}_u$ is a matrix defined as defined as in Section 4.2.2.

Based in the approximation (4.60), it is possible to derive, from (4.52) and (4.53), the following discrete version of the weak form of the problem:

$$\boldsymbol{R}_u = \int_{\Omega} \boldsymbol{B}^T \left\{ [(1-\tilde{d})^2 + \eta] \boldsymbol{D}^{\text{dev}} + \boldsymbol{D}^{\text{vol}} \right\} [\![\boldsymbol{\varepsilon}(\tilde{\boldsymbol{u}})]\!] \, \mathrm{d}V = \mathbf{0} \tag{4.61}$$

$$\begin{aligned} \boldsymbol{R}_d = \int_{\Omega} \boldsymbol{N}_d^T \left[-2(1-\tilde{d}) \, \Psi_0^{\text{dev}} \left(\boldsymbol{\varepsilon}(\tilde{\boldsymbol{u}}) \right) + \frac{3 G_c}{8 l} \right] \mathrm{d}V + \frac{3}{4} G_c l \int_{\Omega} (\nabla \boldsymbol{N}_d)^T \nabla \tilde{d} \mathrm{d}V \\ + \gamma \int_{\Omega} \boldsymbol{N}_d^T \left\langle \tilde{d} - \tilde{d}_n \right\rangle_{-} \alpha \mathrm{d}V = \mathbf{0} \end{aligned} \tag{4.62}$$

where $[\![\boldsymbol{\varepsilon}(\tilde{\boldsymbol{u}})]\!] = \boldsymbol{B}\hat{\boldsymbol{u}}$is the infinitesimal strain vector, and $\boldsymbol{D}^{\text{dev}}$ and $\boldsymbol{D}^{\text{vol}}$ are the deviatoric and the volumetric component of the elasticity matrix $\boldsymbol{D}$, defined as

$$\boldsymbol{D}^{\text{dev}} = \begin{bmatrix} \frac{4}{3}\mu & -\frac{2}{3}\mu & 0 \\ -\frac{2}{3}\mu & \frac{4}{3}\mu & 0 \\ 0 & 0 & \mu \end{bmatrix} \tag{4.63}$$

$$\boldsymbol{D}^{\mathrm{vol}} = \begin{bmatrix} \lambda + \frac{2}{3}\mu & \lambda + \frac{2}{3}\mu & 0 \\ \lambda + \frac{2}{3}\mu & \lambda + \frac{2}{3}\mu & 0 \\ 0 & 0 & 0 \end{bmatrix} \tag{4.64}$$

The systems of equations (4.61) and (4.62) is solved in a staggered way: for every loading step, each system of equations is solved for its main field ($\boldsymbol{u}$ for (4.61) and d for (4.62)) independently, using the last calculated value of the other field as a constant. These procedure is repeated in loop until a convergence condition is satisfied, namely [60]

$$\left\| \hat{\boldsymbol{d}}_{s+1} - \hat{\boldsymbol{d}}_s \right\|_\infty < \mathtt{TOL}_{stag} \tag{4.65}$$

where $s+1$ and s are the current and the previous staggered iteration, respectively. The residual $\boldsymbol{R}_u$ is linear with respect to $\boldsymbol{u}$, so the solution of the discrete equilibrium equation (4.61), with $\tilde{d}$ fixed, is obtained solving the system of equations

$$\boldsymbol{K}_{\tilde{d}} \hat{\boldsymbol{u}} = \boldsymbol{0} \tag{4.66}$$

where

$$\boldsymbol{K}_{\tilde{d}} = \int_{\Omega} \boldsymbol{B}^T \left\{ [(1-\tilde{d})^2 + \eta] \boldsymbol{D}^{\mathrm{dev}} + \boldsymbol{D}^{\mathrm{hyd}} \right\} \boldsymbol{B} \mathrm{d}V \tag{4.67}$$

Due to the presence of the Macaulay brackets, the residual $\boldsymbol{R}_d$ is linear with respect to d, so an iterative procedure has to be used to find a solution of the discrete phase-field evolution equation (4.62) at each staggered iteration within the current loading step. Using the Newton-Raphson method, the solution of (4.62), with $\tilde{\boldsymbol{u}}$ fixed, is obtained solving, at each nonlinear iteration, the system of equations

$$\boldsymbol{J}_d^k \Delta \hat{\boldsymbol{d}}^{k+1} = -\boldsymbol{R}_d^k \tag{4.68}$$

where $k+1$ and k are the current and the previous nonlinear iterations. The solution $\hat{\boldsymbol{d}}$ is updated after each nonlinear iteration, i.e.

$$\hat{\boldsymbol{d}}^{k+1} = \hat{\boldsymbol{d}}^k + \Delta \hat{\boldsymbol{d}}^{k+1} \tag{4.69}$$

The iteration loop is repeated until the residual $\boldsymbol{R}_d^k$ becomes smaller than a certain tolerance.The matrix $\boldsymbol{J}_d^k$, known as Jacobian matrix of $\boldsymbol{R}_d^k$, is defined as

$$\boldsymbol{J}_d^k = \frac{\partial \boldsymbol{R}_d^k}{\partial \hat{\boldsymbol{d}}^k} = \boldsymbol{C} + \boldsymbol{G} + \boldsymbol{P}^k \tag{4.70}$$

where

$$\boldsymbol{C} = \int_{\Omega} \boldsymbol{N}_d^T (2\psi^{dev} + \frac{3G_c}{8l}) \boldsymbol{N}_d \mathrm{d}V \tag{4.71}$$

$$\boldsymbol{G} = \frac{3l}{4} G_c \int_{\Omega} (\nabla \boldsymbol{N}_d)^T (\nabla \boldsymbol{N}_d) \mathrm{d}V \tag{4.72}$$

$$\boldsymbol{P}^k = \gamma \int_{\Omega} \boldsymbol{N}_d^T \left\langle \operatorname{sgn}\left(\tilde{d}^k - \tilde{d}_n\right) \right\rangle_- \boldsymbol{N}_d \mathrm{d}V \tag{4.73}$$

4.3.2 Mixed formulation and stabilization

Because of the volumetric-deviatoric energy split introduced in the functional (4.45), when a fracture occurs the deviatoric stiffness of the material becomes very small, in comparison with the volumetric one, which is not affected by the phase-field variable d. Therefore, a discretization that cannot treat the deviatoric and the volumetric part of the deformation independently can lead to unstable solutions when the fracture localizes. This problem is well known for elastic materials with Poisson modulus $\nu \to 0.5$ ($\lambda \to \infty$). To solve this problem a mixed formulation is generally used, that is a reformulation of the elasticity problem in which, together with the displacement $\boldsymbol{u}$, also the hydrostatic component of the stress p, defined as

$$p = \frac{\operatorname{tr}(\boldsymbol{\sigma})}{3} \tag{4.74}$$

is treated as a primary variable. This hydrostatic component p is related to the volumetric deformation of the body by the constitutive equation

$$p = K \operatorname{tr}(\boldsymbol{\varepsilon}(\boldsymbol{u})) = K \nabla \cdot \boldsymbol{u} \tag{4.75}$$

where $K = \lambda + \frac{2}{3}\mu$ is the material bulk modulus.

Following the procedure shown in [60], we now introduce a mixed formulation $\boldsymbol{u} - p - d$ of the phase-field model presented in Section 4.3.1. Taking into account the elastic constitutive relation (4.75), the volumetric part of the elastic energy (4.44) can be expressed as a function of p, namely

$$\Psi_0^{\mathrm{vol}}(p) = \frac{p^2}{2K} \tag{4.76}$$

With this definition of the volumetric part of the elastic energy density, the functional (4.49) can be rewritten as

$$E_l(\boldsymbol{u}, p, d) = \int_{\Omega} [(1-d)^2 + \eta] \underbrace{\boldsymbol{\varepsilon}(\boldsymbol{u}) : \mathbb{C}^{\mathrm{dev}} : \boldsymbol{\varepsilon}(\boldsymbol{u})}_{\Psi_0^{\mathrm{dev}}} \mathrm{d}V + \int_{\Omega} \underbrace{\frac{p^2}{2K}}_{\Psi_0^{\mathrm{vol}}} \mathrm{d}V$$
$$+ \frac{3}{8} G_c \int_{\Omega} \left(\frac{d}{l} + l \left| \nabla d \right|^2 \right) \mathrm{d}V + \frac{\gamma}{2} \int_{\Omega} \langle d - d_n \rangle_-^2 \, \mathrm{d}V \tag{4.77}$$

where the notation $E_l(\boldsymbol{u}, p, d)$ indicates that the functional E_l depends also on the hydrostatic pressure p as main variable. The evolution of the pressure is related to the volumetric deformation by the constitutive equation (4.75), which can be viewed as a constrain equation, namely

$$\nabla \cdot \boldsymbol{u} - \frac{p}{K} = 0 \tag{4.78}$$

This constrain equation can be taken into account in the variationl problem using the method of the Lagrange multipliers. We define the following lagrangian functional

$$L_l(\boldsymbol{u}, p, d, \eta) = E_l(\boldsymbol{u}, p, d) + \int_{\Omega} \eta \left(\nabla \cdot \boldsymbol{u} - \frac{p}{K} \right) \mathrm{d}V \tag{4.79}$$

where η is a Lagrange multiplier, introduced to enforce the constraint (4.78). The mixed formulation of the variational problem (4.50) reads

$$\arg\min \left\{ L_l(\boldsymbol{u}, p, d, \eta) : \ \boldsymbol{u} \in T_u, \ d \in T_p, \ d \in T_d, \ d \in T_\eta \right\} \tag{4.80}$$

where

$$\begin{aligned} T_u &= \left\{ \boldsymbol{u} : \Omega \to \mathbb{R}^2 \mid \boldsymbol{u} \in \boldsymbol{H}^1, \boldsymbol{u} = \overline{\boldsymbol{u}} \text{ on } \Gamma_{\boldsymbol{u}}^D \right\} \\ T_p &= \left\{ p : \Omega \to \mathbb{R} \mid d \in L^2 \right\} \\ T_d &= \left\{ d : \Omega \to \mathbb{R} \mid d \in H^1 \right\} \\ T_\eta &= \left\{ \eta : \Omega \to \mathbb{R} \mid \eta \in L^2 \right\} \end{aligned} \tag{4.81}$$

are the spaces of the admissible spaces for the field $\boldsymbol{u}$, p, d and η. Necessary optimality conditions for $(\boldsymbol{u}, p, d, \eta)$ ti be a minimum of $L_l(\boldsymbol{u}, p, d, \eta)$ are that

$$L_l'(\boldsymbol{u}, p, d, \eta)\,(\boldsymbol{v}) = 0 \tag{4.82}$$

$$L_l'(\boldsymbol{u}, p, d, \eta)\,(q) = 0 \tag{4.83}$$

$$L_l'(\boldsymbol{u}, p, d, \eta)\,(\alpha) = 0 \tag{4.84}$$

$$L_l'(\boldsymbol{u}, p, d, \xi)\,(\alpha) = 0 \tag{4.85}$$

for every $(\boldsymbol{v}, q, \alpha, \xi) \in W_u \times W_p \times W_d \times W_\lambda$, where

$$\begin{aligned} W_u &= \left\{ \boldsymbol{v} : \Omega \to \mathbb{R}^2 \mid \boldsymbol{v} \in \boldsymbol{H}^1, \boldsymbol{v} = \boldsymbol{0} \text{ on } \Gamma_{\boldsymbol{u}}^D \right\} \\ W_p &= \left\{ q : \Omega \to \mathbb{R} \mid d \in L^2 \right\} \\ W_d &= \left\{ \alpha : \Omega \to \mathbb{R} \mid \alpha \in H^1 \right\} \\ W_\eta &= \left\{ \xi : \Omega \to \mathbb{R} \mid \xi \in L^2 \right\} \end{aligned} \tag{4.86}$$

are the test spaces for the variation $\boldsymbol{v}$, q, α and ξ. From the condition

$$L_l'(\boldsymbol{u}, p, d, \eta)(q) = \textstyle\int_\Omega q(p - \eta) d\Omega = 0 \quad \forall \xi \in W_\lambda \tag{4.87}$$

we obtain that

$$p = \eta$$

This means that the hydrostatic stress p acts as a Lagrange multiplier in the mixed formulation. The lagrangian functional (4.79) becomes therefore

$$L_l(\boldsymbol{u}, p, d) = \int_{\Omega} [(1-d)^2 + \eta] \frac{1}{2} \boldsymbol{\varepsilon}(\boldsymbol{u}) : \mathbb{C}^{\text{dev}} : \boldsymbol{\varepsilon}(\boldsymbol{u}) \, \mathrm{d}V - \int_{\Omega} \frac{p^2}{2K} \mathrm{d}V + \int_{\Omega} p \nabla \cdot \boldsymbol{u} dV + \frac{3}{8} G_c \int_{\Omega} \left(\frac{d}{l} + l \left| \nabla d \right|^2 \right) \mathrm{d}V + \frac{\gamma}{2} \int_{\Omega} \langle d - d_n \rangle_-^2 \, \mathrm{d}V \quad (4.88)$$

and its directional derivatives (4.82), (4.83) and (4.84) read

$$L_l'(\boldsymbol{u}, p, d)(\boldsymbol{v}) = \int_{\Omega} [(1-d)^2 + \eta] \boldsymbol{\varepsilon}(\boldsymbol{u}) : \mathbb{C}^{\text{dev}} : \boldsymbol{\varepsilon}(\boldsymbol{v}) \mathrm{d}V - \int_{\Omega} \frac{p^2}{2K} \mathrm{d}V + \int_{\Omega} p \nabla \cdot \boldsymbol{v} dV = 0 \quad (4.89)$$

$$L_l'(\boldsymbol{u}, p, d)(q) = \int_{\Omega} q \left(\nabla \cdot \boldsymbol{u} - \frac{p}{K} \right) dV = 0 \quad (4.90)$$

$$L_l'(\boldsymbol{u}, p, d)(\alpha) = \int_{\Omega} \left[-2(1-d) \Psi_0^{\text{dev}}(\boldsymbol{\varepsilon}(\boldsymbol{u})) \right] \alpha \mathrm{d}V + \frac{3}{8} G_c \int_{\Omega} \frac{\alpha}{l} \mathrm{d}V + \frac{3}{4} G_c l \int_{\Omega} \nabla d \cdot \nabla \alpha \mathrm{d}V + \gamma \int_{\Omega} \langle d - d_n \rangle_- \alpha \mathrm{d}V = 0 \quad (4.91)$$

for every $(\boldsymbol{v}, q, \alpha) \in W_u \times W_p \times W_d$. After the application of the Green's lemma to the equations (4.89) and (4.91), we ca derived the strong form of the mixed variational formulation, which consists into the differential equations

$$-\nabla \cdot \left[\mathbb{C}^{\text{dev}} : \boldsymbol{\varepsilon}(\boldsymbol{u}) + p \boldsymbol{I} \right] = 0 \quad (4.92)$$

$$\frac{p}{K} - \nabla \cdot \boldsymbol{u} = 0 \quad (4.93)$$

$$-2(1-d) \Psi_0^{\text{dev}} + \frac{G_c}{4C_v} \left(\frac{w'(d)}{l} - 2l\Delta d \right) + \gamma \langle d - d_{n-1} \rangle_- = 0 \quad (4.94)$$

valid on the domain Ω, together with the BCs

$$\boldsymbol{\sigma} \cdot \boldsymbol{n} = \boldsymbol{0} \quad \text{on } \Gamma_{\boldsymbol{u}}^N \tag{4.95}$$

$$\nabla d \cdot \boldsymbol{n} = 0 \quad \text{on } \Gamma_d^N \tag{4.96}$$

where

$$\boldsymbol{\sigma}(\boldsymbol{\varepsilon}, p, d) = [(1-d)^2 + \eta]\mathbb{C}^{\text{dev}} : \boldsymbol{\varepsilon} + \boldsymbol{I}p$$

The Finite Element discretization can be obtained following a procedure similar to the one exposed in Section 4.3.1. Once defined the following approximation of the solution

$$\begin{aligned} \tilde{\boldsymbol{u}} &= \boldsymbol{N}_u \hat{\boldsymbol{u}} \\ \tilde{p} &= \boldsymbol{N}_p \hat{\boldsymbol{p}} \\ \tilde{d} &= \boldsymbol{N}_d \hat{\boldsymbol{d}} \end{aligned} \tag{4.97}$$

where $\boldsymbol{N}_u$, $\boldsymbol{N}_p$ and $\boldsymbol{N}_d$ are the shape functions, defined in the previous sections and used also to interpolate the test function, the following discrete version of the weak form of the problem:

$$\boldsymbol{R}_u = \int_\Omega \boldsymbol{B}^T \left\{ [(1-\tilde{d})^2 + \eta] \boldsymbol{D}^{\text{dev}} \right\} [\![\boldsymbol{\varepsilon}(\tilde{\boldsymbol{u}})]\!] \, \mathrm{d}V + \int_\Omega \boldsymbol{b}^T \tilde{p} \mathrm{d}V = \boldsymbol{0} \tag{4.98}$$

$$\boldsymbol{R}_p = \int_\Omega \boldsymbol{B}^T \nabla \cdot \tilde{\boldsymbol{u}} \mathrm{d}V + \int_\Omega \boldsymbol{N}_p^T \frac{\tilde{p}}{K} \mathrm{d}V = \boldsymbol{0} \tag{4.99}$$

$$\begin{aligned} \boldsymbol{R}_d = \int_\Omega \boldsymbol{N}_d^T \left[-2(1-\tilde{d}) \, \Psi_0^{\text{dev}} \left(\boldsymbol{\varepsilon}(\tilde{\boldsymbol{u}}) \right) + \frac{3 G_c}{8 l} \right] \mathrm{d}V + \frac{3}{4} G_c l \int_\Omega (\nabla \boldsymbol{N}_d)^T \nabla \tilde{d} \mathrm{d}V \\ + \gamma \int_\Omega \boldsymbol{N}_d^T \left\langle \tilde{d} - \tilde{d}_n \right\rangle_- \alpha \mathrm{d}V = \boldsymbol{0} \end{aligned} \tag{4.100}$$

where $\boldsymbol{R}_u$, $\boldsymbol{R}_p$ and $\boldsymbol{R}_d$ are the residuals vector. The residual $\boldsymbol{R}_d$ is identical to the one obtained in Section 4.3.1. Therefore, using a staggered procedure, in which the nonlinear system of equations (4.100) is solved independently from the ones related to the other fields, the solution of (4.100) can be solved using exactly the nonlinear procedure exposed in Section 4.3.1. On the other hand, equations (4.98) and (4.99) are solved with a monolithic approach, which leads to the following linear system of equations:

$$\begin{bmatrix} \boldsymbol{K}_{\tilde{d}}^{\text{dev}} & \boldsymbol{Q} \\ \boldsymbol{Q}^T & -\boldsymbol{M} \end{bmatrix} \begin{Bmatrix} \hat{\boldsymbol{u}} \\ \hat{\boldsymbol{p}} \end{Bmatrix} = \begin{Bmatrix} \boldsymbol{0} \\ \boldsymbol{0} \end{Bmatrix} \tag{4.101}$$

where

$$\boldsymbol{K}_{\tilde{d}}^{\mathrm{dev}} = \int_{\Omega} [(1-\tilde{d})^2 + \eta] \boldsymbol{B}^T \boldsymbol{D}^{\mathrm{dev}} \boldsymbol{B} \mathrm{d}V \tag{4.102}$$

$$\boldsymbol{Q} = \int_{\Omega} \boldsymbol{b}^T \boldsymbol{N}_p \mathrm{d}V \tag{4.103}$$

$$\boldsymbol{M} = \int_{\Omega} \frac{1}{K} \boldsymbol{N}_p^T \boldsymbol{N}_p \mathrm{d}V \tag{4.104}$$

We focus now on the problem of the stability of the formulation. As we saw in the previous section, to ensure the stability of the solution of the mixed formulation, the choice of the shape functions $\boldsymbol{N}_u$and $\boldsymbol{N}_p$ has to satisfy the LBB condition. The combination of quadratic displacements and linear pressure interpolations (Q9P4 for quadrilateral finite elements) satisfies this condition, while the combination of linear displacements and linear pressure interpolations (Q4P4 for quadrilateral finite elements) does not. If we look at the structure of the system of equations (4.101), when the matrix $\boldsymbol{M}$ is zero, we can notice a clear analogy with the structure of the system (4.30), characterizing the numerical solution of the Stokes equations. This is the case of materials with very high volumetric stiffness K, or, as in our case, when, due to the evolution of the phase-field d in a model with a volumetric-deviatoric split of the energy, the deviatoric stiffness becomes very small compared to the volumetric one.

In order to stabilize the solution obtained with the linear-displacements/linear-pressure quadrilateral elements Q4P4, we add to the system (4.101) a stabilization term $\boldsymbol{S}^{pf}$ defined again using the pressure-projection technique exposed in Section 4.2.

As we saw in Section 4.2, the choice of the stabilization coefficient c^{stab}, which depends on a scalar value representative of the damaged tensor

$$\mathbb{C}_d^{\mathrm{dev}} = [(1-\tilde{d})^2 + \eta] \mathbb{C}^{\mathrm{dev}} \tag{4.105}$$

$\boldsymbol{D}^{dev}$, plays an important role in the performance of the stabilized solution. Following the rule (4.38), we define the stabilization coefficient as

$$c^{stab} = (\mathrm{tr}(\mathbb{C}_d^{\mathrm{dev}})/n)^{-1} = \frac{4}{3\mu[(1-\tilde{d})^2 + \eta]} \tag{4.106}$$

The matrix $\boldsymbol{S}^{pf}$ is defined than as

$$\boldsymbol{S}^{pf} = \int_{\Omega} c^{stab} (\boldsymbol{N}_p - \mathit{\Pi} \boldsymbol{N}_p)^T (\boldsymbol{N}_p - \mathit{\Pi} \boldsymbol{N}_p) \mathrm{d}V \tag{4.107}$$

The stabilized counterpart of the mixed formulation (4.101) is defined as

$$\begin{bmatrix} \boldsymbol{K}_{\bar{d}}^{\mathrm{dev}} & \boldsymbol{Q} \\ \boldsymbol{Q}^T & -\boldsymbol{M} - \boldsymbol{S}^{pf} \end{bmatrix} \begin{Bmatrix} \hat{\boldsymbol{u}} \\ \hat{\boldsymbol{p}} \end{Bmatrix} = \begin{Bmatrix} \boldsymbol{0} \\ \boldsymbol{0} \end{Bmatrix} \tag{4.108}$$

4.3.3 Numerical examples

We present now two numerical examples, a one- and a two-dimensional problem, in order to test the performance of different finite element interpolations. In particular, for both the examples, we consider interpolations with with quadrilateral elements Q4/Q4 and Q9/Q4 for the formulation $\boldsymbol{u} - d$, and with the quadrilateral elements Q4P4/Q4, Q4P4s/Q4 and Q9P4/Q4 for the mixed formulation $\boldsymbol{u} - p - d$. The interpolations used for each of these elements are specified in Table 4.1, including an indication of the field in which, if present, the stabilization is applied. In the notation used to identify the elements, the interpolation of the phase-field d is separated by the symbol "/", in order to point out that we use a staggered procedure in which the phase-field equation is solved separately from the other fields. We choose a linear interpolation for the phase-field for all the finite elements considered, in order to enable a better comparison of the results.

	$\boldsymbol{u}$	p	d
Q4/Q4	linear	-	linear
Q9/Q4	quadratic	-	linear
Q4P4/Q4	linear	linear	linear
Q4P4s/Q4	linear	linear - stabilized	linear
Q9P4/Q4	quadratic	linear	linear

Table 4.1: Summary of the different finite elements used for the numerical applications in Section 4.3.3, including the the degree of interpolation used for each field.

With regard to the choice of the penalty coefficient introduced to enforce the irreversibility of the phase-field, we recall the expression (2.144) derived in [26], which for the AT1 model used in this chapter gives

$$\gamma = \frac{G_c}{l} \frac{27}{64 \mathtt{TOL}_{\mathtt{ir}}^2} \tag{4.109}$$

In particular, in [26] the value

$$\mathtt{TOL}_{\mathtt{ir}} = 0.01 \tag{4.110}$$

has been suggested as a practical irreversibility threshold, which leads to

$$\gamma = \frac{G_c}{l}\frac{27}{64 \cdot 0.01^2} \simeq 4000\frac{G_c}{l} \tag{4.111}$$

This expression is used in all the phase-field numerical simulations in this chapter, together with the condition

$$d\left(x, t=0\right) = d_0\left(x\right) = 0, \quad \forall x \in \Omega \cup \Gamma_d^N \tag{4.112}$$

which ensure also the fulfillment of the positiveness constraint

$$d > 0 \tag{4.113}$$

necessary fir the AT1 model (see Section 2.3.3).

One dimensional tension test

In this example we study the numerical solution of the tension test of a bar, with the dimensions shown in Figure 4.3 . The mesh is composed by a regular grid of square elements, with side $h_{el} = 0.01\,m$, and plane strain conditions are assumed. The problems is solved in control of displacement, so a Dirichlet boundary condition $u_x = -\Delta t$ (Δt being the time step) is imposed on the left boundary, while the right one is assumed fixed. Concerning the phase-field variable d, homogeneous Dirichlet boundary conditions are imposed on both sides, in order to maintain the symmetry of the phase-field solution, thus promoting the localization of the fracture in the center of the domain. The parameters of the model are: $E = 1\,Pa$, $\nu = 0,4$, $G_c = 1\,N/m$, $l = 0.005\,m$, $\eta = 10^{-8}, \Delta t = 0,05\,s$. We perform $N_{ts} = 80$ time steps, with a tolerance $\texttt{TOL}_{p-f} = 10^{-8}$ for the phase-field Newton-Raphson iterative scheme, and a tolerance $\texttt{TOL}_{stag} = 10^{-5}$ for the staggered loop. The localization of the fracture occurs at $t_{loc} = 2,7\,s$.

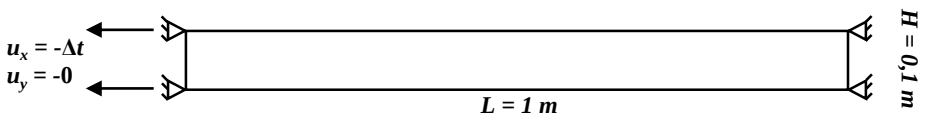

Figure 4.3: Scheme of the problem

Figure 4.4.a shows the profile of the phase-field d obtained, at $t_{end} = 4\,s$, with the standard elements Q9/Q4 and Q4/Q4. The two solutions are compared with the

one obtained analytically [60]. Starting from the element Q9/Q4, we can see that the analytical solution is almost perfectly recovered. The small plateau obtain in correspondence of the cusp of the analytic optimal profile, which has the dimension of one single finite element, is due to the numerical approximation, and will tend to disappear for an element dimension $h_{el} \to 0$. On the other hand, the element Q4/Q4 shows a localization width way significantly larger than the analytical one, with a round profile at the peak instead of the cusp that characterizes the analytical solution. This is how the locking phenomenon manifest itself when the fracture localizes, that is when the deviatoric stiffness, degraded by the phase-field, becomes very small in comparison with the volumetric one.

In Figure 4.4.b we compare the analytical profile with the one obtained with the mixed finite elements Q4P4/Q4, Q4P4s/Q4, Q9P4/Q4. In this case we can notice that all the solutions reproduce very well the analytical one. However the profile obtained with the element Q4P4/Q4 is a slightly wider than the one obtained with the stabilized element Q4P4s/Q4, whose solution coincides with the one of the stable Q9P4/Q4.

In order to compare the general behavior of all the elements, in Figure 4.5 we plot the force-displacement curve relative to all the numerical solutions. We notice that, after the localization of the fracture, the reaction force goes to zero for all the elements, except for the Q4/Q4. This due to an excess of residual stiffness, again characteristic of a locking behavior. A confirmation of this can be obtained by looking at the maximum values of d corresponding to the peak of the damage: while for all the other elements d reaches the unity, with the element Q4/Q4 we have $d \to 1$ but always $d < 1$.

According to these results, except for a small difference in the width of the localization profile, the mixed element Q4P4/Q4 seems to behave as well as the elements Q9/Q4, Q4P4s/Q4 and Q9P4/P4. However, the positive effect of the stabilization becomes evident if we look at the profile of the hydrostatic stress p, obtained with the mixed elements after the localization. In Figure 4.6 we can clearly see that, while the hydrostatic stress at the crack obtained with the stabilized element Q4P4s/Q4 are in good agreement with the one obtained with the stable Q9P4/Q4, the unstable element Q4P4/Q4 leads to large oscillations.

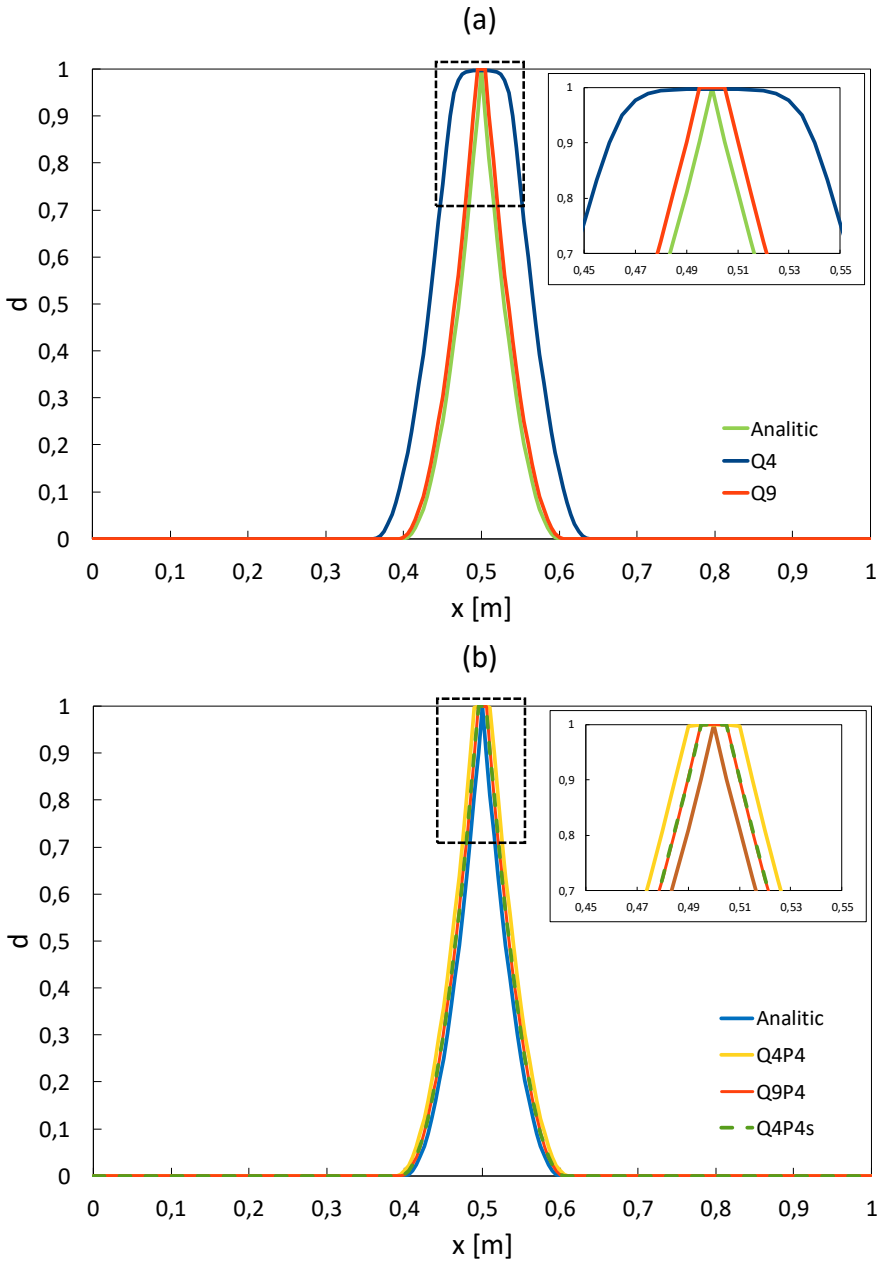

Figure 4.4: Phase field profiles at $t_{end} = 4\,s$: in (a) standard $u - d$ formulation, in (b) mixed $u - p - d$ formulation.

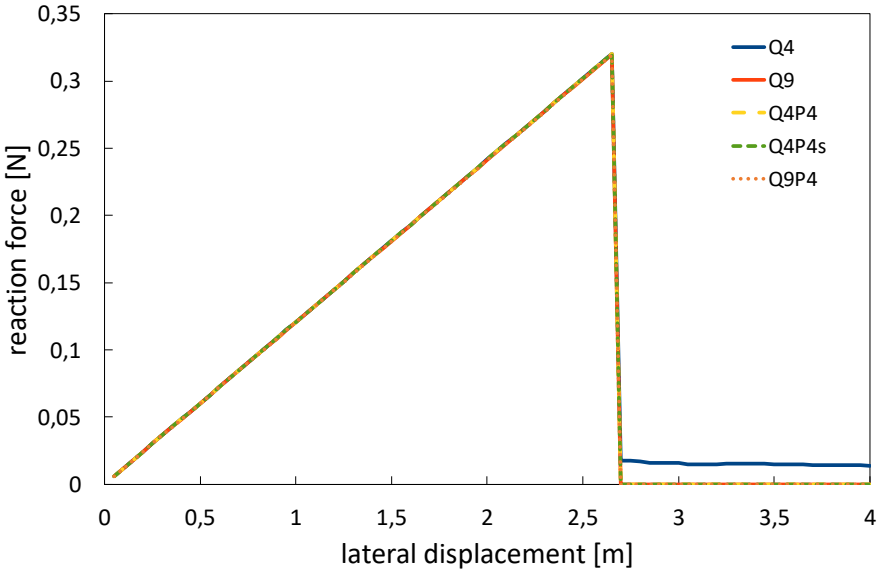

Figure 4.5: Reaction force vs applied displacement curve.

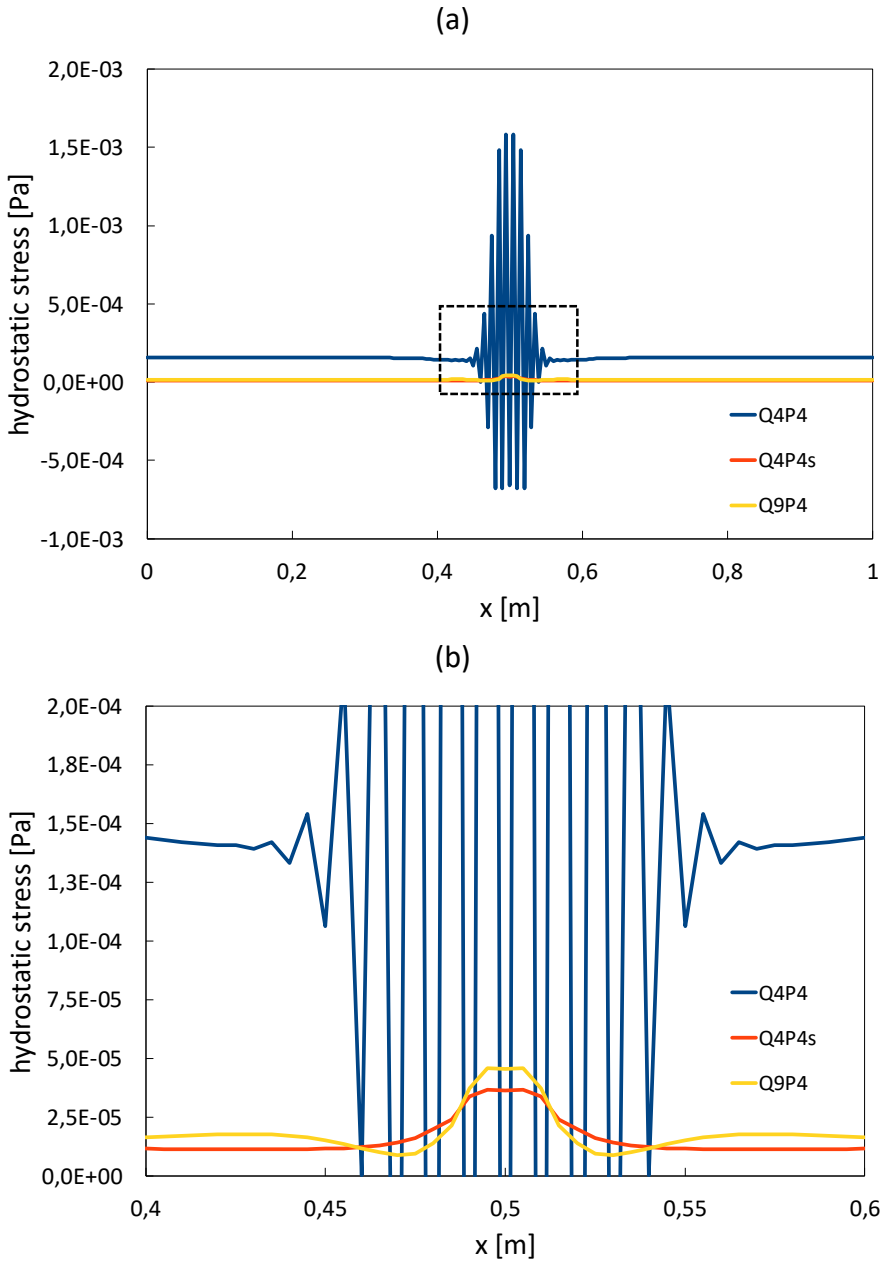

Figure 4.6: Hydrostatic stress p at $t_{end} = 4\,s$ for the mixed $\boldsymbol{u} - p - d$ formulation: (a) interval [0, 1], (b) interval [0.4, 0.6].

Two dimensional shear test

In this example we study the development of a shear fracture in a rectangular domain subjected to lateral compression. This problem, with different dimensions, has been already solved in [60], in order to show the stability of the mixed element Q9P4/Q4, compared to the standard one Q4/Q4. We recompute this example considering all the elements used in the previous one. The mesh is composed by square elements with

side $h_{el} = 0,005\,m$, and the dimensions of the domain are shown in Figure 4.7 along with the BCs. In this case, on the left side we apply symmetry boundary conditions, so no Dirichlet conditions are imposed on the vertical displacements u_y and on the phase-field d. Again the problem is solved in control of displacements, with $u_x = -\Delta t$ on the left side boundary. The parameters of the model are: $E = 1\,kPa$, $\nu = 0,3$, $G_c = 1\,N/m$, $l = 0.02\,m$, $\eta = 10^{-8}$, $\Delta t = 2,5\text{e}^{-4}\,s$. We perform $N_{ts} = 320$ time steps, with a tolerance $\texttt{TOL}_{p-f} = 10^{-8}$ for the phase-field Newton-Raphson iterative scheme, and a tolerance $\texttt{TOL}_{stag} = 10^{-5}$ for the staggered loop. The localization of the fracture occurs at $t_{loc} = 0,07525\,s$.

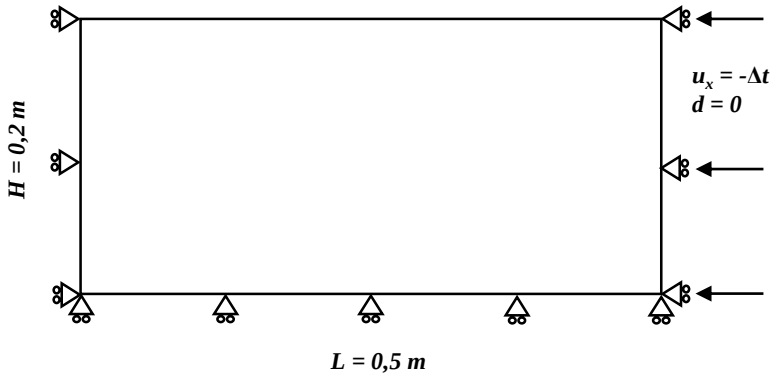

Figure 4.7: Scheme of the problem of shear fracture under compressive load.

In Figure 4.8 we show the contours of the phase-field d obtained at the end of the simulation with the different finite elements. Between the standard elements, we can again notice how the Q9/Q4 element shows a good behavior, leading to a fracture that localizes along an inclined shear band, starting from the center of the domain (considering the symmetry). The standard Q4/Q4 element, instead, localizes along a thick vertical crack, whose width is not controlled by the internal length l anymore. Focusing on the mixed elements, we notice that the stable Q9P4/Q4 and the stabilized Q4P4s/Q4 lead to a good solution, very similar to the one of the standard Q9/Q4. Finally, the unstable Q4P4/Q4 shows, as in the previous example, a width slightly broader than with the stabilized Q4P4s/Q4, but with a localization of the crack along an intermediate pattern among the ones obtained with the other elements.

In Figure 4.9 we show the same results, this time obtained with elements of dimension $h_{el} = 0,01\,m$, that is the coarsest regular mesh respecting the condition $h_{el} \leq l/2$, essential for a correct prediction of the localization profile. In this case

the model discretized with the unstable mixed element Q4P4/Q4 cannot capture at all the shear mode evolution of the fracture, while the standard Q9/Q4, the mixed Q4P4s/Q4 and Q9P4/Q4 can. In particular the element Q4P4s/Q4 seems to behave better than the element Q9P4/Q4 in terms of pattern of the localization profile, but still not as good as the element Q9P4/Q4 in terms of fracture width.

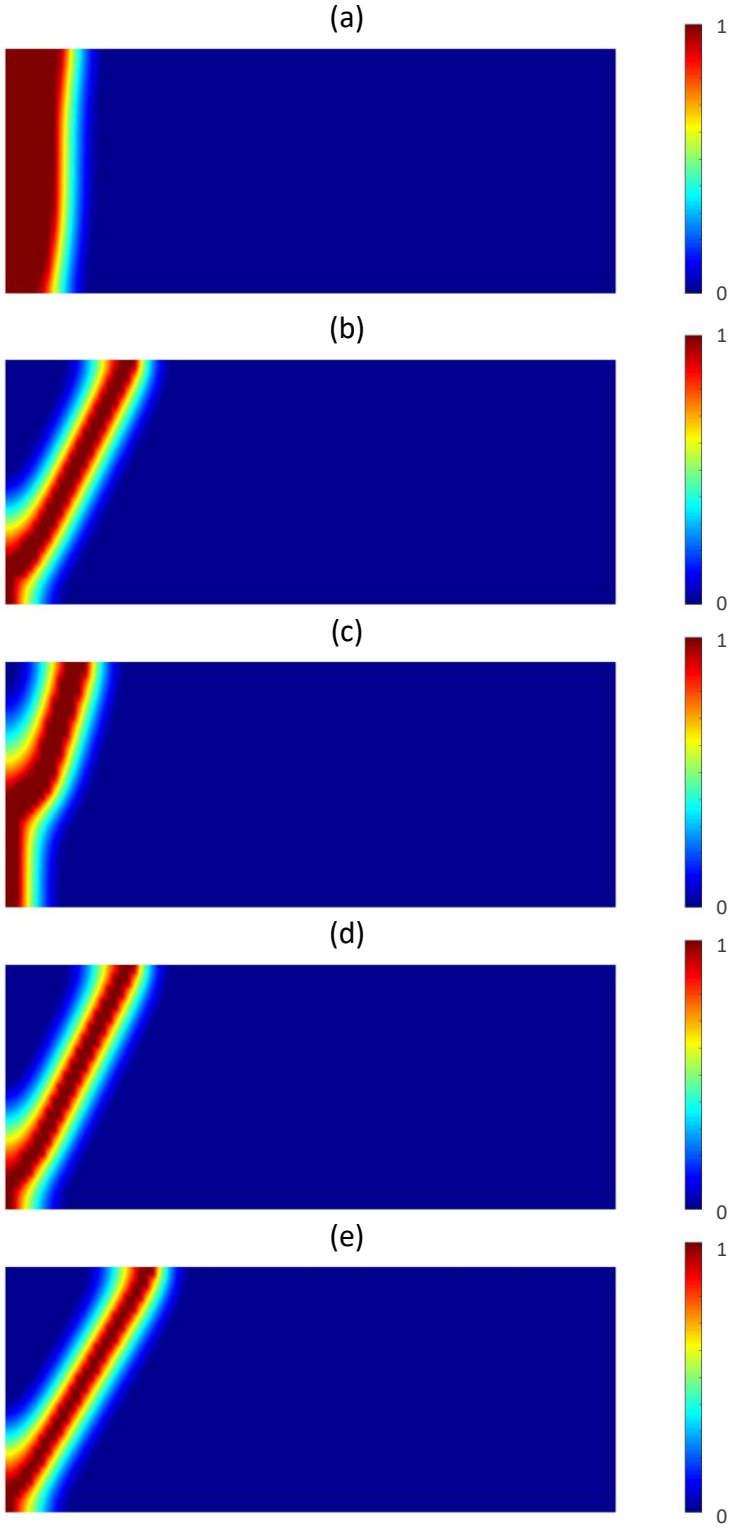

Figure 4.8: Contours of the phase-field d at $t = 0,08\,s$, for $l = 0,005\,m$: (a) Q4/Q4, (b) Q9/Q4, (c) Q4P4/Q4, (d) Q4P4s/Q4, (e) Q9P4/Q4.

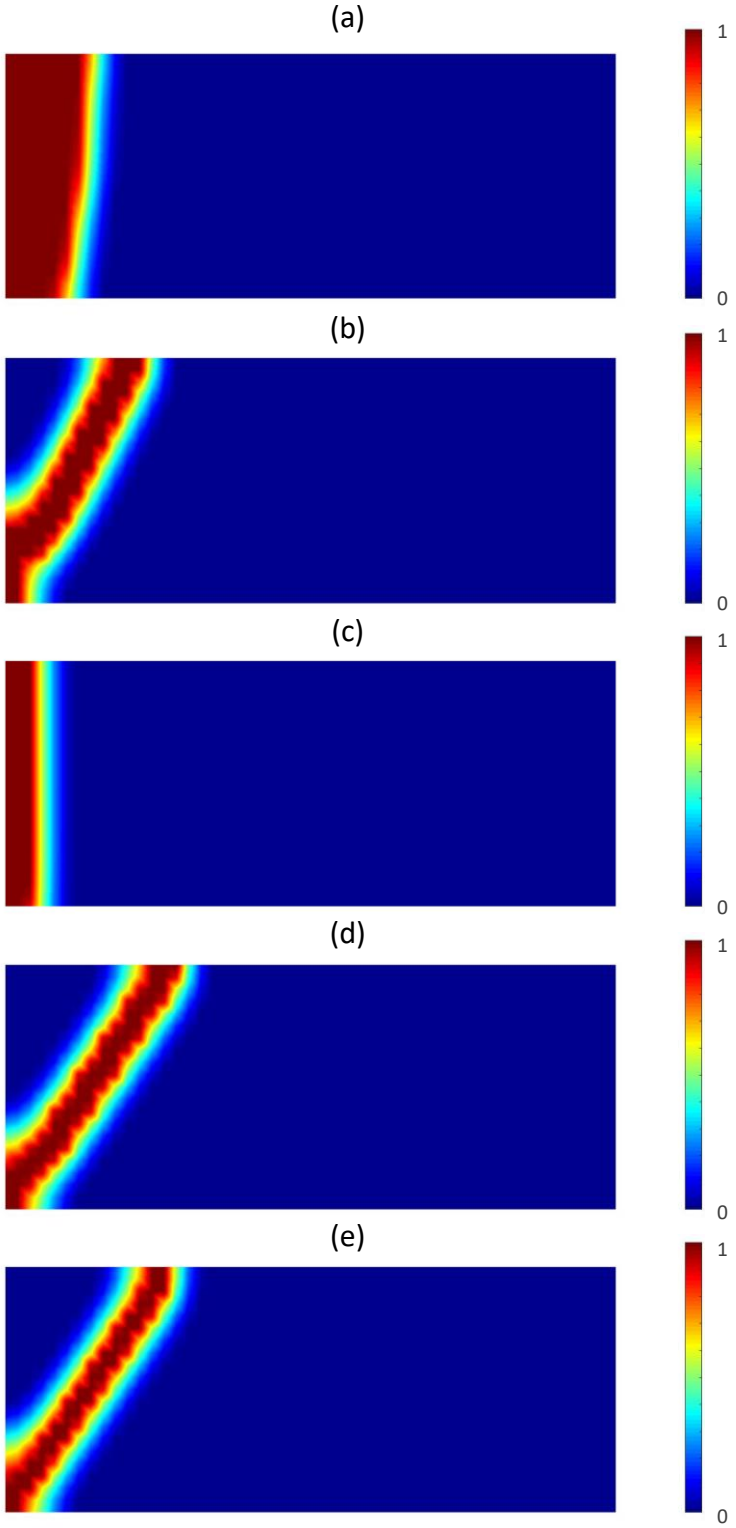

Figure 4.9: Contours of the phase-field d at $t = 0,08\,s$, for $l = 0,01\,m$: (a) Q4/Q4, (b) Q9/Q4, (c) Q4P4/Q4, (d) Q4P4s/Q4, (e) Q9P4/Q4.

4.4 Phase-field model of fractures in a saturated porous medium

4.4.1 Mathematical formulation

In this section we aim to combine the model for fluid flow in a saturated elastic porous media, shown in Section 4.2, with the phase-field model for fracture with volumetric-deviatoric energy split, shown in Section 4.4.

If we add the phase-field equation (4.56) to the system of equations (4.7) and (4.8), we obtain

$$\nabla \cdot \left\{ [(1-d)^2 + \eta] \boldsymbol{D}^{dev} + \boldsymbol{D}^{idr} \right\} : \nabla^s \boldsymbol{u} - \nabla p^w + \rho \boldsymbol{g} = 0 \tag{4.114}$$

$$\nabla \cdot \dot{\boldsymbol{u}} - \nabla \cdot \left[\frac{k^w}{\rho^w g} \boldsymbol{I} \cdot (\nabla p^w - \rho^w \boldsymbol{g}) \right] = 0 \tag{4.115}$$

$$-2(1-d)\,\Psi_0^{\mathrm{dev}} + \frac{G_c}{4C_v}\left(\frac{w'(d)}{l} - 2l\Delta d\right) + \gamma \left\langle d - d_{n-1} \right\rangle_- = 0 \tag{4.116}$$

where the linear elastic constitutive equation (4.5) for $\boldsymbol{\sigma}^e$ has been replaced by the following constitutive relation

$$\boldsymbol{\sigma}^e = \left\{ [(1-d)^2 + \eta] \boldsymbol{D}^{\mathrm{dev}} + \boldsymbol{D}^{\mathrm{vol}} \right\} : \boldsymbol{\varepsilon} \tag{4.117}$$

that is, the same constitutive relation used in Section 4.4. The ICs and BCs of the problem are

$$\begin{array}{ll} \boldsymbol{u} = \boldsymbol{u}_0 & \text{at } t = 0 \\ p^w = p_0^w & \text{at } t = 0 \\ \boldsymbol{u} = \overline{\boldsymbol{u}} & \text{on } \Gamma_{\boldsymbol{u}}^D \\ p^w = \bar{p}^w & \text{on } \Gamma_{p^w}^D \\ \boldsymbol{\sigma} \cdot \boldsymbol{n} = \bar{\boldsymbol{t}} & \text{on } \Gamma_{\boldsymbol{u}}^N \\ \boldsymbol{v}^{ws} \cdot \boldsymbol{n} = \bar{q} & \text{on } \Gamma_q^N \\ \nabla d \cdot \boldsymbol{n} = 0 & \text{on } \Gamma_d^N \end{array} \tag{4.118}$$

Following the same procedure of Section 4.2, we apply the Weighted Residual Method and, after the discretization in time and space, we obtain the following expression for the residuals:

$$\boldsymbol{R}_u = \int_\Omega \boldsymbol{B}^T \left\{ [(1-\tilde{d}_{n+1})^2 + \eta] \boldsymbol{D}^{\mathrm{dev}} + \boldsymbol{D}^{\mathrm{vol}} \right\} [\![\boldsymbol{\varepsilon}(\tilde{\boldsymbol{u}}_{n+1})]\!] \, \mathrm{d}V - \int_\Omega \boldsymbol{b}^T \tilde{p}_{n+1}^w \mathrm{d}V$$
$$- \int_\Omega \boldsymbol{N}_u^T \rho \boldsymbol{g} \mathrm{d}V - \int_{\Gamma_{\boldsymbol{u}}} \boldsymbol{N}_u^T \bar{\boldsymbol{t}}_{n+1} \mathrm{d}\Gamma = \boldsymbol{0} \tag{4.119}$$

$$\boldsymbol{R}_p = \int_\Omega \boldsymbol{B}^T \nabla \cdot \frac{\tilde{\boldsymbol{u}}_{n+1} - \tilde{\boldsymbol{u}}_n}{\Delta t} \mathrm{d}V + \int_\Omega (\nabla \boldsymbol{N}_p)^T \frac{k^w \mathbf{I}}{\rho^w g} (\nabla \tilde{p}^w_{n+1} - \rho^w \boldsymbol{g}) \mathrm{d}V + \int_{\Gamma_{p^w}} \boldsymbol{N}_p^T \bar{q}_{n+1} \mathrm{d}\Gamma = \mathbf{0} \tag{4.120}$$

$$\boldsymbol{R}_d = \int_\Omega \boldsymbol{N}_d^T \left[-2(1-\tilde{d})\, \Psi_0^{\mathrm{dev}} \left(\boldsymbol{\varepsilon}(\tilde{\boldsymbol{u}}_{n+1}) \right) + \frac{3 G_c}{8 l} \right] \mathrm{d}V + \frac{3}{4} G_c l \int_\Omega (\nabla \boldsymbol{N}_d)^T \nabla \tilde{d}_{n+1} \mathrm{d}V + \gamma \int_\Omega \boldsymbol{N}_d^T \left\langle \tilde{d}_{n+1} - \tilde{d}_n \right\rangle_- \alpha \mathrm{d}V = \mathbf{0} \tag{4.121}$$

Again, following the same staggered procedure explained in Section 4.3.1, the problem is split into the two sub-problem, solved for the pair $(\boldsymbol{u}, p^w)$ and for the phase-field d independently. The residual $\boldsymbol{R}_d$ is identical to the one obtained in Section 4.3.1 and the same nonlinear solution scheme is adopted. The fully-coupled sub-problem (4.119) and (4.120) is solved with a monolithic approach, which leads to the linear system

$$\begin{bmatrix} \boldsymbol{K}_{\tilde{d}}^{\mathrm{dev}} & \boldsymbol{Q} \\ \boldsymbol{Q}^T & \Delta t \boldsymbol{H} \end{bmatrix} \begin{Bmatrix} \hat{\boldsymbol{u}} \\ \hat{\boldsymbol{p}}^w \end{Bmatrix}_{n+1} = \begin{bmatrix} \mathbf{0} & \mathbf{0} \\ \boldsymbol{Q}^T & \mathbf{0} \end{bmatrix} \begin{Bmatrix} \hat{\boldsymbol{u}} \\ \hat{\boldsymbol{p}}^w \end{Bmatrix}_{n} + \begin{Bmatrix} \boldsymbol{f}_u \\ \Delta t \boldsymbol{f}_p \end{Bmatrix}_{n+1} \tag{4.122}$$

where $\boldsymbol{K}_{\tilde{d}}^{\mathrm{dev}}$, $\boldsymbol{Q}$, $\boldsymbol{H}$, $\boldsymbol{C}$, $\boldsymbol{G}$, $\boldsymbol{f}_u$ and $\boldsymbol{f}_p$ are defined in the previous sections.

In this case, when deviatoric fractures develops under undrained conditions, both the instabilities analyzed in Section 4.2 and Section 4.3 can appear. The use of a stabilized element Q4Pw4s for the problem (4.122), together with a linear interpolation (Q4) of the phase-field, is expected to be stable under undrained condition, and to become unstable when the fracture develops. The Taylor-Hood element Q9Pw4/Q4 is stable with respect to the undrained condition and, as it has been shown in the numerical application in Section 4.2.4, can lead to acceptable results for the phase-field. Anyway none of these elements is, on principle, stable when the fracture localizes. In the next section we derive two possible mixed formulations, stable both under undrained and fractured conditions.

4.4.2 Mixed formulations and stabilization

As we did for Section 4.3.2, we want to derive a mixed formulation of the model introduced in the previous section. We focus only on the poromechanical sub-problem, governed by equations (4.114) and (4.115), based on the fact that the phase-field equation is solved independently in the staggered procedure adopted. Following the same

procedure of Section 4.3.2, we can derive a mixed formulation of equation (4.114), leaving unchanged equation (4.115), obtaining the system of differential equations

$$\nabla \cdot \left\{ [(1-d)^2 + \eta] \boldsymbol{D}^{\text{dev}} \right\} : \nabla^s \boldsymbol{u} + \nabla(p^e - p^w) + \rho \boldsymbol{g} = \boldsymbol{0} \tag{4.123}$$

$$\frac{p^e}{K} - \nabla \cdot \boldsymbol{u} = 0 \tag{4.124}$$

$$\nabla \cdot \dot{\boldsymbol{u}} - \nabla \cdot \left[\frac{k^w}{\rho^w g} \boldsymbol{I} \cdot (\nabla p^w - \rho^w \boldsymbol{g}) \right] = 0 \tag{4.125}$$

where p^e is the hydrostatic component of the effective stress tensor $\boldsymbol{\sigma}^e$, defined through the effective stress principle (4.4). Equation (4.124) is, therefore, the volumetric part of the elastic constitutive equation (4.117).We apply again the Weighted Residual Method and, after the discretization in time and space, we obtain the following system of equations:

$$\begin{bmatrix} \boldsymbol{K} & \boldsymbol{Q} & -\boldsymbol{Q} \\ \boldsymbol{Q}^T & -\boldsymbol{M} & \boldsymbol{0} \\ \boldsymbol{Q}^T & \boldsymbol{0} & \Delta t \boldsymbol{H} \end{bmatrix} \begin{Bmatrix} \hat{\boldsymbol{u}} \\ \hat{\boldsymbol{p}}^e \\ \hat{\boldsymbol{p}}^w \end{Bmatrix}_{n+1} = \\ = \begin{bmatrix} \boldsymbol{0} & \boldsymbol{0} & \boldsymbol{0} \\ \boldsymbol{0} & \boldsymbol{0} & \boldsymbol{0} \\ \boldsymbol{Q}^T & \boldsymbol{0} & \boldsymbol{0} \end{bmatrix} \begin{Bmatrix} \hat{\boldsymbol{u}} \\ \hat{\boldsymbol{p}}^e \\ \hat{\boldsymbol{p}}^w \end{Bmatrix}_{n} + \begin{Bmatrix} \boldsymbol{f}_u \\ \boldsymbol{0} \\ \Delta t \boldsymbol{f}_p \end{Bmatrix}_{n+1} \tag{4.126}$$

to be solved together with the phase-field equation (4.120). Based on the main variables of the problem, we call this formulation $\boldsymbol{u} - p^e - p^w - d$.

Now, looking at the structure of the matrix on the left side of equation (4.126), we can notice that both equations for the fields p^e and p^w are coupled with the equation for the displacement field $\boldsymbol{u}$. In the perspective of the stability of the formulation it will be necessary either to use stable finite elements, like the quadrilateral element Q9Pe4Pw4 (quadratic-displacement/linear-effective pressure/linear water-pressure), or to define a stabilization term for both fields and dealing with the problem of the correct balance between the two stabilizations.

A possibility to reduce the number of couplings is to perform a change of variables, based on the effective stress principle for the volumetric component of the stresses, namely

$$p^t = p^e - p^w \tag{4.127}$$

where p^t is the hydrostatic part of the total stress tensor $\boldsymbol{\sigma}^t$. After applying the change of variables (4.127), the system of equations (4.123), (4.124) and (4.125) becomes

$$\nabla \cdot \left\{ [(1-d)^2 + \eta] \boldsymbol{D}^{\text{dev}} \right\} : \nabla^s \boldsymbol{u} + \nabla p^t + \rho \boldsymbol{g} = \boldsymbol{0} \tag{4.128}$$

$$\frac{(p^t + p^w)}{K} - \nabla \cdot \boldsymbol{u} = 0 \tag{4.129}$$

$$\nabla \cdot \dot{\boldsymbol{u}} - \nabla \cdot \left[\frac{k^w}{\rho^w g} \boldsymbol{I} \cdot (\nabla p^w - \rho^w \boldsymbol{g}) \right] = 0 \tag{4.130}$$

We can notice that the equation (4.130) is still directly depending from the displacements $\boldsymbol{u}$. But if we take the total time derivative of equation (4.129), namely

$$\nabla \cdot \dot{\boldsymbol{u}} = \frac{(\dot{p}^t + \dot{p}^w)}{K} \tag{4.131}$$

and we insert equation (4.131) into (4.130), we obtain the system of differential equations

$$\nabla \cdot \left\{ [(1-d)^2 + \eta] \boldsymbol{D}^{\text{dev}} \right\} : \nabla^s \boldsymbol{u} + \nabla p^t + \rho \boldsymbol{g} = \boldsymbol{0} \tag{4.132}$$

$$\frac{(p^t + p^w)}{K} - \nabla \cdot \boldsymbol{u} = 0 \tag{4.133}$$

$$\frac{(\dot{p}^t + \dot{p}^w)}{K} - \nabla \cdot \left[\frac{k^w}{\rho^w g} \boldsymbol{I} \cdot (\nabla p^w - \rho^w \boldsymbol{g}) \right] = 0 \tag{4.134}$$

We apply again the Weighted Residual Method and, after the discretization in time and space, we obtain the following corresponding system of equations:

$$\begin{bmatrix} \boldsymbol{K} & \boldsymbol{Q} & \boldsymbol{0} \\ \boldsymbol{Q}^T & -\boldsymbol{M} & -\boldsymbol{M} \\ \boldsymbol{0} & \boldsymbol{M} & \boldsymbol{M} + \Delta t \boldsymbol{H} \end{bmatrix} \begin{Bmatrix} \hat{\boldsymbol{u}} \\ \hat{\boldsymbol{p}}^t \\ \hat{\boldsymbol{p}}^w \end{Bmatrix}_{n+1} =$$

$$= \begin{bmatrix} \boldsymbol{0} & \boldsymbol{0} & \boldsymbol{0} \\ \boldsymbol{0} & \boldsymbol{0} & \boldsymbol{0} \\ \boldsymbol{0} & \boldsymbol{M} & \boldsymbol{M} \end{bmatrix} \begin{Bmatrix} \hat{\boldsymbol{u}} \\ \hat{\boldsymbol{p}}^t \\ \hat{\boldsymbol{p}}^w \end{Bmatrix}_{n} + \begin{Bmatrix} \boldsymbol{f}_u \\ \boldsymbol{0} \\ \Delta t \boldsymbol{f}_p \end{Bmatrix}_{n+1} \tag{4.135}$$

to be solved together with the phase-field equation (4.62). Based on the main variables of the problem, we call this formulation $\boldsymbol{u} - p^t - p^w - d$. Now we can notice that $p^w$is not directly coupled with $\boldsymbol{u}$ anymore.

Both the previous formulations are expected to be stable if we use a higher order of interpolation for $\boldsymbol{u}$ than for pressures. This is the case of the element Q9Pe4Pw4/Q4 (quadratic-linear-linear/linear) for the formulation $\boldsymbol{u} - p^e - p^w - d$, and of the element Q9Pt4Pw4/Q4 (quadratic-linear-linear/linear) for the formulation $\boldsymbol{u} - p^t - p^w - d$. The order of interpolation for the phase-field is assumed always linear.

It is clear that the number of degrees of freedom of a stable finite element, already large for the formulation $\boldsymbol{u} - p^w - d$, becomes even larger for the two developed mixed formulations. For example, if we focus on the interpolation for the poromechanical sub-problem, the standard Taylor-Hood element Q9Pw4 implies 22 degrees

of freedom, while the mixed Q9Pe4Pw4 (or Q9Pt4Pw4) element has 26 degrees of freedom.

Using the results obtained in the previous two sections for the stabilization of the fields of the water pressure p^w and the hydrostatic stress p independently, we define the stabilized versions of the two mixed formulations developed in this section, in order to be able to use finite elements with linear interpolation for all the fields. As a general guideline, we assume that the stabilization of a particular pressure field is needed when this field is directly coupled with the displacement field $\boldsymbol{u}$.

The stabilized version of the discrete system of equations (4.126) is defined as

$$\begin{bmatrix} \boldsymbol{K} & \boldsymbol{Q} & -\boldsymbol{Q} \\ \boldsymbol{Q}^T & -\boldsymbol{M} - \boldsymbol{S}^{pf} & \boldsymbol{0} \\ \boldsymbol{Q}^T & \boldsymbol{0} & \Delta t \boldsymbol{H} + \boldsymbol{S}^{mod} \end{bmatrix} \begin{Bmatrix} \hat{\boldsymbol{u}} \\ \hat{\boldsymbol{p}}^e \\ \hat{\boldsymbol{p}}^w \end{Bmatrix}_{n+1} = \\ = \begin{bmatrix} \boldsymbol{0} & \boldsymbol{0} & \boldsymbol{0} \\ \boldsymbol{0} & \boldsymbol{0} & \boldsymbol{0} \\ \boldsymbol{Q}^T & \boldsymbol{0} & \boldsymbol{0} \end{bmatrix} \begin{Bmatrix} \hat{\boldsymbol{u}} \\ \hat{\boldsymbol{p}}^e \\ \hat{\boldsymbol{p}}^w \end{Bmatrix}_{n} + \begin{Bmatrix} \boldsymbol{f}_u \\ \boldsymbol{0} \\ \Delta t \boldsymbol{f}_p \end{Bmatrix}_{n+1} \tag{4.136}$$

where the matrices $\boldsymbol{S}^{mod}$ and $\boldsymbol{S}^{pf}$ are defined in Section 4.2.3 and Section 4.3.2 respectively. With the stabilization terms, it is now possible to use the finite element Q4Pe4sPw4s, with linear interpolations in all the fields (the letter 's' indicates stabilization of the corresponding field).

The stabilized version of the discrete system of equations (4.135) is instead defined as

$$\begin{bmatrix} \boldsymbol{K} & \boldsymbol{Q} & \boldsymbol{0} \\ \boldsymbol{Q}^T & -\boldsymbol{M} - \boldsymbol{S}^{pf} & -\boldsymbol{M} \\ \boldsymbol{0} & \boldsymbol{M} & \boldsymbol{M} + \Delta t \boldsymbol{H} \end{bmatrix} \begin{Bmatrix} \hat{\boldsymbol{u}} \\ \hat{\boldsymbol{p}}^t \\ \hat{\boldsymbol{p}}^w \end{Bmatrix}_{n+1} = \\ = \begin{bmatrix} \boldsymbol{0} & \boldsymbol{0} & \boldsymbol{0} \\ \boldsymbol{0} & \boldsymbol{0} & \boldsymbol{0} \\ \boldsymbol{0} & \boldsymbol{M} & \boldsymbol{M} \end{bmatrix} \begin{Bmatrix} \hat{\boldsymbol{u}} \\ \hat{\boldsymbol{p}}^t \\ \hat{\boldsymbol{p}}^w \end{Bmatrix}_{n} + \begin{Bmatrix} \boldsymbol{f}_u \\ \boldsymbol{0} \\ \Delta t \boldsymbol{f}_p \end{Bmatrix}_{n+1} \tag{4.137}$$

Also in this case, with the stabilization terms, it is now possible to use the finite element Q4Pt4sPw4/Q4,with linear interpolations in all the fields (again the letter 's' indicates stabilization of the corresponding field).

To conclude we notice that, using the stabilized element Q4Pe4sPw4s (or Q4Pt4sPw4) instead of the stable Q9Pe4Pw4 (or Q9Pt4Pw4), the number of degrees of freedom per element reduces from 26 to 16, becoming now less than the 22 degrees of freedom corresponding to the Taylor-Hood element Q9Pw4.

4.4.3 Numerical examples

In this section two numerical examples are presented, in order to test the performance of different formulations of the phase-field model of brittle fracture in saturated porous media developed in Section 4.4.1 and Section 4.4.2. In particular, for both the examples, we consider interpolations with quadrilateral elements Q4Pw4/Q4, Q4Pw4s/Q4 and Q9Pw4/Q4 for the formulation $\boldsymbol{u} - p^w - d$, with the quadrilateral elements Q4Pe4sPw4s/Q4 and Q9Pe4Pw4/Q4 for the mixed formulation $\boldsymbol{u} - p^e - p^w - d$, and with the quadrilateral elements Q4Pt4sPw4/Q4 and Q9Pt4Pw4sQ4 for the mixed formulation $\boldsymbol{u} - p^t - p^w - d$. The interpolations used for each of these elements are specified in Table 4.2, including an indication of the field in which, if present, the stabilization is applied.

	$\boldsymbol{u}$	p^e	p^t	p^w	d
Q4Pw4/Q4	linear	-	-	linear	linear
Q4Pw4s/Q4	linear	-	-	linear	linear
Q9Pw4/Q4	quadratic	-	-	linear	linear
Q4Pe4sPw4s/Q4	linear	linear - stabilized	-		linear
Q9Pe4Pw4/Q4	quadratic	linear	-	linear	linear
Q4Pt4sPw4/Q4	linear	-	linear - stabilized	linear	linear
Q9Pt4Pw4/Q4	quadratic	-	linear	linear	linear

Table 4.2: Summary of the different finite elements used for the numerical applications in Section 4.4.3, including the the degree of interpolation used for each field.

Terzaghi's problem

In this first example we solve again the Terzaghi's problem analyzed in Section 4.2.4. Our goal is to have a first comparison, without the influence of the phase-field d, between the results obtained with the two mixed formulations $\boldsymbol{u} - p^e - p^w$ and $\boldsymbol{u} - p^t - p^w$ and the one obtained with the standard $\boldsymbol{u} - p^w$ formulation. The finite elements used in the simulation are the stabilized Q4Pe4sPw4s and the stable Q9Pe4Pw4 for the $\boldsymbol{u} - p^e - p^w$ formulation, the stabilized Q4Pt4sPw4 and the stable Q9Pt4Pw4 for the $\boldsymbol{u} - p^t - p^w$ formulation, and the Taylor-Hood Q9Pw4 for the standard $\boldsymbol{u} - p^w$ formulation. The parameter are the same of Section 4.2.4, with $\nu = 0.4$.

In Figure 4.10 the pressure profile after the first time step for the different finite elements is shown. Both two stable elements Q9Pe4Pw4 and Q9Pt4Pw4 lead to the same solution obtained with the standard Q9Pw4, used as reference solution.

Coming to the stabilized elements Q4Pe4sPw4s and Q4Pt4sPw4, we notice that the second one leads to the same results obtained with the reference element Q9Pw4, while the first one shows slightly larger oscillations in the vicinity of the top surface. Moreover, the Q4Pt4sPw4 turns out to be stable for the water pressure field p^w, even if the stabilization is applied only to the equation relative to the total hydrostatic stress field p^t, confirming our assumption that the stabilization is needed only for the field directly coupled with the displacement field $\boldsymbol{u}$. On the other hand, the larger oscillations obtained with the Q4Pe4sPw4s are probably due to the difficulty to define a correct value for the two stabilization terms needed, which, due to the coupling of the equations, need to be also mutually balanced.

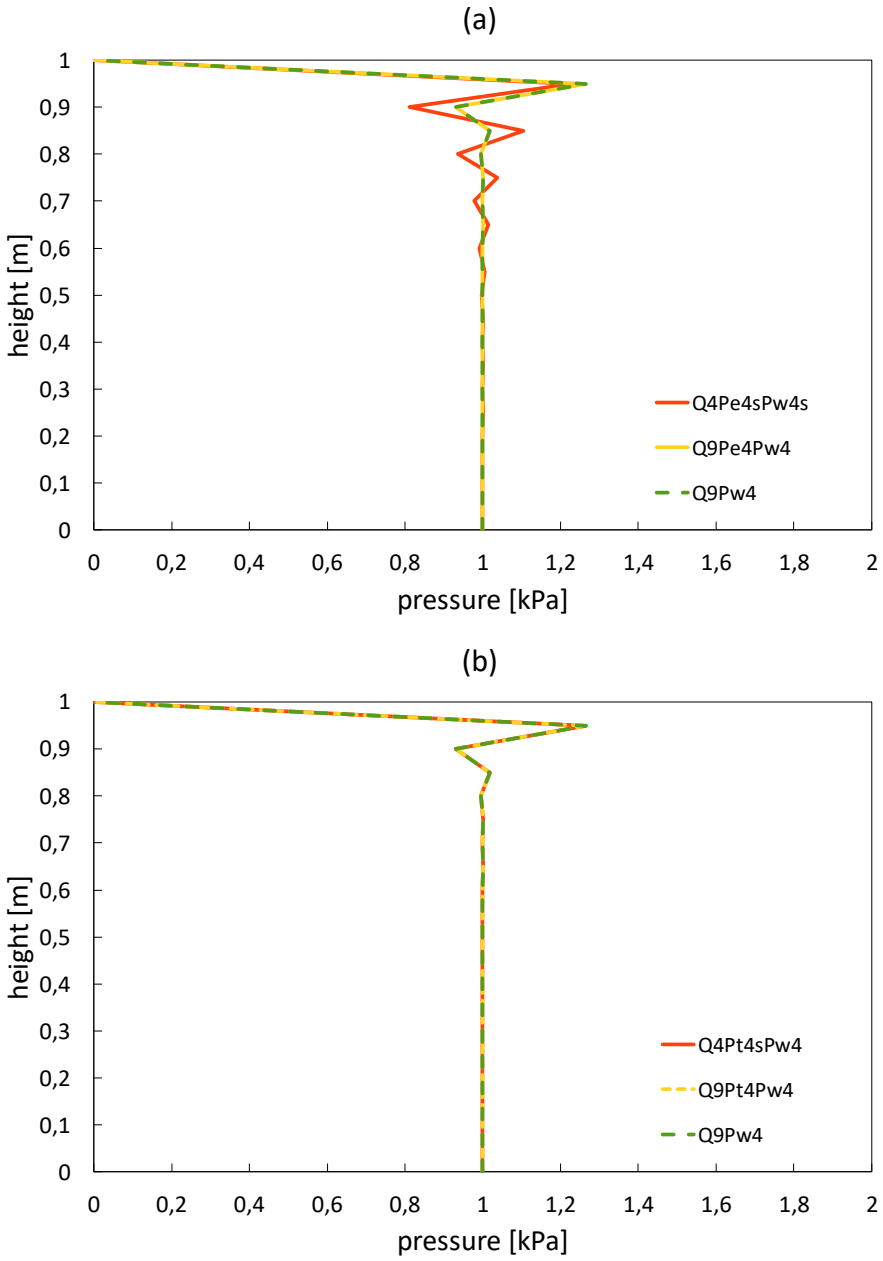

Figure 4.10: Pressure distribution along the column at the first time step for different finite elements. In (a) $\boldsymbol{u} - p^e - p^w$ formulation, in (b) $\boldsymbol{u} - p^t - p^w$ formulation.

Two dimensional saturated shear test

In this second example we solve again the same shear test of Section 4.3.3, but this time considering the material as a saturated porous medium. Additional boundary conditions for the water pressure field are needed, and in this case we consider the lower and the lateral sides impervious, while on the upper one we impose the Dirichlet

boundary condition $p^w = 0$. The finite elements used in the simulations are the unstable Q4Pw4/Q4, the stabilized Q4Pw4s/Q4 and the Taylor-Hood Q9Pw4/Q4 for the $\boldsymbol{u} - p^w - d$ formulation, the stabilized Q4Pe4sPw4s/Q4 and the stable Q9Pe4Pw4/Q4 for the $\boldsymbol{u} - p^e - p^w - d$ formulation, the stabilized Q4Pt4sPw4/Q4 and the stable Q9Pt4Pw4/Q4 for the $\boldsymbol{u} - p^t - p^w - d$ formulation. The parameters for the problem are the same of Section 4.3.3, with the exception of the number of steps $N_{ts} = 240$ (as will be shown, the presence of the water accelerate the process of formation of the crack). The permeability of the porous medium is considered very low, namely $k^w = 10^{-8}\, m/s$.

In Figure 4.11 we show the results relative to the standard $\boldsymbol{u} - p^w - d$ formulation: we can notice how the Q4Pw4/Q4 element shows both oscillations in the water pressure and a wrong localization profile in the phase-field, as we already noticed separately in the previous sections. The Q4Pw4s/Q4 solves the instabilities in the water field, but the phase-field profile still indicates the presence of locking after the fracture localization. The Taylor-Hood element Q9Pw4/Q4 behaves well also in the coupled simulation.

In Figure 4.11 we show the results relative to the mixed $\boldsymbol{u} - p^e - p^w - d$ and $\boldsymbol{u} - p^t - p^w - d$ formulations: we can notice that, if a quadratic interpolation is used for the displacement field (element Q9Pe4Pw4/Q4 and Q9Pt4Pw4/Q4 respectively), both the formulations are stable, and leads to identical results (only the results relative to the element Q9Pe4Pw4/Q4 are reported). The Q4Pe4sPw4s/Q4 element is stable for the pressure field and, looking at the phase-field profile, the crack seems to start vertically, and then take the expected direction. This right failure pattern is, on the other side, perfectly captured by the element Q4Pt4sPw4/Q4, which shows results very similar to the ones obtained with Q9Pt4Pw4/Q4.

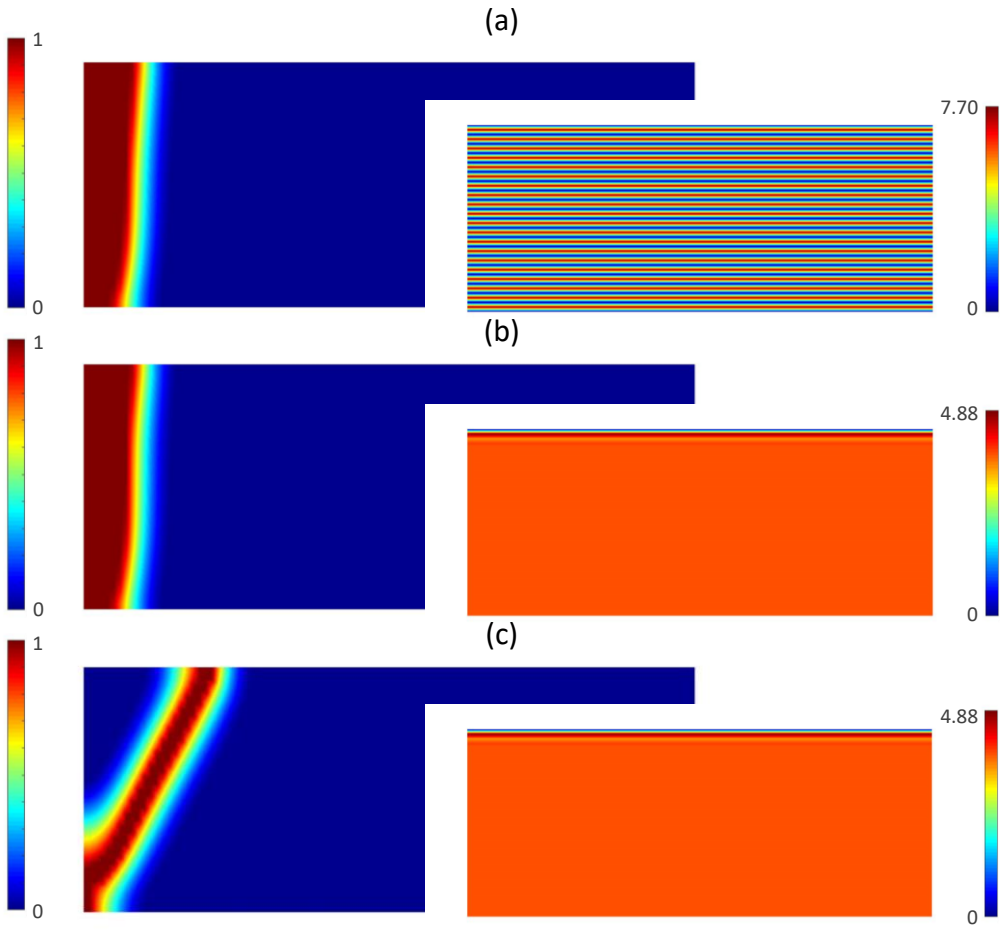

Figure 4.11: Contours of the phase-field d (left) and of the water pressure p^w (right) for $l = 0,005\,m$, at $t = 0,06\,s$: (a) Q4Pw4/Q4, (b) Q4Pw4s/Q4, (c) Q9Pw4/Q4.

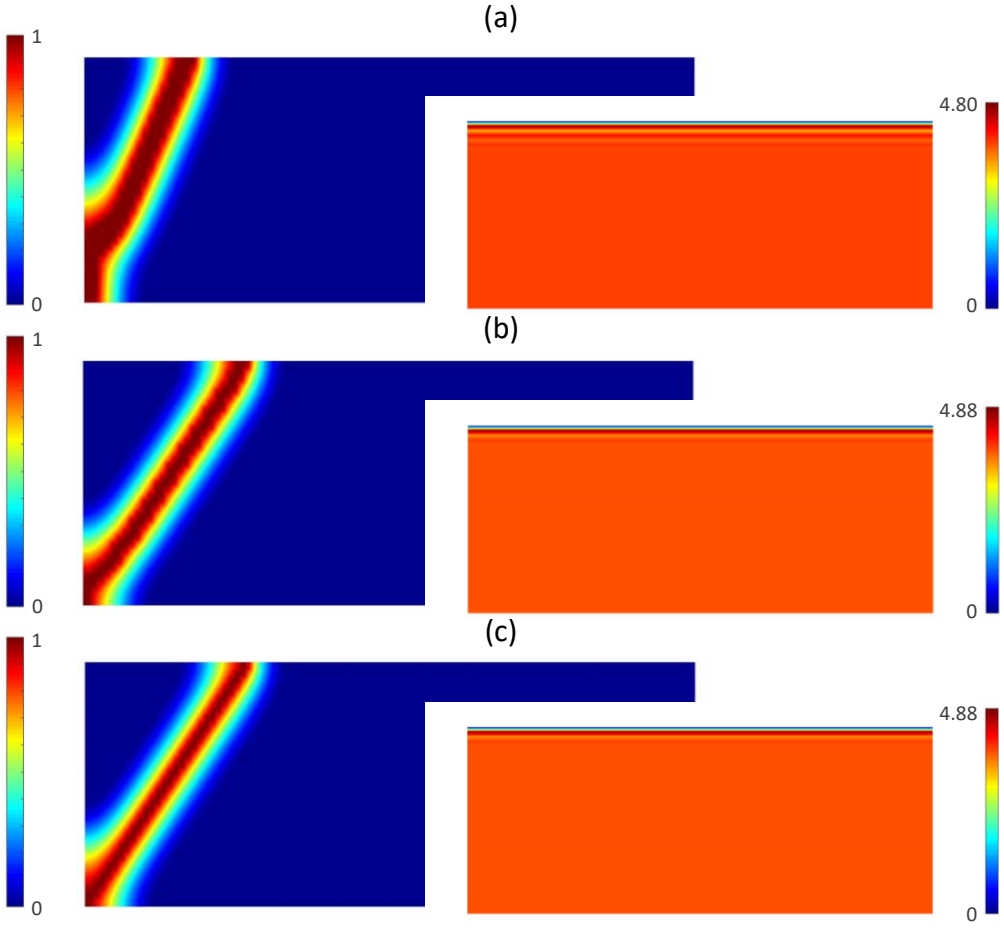

Figure 4.12: Contours of the phase-field d (left) and of the water pressure p^w(right) for $l = 0,005\,m$, at $t = 0,06\,s$: (a) Q4Pe4sPw4s/Q4, (b) Q4Pt4sPw4/Q4, (c) Q9Pt4Pw4/Q4(Q9Pe4Pw4/Q4).

As done in Section 4.3.3, we run again the same simulation whit a mesh composed by elements of dimension $h_{el} = 0,01\,m$, that is the coarsest regular mesh respecting the condition $h_{el} \leq l/2$. Results are shown in Figure 4.13 and Figure 4.14. Also in this case the standard Q9Pw4/Q4 and the stabilized mixed Q4Pt4sPw4/Q4 show again a good behavior for both water pressure and phase-field, when compared to the reference stable mixed Q9Pt4Pw4/Q4 element. On the other hand, the stabilized mixed Q4Pe4sPw4s/Q4 is, in this case, not able to capture the inclined crack pattern, typical of the shear failure mode.

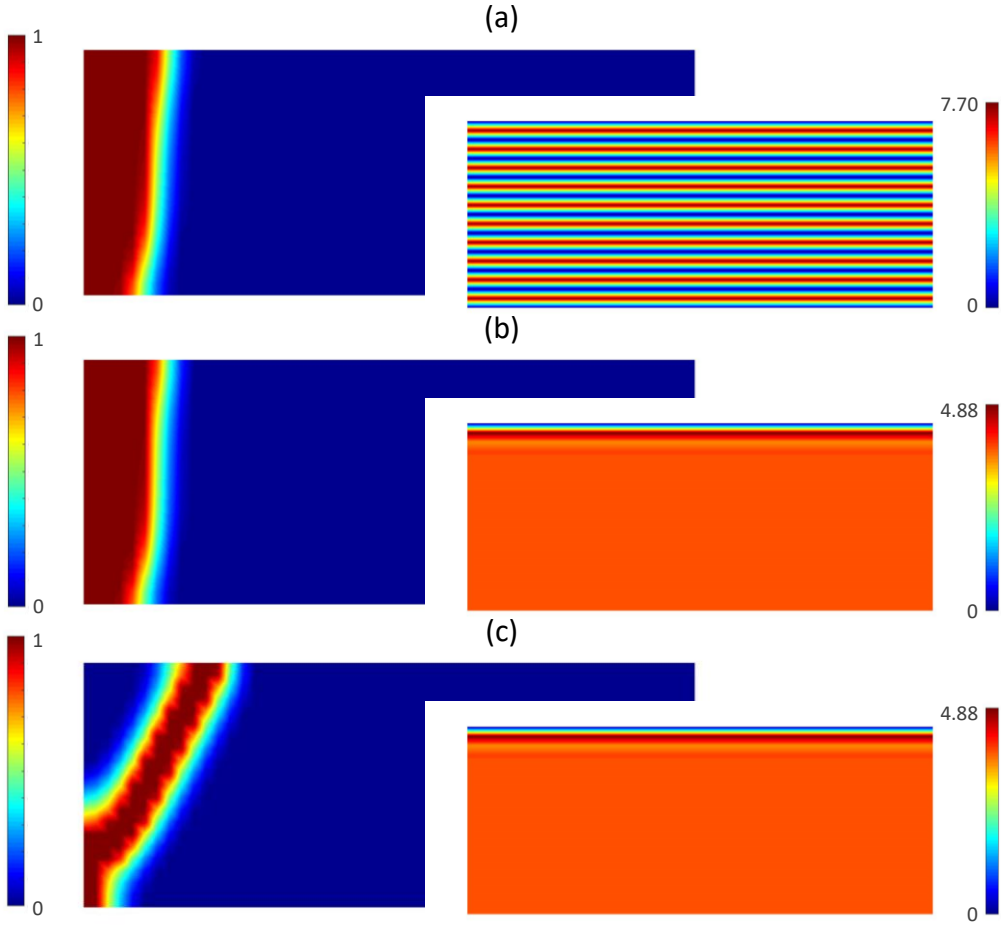

Figure 4.13: Contours of the phase-field d (left) and for the water pressure p^w(right) for $l = 0,01\,m$, at $t = 0,06\,s$: (a) Q4Pw4/Q4, (b) Q4Pw4s/Q4, (c) Q9Pw4/Q4.

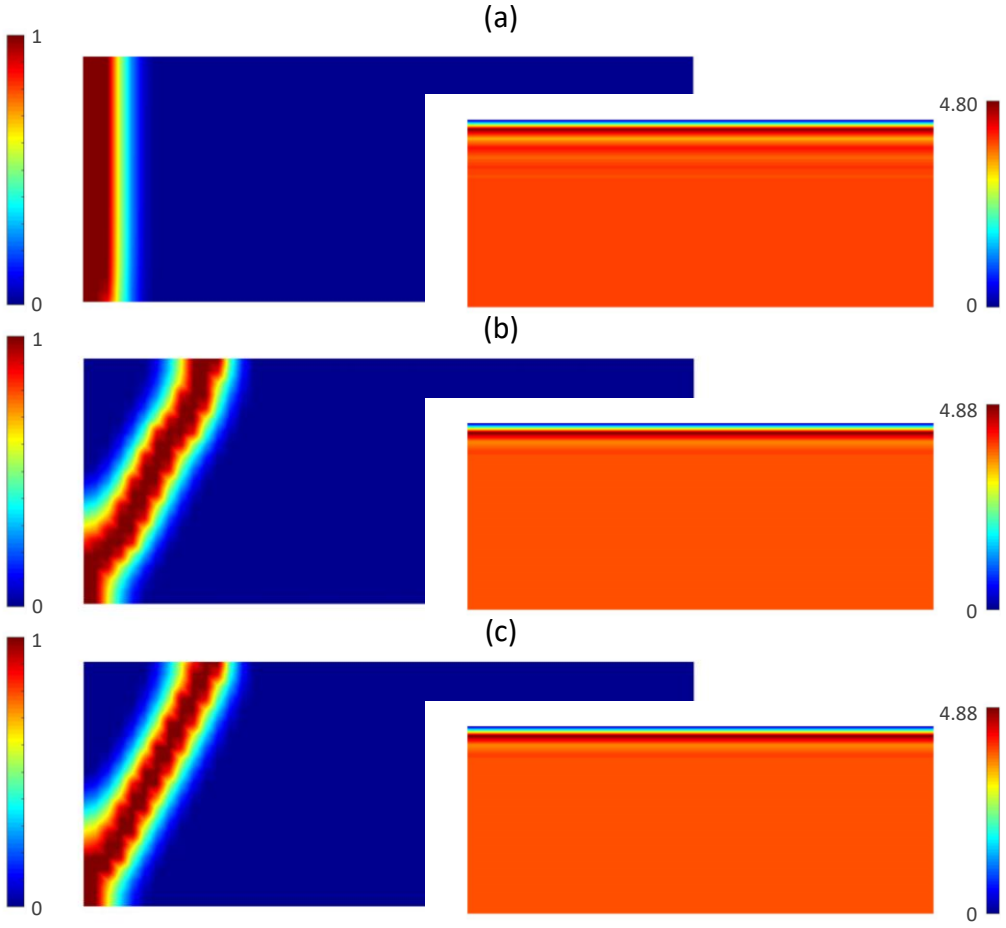

Figure 4.14: Contours of the phase-field d (left) and for the water pressure p^w (right) for $l = 0,01\,m$, at $t = 0,06\,s$: (a) Q4Pe4sPw4s/Q4, (b) Q4Pt4sPw4/Q4, (c) Q9Pt4Pw4/Q4(Q9Pe4Pw4/Q4).

Finally, Figure 4.15 shows the horizontal reaction - applied displacement curves in presence of water ("wet" case) and in absence of water ("dry" case, i.e. the one shown in Section 4.3.3) . Due to the low permeability of the material, under undrained conditions the water acts as a constraint, imposing pure deviatoric deformations on the solid. The pressure of the water causes the development of an effective tension in the vertical direction, equal to $\sigma_y^e = p^w$, obtained from the effective stress principle, considering that $\sigma_y^t = 0$. This vertical stress leads to an increase in the deviatoric energy, and so in the "wet" case the failure stress is reached earlier then in the "dry" case.

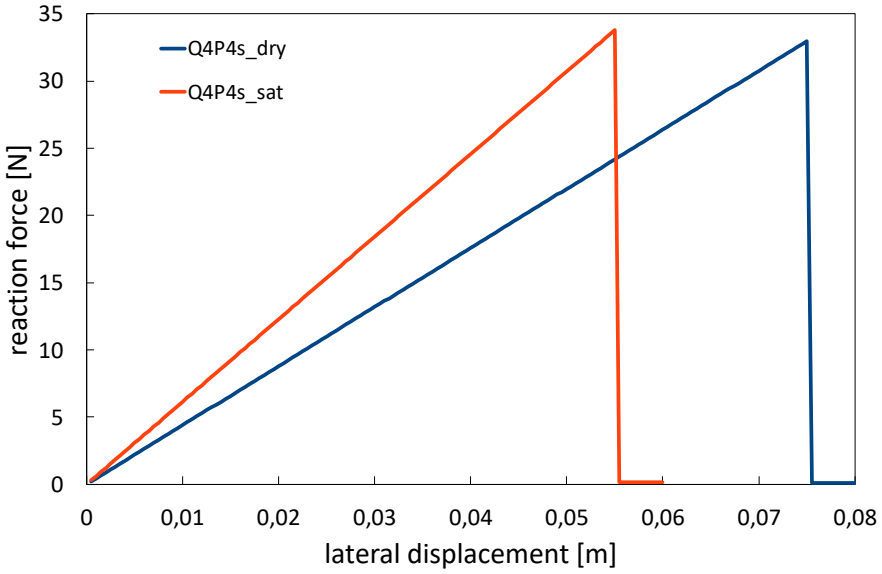

Figure 4.15: Horizontal reaction vs applied displacement curve: (a) "dry" mixed stabilized $\boldsymbol{u} - p - d$ formulation (Section 4.3.3), (b) "wet" mixed stabilized $\boldsymbol{u} - p^t - p^w - d$ formulation.

4.5 Conclusions

In this chapter we focused on the problem of the numerical locking, due to a condition of high volumetric stiffness of the solid matrix, that can occur in the numerical approximation of a phase-field model of fracture in porous media with the Finite Element Method (FEM). The causes of this state of incompressibility can be traced both to the hydraulic and to the mechanical properties of the material.

In the first part of the chapter we introduced the problem of the numerical locking in the simulation of the consolidation process of saturated porous media under undrained condition, which occurs when a linear interpolation for both the solid and the fluid fields is used. In particular a stabilization technique proposed in [66], developed using a polynomial pressure-projection technique originally applied in the field of fluid dynamics, has been reviewed.

In the second part of the chapter the problem of volumetric locking due to the presence of fully developed cracks obtained with a phase-field model based on a decomposition of the elastic energy into volumetric and deviatoric parts has been investigated. It has been noticed how, in this case, the locking is due to the fact that the deviatoric stiffness becomes several order of magnitudes smaller than the volumetric one, causing an enlargement of the localization band of the phase-field variable, and

a dissipative residual force in the crack. To solve this problem, a stabilized mixed $\boldsymbol{u} - p - d$ finite element formulation has been developed, using the same technique applied in the first part of the chapter.

Finally, the model has been extended to variably saturated porous media, and two alternative mixed and mixed stabilized formulations of the problem have been proposed and tested in two numerical application, with successfully results.

Chapter 5

Phase-field model of fracture in three-phase partially saturated porous media

5.1 Introduction

In this chapter we deal with the problem of fracture in partially saturated porous media, governed by the differential equations (2.152), (2.153), (2.154) and (2.155) derived in Chapter 2. In the first part the Finite Element Method is applied, in order to derive the numerical formulation of the governing equations. This model is then applied to the simulation of two different problems of desiccation of initially saturated soil, focusing in particular on the investigation of the influence of the air phase on the onset and the development of desiccation cracks. In addition, the stabilized model developed in Section 4.4.2 is applied in the second example, in order to analyze its behavior when extended to the unsaturated regime.

5.2 Governing equations and finite element discretization

We recall the set of differential equations governing the phase-field model of brittle fracture in three-phase porous media derived in Section 2.4, namely

$$\nabla \cdot \boldsymbol{\sigma}'(\boldsymbol{\varepsilon}, d) - \nabla \left[S^w p^w + (1 - S^w) p^a \right] + \rho \boldsymbol{g} = \mathbf{0} \tag{5.1}$$

$$n \rho^w \dot{S^w} + S^w n \rho^w \frac{\dot{p^w}}{K^w} + S^w \rho^w \nabla \cdot \boldsymbol{v} + \nabla \cdot \left[\rho^w \frac{k^{rw} k^s \boldsymbol{I}}{\mu^w} (-\nabla p^w + \rho^w \boldsymbol{g}) \right] = 0 \tag{5.2}$$

$$- n \rho^a \dot{S^w} + (1 - S^w) n \frac{\dot{p^a}}{K^a} + (1 - S^w) \rho^a \nabla \cdot \boldsymbol{v} + \nabla \cdot \left[\rho^a \frac{k^{ra} k^s \boldsymbol{I}}{\mu^a} (-\nabla p^a + \rho^a \boldsymbol{g}) \right] = 0 \tag{5.3}$$

$$-2(1-d)\mathcal{H}^{+}+G_c(\frac{d}{l}-l\Delta d)=0 \tag{5.4}$$

where equation (5.1) is the equilibrium equation of the three-phase mixture, equation (5.2) is the mass balance equation for the solid and the water phases, equation (5.3) is the mass balance equation for the solid and the air phases, and (5.4) is the evolution equation for the phase-field variable d, in which the AT2 model for the local part of the dissipated density function ($w(d)=d^2$,$C_v=\frac{1}{2}$) has been used, and the quantity

$$\mathcal{H}^{+}=\max_{\tau\in[0,t]}\Psi_0^{+}(\boldsymbol{\varepsilon},\tau)$$

called energy density history variable, has been introduced in order to ensure the irreversibility of the phase-field d. The ICs and BCs of the model are the following

$$\begin{array}{ll}
\boldsymbol{u}(\boldsymbol{x},t))=\boldsymbol{u}(\boldsymbol{x},0)) & \text{at } t=0\\
p^w(\boldsymbol{x},t))=p^w(\boldsymbol{x},0)) & \text{at } t=0\\
p^a(\boldsymbol{x},t))=p^a(\boldsymbol{x},0) & \text{at } t=0\\
\boldsymbol{u}=\overline{\boldsymbol{u}} & \text{on } \Gamma_{\boldsymbol{u}}^{D}\\
p^w=\bar{p}^w & \text{on } \Gamma_{p^w}^{D}\\
p^a=\bar{p}^a & \text{on } \Gamma_{a}^{D}\\
\boldsymbol{\sigma}\cdot\boldsymbol{n}=\bar{\boldsymbol{t}} & \text{on } \Gamma_{\boldsymbol{u}}^{N}\\
\tilde{\boldsymbol{v}}^w\cdot\boldsymbol{n}=\bar{q}^w & \text{on } \Gamma_{p^w}^{N}\\
\tilde{\boldsymbol{v}}^w\cdot\boldsymbol{n}=\bar{q}^a & \text{on } \Gamma_{p^a}^{N}\\
\nabla d\cdot\boldsymbol{n}=0 & \text{on } \Gamma_{d}^{N}
\end{array} \tag{5.5}$$

The quantity $\boldsymbol{\sigma}'$ and $\boldsymbol{\sigma}$ that appear in the equilibrium equation (5.1) and in the BCs (5.5) are respectively the effective and the total stress, and are related by the effective stress principle (2.49), namely

$$\boldsymbol{\sigma}'=\boldsymbol{\sigma}+\left[S^w p^w+(1-S^w)p^a\right]\mathbf{I} \tag{5.6}$$

The coupling between the phase-field equation (5.4) and the equilibrium equation (5.1), is realized assuming a dependency on the phase-field variable d of the elastic constitutive law for the effective stress $\boldsymbol{\sigma}'$, namely

$$\boldsymbol{\sigma}'(\boldsymbol{\varepsilon},d)=\left[(1-d^2)+\eta\right]\frac{\partial\Psi_0^{+}(\boldsymbol{\varepsilon}(\boldsymbol{u}))}{\partial\boldsymbol{\varepsilon}}+\frac{\partial\Psi_0^{-}(\boldsymbol{\varepsilon}(\boldsymbol{u}))}{\partial\boldsymbol{\varepsilon}} \tag{5.7}$$

where $\Psi_0^{+}(\boldsymbol{\varepsilon}(\boldsymbol{u}))$ and $\Psi_0^{-}(\boldsymbol{\varepsilon}(\boldsymbol{u}))$ are the positive and the negative part of the undamaged elastic elastic energy $\Psi_0(\boldsymbol{\varepsilon}(\boldsymbol{u}))$, whose definitions depend on the energy split chosen for the phase-field model (see Section 2.3.3). In this chapter we use the split proposed by Amor *et al.* [3], in which $\Psi_0^{+}(\boldsymbol{\varepsilon}(\boldsymbol{u}))$ and $\Psi_0^{-}(\boldsymbol{\varepsilon}(\boldsymbol{u}))$ are defined as

$$\begin{cases}
\Psi_0^{+}=K_n\langle\mathrm{tr}(\boldsymbol{\varepsilon})\rangle_{+}^{2}+\mu(\boldsymbol{\varepsilon}^{\mathrm{dev}}:\boldsymbol{\varepsilon}^{\mathrm{dev}})\\
\Psi_0^{-}=K_n\langle\mathrm{tr}(\boldsymbol{\varepsilon})\rangle_{-}^{2}
\end{cases} \tag{5.8}$$

where $K_n = \lambda + \frac{\mu}{n}$, with n being the dimension of the problem, is the bulk modulus of the material, and $\langle \mathrm{tr}(\boldsymbol{\varepsilon}) \rangle_{\pm} = \frac{1}{2}(\mathrm{tr}(\boldsymbol{\varepsilon}) \pm |\mathrm{tr}(\boldsymbol{\varepsilon})|)$. This definition of the split is based on the idea that degrading the volumetric part of the energy only if the volumetric part of the deformation tensor $\boldsymbol{\varepsilon}$ is positive should prevent the interpenetration of the crack faces under compression. Furthermore, if $\mathrm{tr}(\boldsymbol{\varepsilon}) < 0$, the volumetric part of the energy is not taken into account in the evolution equation for the phase-field d, avoiding the formation of unrealistic crack patterns in compression. Introducing the following split of the elasticity tensor $\mathbb{C}$

$$\mathbb{C}^{\pm}(\boldsymbol{\varepsilon}) = \frac{\partial^2 \Psi_0^{\pm}}{\partial \boldsymbol{\varepsilon}^2} \tag{5.9}$$

it is possible to rewrite the constitutive relation (5.8) as

$$\boldsymbol{\sigma'} = \left\{ \left[(1-d^2) + \eta \right] \mathbb{C}^{+}(\boldsymbol{\varepsilon}) + \mathbb{C}^{-}(\boldsymbol{\varepsilon}) \right\} : \boldsymbol{\varepsilon} \tag{5.10}$$

In addition to the constitutive relations introduced in Section 2.2.4, for clayey materials a dependency of the Young's modulus E and of the tensile strength σ_t on the water content w has been experimentally observed [58] , namely

$$E = E(w) \tag{5.11}$$

$$\sigma_t = \sigma_t(w) \tag{5.12}$$

where the water content w is defined as

$$w = \frac{n S^w \rho^w}{(1-n)\rho^s} \tag{5.13}$$

Even if the tensile strength of the material is not explicitly modeled in the proposed formulation, as observed in [17], the expression of the critical stress derived from the analytical phase-field solution for the one dimensional tension problem (see Section 2.3.3), which for the AT2 model reads

$$\sigma_c^{AT2} = \frac{9}{16}\sqrt{\frac{G_c E}{3l}} \tag{5.14}$$

can be used to express the value σ_c^{AT2} as a function of the fracture toughness G_c, the Young's modulus E and the characteristic length l. In particular, taking into account the constitutive expressions (5.11) and (5.12), we can derive from equations (5.14) the following expression for the fracture toughness [17]

$$G_c(w) = \left(\frac{16}{9}\right)^2 \sigma_c'(w) \frac{3l}{E(w)} \tag{5.15}$$

which allows to account for (5.12) into the proposed model. Considering constant values for the porosity n and for the intrinsic density of solid ρ^s and of the water ρ^w, the water content w, defined in (5.13), becomes a function of the water saturation S^w alone. Therefore the expressions (5.11) and (5.12) can be rewritten as

$$E = E\left(S^w\right) \tag{5.16}$$

$$G_c = G_c\left(S^w\right) \tag{5.17}$$

The elasticity tensors $\mathbb{C}^{\pm}$ and the effective stress $\boldsymbol{\sigma}'$, which depends on the Young modulus $E\left(S^w\right)$, become also a function of the saturation S^w

$$\mathbb{C}^{\pm} = \mathbb{C}^{\pm}\left(E\left(S^w\right), \boldsymbol{\varepsilon}\right) \tag{5.18}$$

$$\boldsymbol{\sigma}' = \boldsymbol{\sigma}'(E\left(S^w\right), \boldsymbol{\varepsilon}, d) \tag{5.19}$$

Taking into account the expressions (5.17) and (5.19), we can rewrite the equilibrium equation (5.1) and the phase-field evolution equation (5.4) as

$$\nabla \cdot \boldsymbol{\sigma}'(E\left(S^w\right), \boldsymbol{\varepsilon}, d) - \nabla\left[S^w p^w + (1 - S^w)p^a\right] + \rho \boldsymbol{g} = 0 \tag{5.20}$$

$$-2(1-d)\mathcal{H}^+ + G_c\left(S^w\right)\left(\frac{d}{l} - l\Delta d\right) = 0 \tag{5.21}$$

With a procedure similar to the one exposed in Section 3.3, we apply the Backward Euler scheme for the discretization in time. Defined as $n+1$ and n the current and the previous time steps respectively, the equations governing the problem are solved at the current time step $n+1$, substituting the material time derivatives present in the mass balance equations (5.2) and (5.3) with their discrete counterpart

$$\dot{(\,)} = \frac{(\,)_{n+1} - (\,)_n}{\Delta t} \tag{5.22}$$

where Δt is the time step. From equations (5.20), (5.2), (5.3) and (5.21) we obtain

$$\nabla \cdot \boldsymbol{\sigma}'(E\left(S^w_{n+1}\right), \boldsymbol{\varepsilon}_{n+1}, d_{n+1}) - \nabla\left[S^w_{n+1} p^w_{n+1} + (1 - S^w_{n+1})p^a_{n+1}\right] + \rho_{n+1}\boldsymbol{g} = 0 \tag{5.23}$$

$$n\rho^w \frac{S^w_{n+1} - S^w_n}{\Delta t} + S^w_{n+1}\rho^w \nabla \cdot \frac{\boldsymbol{u}_{n+1} - \boldsymbol{u}_n}{\Delta t} + \nabla \cdot \left[\rho^w \frac{k^{rw}_{n+1} k^s \boldsymbol{I}}{\mu^w}(-\nabla p^w_{n+1} + \rho^w \boldsymbol{g})\right] = 0 \tag{5.24}$$

$$\begin{aligned} &- n\rho^a_{n+1}\frac{S^w_{n+1} - S^w_n}{\Delta t} + (1 - S^w_{n+1})\frac{n}{K^a}\frac{p^a_{n+1} - p^a_n}{\Delta t} + (1 - S^w_{n+1})\rho^a_{n+1}\nabla \cdot \frac{\boldsymbol{u}_{n+1} - \boldsymbol{u}_n}{\Delta t} \\ &\qquad + \nabla \cdot \left[\rho^a_{n+1}\frac{k^{ra}_{n+1} k^s \boldsymbol{I}}{\mu^a}(-\nabla p^a_{n+1} + \rho^a_{n+1}\boldsymbol{g})\right] = 0 \end{aligned} \tag{5.25}$$

$$-2(1-d_{n+1})\mathcal{H}^{+}_{n+1} + G_c\left(S^w_{n+1}\right)\left(\frac{d_{n+1}}{l} - l\Delta d_{n+1}\right) = 0 \tag{5.26}$$

We apply now the Weighted Residual method, in order to derive the weak form of the time-discrete problem governed by the equations (5.23), (5.24), (5.25) and (5.26). Once defined the test functions $\boldsymbol{w}_u$, w_w, w_a and w_d, the weak form of the problem reads

$$\begin{aligned} W^u_{n+1} = &\int_\Omega \nabla^s \boldsymbol{w}_u : \boldsymbol{\sigma}'(E\left(S^w_{n+1}\right), \boldsymbol{\varepsilon}_{n+1}, d_{n+1})\mathrm{dV} \\ &- \int_\Omega \nabla\cdot\boldsymbol{w}_u\left[S^w_{n+1}p^w_{n+1} + (1-S^w_{n+1})p^a_{n+1}\right]\mathrm{dV} \\ &- \int_\Omega \boldsymbol{w}_u\cdot\rho_{n+1}\boldsymbol{g}dV - \int_{\Gamma^N_{\boldsymbol{u}}} \boldsymbol{w}_u\cdot\bar{\boldsymbol{t}}\mathrm{d}\Gamma = 0 \end{aligned} \tag{5.27}$$

$$\begin{aligned} W^w_{n+1} = &\int_\Omega w_w n\rho^w \frac{S^w_{n+1}-S^w_n}{\Delta t}\mathrm{dV} + \int_\Omega w_w S^w_{n+1}\rho^w\nabla\cdot\frac{\boldsymbol{u}_{n+1}-\boldsymbol{u}_n}{\Delta t}\mathrm{dV} \\ &+ \int_\Omega \nabla w_w\cdot\left[\rho^w\frac{k^{rw}_{n+1}k^s\boldsymbol{I}}{\mu^w}(\nabla p^w_{n+1} - \rho^w\boldsymbol{g})\right]\mathrm{dV} + \int_{\Gamma^N_p} w_w\bar{q}^w\mathrm{d}\Gamma = 0 \end{aligned} \tag{5.28}$$

$$\begin{aligned} W^a_{n+1} = &-\int_\Omega w_w n\rho^a_{n+1}\frac{S^w_{n+1}-S^w_n}{\Delta t}\mathrm{dV} + \int_\Omega w_w(1-S^w_{n+1})\frac{n}{K^a}\frac{p^a_{n+1}-p^a_n}{\Delta t}\mathrm{dV} \\ &+ \int_\Omega w_w(1-S^w_{n+1})\rho^a_{n+1}\nabla\cdot\frac{\boldsymbol{u}_{n+1}-\boldsymbol{u}_n}{\Delta t}\mathrm{dV} \\ &+ \int_\Omega \nabla w_w\cdot\left[\rho^a_{n+1}\frac{k^{ra}_{n+1}k^s\boldsymbol{I}}{\mu^a}(\nabla p^a_{n+1} - \rho^a_{n+1}\boldsymbol{g})\right]\mathrm{dV} + \int_{\Gamma^N_p} w_w\bar{q}^a\mathrm{d}\Gamma = 0 \end{aligned} \tag{5.29}$$

$$\begin{aligned} W^d_{n+1} = &-\int_\Omega w_d 2(1-d_{n+1})\mathcal{H}^{+}_{n+1}\mathrm{dV} + \int_\Omega w_d G_c\left(S^w_{n+1}\right)\frac{d_{n+1}}{l} \\ &+ \int_\Omega \nabla w_d\cdot\left[G_c\left(S^w_{n+1}\right)l\right]\nabla d_{n+1} = 0 \end{aligned} \tag{5.30}$$

The corresponding discrete system of equations is obtained applying the Bubnov-Galerkin approach. We subdivide our domain in a mesh of finite elements, and we consider an approximation of the spaces T_p and W_p, based on polynomial shape functions with local support, namely

$$\begin{aligned}
\tilde{\boldsymbol{u}} &= \boldsymbol{N}_u \hat{\boldsymbol{u}} \\
\tilde{p}^w &= \boldsymbol{N}_p \hat{\boldsymbol{p}}^w \\
\tilde{p}^a &= \boldsymbol{N}_p \hat{\boldsymbol{p}}^a \\
\tilde{d} &= \boldsymbol{N}_d \hat{\boldsymbol{d}} \\
\tilde{\boldsymbol{w}}_u &= \boldsymbol{N}_u \hat{\boldsymbol{w}}_u \\
\tilde{w}_w &= \boldsymbol{N}_p \hat{\boldsymbol{w}}_w \\
\tilde{w}_a &= \boldsymbol{N}_p \hat{\boldsymbol{w}}_a \\
\tilde{w}_d &= \boldsymbol{N}_d \hat{\boldsymbol{w}}_d
\end{aligned} \tag{5.31}$$

where $\tilde{()}$ are the approximated trials and weighting functions, $\hat{()}$ are the vectors containing the values of those functions on the mesh nodes, and $\boldsymbol{N}_u$, $\boldsymbol{N}_p$ and $\boldsymbol{N}_d$ are the matrix and the vectors containing the nodal shape functions. After the discretization in space, we obtain a system of equations with structure

$$\boldsymbol{R}_{n+1} = \left\{ \begin{array}{c} \boldsymbol{R}^u_{n+1} \\ \boldsymbol{R}^w_{n+1} \\ \boldsymbol{R}^a_{n+1} \\ \boldsymbol{R}^d_{n+1} \end{array} \right\} = \boldsymbol{0} \tag{5.32}$$

where $\boldsymbol{R}^u_{n+1}$, $\boldsymbol{R}^w_{n+1}$, $\boldsymbol{R}^a_{n+1}$ and $\boldsymbol{R}^d_{n+1}$ are the residual vectors relative to the equations (5.27), (5.28), (5.29) and (5.30) respectively. The coupled problem is solved using a staggered iterative procedure similar to the one exposed in Sections 4.3.1, in which the phase-field equation

$$\boldsymbol{R}^d_{n+1} = \boldsymbol{0} \tag{5.33}$$

is solved independently for the variable d, using the last available solution of the sub-problem

$$\underline{\boldsymbol{R}}_{n+1} = \left\{ \begin{array}{c} \boldsymbol{R}^u_{n+1} \\ \boldsymbol{R}^w_{n+1} \\ \boldsymbol{R}^a_{n+1} \end{array} \right\} = \boldsymbol{0} \tag{5.34}$$

and vice versa. The discrete counterpart of the phase-field equation (5.33) turns out to be a linear system of equations with respect to the phase-field solution vector $\hat{\boldsymbol{d}}_{n+1}$, namely

$$\boldsymbol{R}^d_{n+1} = (\boldsymbol{C} + \boldsymbol{G})\hat{\boldsymbol{d}}_{n+1} - \boldsymbol{f}_d = \boldsymbol{0} \tag{5.35}$$

where

$$\boldsymbol{C} = \int_{\Omega^e} \boldsymbol{N}_d^T (\mathcal{H}^+ + \frac{G_c}{2l}) \boldsymbol{N}_d d\Omega \tag{5.36}$$

$$\boldsymbol{G} = \frac{G_c l}{2} \int_{\Omega^e} (\nabla \boldsymbol{N}_d)^T (\nabla \boldsymbol{N}_d) d\Omega \tag{5.37}$$

$$\boldsymbol{f}_d = \int_{\Omega^e} \boldsymbol{N}_d^T \mathcal{H}^+ d\Omega \tag{5.38}$$

Regarding the sub-problem (5.34), we obtain the following expression for the residuals

$$\begin{aligned} \boldsymbol{R}_{n+1}^u = & \int_\Omega \boldsymbol{B}^T \left[\!\!\left[\boldsymbol{\sigma}'(E\left(S_{n+1}^w\right), \boldsymbol{\varepsilon}\left(\tilde{\boldsymbol{u}}_{n+1}\right), \tilde{d}_{n+1}) \right]\!\!\right] \mathrm{dV} - \int_\Omega \boldsymbol{b}^T S_{n+1}^w \tilde{p}_{n+1}^w \mathrm{dV} \\ & - \int_\Omega \boldsymbol{b}^T (1 - S_{n+1}^w) \tilde{p}_{n+1}^a \mathrm{dV} - \int_\Omega \boldsymbol{N}_u^T \rho_{n+1} \boldsymbol{g} \mathrm{dV} - \int_{\Gamma_{\boldsymbol{u}}^N} \boldsymbol{N}_u^T \bar{\boldsymbol{t}} \mathrm{d}\Gamma = 0 \end{aligned} \tag{5.39}$$

$$\begin{aligned} \boldsymbol{R}_{n+1}^w = & \int_\Omega \boldsymbol{N}_p^T n \rho^w \frac{S_{n+1}^w - S_n^w}{\Delta t} \mathrm{dV} + \int_\Omega \boldsymbol{N}_p^T S_{n+1}^w \rho^w \nabla \cdot \frac{\tilde{\boldsymbol{u}}_{n+1} - \tilde{\boldsymbol{u}}_n}{\Delta t} \mathrm{dV} \\ & + \int_\Omega (\nabla \boldsymbol{N}_p)^T \left[\rho^w \frac{k_{n+1}^{rw} k^s \boldsymbol{I}}{\mu^w} (\nabla \tilde{p}_{n+1}^w - \rho^w \boldsymbol{g}) \right] \mathrm{dV} + \int_{\Gamma_p^N} \boldsymbol{N}_p^T \bar{q}^w \mathrm{d}\Gamma = 0 \end{aligned} \tag{5.40}$$

$$\begin{aligned} \boldsymbol{R}_{n+1}^a = & -\int_\Omega \boldsymbol{N}_p^T n \rho_{n+1}^a \frac{S_{n+1}^w - S_n^w}{\Delta t} \mathrm{dV} + \int_\Omega \boldsymbol{N}_p^T (1 - S_{n+1}^w) \frac{n}{K^a} \frac{\tilde{p}_{n+1}^a - \tilde{p}_n^a}{\Delta t} \mathrm{dV} \\ & + \int_\Omega \boldsymbol{N}_p^T (1 - S_{n+1}^w) \rho_{n+1}^a \nabla \cdot \frac{\tilde{\boldsymbol{u}}_{n+1} - \tilde{\boldsymbol{u}}_n}{\Delta t} \mathrm{dV} \\ & + \int_\Omega (\nabla \boldsymbol{N}_p)^T \left[\rho_{n+1}^a \frac{k_{n+1}^{ra} k^s \boldsymbol{I}}{\mu^a} (\nabla \tilde{p}_{n+1}^a - \rho_{n+1}^a \boldsymbol{g}) \right] \mathrm{dV} + \int_{\Gamma_p^N} \boldsymbol{N}_p^T \bar{q}^a \mathrm{d}\Gamma = 0 \end{aligned} \tag{5.41}$$

where

$$[\![\boldsymbol{\sigma}']\!] = \left\{ \left[(1 - d^2) + \eta \right] \boldsymbol{D}^+ \left(E\left(S^w\right), \boldsymbol{\varepsilon} \right) + \boldsymbol{D}^- \left(E\left(S^w\right), \boldsymbol{\varepsilon} \right) \right\} [\![\boldsymbol{\varepsilon}]\!] \tag{5.42}$$

is the constitutive law (5.10) written in Voigt notation. If we consider a two-dimensional problem, the bulk modulus of the solid matrix becomes

$$K_2 = \lambda + \mu \tag{5.43}$$

and the positive and the negative parts of the elasticity matrix $\boldsymbol{D}$ are defined as

$$\boldsymbol{D}^{+}\left(E\left(S^{w}\right),\boldsymbol{\varepsilon}\right)=\frac{E\left(S^{w}\right)}{2\left(1-2\nu\right)\left(1+\nu\right)}\begin{bmatrix}1&1&0\\1&1&0\\0&0&0\end{bmatrix}\left\langle \operatorname{sgn}\left(\operatorname{tr}(\boldsymbol{\varepsilon})\right)\right\rangle_{+}$$

$$+\frac{E}{2\left(1+\nu\right)}\begin{bmatrix}1&-1&0\\-1&1&0\\0&0&1\end{bmatrix} \tag{5.44}$$

$$\boldsymbol{D}^{-}\left(E\left(S^{w}\right),\boldsymbol{\varepsilon}\right)=\frac{E\left(S^{w}\right)}{2\left(1-2\nu\right)\left(1+\nu\right)}\begin{bmatrix}1&1&0\\1&1&0\\0&0&0\end{bmatrix}\left\langle \operatorname{sgn}\left(\operatorname{tr}(\boldsymbol{\varepsilon})\right)\right\rangle_{-} \tag{5.45}$$

If we call $\underline{\hat{\boldsymbol{U}}}_{n+1}$ the generalized solution vector of the sub-problem (5.34), defined as

$$\underline{\hat{\boldsymbol{U}}}_{n+1}=\begin{Bmatrix}\hat{\boldsymbol{u}}_{n+1}\\ \hat{\boldsymbol{p}}^{w}_{n+1}\\ \hat{\boldsymbol{p}}^{a}_{n+1}\end{Bmatrix} \tag{5.46}$$

the generalized residual $\underline{\boldsymbol{R}}_{n+1}$ turns out to be a nonlinear function in $\underline{\hat{\boldsymbol{U}}}_{n+1}$, and so has to be linearized and solved using an iterative scheme. In this section we apply the Newton-Raphson method, in which the solution of the current time step $n+1$ is searched iteratively, approximating the function $\underline{\boldsymbol{R}}_{n+1}$ with its tangent. The approximation solution $\hat{\boldsymbol{U}}^{k+1}_{n+1}$, where $k+1$ indicates the current Newton-Raphson iteration $k+1$, , is obtained solving the linear system of equations

$$\boldsymbol{J}^{k}_{n+1}\Delta\underline{\hat{\boldsymbol{U}}}^{k+1}_{n+1}=-\underline{\boldsymbol{R}}^{k}_{n+1} \tag{5.47}$$

and then computing

$$\underline{\hat{\boldsymbol{U}}}^{k+1}_{n+1}=\underline{\hat{\boldsymbol{U}}}^{k}_{n+1}+\Delta\underline{\hat{\boldsymbol{U}}}^{k+1}_{n+1} \tag{5.48}$$

The matrix $\boldsymbol{J}^{k}_{n+1}$, known as Jacobian matrix of $\underline{\boldsymbol{R}}^{k}_{n+1}$, is defined as

$$\boldsymbol{J}^{k}_{n+1}=\frac{\partial\underline{\boldsymbol{R}}^{k}_{n+1}}{\partial\underline{\hat{\boldsymbol{U}}}^{k}_{n+1}}=\begin{bmatrix}\frac{\partial\boldsymbol{R}_{u}}{\partial\hat{\boldsymbol{u}}}&\frac{\partial\boldsymbol{R}_{u}}{\partial\hat{\boldsymbol{p}}^{w}}&\frac{\partial\boldsymbol{R}_{u}}{\partial\hat{\boldsymbol{p}}^{a}}\\ \frac{\partial\boldsymbol{R}_{w}}{\partial\hat{\boldsymbol{u}}}&\frac{\partial\boldsymbol{R}_{w}}{\partial\hat{\boldsymbol{p}}^{w}}&\frac{\partial\boldsymbol{R}_{w}}{\partial\hat{\boldsymbol{p}}^{a}}\\ \frac{\partial\boldsymbol{R}_{a}}{\partial\hat{\boldsymbol{u}}}&\frac{\partial\boldsymbol{R}_{a}}{\partial\hat{\boldsymbol{p}}^{w}}&\frac{\partial\boldsymbol{R}_{a}}{\partial\hat{\boldsymbol{p}}^{a}}\end{bmatrix} \tag{5.49}$$

The complete derivation of the Jacobian matrix $\boldsymbol{J}^{k}_{n+1}$ is reported in Appendix A

5.3 Numerical applications

5.3.1 The constrained Liakopoulos experiment

In this section we introduce a modify version of the Liakopoulos test presented in Section 3.3.4. In this case the upper boundary is constrained in the vertical direction, and the gravitational force is maintained in the equation of conservation of mass, as a driving force for the fluid flow, but its effect is not consider into the equilibrium equation. The initial and the boundary conditions, together with the dimensions of the domain are shown in Figure 5.1. This modification implies only a change in the stress state of the material in the initial condition, but has no influence on the evolution of displacements and pressure in the transient phase of the desiccation process. The modification is done in order to isolate the pressure as fracture driving force in the porous material. All the analysis are developed with a a two-phase (passive air pressure) and a three-phase model. We use the same parameter of the example in Section 3.3.4. summarized in the Table 3.2. The addition parameters for the air phase and the phase-field equation are $p_0^a = 101325\,Pa$, $\rho_0^a = 1,25\,Kg,m^3$,$\mu^a = 0,000018\,Pas$, $l = 0,01\,m$, $G_c = 0,3\,N/m$. The permeability of the gas is assumed to be as given by Brooks and Corey [16]

$$k^{ra} = (1 - S_e)^2 \left(1 - S_e^{\frac{5}{3}}\right) \tag{5.50}$$

$$S_e = \frac{S^w - 0,2}{0,8} \tag{5.51}$$

Three different cases, for both the two- and the three-phase model, are studied:

- NC case: vertical displacement non constrained at the upper boundary (Liakopoulos solution), without phase-field equation.
- C case: vertical displacement constrained at the upper boundary , without phase-field equation.
- C-PF case: vertical displacement constrained at the upper boundary , with phase-field equation.

The quadrilateral finite elements Q9Pw4/Q9 and Q9Pw4Pa4/Q9 are used for the two- and the three-phase model respectively.

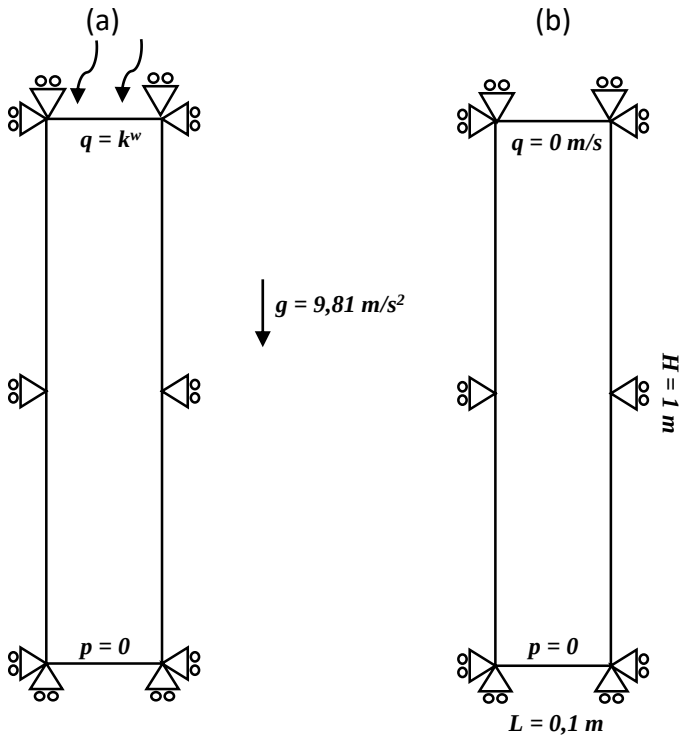

Figure 5.1: Scheme of the constrained Liakopoulos experiment: in (a) the initial conditions at $t = 0$ s, in (b) the boundary conditions for the desiccation process. The gravity $\boldsymbol{g}$ is taken into account only in the mass balance equation.

In Figure 5.2 the evolution in time of the variables p^w, p^a and $\boldsymbol{u}$ is shown, for the two- and the three-phase model, and without constraint on the top (NC case). The solution coincides with the reference solution of the classical Liakopouls problem [37] obtained in Section 3.3.4, confirming that the assumption done on the gravitational force does not influence the solution in the desiccation phase. These results are also useful to understand the influence of the air phase, in particular with respect to the time evolution of the problem. In fact, when the air phase is assumed constant, the desiccation process turns out to last longer than in the thee-phase case.

Figure 5.3 and Figure 5.4 show, for the two- and the three-phase model respectively, the comparison between the cases NC, C and C-PF. It is clear, looking at the displacements curves, that, for both two- and the three-phase models, the solution for the displacement field obtained in the C-PF case follows the one obtained in the C case, until a point in which it shows an abrupt jump, beginning to follow the one obtained in the NC case. This phenomenon is even more clear if we look at the evolution of the outgoing mass. This jump can be then consider as an indicator of

the development of a fracture. We notice also that this jump occurs earlier in the desiccation process, when three-phase model is used.

Finally, in Figure 5.5 and Figure 5.6 the results for the phase-field variable d are shown. In Figure 5.5.a and 5.5.b the evolution in time of the phase-field obtained with the two different models is shown. In both the cases, the cracking occurs at the lower boundary of the column. In Figure 5.6, for both models, the time evolution of the phase-field variable at bottom of the column is plotted together with the evolution of the water pressure at the top of the column: it can be noticed that, the crack localizes approximately at the same value of the pressure p^w for both models (green line in the figure). This is because the water pressure is strictly correlated to the effective stress throw the effective stress principle (5.6). Due to the fact that the minimum value reached by the water saturation, for both the models, is $S^w \simeq 0.91$, the contribution of the air pressure in the effective stress principle (5.6) is negligible also in the three-phase model. Therefore, taking into account the air phase is not important in terms of effect of the air pressure in the equilibrium equation. The importance of its contribution lies in the influence that the air flows has in the time scale of the fracture process.

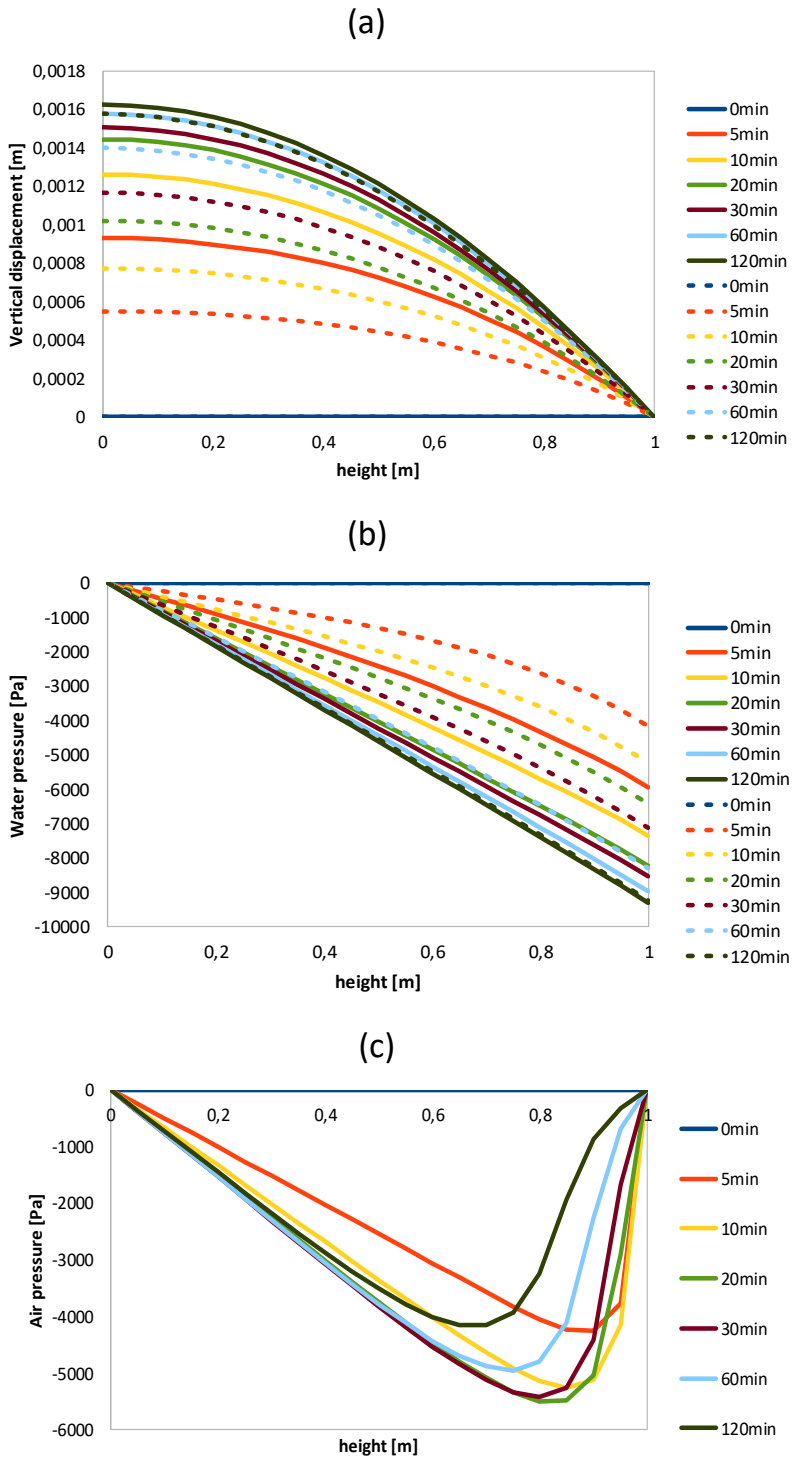

Figure 5.2: Comparison between the one phase (- -) and the two phase (—) model: (a) relative water pressure, (b) vertical displacement, (c) relative air pressure.

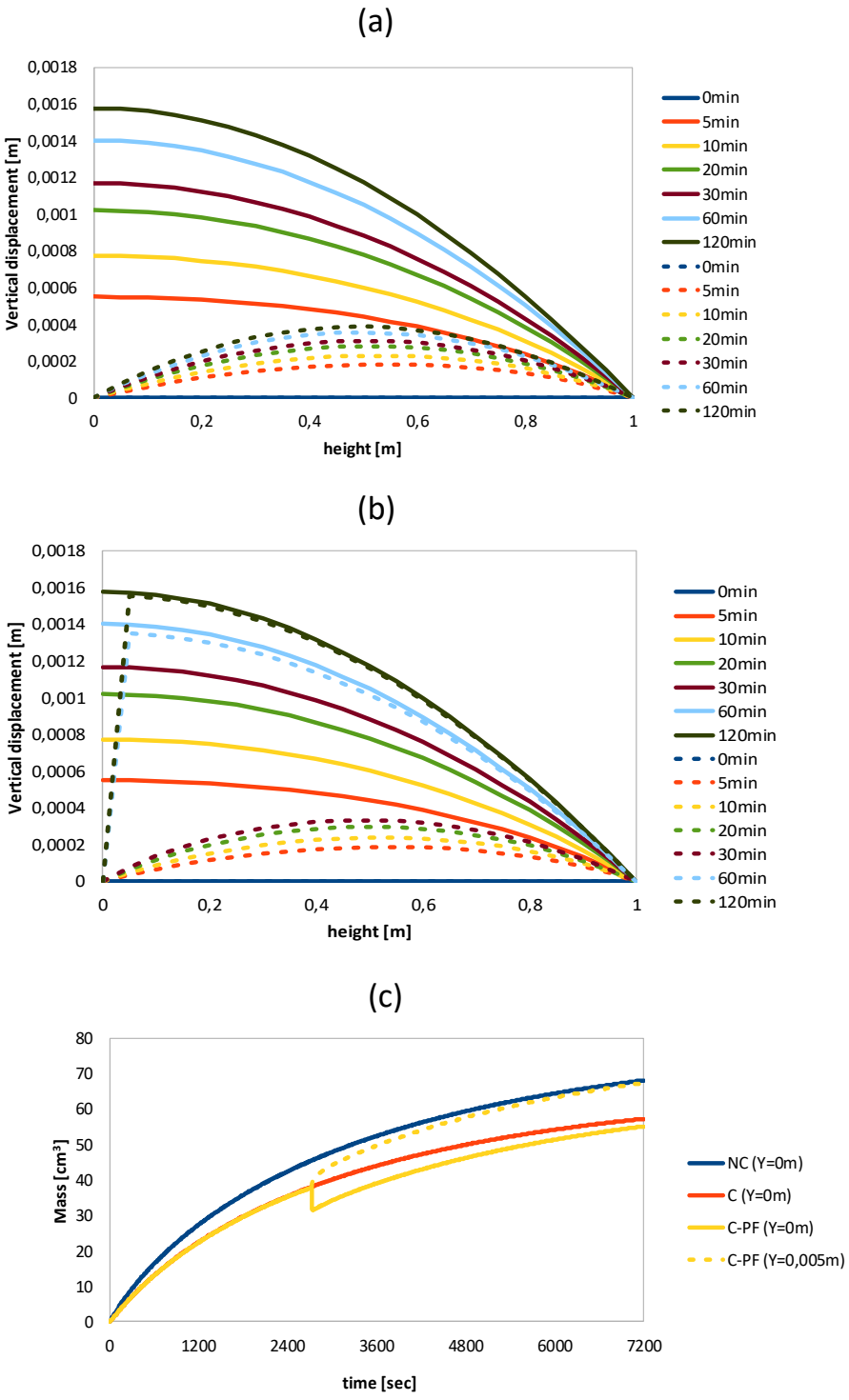

Figure 5.3: Solution for the two-phase model: (a) vertical displacement: comparison between the NC (—) and the C (- -) case, (b) vertical displacement: comparison between the NC (—) and the C-PF (- -) case, (c) evolution in time of the outgoing water mass.

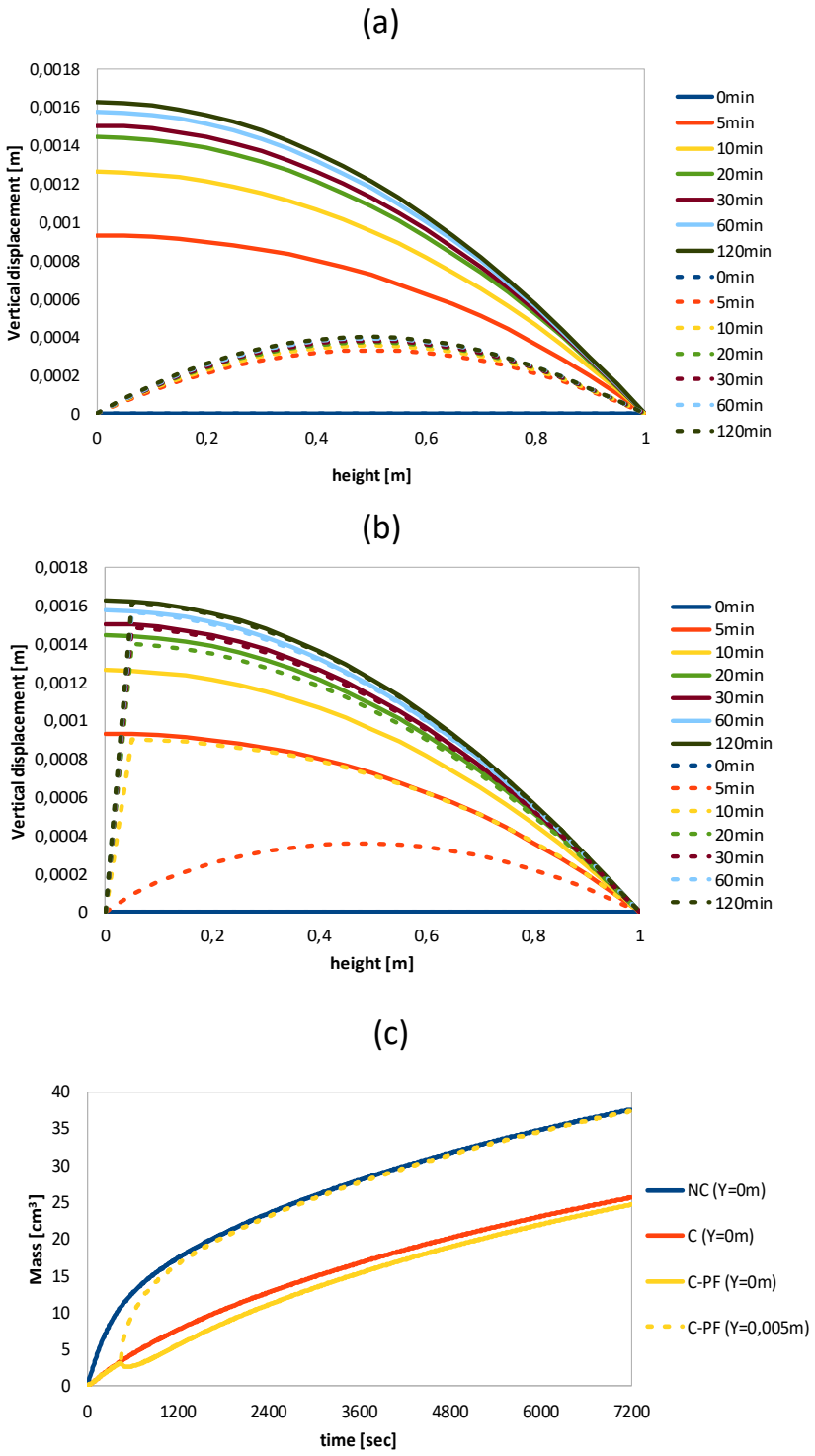

Figure 5.4: Solution for the three-phase model: (a) vertical displacement: comparison between the NC (—) and the C (- -) case, (b) vertical displacement: comparison between the NC (—) and the C-PF (- -) case, (c) evolution in time of the outgoing water mass.

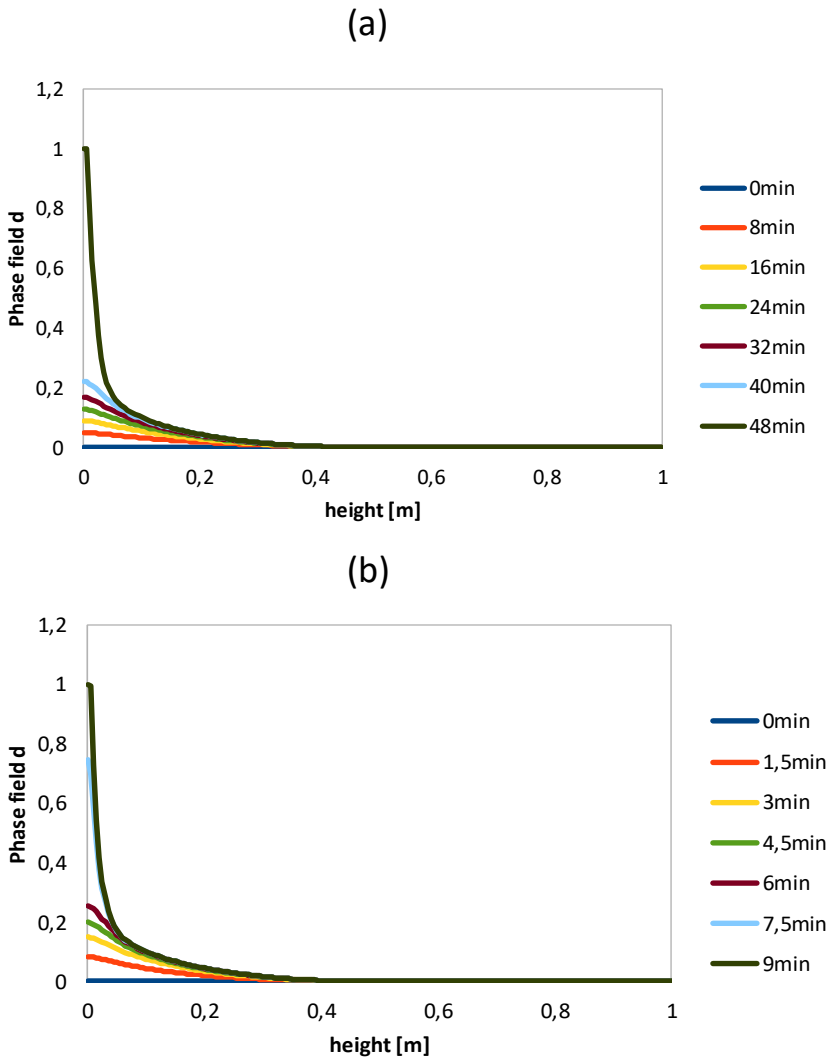

Figure 5.5: Phase-field solution: (a) evolution of the phase-field profile obtained with the two-phase model (a) and with the three-phase model (b).

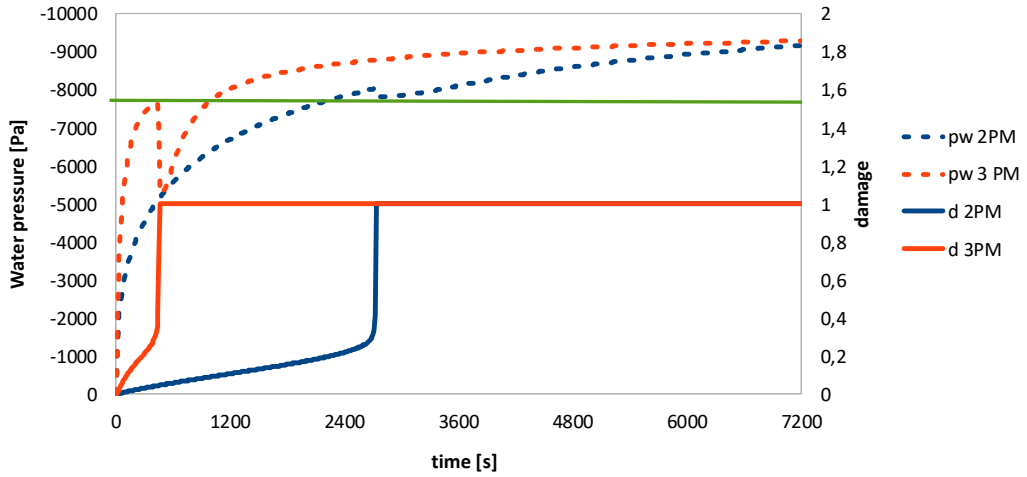

Figure 5.6: Phase-field solution: comparison between the time evolution of the phase-field at the bottom boundary and the evolution of the water pressure at the top boundary for the two models.

5.3.2 Desiccation cracking in clayey materials

Description of the problem

In this example we simulate the cracking of clayey materials during a desiccation process. This is a numerical application proposed in Cajuhi *et al.*[17] and based on the experimental results reported in [49] and [58] (see Figure 5.7). In the simulation presented in [17], taken as reference numerical test, the porous medium is considered partially saturated, with constant air pressure. The aim of this numerical investigation is to compare the results of the reference tests with the ones obtained considering the air flow in the medium.

The geometry and the boundary conditions are shown in Figure 5.8. The applied flux is $q^w = 6\,e^{-7}\,m/s$, and the desiccation is studied for a time $T = 60\,min$, with a regular time stepping of $\Delta t = 1\,s$. The mesh is discretized with square finite elements of dimension $h^e = 0,01\,cm$. The tolerance for the Newton-Raphson iterative scheme is $\texttt{TOL}_{\texttt{N-R}} = 10^{-5}$ and only one staggered iteration per time step is performed, due to the small dimension of the chosen time step [17]. The problem is assumed to be a pure 2D problem, with the deviatoric energy defined as $\boldsymbol{\varepsilon}^{dev} = \boldsymbol{\varepsilon} - \frac{1}{2}\text{tr}(\boldsymbol{\varepsilon})\boldsymbol{I}$, and no stress nor strain along the third dimension are present. The parameter of the model are $n = 0.41$, $\rho^s = 2800\,Kg/m^3$, $k^s = 10^{-15}\,m^3$, $l = 0.02\,m$. For the SWCC the Van

Genuchten model [64] is used, namely

$$\begin{cases} S^w = 1 & \text{for } p^c \leq 0 \\ S^w = (1 - S_r^w)\left[1 + \left(\frac{\alpha_{vg} p^c}{\rho^w g}\right)^{n_{vg}}\right]^{-m_{vg}} + S_r^w & \text{for } p^c > 0 \end{cases} \tag{5.52}$$

with $\alpha^{vg} = 0.028$, $n^{vg} = 1.3$. For the relative pressure k^{rw} and the air relative pressure k^{ws} the Mualem model [45]

$$k^{rw} = \sqrt{S_e^w}\left\{1 - \left[1 - (S_e^w)^{\frac{1}{m_{vg}}}\right]^{m_{vg}}\right\}^2 \tag{5.53}$$

$$k^{ra} = \left\{(1 - S_e^w)\left[1 - (S_e^w)^{\frac{1}{m_{vg}}}\right]^{m_{vg}}\right\}^2 + k_{RES}^{ra} \tag{5.54}$$

is used, where $S_e^w = (S^w - S_r^w)/(1 - S_r^w)$ is the effective saturation, m_{vg} is the same parameter used in the Van Genuchten model, and $k_{RES}^{ra} = 0.01$ is an artificial residual air relative permeability, fundamental in the numerical application because it allows to maintain the mass balance equation of solid and air (2.30) always "active", also when $S^w = 1$.

For the elastic parameter, as done in [17], we assume $\nu = 0.4$, and the relations

$$E = 1770 exp(-0.297 w)\, MPa$$

$$\sigma^c = 228.85 exp(-0.14 w)\, MPa$$

proposed in [58]. As pointed out in [17], it is possible to use the formula (2.132), to derive the following expression for the fracture toughness

$$G_c(w) = \left(\frac{16}{9}\right)^2 \sigma^c(w) \frac{3l}{E(w)} \tag{5.55}$$

obtaining a value of G_c depending on the water content, and therefore on the saturation. The finite elements used for the solution of the problem are quadrilateral elements Q9Pw4/Q9 for the two-phase formulation $\boldsymbol{u} - p^w - d$ and quadrilateral elements Q9Pw4Pa4/Q9 for the three-phase formulation $\boldsymbol{u} - p^w - p^a - d$. In addition, the numerical problem is also solved using the mixed two-phase formulation $\boldsymbol{u} - p^t - p^w - d$, developed in Section 4.4.2, and extended to take into account the partial saturated condition with constant air pressure, in order to test again the stabilization proposed. For the mixed formulation the quadrilateral elements Q4Pt4Pw4/Q4 and quadrilateral elements Q4Pt4sPw4/Q4 are used. The interpolations used for all of these elements are summarized in Table 5.1.

	$\boldsymbol{u}$	p^t	p^w	p^a	d
Q9Pw4/Q9	quadratic	-	linear	-	quadratic
Q9Pw4Pa4/Q9	quadratic	-	linear	linear	quadratic
Q4Pt4Pw4/Q4	linear	linear	linear	-	linear
Q4Pt4sPw4/Q4	linear	linear - stabilized	linear	-	linear

Table 5.1: Summary of the different finite elements used in the simulation.

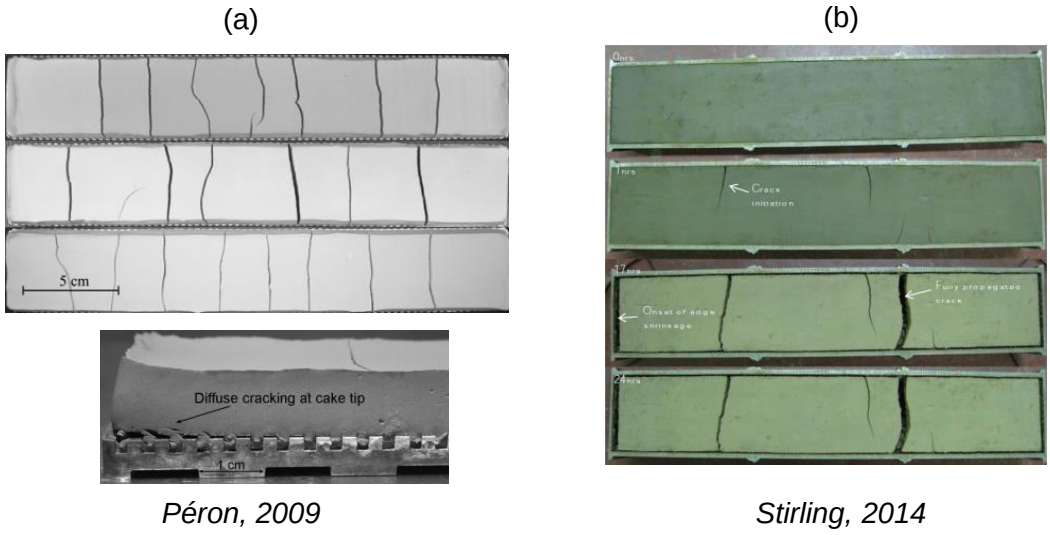

Figure 5.7: Experiments on desiccation cracking in clays: (a) Peron *et al.* [49], (b) Stirling *et al.* [58]

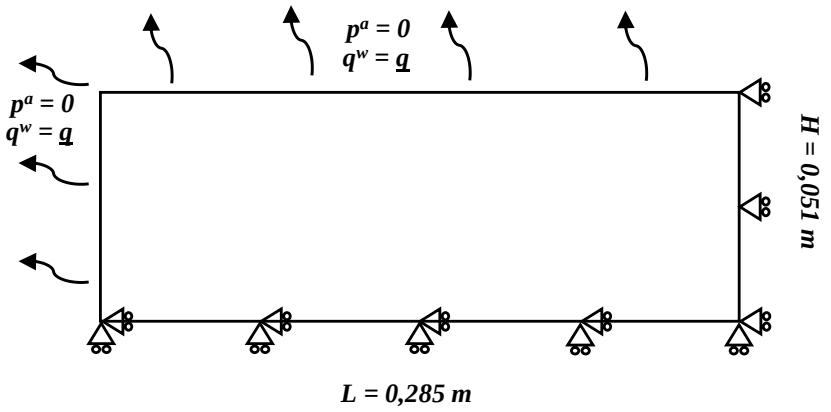

Figure 5.8: Scheme of the desiccation problem.

Reference numerical test

In Figure 5.9, Figure 5.10 and Figure 5.11 the evolution in time of the phase-field d, the water pressure p^w and the water saturation S^w, obtained with the two-phase $\boldsymbol{u} - p^w - d$ formulation, are shown. These results are obtained using a discretization with quadrilateral elements (Q9Pw4/Q9), the same used in [17], and are in good agreement with the one shown in the article. In particular, looking at the evolution of the crack pattern in Figure 5.9, it can be noticed that the first crack to occur is a shear crack at the lower left corner of the domain. As underlined in [17], the presence of this shear crack is in agreement with the experimental observation done in [49], and is due to the Dirichlet homogeneous constraint applied on the horizontal displacements in the lowed boundary, condition similar to the one created in the experiment of Peron [49] (Figure 5.7.a). After a time $t \simeq 27\,min$ a second crack nucleates on the upper part of the domain, and propagates almost vertically throw the entire domain, dividing the body in two parts. The nucleation of a second vertical crack is observed at the end of the simulation. Comparing the evolution of the water saturation (Figure 5.11) with the one of the phase-field, an other correspondence with the experimental observations can be found. At the crack onset in fact the water saturation is closed to the unit value, which have been noticed also in the experiments reported in [49].

In Figure 5.12 and 5.13 the results relative to evolution in time of the phase-field d obtained with the mixed two-phase formulation $\boldsymbol{u} - p^t - p^w - d$ are shown. Two different mixed elements are used in the simulation, i.e. the element Q4Pw4/Q4

(Figure 5.12) and the stabilized element Q4Pt4sPw4/Q4 (Figure). The location of the cracks in the domain obtained with the non stabilized element Q4Pw4/Q4 is the same of the one obtained with the standard Q9Pw4/Q9, but it can be noticed that the width of the cracks is larger, although the characteristic length l has not been changed. On the other hand, if we look at the solution obtained with the stabilized element Q4Pt4sPw4/Q4, not only the same crack pattern of the reference solution (Q9Pw4/Q9) is obtain, but also the width of the crack is the same. Anyway, in this application it has been necessary to introduce a coefficient $\tau = 0.03$, similar to the one used in [66], in order to slightly penalized the effect of the stabilization term, which otherwise would lead to irregular crack patterns.

Finally, in Figure 5.14 and Figure 5.14 the evolution in time of the phase-field d, and of the water saturation S^w, obtained with the three-phase $\boldsymbol{u} - p^w - p^a - d$ formulation, are shown. We can immediately notice that the solution for the both field is almost coincident to the one obtained without considering the flow of the gaseous phase. Even if at a glance this results seems to lead to the conclusion that the modeling of the air phase is not needed for a correct simulation of the desiccation process, further investigation is needed to understand if this coincidence of the solutions is a result of the particular geometry and boundary conditions of the problem. The effect of the air phase is in fact expected to be mitigated in the vicinity of the boundaries where homogeneous condition on the air pressure are applied. This could be exactly the case of the problem in analysis, where due to the small height of the domain, the effect of the Dirichlet condition on the air pressure imposed on two sides mitigates the effect of the air phase. This consideration leads to the numerical experiment presented in the next section, in which the same desiccation problem is solved for an higher domain and different BCs.

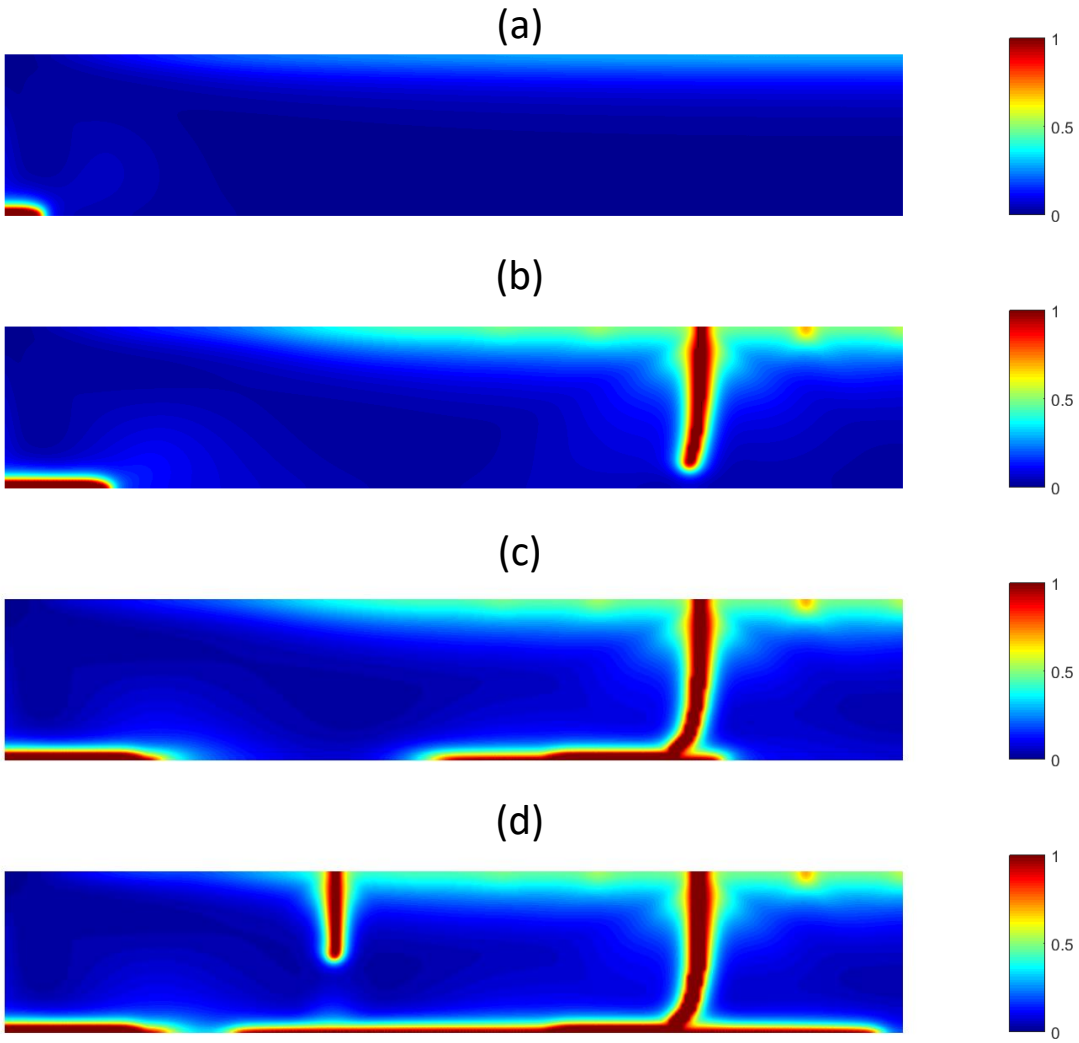

Figure 5.9: Phase-field contours for the two-phase model (Q9Pw4/Q9 elements): (a) 15 min, (b) 30min, (c) 45 min, (d) 60 min.

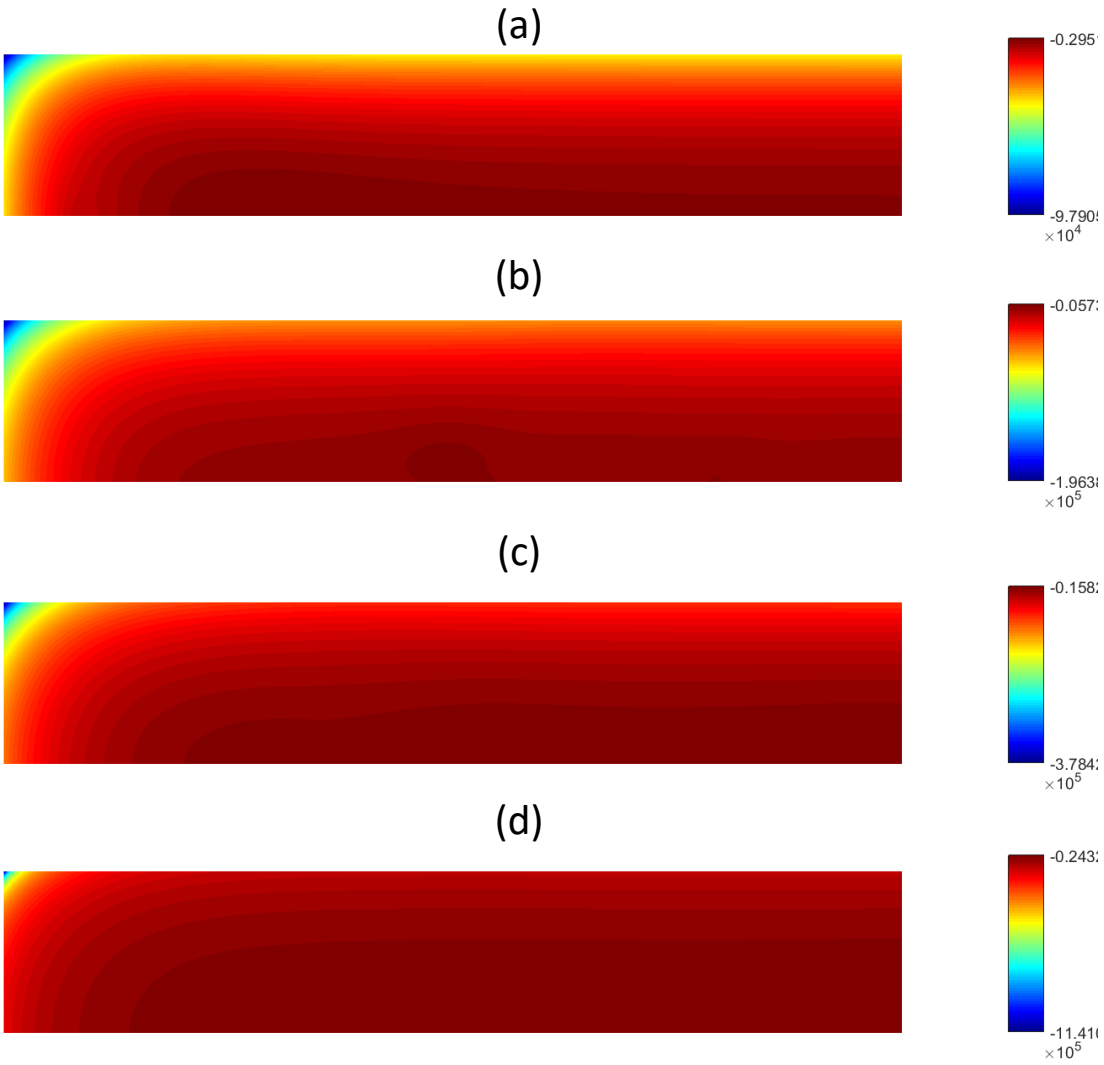

Figure 5.10: Water pressure contours for the two-phase model (Q9Pw4/Q9 elements): (a) 15 min, (b) 30min, (c) 45 min, (d) 60 min.

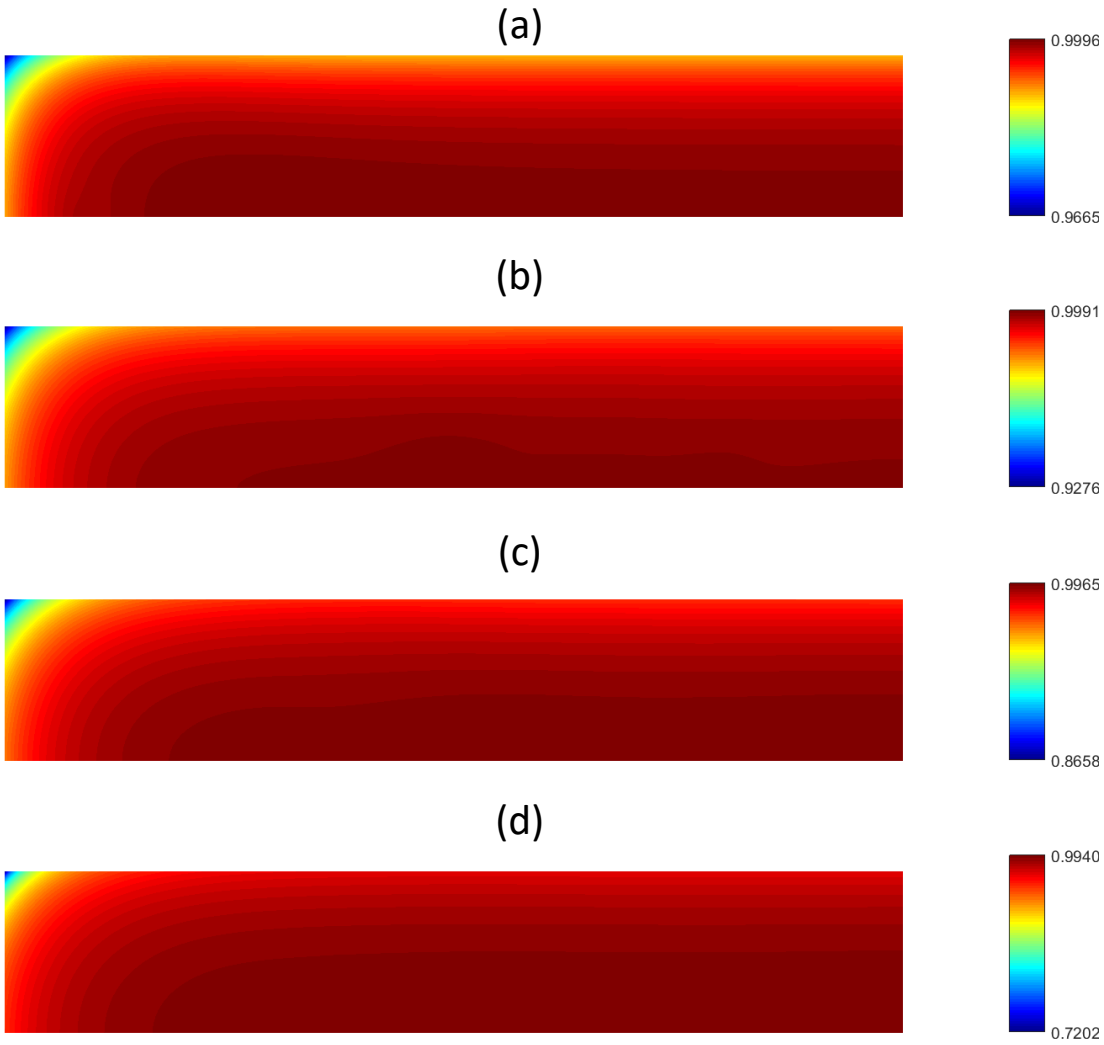

Figure 5.11: Water saturation contours for the two-phase model (Q9Pw4/Q9 elements): (a) 15 min, (b) 30min, (c) 45 min, (d) 60 min.

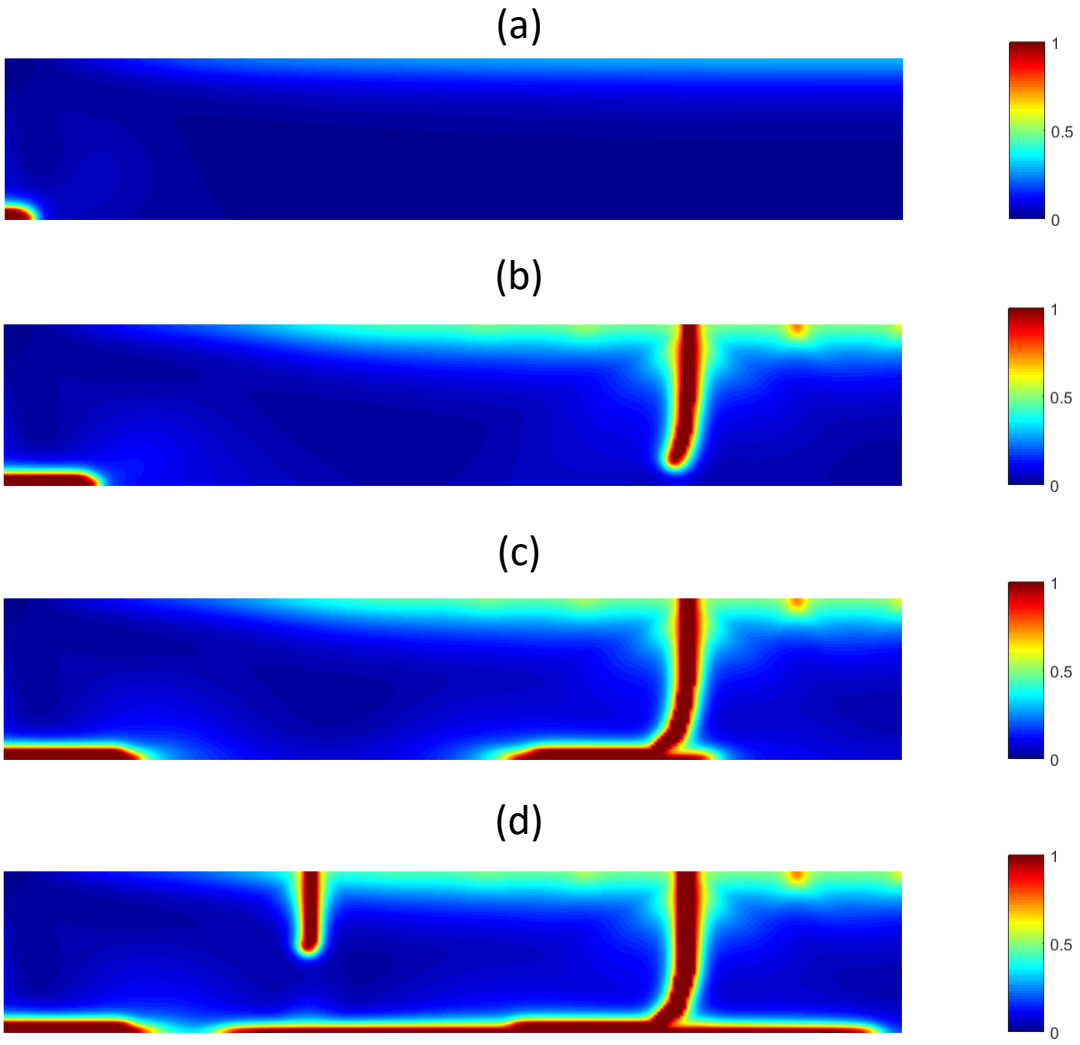

Figure 5.12: Phase-field contours for the mixed two-phase model (Q4Pt4Pw4/Q4 elements): (a) 15 min, (b) 30min, (c) 45 min, (d) 60 min.

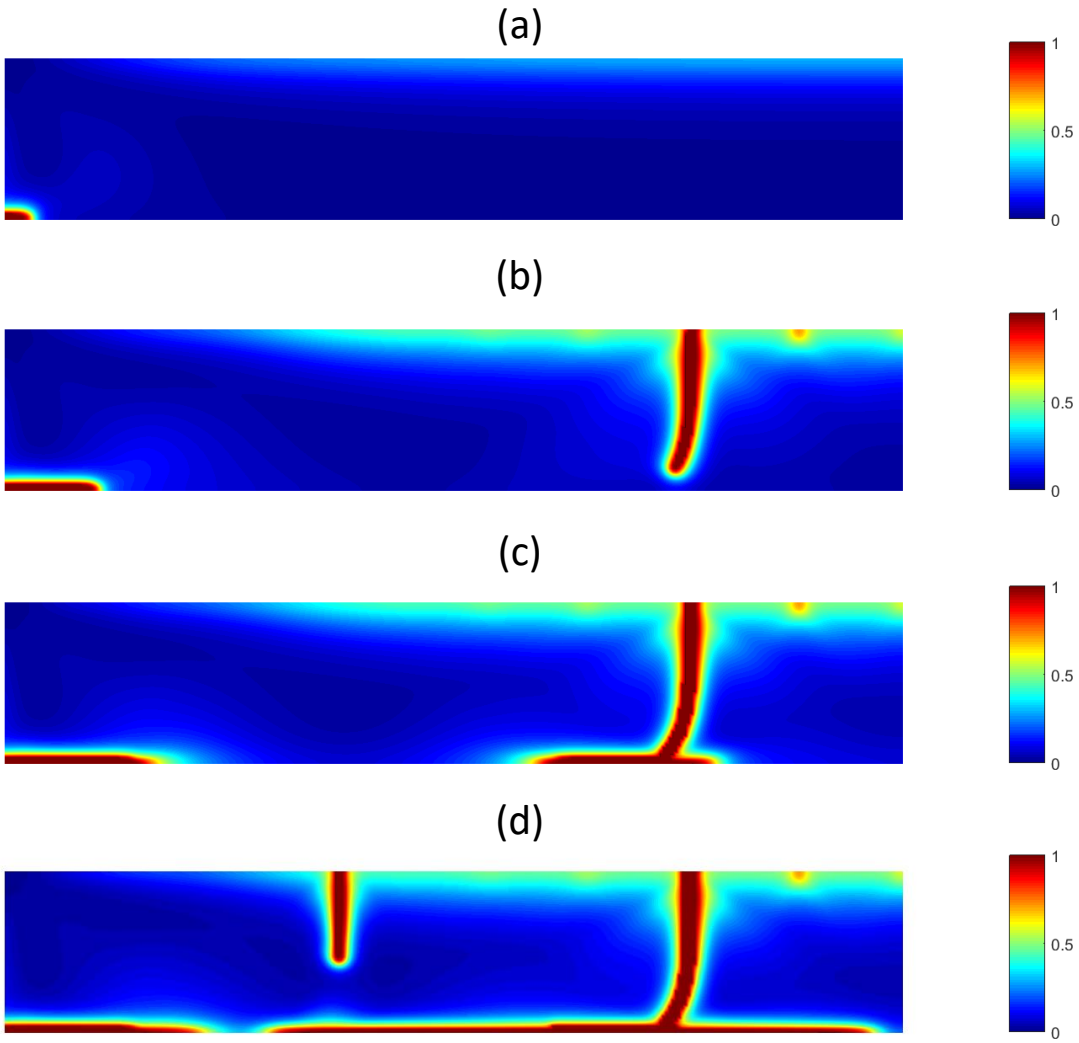

Figure 5.13: Phase-field contours for the stabilized mixed two-phase model (mixed stabilized Q4Pt4sPw4s/Q4 elements): (a) 15 min, (b) 30min, (c) 45 min, (d) 60 min.

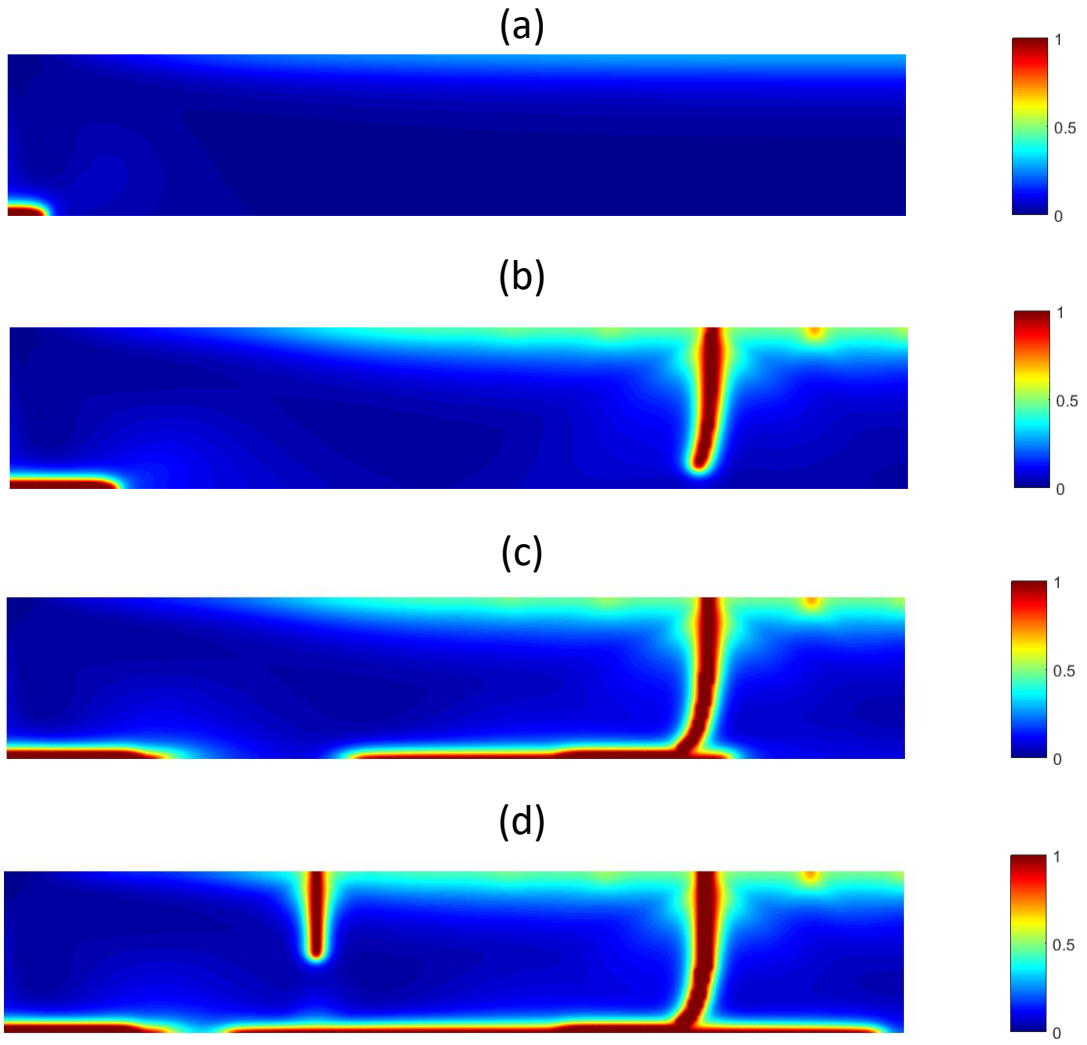

Figure 5.14: Phase-field contours for the three-phase model (Q9Pt4Pw4Pa4/Q9 elements): (a) 15 min, (b) 30min, (c) 45 min, (d) 60 min.

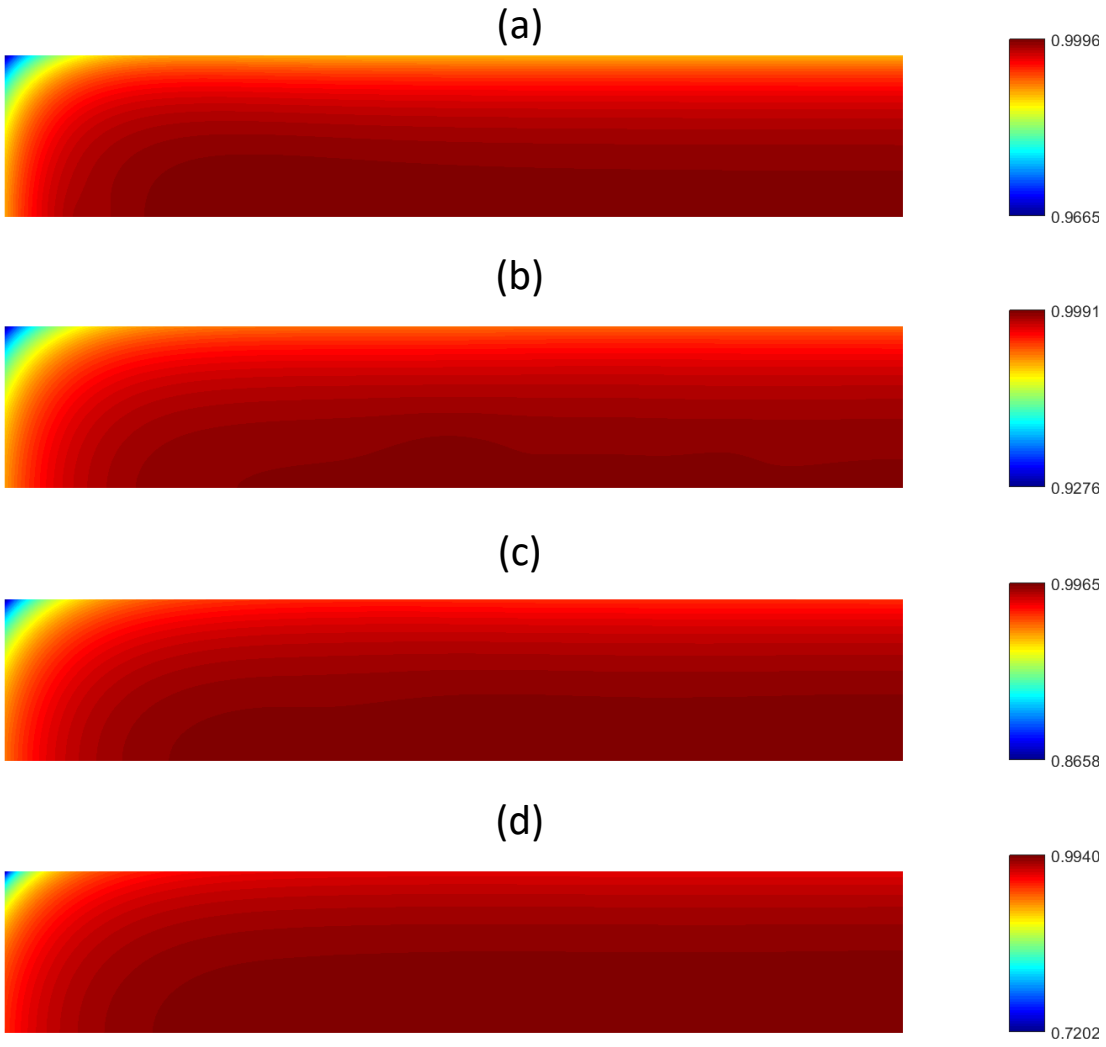

Figure 5.15: Water saturation contours for the three-phase model (Q9Pw4/Q9 elements): (a) 15 min, (b) 30min, (c) 45 min, (d) 60 min.

Modified desiccation test

We propose in this section a modification of the previous numerical test, in which a higher domain is considered. Different BCs are also applied on the left side: no water and air flux. These BCs are expected to be more similar to the ones of the the experiment presented in [58] (Figure 5.7.b). The new geometry and the BCs are shown in Figure 5.16. All the material properties and the parameter of the simulation coincides with the ones of the reference test. The total time of the simulation is $T = 120\,min$.

In Figure 5.17 the evolution in time of the phase-field d, for the two- and the three-phase model, is shown. In this case the influence of the air phase becomes relevant. In contrast with the reference test modeled in the previous section, for both models, the first crack to appear is a vertical crack starting from the upper boundary, while in a second stage a shear crack appears on the lower left corner. Anyway the moment in which these two cracks nucleate is different for the two models. In particular, the first vertical crack appears earlier in the two-phase model ($t = 23\,min$) and, slightly later, in the three-phase model ($t = 28\,min$). The difference becomes event more evident for the second crack: it appears first in the three-phase model ($t = 28\,min$), and then in the two-phase model ($t = 28\,min$), showing a difference close to the 20% of the total simulation time. A difference can be noticed also in the final crack pattern.

Finally, looking at the contours of the saturation S^w at the end of the simulation, shown in Figure 5.18, it can be noticed that, with the three-phase model, the gradient of the saturation is slightly more concentrated in the vicinity of the upper boundary, with respect to the solution obtained using the two-phase model.

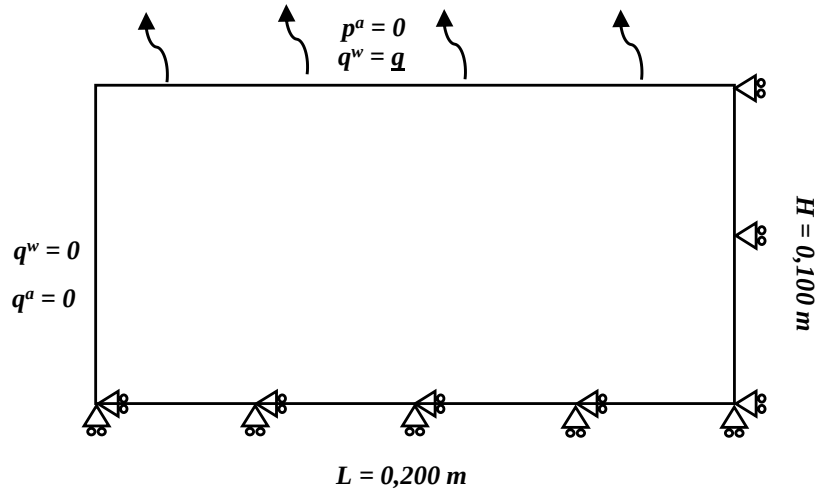

Figure 5.16: Scheme of the modified desiccation problem.

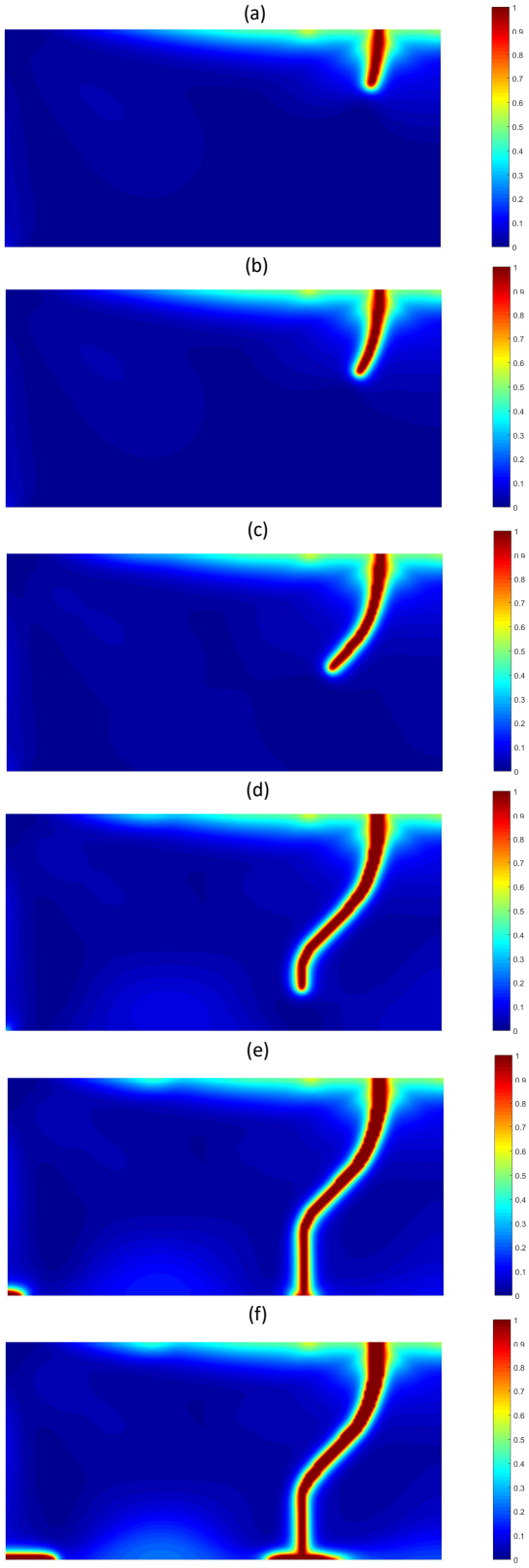

Figure 5.17: Phase-field contours for the two-phase model (Q9Pt4Pw4/Q9 elements): (a) 23 min (first crack), (b) 28min, (c) 40 min, (d) 75 min, (d) 95 min (second crack), (d) 120 min.

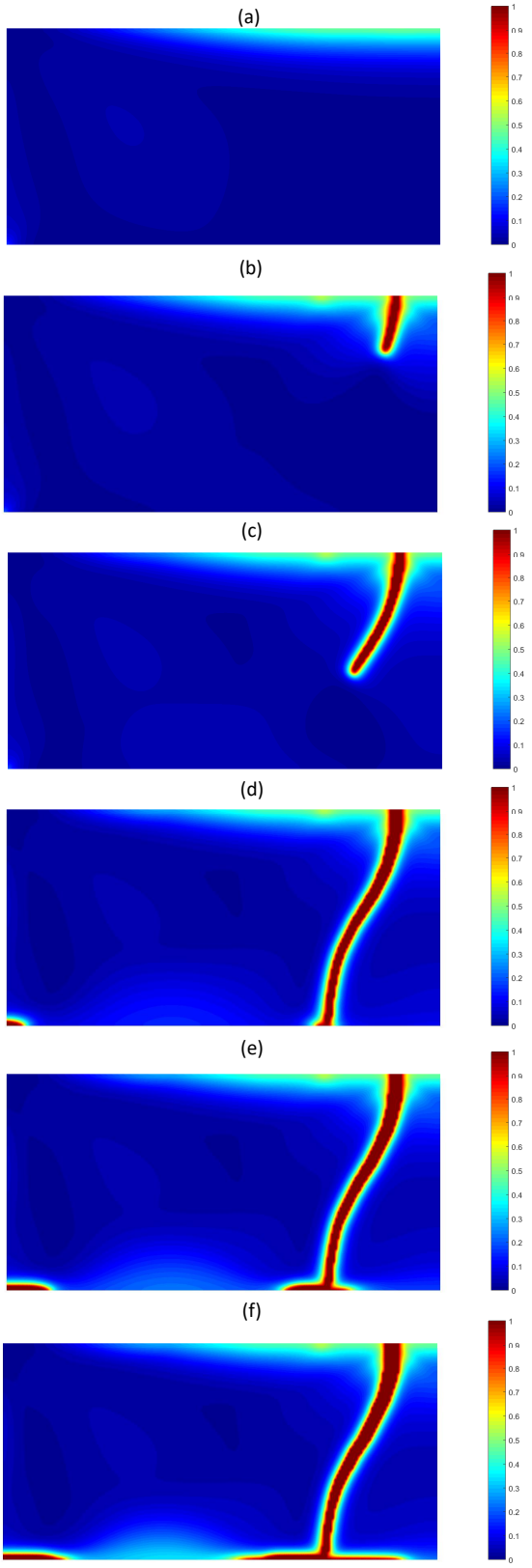

Figure 5.18: Phase-field contours for the three-phase model (Q9Pt4Pw4Pa4/Q9 elements): (a) 23 min, (b) 28min (first crack), (c) 40 min, (d) 75 min (second crack), (d) 95 min , (d) 120 min.

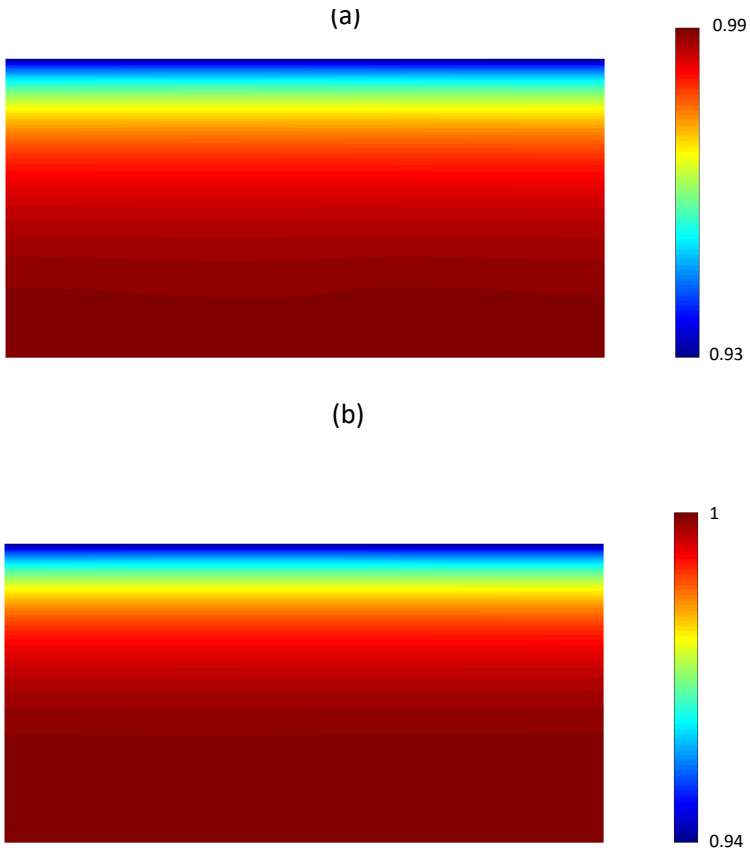

Figure 5.19: Water saturation contours at $t = 120$ min: (a) two-phase model, (b) three-phase model.

5.4 Conclusions

In the first part of this chapter the finite element implementation of the phase-field model for fracture in three-phase porous media has been derived, with particular attention on the nonlinear constitutive dependency of the elastic and the fracture parameters that characterizes certain soil materials. A staggered procedure for the solution of the problem has been adopted, in which the phase-field evolution equations is solved independently, while the equilibrium and the mass conservation equations are solved with a monolithic approach.

This numerical model has been applied to the solution of two different cases of constrained desiccation, and the results have been compared with the ones obtained assuming the passive air condition, i.e. without taking into account the mass conservation equation for the air phase. The results show how taking into account the air phase influences the time evolution of the fracture process, as well as the final

cracking pattern. Anyway, for certain specific boundary conditions and geometries, it has been noticed that the influence of the air phase becomes negligible. Finally the stabilized mixed formulation proposed in the previous chapter has been applied successfully to the second desiccation problem, although in this case the introduction of a coefficient which mitigates the effect of the stabilization is found to be needed.

Conclusions

In this work a phase-field model for the fracture in three-phase partially saturated porous media has been developed. The numerical discretization of the model has been derived using the Finite Element Method, with particular attention on some numerical issues due to the coupled nature of the problem.

In particular, the mass conservation properties of different numerical schemes for the discretization of the mass balance equation of the water in partially saturated porous media have been investigate, both considering the solid skeleton rigid and deformable. A new conservative scheme for the deformable case has been derived and successfully tested in the simulation of a desiccation process.

Furthermore, the problem of the numerical locking due to undrained conditions in saturated porous media has been reviewed, including the study of a stabilization technique, called polynomial pressure-projection, for finite elements with linear interpolation for the displacement field. This stabilization technique has been extended to different mixed formulations of the phase-field model for fracture in elastic and poroelastic materials.

In the last part of the thesis the finite element implementation of the equations governing the phase-field model of fracture in three-phase partially saturated porous media has been developed, and applied to two different problems of constrained desiccation. It has been shown how considering the flow of the air in the medium can significantly influence the time scale of the evolution of the fractures.

Finally we notice how taking into account in the model the mass balance equation for the gaseous phase, considered in this work as dry air, can also be considered as a starting point for an extension of the model in which the gas is considered as a mixture of dry air and vapor, which would allow to model more accurately the real physical processes which characterize the problem of desiccation.

Appendix A

Derivation of the Jacobian matrix for the three-phase model

In this section we derive, from the expressions (5.39), (5.40) and (5.41) the Jacobian matrix $\boldsymbol{J}_{n+1}$ for the nonlinear solution of the system of equations

$$\underline{\boldsymbol{R}}_{n+1} = \left\{ \begin{array}{c} \boldsymbol{R}^u_{n+1} \\ \boldsymbol{R}^w_{n+1} \\ \boldsymbol{R}^a_{n+1} \end{array} \right\} = \boldsymbol{0} \tag{A.1}$$

The Jacobian matrix $\boldsymbol{J}_{n+1}$ is defined as

$$\boldsymbol{J}_{n+1} = \frac{\partial \underline{\boldsymbol{R}}_{n+1}}{\partial \underline{\hat{\boldsymbol{U}}}^k_{n+1}} = \left[\begin{array}{ccc} \frac{\partial \boldsymbol{R}_u}{\partial \hat{\boldsymbol{u}}} & \frac{\partial \boldsymbol{R}_u}{\partial \hat{\boldsymbol{p}}^w} & \frac{\partial \boldsymbol{R}_u}{\partial \hat{\boldsymbol{p}}^a} \\ \frac{\partial \boldsymbol{R}_w}{\partial \hat{\boldsymbol{u}}} & \frac{\partial \boldsymbol{R}_w}{\partial \hat{\boldsymbol{p}}^w} & \frac{\partial \boldsymbol{R}_w}{\partial \hat{\boldsymbol{p}}^a} \\ \frac{\partial \boldsymbol{R}_a}{\partial \hat{\boldsymbol{u}}} & \frac{\partial \boldsymbol{R}_a}{\partial \hat{\boldsymbol{p}}^w} & \frac{\partial \boldsymbol{R}_a}{\partial \hat{\boldsymbol{p}}^a} \end{array} \right] \tag{A.2}$$

The expression obtained for the matrix $\boldsymbol{J}^{uu}_{n+1}$ is

$$\boldsymbol{J}^{uu}_{n+1} = \frac{\partial \boldsymbol{R}_u}{\partial \hat{\boldsymbol{u}}} = \int_\Omega \boldsymbol{B}^T \left\{ \left[(1 - \tilde{d}^2_{n+1}) + \eta \right] \boldsymbol{D}^+_{n+1} + \boldsymbol{D}^-_{n+1} \right\} \boldsymbol{B} \mathrm{dV} \tag{A.3}$$

The expression obtained for the matrix $\boldsymbol{J}^{uw}_{n+1}$ is

$$\boldsymbol{J}^{uw}_{n+1} = \frac{\partial \boldsymbol{R}_u}{\partial \hat{\boldsymbol{p}}^w} = \boldsymbol{J}^{uw1}_{n+1} + \boldsymbol{J}^{uw2}_{n+1} + \boldsymbol{J}^{uw3}_{n+1} + \boldsymbol{J}^{uw4}_{n+1} + \boldsymbol{J}^{uw5}_{n+1} \tag{A.4}$$

where

$$\boldsymbol{J}^{uw1}_{n+1} = \int_\Omega \boldsymbol{B}^T \left\{ \left[(1 - \tilde{d}^2_{n+1}) + \eta \right] \frac{\partial \boldsymbol{D}^+}{\partial E} + \frac{\partial \boldsymbol{D}^+}{\partial E} \right\} \frac{\partial E}{\partial S^w} \frac{\partial S^w}{\partial p^w} [\![\boldsymbol{\varepsilon}_{n+1}]\!] \boldsymbol{N}_p \mathrm{dV} \tag{A.5}$$

$$\boldsymbol{J}^{uw2}_{n+1} = - \int_\Omega \boldsymbol{b}^T S^w_{n+1} \boldsymbol{N}_p \mathrm{dV} \tag{A.6}$$

$$\boldsymbol{J}_{n+1}^{uw3} = -\int_{\Omega} \boldsymbol{b}^T \frac{\partial S^w}{\partial p^w} \tilde{p}_{n+1}^w \boldsymbol{N}_p \mathrm{dV} \tag{A.7}$$

$$\boldsymbol{J}_{n+1}^{uw4} = \int_{\Omega} \boldsymbol{b}^T \frac{\partial S^w}{\partial p^w} \tilde{p}_{n+1}^a \boldsymbol{N}_p \mathrm{dV} \tag{A.8}$$

$$\boldsymbol{J}_{n+1}^{uw5} = -\int_{\Omega} \boldsymbol{N}_u^T \frac{\partial \rho}{\partial S^w} \frac{\partial S^w}{\partial p^w} \boldsymbol{g} \boldsymbol{N}_p \mathrm{dV} \tag{A.9}$$

The expression obtained for the matrix $\boldsymbol{J}_{n+1}^{ua}$ is

$$\boldsymbol{J}_{n+1}^{ua} = \frac{\partial \boldsymbol{R}_u}{\partial \hat{\boldsymbol{p}}^a} = \boldsymbol{J}_{n+1}^{ua1} + \boldsymbol{J}_{n+1}^{ua2} + \boldsymbol{J}_{n+1}^{ua3} + \boldsymbol{J}_{n+1}^{ua4} + \boldsymbol{J}_{n+1}^{ua5} + \boldsymbol{J}_{n+1}^{ua6} \tag{A.10}$$

where

$$\boldsymbol{J}_{n+1}^{ua1} = \int_{\Omega} \boldsymbol{B}^T \left\{ \left[(1 - \tilde{d}_{n+1}^2) + \eta \right] \frac{\partial \boldsymbol{D}_{n+1}^+}{\partial E} + \frac{\partial \boldsymbol{D}_{n+1}^+}{\partial E} \right\} \frac{\partial E}{\partial S^w} \frac{\partial S^w}{\partial p^a} [\![\boldsymbol{\varepsilon}_{n+1}]\!] \boldsymbol{N}_p \mathrm{dV} \tag{A.11}$$

$$\boldsymbol{J}_{n+1}^{ua2} = -\int_{\Omega} \boldsymbol{b}^T \frac{\partial S^w}{\partial p^a} \tilde{p}_{n+1}^w \boldsymbol{N}_p \mathrm{dV} \tag{A.12}$$

$$\boldsymbol{J}_{n+1}^{ua3} = -\int_{\Omega} \boldsymbol{b}^T (1 - S_{n+1}^w) \boldsymbol{N}_p \mathrm{dV} \tag{A.13}$$

$$\boldsymbol{J}_{n+1}^{ua4} = \int_{\Omega} \boldsymbol{b}^T \frac{\partial S^w}{\partial p^a} \tilde{p}_{n+1}^a \boldsymbol{N}_p \mathrm{dV} \tag{A.14}$$

$$\boldsymbol{J}_{n+1}^{ua5} = -\int_{\Omega} \boldsymbol{N}_u^T \frac{\partial \rho}{\partial S^w} \frac{\partial S^w}{\partial p^a} \boldsymbol{g} \boldsymbol{N}_p \mathrm{dV} \tag{A.15}$$

$$\boldsymbol{J}_{n+1}^{ua6} = -\int_{\Omega} \boldsymbol{N}_u^T \frac{\partial \rho}{\partial \rho^a} \frac{\partial \rho^a}{\partial p^a} \boldsymbol{g} \boldsymbol{N}_p \mathrm{dV} \tag{A.16}$$

The expression obtained for the matrix $\boldsymbol{J}_{n+1}^{wu}$ is

$$\boldsymbol{J}_{n+1}^{wu} = \frac{\partial \boldsymbol{R}_w}{\partial \hat{\boldsymbol{u}}} = \int_{\Omega} \boldsymbol{N}_p^T S_{n+1}^w \rho^w \boldsymbol{b} \mathrm{dV} \tag{A.17}$$

The expression obtained for the matrix $\boldsymbol{J}_{n+1}^{ww}$ is

$$\boldsymbol{J}_{n+1}^{ww} = \frac{\partial \boldsymbol{R}_w}{\partial \hat{\boldsymbol{p}}^w} = \boldsymbol{J}_{n+1}^{ww1} + \boldsymbol{J}_{n+1}^{ww2} + \boldsymbol{J}_{n+1}^{ww3} + \boldsymbol{J}_{n+1}^{ww4} \tag{A.18}$$

where

$$\boldsymbol{J}_{n+1}^{ww1} = \int_{\Omega} \boldsymbol{N}_p^T \frac{n \rho^w}{\Delta t} \frac{\partial S^w}{\partial p^w} \boldsymbol{N}_p \mathrm{dV} \tag{A.19}$$

$$\boldsymbol{J}_{n+1}^{ww2} = \int_{\Omega} \boldsymbol{N}_p^T \rho^w \left(\nabla \cdot \frac{\tilde{\boldsymbol{u}}_{n+1} - \tilde{\boldsymbol{u}}_n}{\Delta t} \right) \frac{\partial S^w}{\partial p^w} \boldsymbol{N}_p \mathrm{dV} \tag{A.20}$$

$$\boldsymbol{J}_{n+1}^{ww3} = \int_{\Omega} (\nabla \boldsymbol{N}_p)^T \rho^w \frac{k_{n+1}^{rw} k^s \boldsymbol{I}}{\mu^w} \boldsymbol{N}_p \mathrm{dV} \tag{A.21}$$

$$\boldsymbol{J}_{n+1}^{ww4} = \int_{\Omega} (\nabla \boldsymbol{N}_p)^T \left[\rho^w \frac{k^s \boldsymbol{I}}{\mu^w} (\nabla \tilde{p}_{n+1}^w - \rho^w \boldsymbol{g}) \right] \frac{\partial k^{rw}}{\partial S^w} \frac{\partial S^w}{\partial p^w} \boldsymbol{N}_p \mathrm{dV} \tag{A.22}$$

The expression obtained for the matrix $\boldsymbol{J}_{n+1}^{wa}$ is

$$\boldsymbol{J}_{n+1}^{wa} = \frac{\partial \boldsymbol{R}_w}{\partial \hat{\boldsymbol{p}}^a} = \boldsymbol{J}_{n+1}^{wa1} + \boldsymbol{J}_{n+1}^{wa2} + \boldsymbol{J}_{n+1}^{wa3} \tag{A.23}$$

where

$$\boldsymbol{J}_{n+1}^{wa1} = \int_{\Omega} \boldsymbol{N}_p^T \frac{n \rho^w}{\Delta t} \frac{\partial S^w}{\partial p^a} \boldsymbol{N}_p \mathrm{dV} \tag{A.24}$$

$$\boldsymbol{J}_{n+1}^{wa2} = \int_{\Omega} \boldsymbol{N}_p^T \rho^w \left(\nabla \cdot \frac{\tilde{\boldsymbol{u}}_{n+1} - \tilde{\boldsymbol{u}}_n}{\Delta t} \right) \frac{\partial S^w}{\partial p^a} \boldsymbol{N}_p \mathrm{dV} \tag{A.25}$$

$$\boldsymbol{J}_{n+1}^{wa3} = \int_{\Omega} (\nabla \boldsymbol{N}_p)^T \left[\rho^w \frac{k^s \boldsymbol{I}}{\mu^w} (\nabla \tilde{p}_{n+1}^w - \rho^w \boldsymbol{g}) \right] \frac{\partial k^{rw}}{\partial S^w} \frac{\partial S^w}{\partial p^a} \boldsymbol{N}_p \mathrm{dV} \tag{A.26}$$

The expression obtained for the matrix $\boldsymbol{J}_{n+1}^{au}$ is

$$\boldsymbol{J}_{n+1}^{au} = \frac{\partial \boldsymbol{R}_a}{\partial \hat{\boldsymbol{u}}} = \int_{\Omega} \boldsymbol{N}_p^T (1 - S_{n+1}^w) \rho_{n+1}^a \boldsymbol{b} \mathrm{dV} \tag{A.27}$$

The expression obtained for the matrix $\boldsymbol{J}_{n+1}^{aw}$ is

$$\boldsymbol{J}_{n+1}^{aw} = \frac{\partial \boldsymbol{R}_a}{\partial \hat{\boldsymbol{p}}^w} = \boldsymbol{J}_{n+1}^{aw1} + \boldsymbol{J}_{n+1}^{aw2} + \boldsymbol{J}_{n+1}^{aw3} + \boldsymbol{J}_{n+1}^{aw4} \tag{A.28}$$

where

$$\boldsymbol{J}_{n+1}^{aw1} = \int_{\Omega} \boldsymbol{N}_p^T \frac{n \rho_{n+1}^a}{\Delta t} \frac{\partial S^w}{\partial p^w} \boldsymbol{N}_p \mathrm{dV} \tag{A.29}$$

$$\boldsymbol{J}_{n+1}^{aw2} = -\int_{\Omega} \boldsymbol{N}_p^T \frac{n}{K^a} \frac{\tilde{p}_{n+1}^a - \tilde{p}_n^a}{\Delta t} \frac{\partial S^w}{\partial p^w} \boldsymbol{N}_p \mathrm{dV} \tag{A.30}$$

$$\boldsymbol{J}_{n+1}^{aw3} = -\int_{\Omega} \boldsymbol{N}_p^T \rho_{n+1}^a \left(\nabla \cdot \frac{\tilde{\boldsymbol{u}}_{n+1} - \tilde{\boldsymbol{u}}_n}{\Delta t} \right) \frac{\partial S^w}{\partial p^w} \boldsymbol{N}_p \mathrm{dV} \tag{A.31}$$

$$\boldsymbol{J}_{n+1}^{aw4} = \int_{\Omega} (\nabla \boldsymbol{N}_p)^T \left[\rho_{n+1}^a \frac{k_{n+1}^{ra} k^s \boldsymbol{I}}{\mu^a} (\nabla \tilde{p}_{n+1}^a - \rho_{n+1}^a \boldsymbol{g}) \right] \frac{\partial k^{rw}}{\partial S^w} \frac{\partial S^w}{\partial p^a} \boldsymbol{N}_p \mathrm{dV} \tag{A.32}$$

The expression obtained for the matrix $\boldsymbol{J}^{aa}_{n+1}$ is

$$\boldsymbol{J}^{aa}_{n+1} = \frac{\partial \boldsymbol{R}_a}{\partial \hat{\boldsymbol{p}}^a} = \boldsymbol{J}^{aa1}_{n+1} + \boldsymbol{J}^{aa2}_{n+1} + \boldsymbol{J}^{aa3}_{n+1} + \boldsymbol{J}^{aa4}_{n+1} + \boldsymbol{J}^{aa5}_{n+1} + \boldsymbol{J}^{aa6}_{n+1} + \boldsymbol{J}^{aa7}_{n+1} + \boldsymbol{J}^{aa8}_{n+1} + \boldsymbol{J}^{aa9}_{n+1} \quad \text{(A.33)}$$

where

$$\boldsymbol{J}^{aa1}_{n+1} = -\int_{\Omega} \boldsymbol{N}_p^T \frac{n\rho^a_{n+1}}{\Delta t} \frac{\partial S^w}{\partial p^a} \boldsymbol{N}_p \mathrm{dV} \quad \text{(A.34)}$$

$$\boldsymbol{J}^{aa2}_{n+1} = -\int_{\Omega} \boldsymbol{N}_p^T n \frac{S^w_{n+1} - S^w_n}{\Delta t} \frac{\partial \rho^a}{\partial p^a} \boldsymbol{N}_p \mathrm{dV} \quad \text{(A.35)}$$

$$\boldsymbol{J}^{aa3}_{n+1} = \int_{\Omega} \boldsymbol{N}_p^T \frac{n}{K^a} \frac{(1 - S^w_{n+1})}{\Delta t} \boldsymbol{N}_p \mathrm{dV} \quad \text{(A.36)}$$

$$\boldsymbol{J}^{aa4}_{n+1} = -\int_{\Omega} \boldsymbol{N}_p^T \frac{n}{K^a} \frac{\tilde{p}^a_{n+1} - \tilde{p}^a_n}{\Delta t} \frac{\partial S^w}{\partial p^a} \boldsymbol{N}_p \mathrm{dV} \quad \text{(A.37)}$$

$$\boldsymbol{J}^{aa5}_{n+1} = -\int_{\Omega} \boldsymbol{N}_p^T \rho^a_{n+1} \left(\nabla \cdot \frac{\tilde{\boldsymbol{u}}_{n+1} - \tilde{\boldsymbol{u}}_n}{\Delta t} \right) \frac{\partial S^w}{\partial p^a} \boldsymbol{N}_p \mathrm{dV} \quad \text{(A.38)}$$

$$\boldsymbol{J}^{aa6}_{n+1} = \int_{\Omega} \boldsymbol{N}_p^T (1 - S^w_{n+1}) \left(\nabla \cdot \frac{\tilde{\boldsymbol{u}}_{n+1} - \tilde{\boldsymbol{u}}_n}{\Delta t} \right) \frac{\partial \rho^a}{\partial p^a} \boldsymbol{N}_p \mathrm{dV} \quad \text{(A.39)}$$

$$\boldsymbol{J}^{aa7}_{n+1} = \int_{\Omega} (\nabla \boldsymbol{N}_p)^T \rho^a_{n+1} \frac{k^{ra}_{n+1} k^s \boldsymbol{I}}{\mu^a} \boldsymbol{N}_p \mathrm{dV} \quad \text{(A.40)}$$

$$\boldsymbol{J}^{aa8}_{n+1} = \int_{\Omega} (\nabla \boldsymbol{N}_p)^T \left[\rho^a_{n+1} \frac{k^{ra}_{n+1} k^s \boldsymbol{I}}{\mu^a} (\nabla \tilde{p}^a_{n+1} - \rho^a_{n+1} \boldsymbol{g}) \right] \frac{\partial k^{rw}}{\partial S^w} \frac{\partial S^w}{\partial p^a} \boldsymbol{N}_p \mathrm{dV} \quad \text{(A.41)}$$

$$\boldsymbol{J}^{aa9}_{n+1} = \int_{\Omega} (\nabla \boldsymbol{N}_p)^T \left[\frac{k^{ra}_{n+1} k^s \boldsymbol{I}}{\mu^a} (\nabla \tilde{p}^a_{n+1} - 2\rho^a_{n+1} \boldsymbol{g}) \right] \frac{\partial \rho^a}{\partial p^a} \boldsymbol{N}_p \mathrm{dV} \quad \text{(A.42)}$$

Bibliography

[1] M. Ambati, T. Gerasimov, and L. De Lorenzis. A review on phase-field models of brittle fracture and a new fast hybrid formulation. *Computational Mechanics*, 2014.

[2] L. Ambrosio and V. M. Tortorelli. Approximation of functional depending on jumps by elliptic functional via gamma convergence. *Communications on Pure and Applied Mathematics*, 1990.

[3] H. Amor and C. Marigo, J. J.and Maurini. Regularized formulation of the variational brittle fracture with unilateral contact: Numerical experiments. *Journal of the Mechanics and Physics of Solids*, 2009.

[4] M. A. Biot. General theory of three-dimensional consolidation. *Journal of Applied Physics*, 1941.

[5] M. A. Biot. General solutions of the equation of elasticity and consolidation for a porous material. *Journal of Applied Mechanics*, 1956.

[6] A.W. Bishop. The principle of effective stress., 1959.

[7] P. B. Bochev and C. R. Dohrmann. A computational study of stabilized, low-order C0finite element approximations of darcy equations. *Computational Mechanics*, 2006.

[8] P. B. Bochev, C. R. Dohrmann, and M. D. Gunzburger. Stabilization of Low-order Mixed Finite Elements for the Stokes Equations. *SIAM Journal on Numerical Analysis*, 2006.

[9] M. J. Borden, C. V. Verhoosel, M. A. Scott, T. J.R. Hughes, and C. M. Landis. A phase-field description of dynamic brittle fracture. *Computer Methods in Applied Mechanics and Engineering*, 2012.

[10] R. I. Borja. On the mechanical energy and effective stress in saturated and unsaturated porous continua. *International Journal of Solids and Structures*, 2006.

[11] B. Bourdin, C. P. Chukwudozie, and K. Yoshioka. A Variational Approach to the Numerical Simulation of Hydraulic Fracturing. 2012.

[12] B. Bourdin, G. A. Francfort, and J. J. Marigo. Numerical experiments in revisited brittle fracture. *Journal of the Mechanics and Physics of Solids*, 2000.

[13] B. Bourdin, G. A. Francfort, and J. J. Marigo. *The variational approach to fracture*. 2008.

[14] R. M. Bowen. Compressible porous media models by use of the theory of mixtures. *International Journal of Engineering Science*, 1982.

[15] F. Brezzi and M. Fortin. *Mixed and hybrid finite element methods*. 2012.

[16] R. H. Brooks and A. T. Corey. Properties of Porous Media Affecting Fluid Flow, 1966.

[17] T. Cajuhi, L. Sanavia, and L. De Lorenzis. Phase-field modeling of fracture in variably saturated porous media. *Computational Mechanics*, 2017.

[18] M. A. Celia, E. T. Bouloutas, and R. L. Zarba. A general massâconservative numerical solution for the unsaturated flow equation. *Water Resources Research*, 1990.

[19] A. Chambolle, G. A. Francfort, and J. J. Marigo. When and how do cracks propagate? *Journal of the Mechanics and Physics of Solids*, 2009.

[20] S. Cola, L. Sanavia, P. Simonini, and B. A. Schrefler. Coupled thermohydromechanical analysis of Venice lagoon salt marshes. *Water Resources Research*, 2008.

[21] R. de Boer. Highlights in the Historical Development of the Porous Media Theory: Toward a Consistent Macroscopic Theory. *Applied Mechanics Reviews*, 1996.

[22] R. De Boer. *Trends in Continuum Mechanics of Porous Media*. 2005.

[23] C. R. Dohrmann and P. B. Bochev. A stabilized finite elements method for the Stokes problem based on polynomial pressure projections. *International Journal for Numerical Methods in Fluids*, 2004.

[24] P. A. Forsyth, Y. S. Wu, and K. Pruess. Robust numerical methods for saturated-unsaturated flow with dry initial conditions in heterogeneous media. *Advances in Water Resources*, 1995.

[25] G.A. Francfort and J.-J. Marigo. Revisiting brittle fracture as an energy minimization problem. *Journal of the Mechanics and Physics of Solids*, 1998.

[26] T. Gerasimov and L. De Lorenzis. On penalization in variational phase-field models of brittle fracture. (November), 2018.

[27] M. A. Goodman and S. C. Cowin. A continuum theory for granular materials. *Archive for Rational Mechanics and Analysis*, 1972.

[28] W. G. Gray and B. A. Schrefler. Thermodynamic approach to effective stress in partially saturated porous media. *European Journal of Mechanics, A/Solids*, 2001.

[29] A. A. Griffith. The Phenomena of Rupture and Flow in Solids. *Philosophical Transactions of the Royal Society A: Mathematical, Physical and Engineering Sciences*, 1921.

[30] M. Hassanizadeh and W. G. Gray. General conservation equations for multi-phase systems: 1. Averaging procedure. *Advances in Water Resources*, 1979.

[31] M. Hassanizadeh and W. G. Gray. General conservation equations for multi-phase systems: 2. Mass, momenta, energy, and entropy equations. *Advances in Water Resources*, 1979.

[32] M. Hassanizadeh and W. G. Gray. General conservation equations for multi-phase systems: 3. Constitutive theory for porous media flow. *Advances in Water Resources*, 1980.

[33] S. M. Hassanizadeh and W. G. Gray. Mechanics and thermodynamics of multi-phase flow in porous media including interphase boundaries. *Advances in Water Resources*, 1990.

[34] Y. Heider and B. Markert. A phase-field modeling approach of hydraulic fracture in saturated porous media. *Mechanics Research Communications*, 2017.

[35] R. Krueger. Virtual crack closure technique: History, approach, and applications. *Applied Mechanics Reviews*, 2004.

[36] G. Lancioni and G. Royer-Carfagni. The variational approach to fracture mechanics. a practical application to the french panthéon in Paris. *Journal of Elasticity*, 2009.

[37] R Lewis and B Schrefler. *Finite Element Method in the Deformation and Consolidation of Porous Media*. 1998.

[38] A. C. Liakopoulos. Theoretical solution of the gravity drainage problem. *Journal of Hydraulic Research*, 1964.

[39] C. Miehe, M. Hofacker, and F. Welschinger. A phase field model for rate-independent crack propagation: Robust algorithmic implementation based on operator splits. *Computer Methods in Applied Mechanics and Engineering*, 2010.

[40] C. Miehe, S. Mauthe, and S. Teichtmeister. Minimization principles for the coupled problem of Darcy-Biot-type fluid transport in porous media linked to phase field modeling of fracture. *Journal of the Mechanics and Physics of Solids*, 2015.

[41] A. Mikelić, M. F. Wheeler, and T. Wick. A Phase-Field Method for Propagating Fluid-Filled Fractures Coupled to a Surrounding Porous Medium. *Multiscale Modeling Simulation*, 2015.

[42] C. T. Miller, G. A. Williams, C. T. Kelley, and M. D. Tocci. Robust solution of Richards' equation for nonuniform porous media. *Water Resources Research*, 1998.

[43] N. Moës, J. Dolbow, and T. Belytschko. A finite element method for crack growth without remeshing. *International Journal for Numerical Methods in Engineering*, 1999.

[44] L. W. Morland. A simple constitutive theory for a fluid-saturated porous solid. *Journal of Geophysical Research*, 2008.

[45] Y. Mualem. A new model for predicting the hydraulic conductivity of unsaturated porous media. *Water Resources Research*, 1976.

[46] O.C.Zienkiewicz, R.L.Taylor, K Morgan, O Hassan, and N P Weatherill. The Finite Element Method. *Academy of Engineering Polish Academy of Science Chinese Academy of Sciences National Academy of Science Italy (Academia dei Lincei)*, 1981.

[47] M. Ortiz and A. Pandolfi. Finite-deformation irreversible cohesive elements for three-dimensional crack-propagation analysis. *International Journal for Numerical Methods in Engineering*, 1999.

[48] C. Paniconi and M. Putti. A comparison of Picard and Newton iteration in the numerical solution of multidimensional variably saturated flow problems. *Water Resources Research*, 1994.

[49] H. Peron, L. Laloui, T. Hueckel, and L. B. Hu. Desiccation cracking of soils. *European Journal of Environmental and Civil Engineering*, 2009.

[50] K. Pham, H. Amor, J. J. Marigo, and C. Maurini. Gradient damage models and their use to approximate brittle fracture. In *International Journal of Damage Mechanics*, 2011.

[51] R. Sampaio and W.O. Williams. Thermodynamics of diffusing mixtures. *Journal de Méchanique*, 1979.

[52] L. Sanavia. Numerical modelling of a slope stability test by means of porous media mechanics. *Engineering Computations (Swansea, Wales)*, 2009.

[53] B. A. Schrefler, L. Simoni, Li Xikui, and O. C. Zienkiewicz. Mechanics of Partially Saturated Porous Media. 2014.

[54] B.A. Schrefler. Mechanics and thermodynamics of saturated/unsaturated porous materials and quantitative solutions. *Applied Mechanics Reviews*, 2002.

[55] S. Secchi and B. A. Schrefler. A method for 3-D hydraulic fracturing simulation. In *International Journal of Fracture*, 2012.

[56] S. Secchi and B. A Schrefler. Hydraulic fracturing and its peculiarities. *Asia Pacific Journal on Computational Engineering*, 2014.

[57] A. W. Skempton. Effective Stress in Soils, Concrete and Rocks. In *Selected papers in soil mechanics*. 2015.

[58] R. A Stirling, C.T. Davie, and S. Glendinning. Multiphase modelling of desiccation cracking in the near-surface of compacted soils. *Géotechnique*, 2011.

[59] K. Terzaghi. *Theoretical Soil Mechanics*. 2007.

[60] N. Traore. *Modélisation numérique de la propagation des failles décrochantes dans la lithosphère*. 2014.

[61] C. Truesdell and R. Baierlein. Rational Thermodynamics. *American Journal of Physics*, 2005.

[62] C. Truesdell, W. Noll, and A. C. Pipkin. The Non-Linear Field Theories of Mechanics. *Journal of Applied Mechanics*, 2011.

[63] C. Truesdell and R. Toupin. The Classical Field Theories. In *Principles of Classical Mechanics and Field Theory*. 1960.

[64] M. Th. van Genuchten. A Closed-form Equation for Predicting the Hydraulic Conductivity of Unsaturated Soils1. *Soil Science Society of America Journal*, 1980.

[65] S. Whitaker. Simultaneous Heat, Mass, and Momentum Transfer in Porous Media: A Theory of Drying. *Advances in Heat Transfer*, 1977.

[66] J. A. White and R. I. Borja. Stabilized low-order finite elements for coupled solid-deformation/fluid-diffusion and their application to fault zone transients. *Computer Methods in Applied Mechanics and Engineering*, 2008.

[67] F. Zanello. *Contributions to modeling of Venice coastal peatlands and wetlands*. 2011.

[68] O. C. Zienkiewicz, a. H. C. Chan, M. Pastor, B. a. Schrefler, and T. Shiomi. *Computational Geomechanics with Special Reference to Earthquake Engineering*, volume 25. 2001.